2015

Antenna selection for energy-efficient MIMO-OFDM wireless systems

Phuc Ngoc Le
University of Wollongong

Antenna Selection for Energy-Efficient MIMO-OFDM Wireless Systems

A thesis submitted in partial fulfilment of the
requirements for the award of the degree

Doctor of Philosophy

from

THE UNIVERSITY OF WOLLONGONG

by

Phuc Ngoc Le

B.E. (2004) and M.E. (2006) in Electronics & Telecommunications Engineering,
Ho Chi Minh City University of Technology (HCMUT), Vietnam

School of Electrical, Computer and Telecommunications Engineering

Australia, March 2015

Abstract

Orthogonal frequency division multiplexing (OFDM) and multi-input multi-output (MIMO) are key techniques for high-speed wireless communications. Besides, there are raising energy costs and carbon footprint associated with the operation of wireless networks. Consequently, it is important to design MIMO-OFDM systems with high energy-efficiency for the next generation of wireless systems.

This thesis studies antenna selection MIMO-OFDM systems from an energy-efficiency perspective. The aim of the thesis is to propose and analyse novel antenna selection methods to improve the energy efficiency of the systems. The proposed methods include: *i*) adaptive antenna selection that jointly selects the number of active radio frequency (RF) chains and antenna indices; *ii*) power-amplifier aware antenna selection; and *iii*) jointly optimising transmit power allocation and antenna selection under quality-of-service (QoS) constraints.

Firstly, this thesis analyses energy efficiency in MIMO-OFDM systems that deploy conventional antenna selection approaches. The results show that these antenna systems are not effective from an energy-efficiency viewpoint. Thus, an adaptive selection method is proposed to improve energy efficiency. In the adaptive scheme, the number of active RF chains and the antenna indices are jointly selected to attain maximum energy efficiency. This proposed scheme is shown to achieve a better energy efficiency-spectral efficiency (EE-SE) trade-off compared to the existing selection schemes. In addition, the efficacy of power loading across subcarriers for improved energy-efficiency in antenna selection MIMO-OFDM systems is investigated.

Secondly, this thesis considers energy efficiency of antenna selection MIMO-OFDM systems from a power amplifier (PA) perspective. The PA aware antenna selection approach exploits the fact that antenna selection schemes that involve selecting antennas independently for each subcarrier result in power unbalance across transmit antennas, which affects power amplifier. A constrained selection scheme that can equally allocate data subcarriers among antennas by means of linear optimisation is proposed for the systems with an arbitrary number of multiplexed data streams. Moreover, the

effectiveness of this scheme is analysed directly in the nonlinear fading channels. Additionally, to overcome the issue of significant fluctuations of both the average power and peak power across transmit antennas, this thesis proposes and analyses a two-step strategy for data allocation in a space-frequency domain. This strategy is based on the aforementioned equal allocation of data subcarriers and the proposed peak-power reduction using cross-antenna permutations. The results demonstrate that a significant improvement in terms of energy efficiency could be achieved in the proposed systems in comparison with the conventional systems.

Lastly, this thesis investigates energy efficiency in antenna selection MIMO systems under QoS constraints. Both antenna selection MIMO and antenna selection MIMO automatic repeat request (ARQ) schemes are considered. Analytical expressions of the achieved energy efficiency in these systems over quasi-static Nakagami-*m* fading channels are derived. The energy-efficiency metrics take into account several important system parameters, such as channel codes, modulation schemes and detection methods, which is of great significance to practical system designs. Based on a convexity analysis of the energy-efficiency expressions, the optimal average energy per transmitted symbol is determined such that the energy efficiency of the systems is maximised.

Declaration

I, Phuc Ngoc Le, declare that this thesis, submitted in partial fulfilment of the requirements for the award of Doctor of Philosophy, in the School of Electrical, Computer and Telecommunications Engineering, University of Wollongong, is wholly my own work unless otherwise referenced or acknowledged.

Also, this thesis has not been submitted for qualifications at any other academic institution.

Signed

Phuc Ngoc Le

March 02, 2015

Acknowledgements

I first would like to express my gratitude to the Vietnamese Government's Project 322 for offering me an opportunity to pursue the PhD degree in Australia. Being a recipient of this program is my personal honour, which has deepened my commitment to my research and made me stronger to overcome challenges on my journey towards this thesis.

I would like to thank Dr Le Chung Tran and Prof Farzad Safaei for giving me an opportunity to be a part of their research group. I acknowledge them for fruitful discussions, insightful comments on my research work, as well as their supports over the last few years.

I would like to take this opportunity to thank many friendly staffs from the School of Electrical, Computer and Telecommunications Engineering, ICT Research Institute, SMART Facility, Faculty of Engineering and Information Sciences, the Library, and Research Student Centre, for their kindly supports during my PhD study. In addition, an International Postgraduate Tuition Award provided by the University of Wollongong (UOW) for my PhD course is gratefully appreciated.

I also would like to thank many research students at UOW, especially Mr Miftadi Sudjai, for interesting discussions. Many thanks also go to my friends and my colleagues in Vietnam for their encouragement.

Last but not least, I would like to thank my parents Lê Ngọc Quát and Nguyễn Thị Cúc, my brother, my sisters, and my relatives for their love, care and encouragement.

Wollongong, Australia

January 25, 2015

To my family

Table of Contents

List of Figures

List of Tables

List of Abbreviations

3GPPP	the 3rd Generation Partnership Project
AS	Antenna Selection
ARQ	Automatic Repeat Request
AWGN	Additive White Gaussian Noise
BER	Bit Error Rate
CCDF	Complementary Cumulative Distribution Function
CDF	Cumulative Distribution Function
CSI	Channel State Information
DFT	Discrete Fourier Transform
EE	Energy Efficiency
EIRP	Equivalent Isotropic Radiated Power
FDD	Frequency Division Duplex
FER	Frame Error Rate
FFT	Fast Fourier Transform
GI	Guard Interval
HARQ	Hybrid ARQ
HPA	High Power Amplifier
IBO	Input Back-Off
IEEE	Institute of Electrical and Electronics Engineers
IFFT	Inverse Fast Fourier Transform
i.i.d.	independent, identically distributed
ISI	Inter-Symbol Interference
LDPC	Low-Density Parity-Check code
LP	Linear Programming
LS	Least-Square
LTE	Long Term Evolution
MDCM	Modified Dual Carrier Modulation
MIMO	Multi-Input Multi-Output
MMSE	Minimum Mean Squared Error

M-PSK	*M-ary* Phase Shift Keying
M-QAM	*M-ary* Quadrature Amplitude Modulation
MRC	Maximum Ratio Combining
MRT	Maximum Ratio Transmission
MSE	Mean Squared Error
NACK	Negative ACKnowledgement
NLOS	Non-Line-Of-Sight
OFDM	Orthogonal Frequency Division Multiplexing
OFDMA	Orthogonal frequency Division Multiple Access
OSTBC	Orthogonal Space-Time Block Code
PA	Power Amplifier
PAPR	Peak-to-Average Power Ratio
PDF	Probability Density Function
PE	Power Efficiency
PSD	Power Spectral Density
QoS	Quality of Service
QPSK	Quadrature Phase Shift Keying
RAS	Receive Antenna Selection
RF	Radio Frequency
SE	Spectral Efficiency
SEL	Soft Envelope Limiter
SISO	Single-Input Single-Output
SLM	SeLect Mapping
SNDR	Signal-to-Noise-plus-Distortion Ratio
SNR	Signal-to-Noise Ratio
s.t.	subject to
TAS	Transmit Antenna Selection
TDD	Time-Division Duplex
UWB	Ultra-Wide Band
V-BLAST	Vertical-Bell Labs Layered Space-Time
WiMAX	Worldwide Interoperability for Microwave Access
WLAN	Wireless Local Area Network
ZF	Zero-Forcing
ZPS	Zero-Padded Suffix

Notation

$\mathbf{A}$	the matrix **A** (boldface uppercase)
$\mathbf{x}$	the vector **x** (boldface lowercase)
A or a	the scalar number (italic)
$:=$	defined as
$(.)^*$	complex conjugate
$(.)^{-1}$	inverse of a scalar number or a square matrix
$(.)^T$	transpose of a vector or a matrix
$(.)^H$	Hermitian transpose of a vector or a matrix
$\otimes$	the Kronecker product
$\|\|.\|\|$	the Frobenius norm
$\|a\|$	absolute value of the scalar number a
$\mathbf{I}_n$	an identity matrix with size $n \times n$
$\mathbf{1}_n$	a $n \times 1$ vector of ones
$[\mathbf{A}]_{i,j}$	the (i,j) entry of the matrix **A**
$\det(\mathbf{A})$	determinant of the matrix **A**
$\mathrm{tr}\{\mathbf{A}\}$	trace of the matrix **A**
$\mathrm{diag}(\mathbf{x})$	diagonal matrix defined by **x**
$C_a^b = b!/a!(b-a)!$	the binomial coefficient
$erfc(x) = \frac{2}{\sqrt{\pi}} \int_x^\infty e^{-t^2} dt$	the complementary error function
$\Gamma(a,x) = \int_x^{+\infty} e^{-t} t^{a-1} dt$	the incomplete gamma function
$\log(.)$	logarithm with base 10
$\log_2(.)$	logarithm with base 2
$\ln(.)$	natural logarithm

Pr(.)	probability of an even
$\varepsilon\{.\}$	expectation of random variables
Re{.}	real part of a scalar, vector or matrix
Im{.}	imaginary part of a scalar, vector or matrix
$\Re$	field of real numbers
$O(.)$	an order of complexity

Chapter 1

Introduction

In this chapter, the motivation of this thesis on energy-efficient antenna selection multi-input multi-output orthogonal frequency division multiplexing (MIMO-OFDM) wireless systems is first introduced. After that, the outline and contributions of the thesis are presented. Finally, journal and conference papers that are published or submitted for publication based on this research work are provided.

1.1 Motivation

The next generation of wireless networks are expected to provide ubiquitous access with high speed and high reliability. In cellular networks, there has been a transition from UMTS (Universal Mobile Telecommunications System) to LTE (Long Term Evolution)/LTE-Advanced for enhanced data-rates and expanded coverage areas. Similarly, there has been an evolution in wireless local area networks (WLAN) from IEEE 802.11n to IEEE 802.11ac and IEEE802.11ad to meet increasing demands for high-speed wireless applications. Besides, reducing energy consumption in wireless networks is of significant interest among academic and industrial researchers. This is due to the fact that there are rising energy costs and carbon footprint of operating wireless networks with an increasing number of customers [1]. Consequently, a high-speed system with high energy-efficiency has become one of the main streams for the design of future wireless systems.

A combination of multi-input multi-output (MIMO) techniques and orthogonal frequency division multiplexing (OFDM) has been considered as a key technique for high-speed wireless communications [2, 3]. This is because OFDM transmission offers high spectral efficiency and robustness against intersymbol interference (ISI) in multipath fading channels. Meanwhile, MIMO techniques significantly increase data rate and/or link reliability. Specifically, the ergodic capacity of MIMO systems over fading channels is shown to increase linearly with the minimum of the number of transmit and receive antennas [4]. In fact, MIMO-OFDM has been adopted in current

and future standards, including WiMAX (Worldwide Interoperability for Microwave Access) IEEE 802.16m [5], WLAN IEEE 802.11n [6], and 3GPP LTE/LTE-Advanced [7, 8].

Among a variety of MIMO schemes, antenna selection appears to be a promising approach for OFDM systems. In antenna selection, only a subset of antennas is selected for transmissions subject to a given selection criterion. Therefore, this technique requires a low implementation cost and small amount of feedback information, compared to other beamforming or precoding techniques [9, 10]. Also, antenna selection is robust to channel estimation errors because the phase information is generally not required. Owing to these advantageous properties, antenna selection has been considered for the uplink of 4G LTE-Advanced [11].

Some research works have considered antenna selection MIMO-OFDM systems in the literature. However, these studies only investigated the systems from either capacity or error-performance perspective. Consequently, it is unknown if the existing antenna selection approaches are optimal in terms of energy efficiency. In addition, some recent works on energy-efficient MIMO-OFDM systems, e.g., [12, 13], focused only on spatial multiplexing MIMO schemes, which did not address the above concerns. Consequently, energy-efficient antenna selection MIMO-OFDM systems remains an open research problem. Motivated by this, the thesis focuses on investigating energy efficiency in MIMO-OFDM systems. It aims to propose and analyse novel antenna selection methods for improved energy-efficiency. Details about a literature review on the state-of-the-art of antenna selection MIMO-OFDM systems and specific research problems considered in this thesis will be provided in Chapter 2.

1.2 Thesis Outline

The focus of this thesis is on energy-efficient antenna selection MIMO-OFDM wireless systems. The thesis comprises of seven chapters, which is outlined as follows.

Chapter 1 describes the motivation, the outline and the contributions of this thesis.

Chapter 2 first provides some fundamental background on MIMO and OFDM techniques. It then focuses on a literature review of related works on antenna selection for OFDM systems. In addition, metrics often used to measure energy efficiency of MIMO systems are described in this chapter.

Chapter 3 investigates antenna selection strategies for MIMO-OFDM wireless systems from an energy efficiency perspective. Closed-form expressions of energy efficiency in MIMO-OFDM systems that deploy conventional antenna selection approaches are first derived. Numerical results based on these analytical results are then provided and discussed. To achieve better energy-efficiency performance, this chapter proposes an adaptive antenna selection method in which both the number of active radio frequency (RF) chains and the antenna indices are jointly selected depending on the channel conditions. Exhaustive search is considered to realize this selection method for small numbers of antennas. Moreover, a low-complexity algorithm that can achieve a near-optimal performance, as compared to the (optimal) exhaustive search method, is developed when the number of equipped antennas is large. In addition, the effectiveness of power loading across subcarriers for improved energy efficiency in the context of antenna selection MIMO-OFDM systems is considered.

Chapter 4 develops a constrained antenna selection scheme to improve energy efficiency in MIMO-OFDM systems from a power amplifier perspective. Specifically, this chapter considers antenna selection MIMO-OFDM systems that suffer from nonlinear distortions due to high-power amplifiers. At first, some problems pertaining to the implementation of per-subcarrier antenna selection approaches are identified. Next, a constrained selection scheme that can equally allocate data subcarriers among antennas by means of linear optimisation is proposed for the systems with an arbitrary number of multiplexed data streams. A reduced complexity strategy that requires smaller feedback information and lower computational effort for solving the optimisation problem is also developed. Moreover, an analysis of the efficacy of the constrained selection approach is performed directly in nonlinear fading channels.

Chapter 5 continues to consider energy efficiency in MIMO-OFDM systems with per-subcarrier antenna selection from a power amplifier perspective. Unlike Chapter 4, this chapter focuses on an antenna selection MIMO-OFDM system with linear scaling for non-distortion transmissions. Specifically, a two-step strategy for data-subcarrier allocation is proposed to deliver the maximum overall power efficiency. This strategy consists of an equal allocation of data subcarriers based on linear optimisation (as proposed in Chapter 4) and peak-power reduction via cross-antenna permutations. The complementary cumulative distribution function (CCDF) of the power efficiency and the analytical expressions of the average power efficiency are derived to provide insight

into the system characteristics. An analysis of the efficacy of the proposed method is also performed from both the power efficiency of power amplifiers perspective and the system's energy-efficiency perspective.

Chapter 6 analyses energy efficiency in both antenna selection MIMO and antenna selection MIMO automatic repeat request (ARQ) systems, in which the energy-efficiency metric takes into consideration several important parameters, such as channel coding, modulation scheme, and detection methods. At first, this chapter derives accurate approximate expressions of the average frame-error rate (FER) in these systems over quasi-static Nakagami-*m* fading channels. The FER approximations are then used to obtain analytical expressions of an energy-efficiency metric. Based on a convexity analysis of the energy-efficiency expressions, the optimal value of the average energy per transmitted data symbol is determined such that the energy efficiency in the antenna selection MIMO system is maximised given quality-of-service (QoS) constraints. For the antenna selection MIMO ARQ system, the optimal average energy per symbol to minimise the total energy consumption is obtained.

Finally, Chapter 7 summarises the thesis and highlights the main results. Suggestions for future work based on this research are also provided.

1.3 Contributions of the Thesis

This thesis proposes and analyses novel antenna selection methods to improve energy efficiency in MIMO-OFDM wireless systems. These methods are presented in Chapter 3 to Chapter 6. The research contributions in each chapter are summarised below.

Chapter 3

- Analysis of energy efficiency in MIMO-OFDM systems that deploy conventional antenna selection schemes.
- Analysis of the optimal number of equipped antennas at the transmitter to achieve the maximum energy-efficiency in per-subcarrier antenna selection MIMO-OFDM systems.
- Proposition of an adaptive antenna selection method that jointly selects the number of active RF chains and the antenna indices to significantly improve energy efficiency in MIMO-OFDM systems.

- Evaluation of the efficacy of power loading across subcarriers for improved energy-efficiency in several antenna selection MIMO-OFDM systems.
- Analysis of the trade-off between energy efficiency and spectral efficiency in several antenna selection MIMO-OFDM systems.

The results in this chapter have been accepted for publication in two journal papers [J1] and [J2], and published in a conference paper [C1] (see Section 1.4).

Chapter 4

- Proposition of a constrained antenna selection scheme to deal with the issue of power unbalance across antennas for MIMO-OFDM systems with an arbitrary number of multiplexed data streams. This scheme, devised by means of linear optimisation, optimally allocates data subcarriers under the constraint that all antennas have the same number of data symbols.
- Analysis of the efficacy of the proposed constrained antenna selection approach over the conventional approach directly in the nonlinear fading channels.
- Analysis of the trade-off between energy efficiency and spectral efficiency in antenna selection MIMO-OFDM systems suffering nonlinear distortions.

The results in this chapter have been published in a journal paper [J3] and a conference paper [C2].

Chapter 5

- Proposition of a two-step strategy for data-subcarrier allocation to deliver the maximum overall power efficiency of power amplifiers in MIMO-OFDM systems with linear scaling. This scheme consists of an equal allocation of data subcarriers based on linear optimisation and peak-power reduction via cross-antenna permutations.
- Analysis of the power efficiency of power amplifier and energy efficiency in MIMO-OFDM systems with linear scaling.

The results in this chapter have been published in a journal paper [J4].

Chapter 6

- Convexity analysis of the derived energy-efficiency expressions in both antenna selection MIMO and antenna selection MIMO ARQ systems.

- Analysis of the optimal average energy per transmitted symbol to achieve the maximum energy efficiency antenna selection MIMO systems under QoS constraints.
- Analysis of the optimal value of the average energy per transmitted data symbol such that the total energy consumption in antenna selection MIMO ARQ systems is minimised.

Some results in this chapter have been accepted for publication in a journal paper [J5]. The others have been submitted to the another journal for possible publication [J6].

1.4 Publications

The main contributions of this thesis are published/submitted for publication in the following journal and conference papers.

Journal papers

[J1] N. P. Le, F. Safaei, and L. C. Tran, "Antenna selection strategies for MIMO-OFDM wireless systems: an energy efficiency perspective," *IEEE Transactions on Vehicular Technology,* accepted for publication, April 2015.

[J2] N. P. Le, L. C. Tran, and F. Safaei, "Optimal design for energy-efficient per-subcarrier antenna selection MIMO-OFDM wireless systems," *Wireless Personal Communications,* accepted for publication, April 2015.

[J3] N. P. Le, F. Safaei, and L. C. Tran, "Transmit antenna subset selection for high-rate MIMO-OFDM systems in the presence of nonlinear power amplifiers," *EURASIP Journal on Wireless Communications and Networking*, vol. 2014, Feb. 2014.

[J4] N. P. Le, L. C. Tran, and F. Safaei, "Energy-efficiency analysis of per-subcarrier antenna selection with peak-power reduction in MIMO-OFDM wireless systems," *International Journal of Antennas and Propagation*, vol. 2014, June 2014.

[J5] N. P. Le, L. C. Tran, F. Safaei, and V. S. Varma, "Energy-efficiency analysis of antenna selection MIMO ARQ systems over Nakagami-*m* fading channels," *IET Communications,* accepted for publication, March 2015.

[J6] N. P. Le, F. Safaei, and L. C. Tran, "Maximizing energy efficiency in antenna selection MIMO systems subject to a QoS constraint," *Electronics Letters,* under review.

Conference papers

[C1] N. P. Le, L. C. Tran, and F. Safaei, "Adaptive antenna selection for energy-efficient MIMO-OFDM wireless systems", in *Proc. 17th International Symposium on Wireless Personal Multimedia Communications (WPMC 2014)*, Sydney, Australia, pp. 60-64, Sept. 2014.

[C2] N. P. Le, L. C. Tran, and F. Safaei, "Transmit antenna subset selection with power balancing for high data rate MIMO-OFDM UWB systems", in *Proc. 2013 IEEE International Conference on Ultra-Wideband (ICUWB 2013)*, Sydney, Australia, pp. 159-164, Sept. 2013.

Besides the main focus on antenna selection, the author has considered other MIMO techniques to improve the performance of MIMO-OFDM wireless systems during his PhD study. The proposed ideas include: *i*) space-time-frequency trellis coding for MIMO-OFDM systems to further extract the coding gain that is inherent in a trellis structure of space-time trellis codes for improved performance; *ii*) space-time-frequency coding of the Alamouti code and DSTTD (double space-time transmit diversity) code in conjunction with LDPC (low-density parity-check) channel coding and MDCM (modified dual-carrier modulation) modulation for very high rate MIMO-OFDM systems; and *iii*) combining lattice-reduction detection and antenna shuffling to achieve near-optimal performance in DSTTD MIMO-OFDM systems over correlated fading channels. The results, which are not included in the thesis, are published in the following conference papers.

[C3] N. P. Le, L. C. Tran, and F. Safaei, "Space-time-frequency trellis coding for multiband OFDM ultra wideband wireless systems", in *Proc. 75th IEEE Vehicular Technology Conference (VTC2012-Spring)*, Yokohama, Japan, pp. 1-5, May 2012.

[C4] N. P. Le, L. C. Tran, and F. Safaei, "Very high data rate MB-OFDM UWB systems with transmit diversity techniques", in *Proc. 12nd International Symposium on Communications and Information Technologies (ISCIT 2012)*, Gold Coast, Australia, pp. 508-512, Oct. 2012.

[C5] N. P. Le, L. C. Tran, and F. Safaei, "Double space-time transmit diversity for very high data rate MB-OFDM UWB systems", in *Proc. 12nd International*

Symposium on Communications and Information Technologies (ISCIT 2012), Gold Coast, Australia, pp. 926-930, Oct. 2012.

[C6] N. P. Le, L. C. Tran, and F. Safaei, "Combined adaptive lattice reduction-aided detection and antenna shuffling for DSTTD-OFDM systems", in *Proc. 14th IEEE International Workshop on Signal Processing Advances in Wireless Communications (SPAWC 2013)*, Darmstadt, Germany, pp. 100-104, June 2013.

Chapter 2

Background

In this chapter, an overview of multi-input multi-output (MIMO) and orthogonal frequency division multiplexing (OFDM) techniques is presented. Then, a mathematical model for a MIMO-OFDM system is described. Basic concepts of energy efficiency communications, including a power consumption model and energy-efficiency metrics, are introduced next. Finally, a literature review of antenna selection techniques is provided. This review covers the state-of-the-art of antenna selection for wireless systems. Based on this, open research questions considered in this thesis are formulated.

2.1 MIMO Techniques

Wireless systems can be classified as single-input single-output (SISO), single-input multi-output (SIMO), multi-input single-output (MISO), and multi-input multi-output (MIMO), depending on the numbers of antennas at the transmitter and receiver. These antenna configurations are illustrated in Figure 2.1. Recently, MIMO has been widely adopted in wireless communications. In this section, fundamentals on MIMO techniques are described.

2.1.1 MIMO System Model

Let us consider a point-to-point MIMO system with n_T transmit antennas and n_R receive antennas over flat fading channels as shown in Figure 2.2. Denote $\mathbf{x}$ to be a $n_T \times 1$ transmit signal vector with the covariance matrix $\mathbf{R}_{xx} = \varepsilon\{\mathbf{x}\mathbf{x}^H\}$, where $\varepsilon\{.\}$ is an expectation operation and $(.)^H$ denotes the Hermitian transpose operation. The total transmit power across antennas is constrained to P_t, which implies that $\mathrm{tr}\{\mathbf{R}_{xx}\} = n_T$, where $\mathrm{tr}\{.\}$ denotes a trace of a matrix. The received signal in the MIMO system can be expressed as [14]

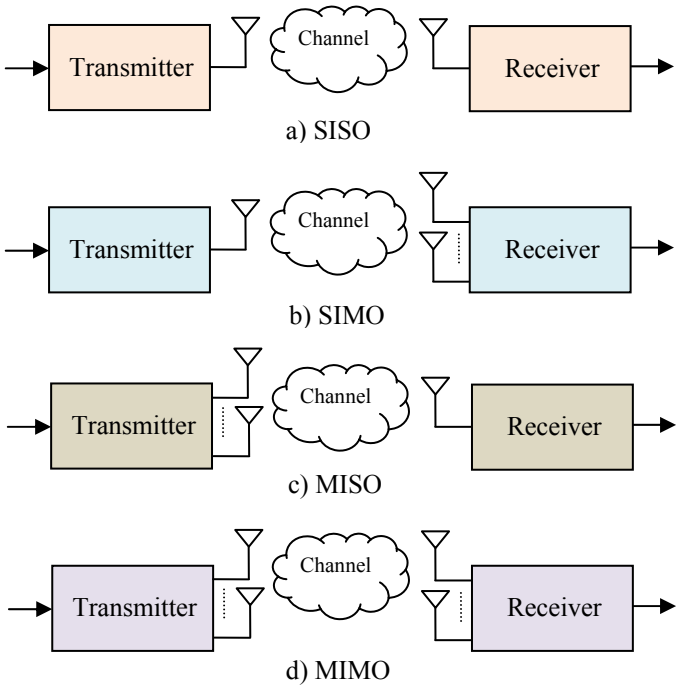

Figure 2.1. Antenna configurations in wireless systems.

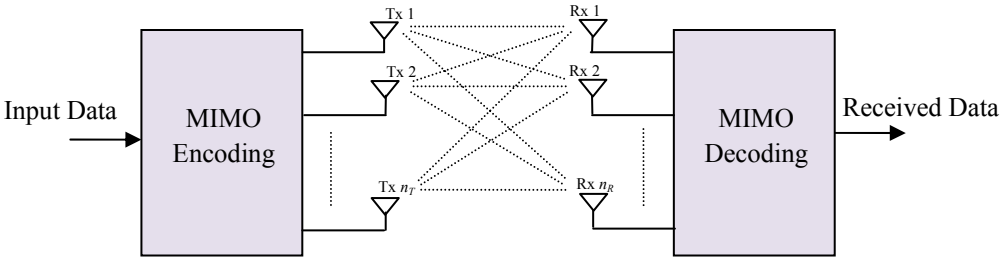

Figure 2.2. Block diagram of a MIMO wireless system.

$$\mathbf{y} = \sqrt{\frac{P_t}{n_T}}\mathbf{H}\mathbf{x} + \mathbf{n}, \tag{2.1}$$

where $\mathbf{y}$ is a $n_R \times 1$ received signal vector, $\mathbf{H}$ is a $n_R \times n_T$ channel matrix whose element $h_{j,i}$ is the fading coefficient between the i^{th} transmit antenna and the j^{th} receive antenna, and $\mathbf{n}$ is a $n_R \times 1$ noise vector with the covariance matrix $\varepsilon\{\mathbf{n}\mathbf{n}^H\} = \sigma_n^2 \mathbf{I}_{n_R}$. The elements of $\mathbf{n}$ are assumed to be zero-mean circularly symmetrical complex Gaussian variables, i.e., $\mathbf{n} \sim CN(0, \sigma_n^2)$. Also, in this section, the elements of matrix $\mathbf{H}$ can be deterministic or random. For the deterministic channel, a normalization of $\sum_{i=1}^{n_T} |h_{j,i}|^2 = n_T, \forall j = 1,2,...,n_R,$ is assumed. If the channel is random, this normalization

will apply to the expected value of the channel coefficients. Consequently, the receive signal-to-noise ratio (SNR) can be written as

$$\rho = \frac{P_t}{\sigma_n^2}. \tag{2.2}$$

Note that Eq. (2.2) is also the average SNR when the channel is random.

2.1.2 MIMO Capacity

Channel capacity is defined as the maximum possible transmission rate that a channel can support with an arbitrary small probability of errors [14]. The capacity of additive white Gaussian noise (AWGN) channels was first introduced by Claude Shannon in 1948 [15]. In this section, capacity of MIMO systems over flat fading channels is described. An extension to frequency-selective fading channels will be discussed in Section 2.2.4.

2.1.2.1 Capacity in Deterministic Flat Fading Channel

In a MIMO channel, capacity is defined as [14, 16]

$$C = \max_{f(\mathbf{x})} I(\mathbf{x};\mathbf{y}), \tag{2.3}$$

where $f(\mathbf{x})$ is the probability distribution of $\mathbf{x}$ and $I(\mathbf{x};\mathbf{y})$ is the mutual information between $\mathbf{x}$ and $\mathbf{y}$. The value of $I(\mathbf{x};\mathbf{y})$ is given as [16]

$$I(\mathbf{x};\mathbf{y}) = \log_2 \det\left(\mathbf{I}_{n_R} + \frac{\rho}{n_T} \mathbf{H}\mathbf{R}_{xx}\mathbf{H}^H \right) \quad \text{(bits/s/Hz)}. \tag{2.4}$$

Therefore, the capacity in Eq. (2.3) can be rewritten as

$$C = \max_{\mathrm{tr}\{\mathbf{R}_{xx}\}=n_T} \log_2 \det\left(\mathbf{I}_{n_R} + \frac{\rho}{n_T} \mathbf{H}\mathbf{R}_{xx}\mathbf{H}^H \right) \text{ (bits/s/Hz)}. \tag{2.5}$$

Note that Eq. (2.5) is a normalized capacity (bits/s/Hz) with respect to the bandwidth. If the bandwidth is W (Hz), the maximum achievable data rate supported by the channel is $W \times C$ (bits/s). Moreover, the capacity formula Eq. (2.5) can be further simplified depending on whether the channel state information (CSI) is available at transmitter or not.

a. Channel unknown to the transmitter

When the channel is unknown to the transmitter, the signals are independent and the power is equally allocated among the transmit antennas, i.e., $\mathbf{R}_{xx} = \mathbf{I}_{n_T}$. Thus, Eq. (2.5) can be rewritten as

$$C = \log_2 \det\left(\mathbf{I}_{n_R} + \frac{\rho}{n_T} \mathbf{H}\mathbf{H}^H \right) \quad \text{(bits/s/Hz)}. \tag{2.6}$$

By performing the eigen-decomposition of $\mathbf{H}\mathbf{H}^H$ as $\mathbf{H}\mathbf{H}^H = \mathbf{U}\mathbf{\Lambda}\mathbf{U}^H$, where $\mathbf{U}$ is a unitary matrix and $\mathbf{\Lambda}$ is the diagonal matrix whose diagonal elements are eigenvalues $\lambda_r, r = 1,2,..., R$, Eq. (2.6) can be expressed as

$$C = \sum_{r=1}^{R} \log_2 \left(1 + \frac{\rho}{n_T} \lambda_r \right) \text{ (bits/s/Hz)}. \tag{2.7}$$

Note that the value R in Eq. (2.7) is referred to as the rank of the channel matrix. Also, it can be seen from Eq. (2.7) that the capacity of MIMO channel is a sum of the capacities of R SISO sub-channels where the r^{th} sub-channel has a power gain λ_r and the corresponding transmit power is P_t / n_T.

b. Channel known to the transmitter

In MIMO schemes where the channel is known to the transmitter, capacity can be increased by optimal allocation of transmit power using a water-filling algorithm [14]. The basic idea behind the water-filling method is assigning more power on the channel with good condition and vice versa.

Let ψ_r denote the optimal transmit power for the r^{th} SISO sub-channel. This power is found using the water-filling algorithm as [14]

$$\psi_r = \left[\upsilon - \frac{n_T}{\rho \lambda_r} \right]_+, \; r = 1,2,..., R, \tag{2.8}$$

where $\upsilon > 0$ is the water level that is chosen to satisfy a constraint $\sum_{r=1}^{R} \psi_r = n_T$ and $[x]_+ = \max(x, 0)$. The capacity in this channel is now obtained as

$$C = \sum_{r=1}^{R} \log_2 \left(1 + \psi_r \frac{\rho}{n_T} \lambda_r \right) \text{ (bits/s/Hz)}. \tag{2.9}$$

As the channel information is exploited at the transmitter, the obtained capacity in Eq. (2.9) is better than its counterpart, i.e., Eq. (2.7).

c. Special cases: SIMO and MISO schemes

In a SIMO scheme with a $n_R \times 1$ channel vector $\mathbf{h}$, we have $R = 1$ and $\lambda_1 = \| \mathbf{h} \|^2$. Thus, the capacity when the channel is unknown to the transmitter is simplified to as (cf. Eq. (2.7))

$$C = \log_2\left(1 + \rho \| \mathbf{h} \|^2\right) \text{ (bits/s/Hz)}. \tag{2.10}$$

It can be seen from Eq. (2.10) that the use of multiple receive antennas increases the effective SNR, thereby improving capacity compared to the SISO channel. Also, it is noted that, in this scheme, the availability of CSI at the transmitter provides no benefit in terms of capacity.

In a MISO scheme without CSI at the transmitter, the capacity is obtained by (cf. Eq. (2.7))

$$C = \log_2\left(1 + \frac{\rho}{n_T} \| \mathbf{h} \|^2\right) \text{ (bits/s/Hz)}. \tag{2.11}$$

From Eq. (2.10) and Eq. (2.11), it can be seen that the SIMO channel offers higher capacity than MISO channel when CSI is not available at the transmitter. This can be explained by the fact that array gain is not exploited in the MISO scheme. However, when CSI is available at the transmitter in a MISO scheme, the obtained capacity with water-filling optimisation is given by

$$C = \log_2\left(1 + \rho \| \mathbf{h} \|^2\right) \text{ (bits/s/Hz)}. \tag{2.12}$$

This implies that the capacity is equal to the SIMO scheme.

2.1.2.2 Capacity in Random Flat Fading Channel

When the channel is random, the information rate is random as well. To characterize capacity in MIMO systems in this case, ergodic capacity is usually used. This capacity is the ensemble average of instantaneous capacity over the distribution of the elements in the channel matrix [14]. This capacity is useful when the channel experiences independent realizations for every use of the channel. In a SISO system with a random complex channel gain h, the ergodic capacity is given by [17]

$$C = \varepsilon\{\log_2(1 + \rho | h |^2)\} \text{ (bits/s/Hz)}, \tag{2.13}$$

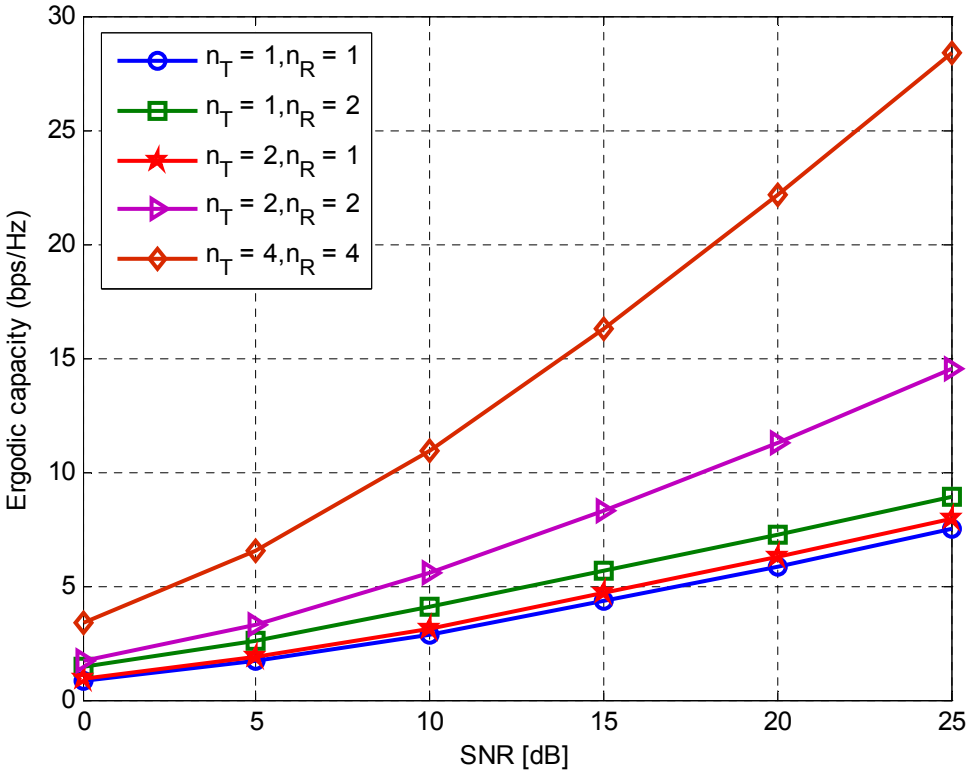

Figure 2.3. Ergodic capacity for different MIMO configurations (no CSI at transmitter).

where $\rho = P_t/\sigma_n^2$ is the average SNR.

In a MIMO system without CSI at the transmitter, ergodic capacity is obtained as (cf. Eq. (2.7))

$$C = \varepsilon\left\{\sum_{r=1}^{R}\log_2\left(1+\frac{\rho}{n_T}\lambda_r\right)\right\} \text{ (bits/s/Hz).} \tag{2.14}$$

Figure 2.3 plots the ergodic capacity for different MIMO configurations without CSI at the transmitter. It can be seen that ergodic capacity increases when the SNR value increases. Also, a larger number of antennas results in a higher ergodic capacity.

When the channel is known to the transmitter, ergodic capacity in a MIMO system with water-filling power allocation is given by (cf. Eq. (2.9))

$$C = \varepsilon\left\{\sum_{r=1}^{R}\log_2\left(1+\psi_r\frac{\rho}{n_T}\lambda_r\right)\right\} \text{ (bits/s/Hz).} \tag{2.15}$$

Note that a MIMO system with CSI at transmitter always achieves higher ergodic capacity than that without CSI at transmitter. However, this advantage diminishes when the SNR value is large enough.

Besides the ergodic capacity, outage capacity, referred to as a capacity that is guaranteed with a certain level of reliability, is often used to characterize capacity of MIMO channels. More specifically, *p*% outage capacity, denoted as $C_{out,q}$, is defined such that the information rate is guaranteed for (100-*p*) % channel realizations, i.e., $\Pr(C \le C_{out,q}) = p\%$. This kind of capacity is useful when evaluating capacity of MIMO channels that the channel matrix is to remain constant for each use of the channel.

It is also worth mentioning that in practical scenarios, there exist some factors that could degrade capacity of MIMO systems. Some of the important factors are spatial correlation due to insufficient scattering or spacing between antennas, the presence of a line-of-sight (LOS) component, and keyhole effects. Detailed discussions about these issues can be found in [14].

2.1.3 MIMO Encoding/Decoding Schemes

MIMO system models and the corresponding capacities have been described in the previous section. Let us now consider MIMO encoding and decoding methods. Numerous MIMO encoding/decoding schemes have been proposed so far. In general, they can be categorized into three main types, namely spatial diversity, spatial multiplexing, and beamforming. This section briefly reviews some MIMO schemes that are relevant to the subsequent chapters of this thesis. A more comprehensive literature review of MIMO encoding/decoding techniques can be found in [18].

2.1.3.1 Spatial Diversity

In wireless fading channels, signal power fluctuates randomly. Diversity is a powerful technique to mitigate the effects of fading. The basic idea behind the diversity technique is to provide the receiver several replicas of the same transmit signal over independent fading links and then perform a proper combining at the receiver [14]. The efficacy of diversity is characterized by the number of independent fading links, and is known as *diversity order*. Diversity techniques can be classified into time diversity, frequency diversity, and spatial diversity, depending on the domain in which the redundancy is introduced. The main advantage of spatial diversity over time diversity and frequency diversity is that no expenditure in transmission time or bandwidth is

incurred. Spatial diversity can be categorized into receive diversity and transmit diversity.

Receive diversity techniques perform a combining of the individual received signals for improved signal quality. Some popular receive diversity schemes are maximum ratio combining (MRC), equal gain combining (EGC), and selection combining (SC). In MRC, each signal branch is first multiplied by a weight factor that is proportional to the signal amplitude. The resultant signals are then co-phased and added up. The MRC scheme is optimal in the sense of maximising the output SNR. Meanwhile, in EGC scheme, the signal branches are only co-phased and added up. This scheme is suboptimal in terms of SNR performance but simpler than MRC. For a SC scheme, the signal branch with the maximum instantaneous SNR is selected, whereas other signal branches are discarded.

Unlike receive diversity, transmit diversity techniques provide diversity gain by sending redundant signals over multiple transmit antennas. As multiple receive antennas are optional, transmit diversity is more preferred (over receive diversity) from a practical viewpoint in downlink cellular networks. Specifically, multiple antennas are required only at the base station, instead of at mobile terminals where cost, size and power consumption are major concerns. Transmit diversity can be realized by means of space-time coding.

There are several classes of space-time codes (STCs) in the literature. One of the most popular STCs is orthogonal space-time block codes (OSTBCs). This kind of STCs is constructed based on orthogonal designs. Accordingly, given a set of data symbols, a codeword matrix is constructed such that the columns (and the rows) are orthogonal to one another. Due to the orthogonality, OSTBCs possess simple maximum-likelihood decoding. A very simple but efficient (in terms of full-diversity and full-rate) OSTBCs was proposed by Alamouti [19]. The Alamouti code is designed for a system with two transmit antennas as shown in Figure 2.4. Accordingly, two data symbols x_1 and x_2 are transmitted simultaneously during the first symbol period from antenna 1 and 2, respectively. During the next symbol period, $-x_2^*$ and x_1^* are transmitted from antenna 1 and antenna 2, respectively. Several OSTBCs designed for systems with more transmit antennas were presented in [20]. It is worth noting that OSTBCs in conjunction with complex modulation while achieving full diversity generally cause rate-loss in comparison to single-antenna systems. Thus, some design approaches to improve data

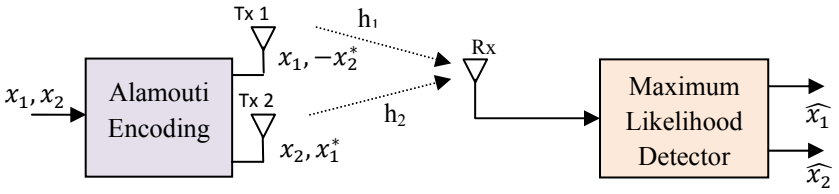

Figure 2.4. Block diagram of the Alamouti space-time coding based system.

rate were proposed, e.g., quasi-orthogonal STBCs [21] or linear dispersion codes [22]. In these STCs codes, higher rates are obtained by relaxing the orthogonal constraint. Hence, diversity gain is typically reduced compared to OSTBCs.

Space time trellis code (STTC) is another class of STCs, which is based on joint design of channel coding, modulation and transmit diversity. Unlike OSTBCs, STTCs could achieve a coding gain in addition to diversity gain. STTC was first introduced by Tarokh *et al.* for narrowband systems over flat fading channels [23]. However, the codes in [23] were manually derived and not optimal with respect to coding gain. Consequently, optimal codes for different system configurations and channel conditions have been reported, see, e.g., [24].

2.1.3.2 Spatial Multiplexing

In spatial multiplexing MIMO systems, the input data stream is first split into sub-streams, known as *layers*. These sub-streams are then transmitted simultaneously over the transmit antennas using the same frequency band. At the receiver, interference cancellation techniques are employed to detect signals. Capacity in spatial multiplexing schemes increases linearly with the minimum of the numbers of transmit and receive antennas at no additional power consumption or bandwidth extension. This benefit is referred to as *multiplexing gain*.

In general, there are three spatial multiplexing MIMO transceiver architectures in the literature, namely Diagonal Bell Labs Layered Space-Time (D-BLAST), Vertical-BLAST (V-BLAST), and Horizontal-BLAST (H-BLAST). The difference among these schemes lies in an overall coding structure in space-time domains, i.e., diagonal structure, vertical structure, or horizontal structure. A performance comparison among these schemes was presented in [25]. Figure 2.5 plots a V-BLAST scheme with channel codes. This scheme will be considered in Chapter 4 and Chapter 5 of this thesis.

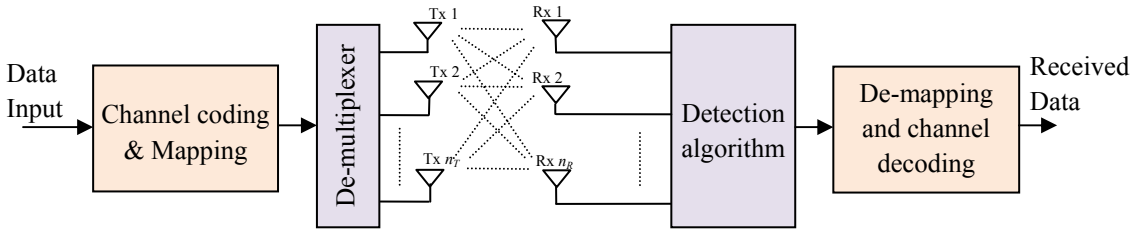

Figure 2.5. Block diagram of a V-BLAST architecture with channel codes.

Several detection methods can be employed in spatial multiplexing MIMO systems, which characterize a trade-off between error-performance and complexity. The maximum-likelihood (ML) method that performs a brute-force search for all possible transmitted signal vectors could achieve the optimal error-performance. However, its complexity increases exponentially with the number of transmit antennas and the number of bits per modulated symbol, which is prohibitive in practice. Therefore, many suboptimal but simpler methods are considered for signal detection.

The first class of suboptimal methods is linear detection, including zero-forcing (ZF) and minimum mean-squared error (MMSE). An advantage of ZF is low-complexity. However, this detection method suffers from an issue of noise enhancement, which reduces error-performance. Meanwhile, MMSE offers better performance than ZF at the cost of the required information of SNR. Besides linear detectors, nonlinear detectors, e.g., SIC (successive interference cancellation) or PIC (parallel interference cancellation), are considered for spatial multiplexing MIMO systems. For example, the V-BLAST scheme proposed in [26] used an ordered SIC detector. In addition, sphere decoding [27] and lattice-reduction [28] were proposed for MIMO detection. These two methods can achieve near-optimal performance at the cost of higher complexity compared to linear detection.

2.1.3.3 Beamforming

In addition to achieving higher data rates and better error-performance, MIMO can be used to improve the received SNR or to suppress co-channel interference (CCI) in a multiuser scenario, thereby improving SINR (signal-to-interference-plus-noise ratio) at the receiver. This kind of MIMO schemes is referred to as beamforming MIMO [29]. Also, the achieved gain in terms of SNR or SINR is called *array gain* in the literature.

In beamforming techniques, the beam patterns of transmit and/or receive antenna array can be steered in the desired directions while being suppressed at undesired

directions. To achieve this, a beamformer controls the phases and/or amplitudes of the signals at all antenna elements. Unlike space-time codes or spatial multiplexing, in beamforming techniques, channel state information is required to achieve array gain. Readers are referred to [4], [29] for details about beamforming techniques.

2.1.3.4 Hybrid MIMO Techniques

The three types of MIMO schemes described above are designed to achieve diversity gain, multiplexing gain, and array gain separately. There exist some MIMO schemes that aim to realize a combination of the different gains in the literature. These MIMO schemes are known as hybrid MIMO or multifunctional MIMO schemes [30]. For example, a hybrid scheme of beamforming and space-time codes was proposed in [31]. Also, a combination of the Alamouti code and spatial multiplexing, namely double space-time transmit diversity (DSTTD), was introduced in [32]. This DSTTD scheme could offer diversity gain (resulting from the Alamouti structure) and multiplexing gain as data streams are multiplexed in the spatial domain. It is worth mentioning here that, for a given MIMO scheme, both diversity and multiplexing gains can be obtained simultaneously. However, there exists a fundamental trade-off between them as analysed in [33]. This trade-off has become a powerful tool for designing, evaluating and comparing MIMO schemes since its introduction.

2.2 MIMO-OFDM Systems

MIMO systems over flat fading channels have been presented in Section 2.1. In this section, MIMO systems are considered for frequency-selective fading channels. In particular, orthogonal frequency division multiplexing (OFDM) and its related issues are first introduced. Then, a mathematical model for a MIMO-OFDM system is described. Finally, capacity in MIMO-OFDM systems is discussed.

2.2.1 OFDM Technique

OFDM is a kind of multi-carrier transmission techniques where a high-rate data stream is split into a set of low-rate sub-streams. Each sub-stream is then modulated by a separate subcarrier. In OFDM, the subcarriers overlap in the frequency-domain, but the subcarrier frequencies are chosen such that the subcarriers are orthogonal to each other. Due to the orthogonality, interference among adjacent subcarriers known as inter-carrier interference (ICI) is eliminated. Moreover, as subcarriers overlap in the frequency-domain, spectral efficiency in OFDM systems is significantly improved. This

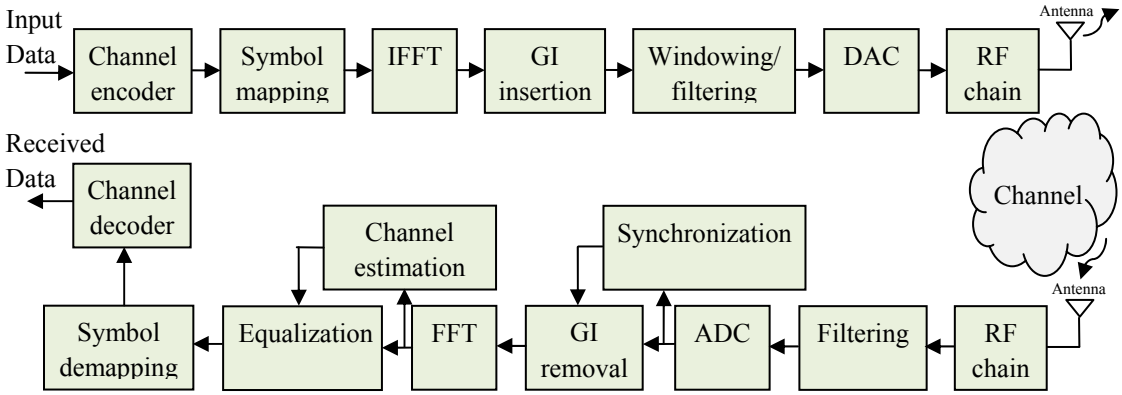

Figure 2.6. Transceiver architecture for an OFDM wireless system.

is one of the most attractive benefits of the OFDM technique. In addition, OFDM converts wideband frequency-selective fading channel into a collection of narrowband flat fading channels. Thus, one-tap equalizers can be used to detect symbols on each subcarrier. In the following, a system architecture for an OFDM system that can be implemented efficiently based on FFT/IFFT (fast Fourier transform) is described.

2.2.1.1 OFDM Transceiver Architecture

A block diagram of an OFDM wireless system is shown in Figure 2.6. The input data bits are first encoded and mapped into a constellation (e.g., *M-ary* quadrature amplitude modulation (*M*-QAM) or *M-ary* phase shift keying (*M*-PSK)). These mapped symbols are then fed into an IFFT (inverse fast Fourier transform) block. Let $\mathbf{x}=[x(0)\ x(1)\ldots x(K-1)]^T$ denote a block of K mapped symbols with a unit-energy. The time-domain complex baseband OFDM signal can be expressed as [34]

$$s(t)=\frac{1}{\sqrt{K}}\sum_{k=0}^{K-1}x(k)e^{j2\pi k\Delta ft},0\le t<KT, \tag{2.16}$$

where T is the sample interval, KT is the data symbol period, and Δf is the subcarrier spacing. In OFDM, subcarriers are chosen to be orthogonal, i.e., $\Delta f=1/KT$. Thus, the time-domain signal samples are obtained as

$$s_n=s(nT)=\frac{1}{\sqrt{K}}\sum_{k=0}^{K-1}x(k)e^{j2\pi kn/K},0\le n<K-1. \tag{2.17}$$

To mitigate the inter-symbol interference (ISI) effects, a guard interval (GI) is appended to the sequences $\{s_n\}$. In multipath fading channels, ISI is induced as the tail of previous symbols overlap with the current symbol. To completely remove ISI, the

length of *GI* should be larger than or equal to the maximum number of multipath taps *L*. Also, as the guard interval wastes transmission resources, the ratio between the guard interval length and the data symbol period is not larger than 1/4 in practical systems. The obtained OFDM symbol is passed through a windowing/filtering block and a DAC block, and then is up-converted to an RF carrier frequency before being transmitted via a transmit antenna.

At the receiver, the pass-band OFDM signal is received and down-converted to its equivalent baseband signal. Due to the guard interval, the discrete linear convolution of the transmitted samples and the channel impulse response becomes a circular convolution. Therefore, the received samples after FFT can be expressed as

$$z(k) = \sqrt{P_t} h(k) x(k) + n(k), 0 \le n < K - 1, \tag{2.18}$$

where P_t is the transmit power, $h(k)$ and $n(k)$ are the fading coefficient and AWGN noise at the k^{th} subcarrier. It can be seen from Eq. (2.18) that a low-complexity one-tap equalizer can be used to detect OFDM signals.

OFDM has been adopted in many current and future wireless systems, including digital broadcasting (i.e., digital audio broadcasting (DAB), terrestrial digital video broadcasting (DVB-T)), worldwide interoperability for microwave access (WiMax IEEE 802.16e), wireless local area network (WLAN IEEE 802.11a/g/n/ac), wireless personal area network WPAN (e.g., multiband OFDM ultra-wideband IEEE 802.15.3a), and cellular networks (i.e., LTE/LTE-Advanced). System parameters of some OFDM-based wireless standards are provided in Table 2.1.

2.2.1.2 Peak-to-Average Power Ratio (PAPR)

Besides the aforementioned advantages, OFDM itself has some disadvantages. One of the challenging issues for OFDM is the high peak-to-average power ratio (PAPR) of time-domain OFDM signals. Here, the PAPR value is defined as the ratio between the peak power and the average power, i.e., [35]

$$PAPR = \frac{\max |s(t)|^2}{\varepsilon\{|s(t)|^2\}}. \tag{2.19}$$

An occurrence of high PAPR results in deleterious effects on the efficacy of OFDM systems. First, when PAPR is large, the amplitude of an OFDM signal varies significantly. If the peak power of an OFDM signal is limited by regulation, the average

Table 2.1. System parameters of some wireless standards using OFDM [34, 36].

	DAB	DVB-T	WLAN (802.11a/g)	WiMAX (802.16e)	UWB (802.15.3a)	3GPP-LTE
Carrier frequency (GHz)	**<3**	**0.4 - 0.8**	**2.5; 5.8**	**2 - 11**	**3.1 - 10.6**	**2**
Bandwidth (MHz)	**1.5**	**8**	**20**	**28**	**500**	**20**
Sample Frequency (MHz)	**2**	**9.14**	**20**	**32.67**	**528**	**30.72**
FFT size	**256**	**2048**	**64**	**256**	**128**	**2048**
Number of Subcarriers Used	**192**	**1705**	**52**	**200**	**122**	**1201**
Subcarrier Spacing (KHz)	**8**	**4.464**	**312.5**	**125**	**4125**	**15**
FFT Period (μs)	**125**	**224**	**3.2**	**8**	**0.24242**	**66.7**
Guard Interval (μs)	**31**	**7**	**0.8**	**0.25**	**0.07008**	**16.67**
Modulation	**DQPSK[(1)]**	**QPSK/ 16-QAM/ 64-QAM**	**BPSK/QPSK/ 16-QAM/ 64-QAM**	**BPSK/QPSK/ 16-QAM/ 64-QAM**	**QPSK/ DCM[(2)]/ MDCM[(3)]**	**QPSK/ 16-QAM/ 64-QAM**
Max. Data Rate	**1.8Mbps**	**31.67Mbps**	**54Mbps**	**104.7Mbps**	**1Gbps**	**100Mbps**

[(1)]: Differential quadrature phase shift keying; [(2)]: Dual carrier modulation; [(3)]: Modified DCM.

signal power is reduced significantly, which in turns shortens the transmission range. Second, to prevent out-of-band radiation and error-performance degradation due to inter-modulation among subcarriers, transmit power amplifier must operate in its linear region where the power efficiency is low. When PAPR is high, a large power back-off is required, which reduces the power efficiency of a power amplifier. In addition, when PAPR is large, a DAC converter with a wide dynamic range is required, which increases the implementation cost.

It is obvious that a high PAPR affects the efficacy of the OFDM system. Therefore, numerous techniques have been proposed to reduce the PAPR in the literature. These techniques include clipping and filtering, coding schemes, nonlinear companding transform, tone reservation, tone injection, active constellation extension, and multiple signal representation methods such as partial transmit sequence (PTS) and selected mapping (SLM) [35]. In essence, these techniques reduce PAPR at the cost of loss in data rate, increase on transmit power, degradation in error-rate performance, or increased implementation complexity. Also, each specific PAPR technique can achieve a different trade-off among those factors. Thus, the choice of PAPR technique depends

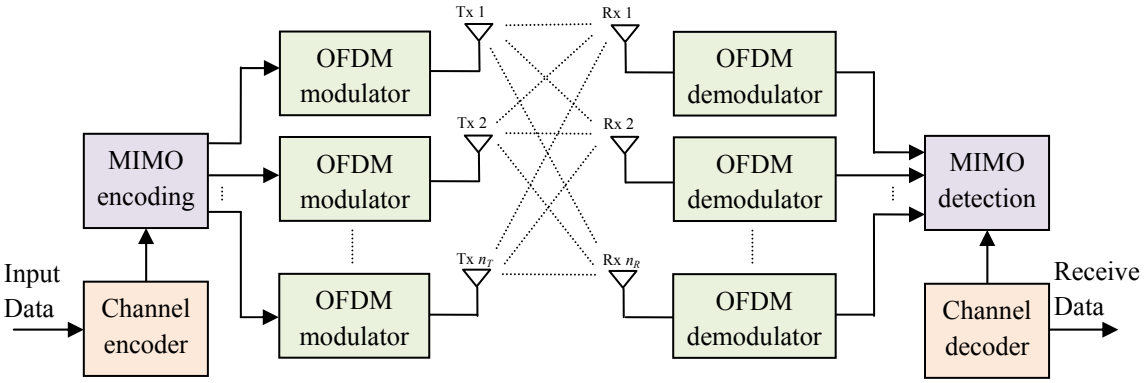

Figure 2.7. Block diagram of a MIMO-OFDM system.

on particular system requirements. Readers are referred to [35] and the references therein for more details.

2.2.2 MIMO-OFDM System Model

In this section, a system model for MIMO-OFDM over frequency-selective fading channels is considered. A block diagram of a MIMO-OFDM system with n_T transmit antennas and n_R receive antennas is shown in Figure 2.7. The baseband sampled channel impulse response between the i^{th} transmit antenna and the j^{th} receive antenna is given as $g_{j,i}(l)$, $l = 0,1,...,L\text{-}1$, where L is the maximum number of multipath taps among all transmit-receive links. Similar to SISO-OFDM systems, the received signal in the MIMO-OFDM system that is corresponding to the j^{th} receive antenna and the k^{th} subcarrier is obtained as

$$y_j(k) = \sqrt{\frac{P_t}{n_T}} \sum_{i=1}^{n_T} h_{j,i}(k) x_i(k) + n_j(k), \; j = 1,2,...,n_R, \tag{2.20}$$

where $x_i(k)$ is the transmit symbol associated with the i^{th} transmit antenna and the k^{th} subcarrier, $h_{j,i}(k)$ is the channel gain between the i^{th} transmit antenna and the j^{th} receive antenna on the k^{th} subcarrier, and $n_j(k)$ is the noise at the j^{th} receive antenna corresponding to the k^{th} subcarrier. Note that the channel gain $h_{j,i}(k)$ can be computed via the channel impulse response $g_{j,i}(l)$ as

$$h_{j,i}(k) = \sum_{l=0}^{L-1} g_{j,i}(l) e^{-\frac{j2\pi lk}{K}}, \; k = 0,1,...,K-1. \tag{2.21}$$

Note that Eq. (2.20) can be expressed in a matrix form as

$$\mathbf{y}(k) = \sqrt{\frac{P_t}{n_T}}\mathbf{H}(k)\mathbf{x}(k) + \mathbf{n}(k), \tag{2.22}$$

where $\mathbf{y}(k)=[y_1(k)\ y_2(k)\ldots y_{n_R}(k)]^T$, $\mathbf{x}(k)=[x_1(k)\ x_2(k)\ldots x_{n_T}(k)]^T$, $\mathbf{n}(k)=[n_1(k)\ n_2(k)\ldots n_{n_R}(k)]^T$, and $\mathbf{H}(k)$ is the $n_R \times n_T$ channel matrix whose the $(j,i)^{\text{th}}$ entry is $h_{j,i}(k)$ calculated in Eq. (2.21). Also, the overall input-output relation in the MIMO-OFDM system can be concisely expressed as [14]

$$\mathbf{y} = \sqrt{\frac{P_t}{n_T}}\mathbf{H}\mathbf{x} + \mathbf{n}, \tag{2.23}$$

where the composite channel $\mathbf{H}$ is a $n_R K \times n_T K$ block diagonal vector whose the block elements are $\mathbf{H}(k), k = 0,1,..., K-1$, $\mathbf{y} = [\mathbf{y}^T(0)\ \mathbf{y}^T(1)\ ...\ \mathbf{y}^T(K-1)]^T$ is the $n_R K \times 1$ receive signal vector, $\mathbf{x} = [\mathbf{x}^T(0)\ \mathbf{x}^T(1)\ ...\ \mathbf{x}^T(K-1)]^T$ is the $n_T K \times 1$ transmit signal vector, and $\mathbf{n} = [\mathbf{n}^T(0)\ \mathbf{n}^T(1)\ ...\ \mathbf{n}^T(K-1)]^T$ is the $n_R K \times 1$ noise vector.

It is also worth mentioning that space-time codes were originally designed in flat-fading MIMO channels. In MIMO-OFDM systems, there exists the additional frequency diversity of frequency-selective fading channels. Therefore, MIMO encoding strategies in MIMO-OFDM systems can be either space-time, space-frequency, or space-time-frequency approach [2]. In other words, information symbols can be jointly mapped into transmit antennas (i.e., space domain), subcarriers (i.e., frequency domain), and subsequent OFDM symbols (i.e., time domain). Theoretically, the maximum achievable diversity order is $n_T \times n_R \times \min(L, K)$, where L is the number of resolvable propagation paths and K is the FFT size [37, 38]. Guidelines for the design of full-diversity space-frequency codes and full-diversity space-time-frequency codes can be found in [39] and [37], respectively.

With respect to channel estimation in MIMO-OFDM systems, time and frequency correlation of the channel parameters can be exploited for the estimation process, which is similar to SISO-OFDM systems. Note that in MIMO-OFDM systems a channel matrix of size $n_R \times n_T$ needs to be estimated, instead of the scalar as in SISO-OFDM systems. The channel estimation can be performed based on space-time pilot insertion [40] or space-frequency insertion [41]. This thesis assumes that the channel state

information is available. Readers are referred to, e.g., [2, 40-42], for more details about channel estimation in MIMO-OFDM systems.

2.2.3 Capacity of MIMO-OFDM Systems

The capacity of MIMO systems over flat fading channels has been considered in Section 2.1.2. In MIMO-OFDM systems over frequency-selective fading channels, capacity can be calculated in a similar manner. In particular, the capacity of MIMO-OFDM system is given by [14] (cf. Eq. (2.5))

$$C_{MIMO-OFDM} = \frac{1}{K} \max_{\mathrm{tr}\{\mathbf{R}_{\mathrm{xx}}\}=n_T K} \log_2 \det\left(\mathbf{I}_{n_R K} + \frac{\rho}{n_T} \mathbf{H} \mathbf{R}_{\mathrm{xx}} \mathbf{H}^H \right) \text{ (bits/s/Hz)}, \tag{2.24}$$

where $\mathbf{R}_{\mathrm{xx}} = \varepsilon\{\mathbf{x}\mathbf{x}^H\}$ is the covariance matrix of $\mathbf{x}$. Note that the total transmit power across antennas is constrained to P_t, i.e., $\mathrm{tr}\{\mathbf{R}_{\mathrm{xx}}\} = n_T K$.

❖ **Channel is unknown to the transmitter**

When the channel state information is not available at the transmitter, the transmit power is allocated equally across antennas and subcarriers, i.e., $\mathbf{R}_{\mathrm{xx}} = \mathbf{I}_{n_T K}$. Therefore, the capacity now becomes (cf. Eq. (2.6))

$$C_{MIMO-OFDM} = \frac{1}{K} \sum_{k=0}^{K-1} \log_2 \det\left(\mathbf{I}_{n_R} + \frac{\rho}{n_T} \mathbf{H}(k) \mathbf{H}^H(k) \right) \text{ (bits/s/Hz)}. \tag{2.25}$$

It can be seen from Eq. (2.25) that the capacity in MIMO-OFDM systems is equivalent to a summation of the capacities across K subcarriers.

For the case of random channels, ergodic capacity and outage capacity are used to characterize the information rate of MIMO-OFDM systems, which is similar to MIMO systems over flat fading channels. In particular, the ergodic capacity on the MIMO-OFDM system is obtained as

$$C_{MIMO-OFDM} = \varepsilon\left\{ \frac{1}{K} \sum_{k=0}^{K-1} \log_2 \det\left(\mathbf{I}_{n_R} + \frac{\rho}{n_T} \mathbf{H}(k) \mathbf{H}^H(k) \right) \right\} \text{ (bits/s/Hz)}. \tag{2.26}$$

❖ **Channel is known to the transmitter**

When the channel state information is available at the transmitter, MIMO-OFDM systems can optimally allocate the transmit power across antennas (i.e., space domain) and subcarriers (i.e., frequency domain) to maximise the information rate. Similar to the case of flat fading channels, a water-filling algorithm can be employed to accomplished this task as shown in [43]. Let $R(\mathbf{H})$ denote the rank of the matrix $\mathbf{H}$, which implies

that the channel is decomposed into $R(\mathbf{H})$ space-frequency sub-channels. The capacity in MIMO-OFDM system with CSI at the transmitter is obtained as

$$C_{MIMO-OFDM} = \frac{1}{K}\sum_{r=1}^{R(\mathbf{H})} \log_2\left(1+\psi_r \frac{\rho}{n_T}\lambda_r(\mathbf{H}\mathbf{H}^H)\right) \text{ (bits/s/Hz)}, \quad (2.27)$$

where $\lambda_r(\mathbf{H}\mathbf{H}^H), r = 1,2,..., R(\mathbf{H})$, is the r^{th} eigenvalue of $\mathbf{H}\mathbf{H}^H$, ψ_r is the power allocated to the r^{th} space-frequency sub-channel that is chosen based on a water-filling algorithm to satisfy a constraint $\sum_{r=1}^{R(\mathbf{H})}\psi_r = n_T K$. If the channel is random, the ergodic capacity in the MIMO-OFDM system with water-filling power allocation is given by (cf. Eq. (2.15))

$$C_{MIMO-OFDM} = \frac{1}{K}\varepsilon\left\{\sum_{r=1}^{R(\mathbf{H})} \log_2\left(1+\psi_r \frac{\rho}{n_T}\lambda_r(\mathbf{H}\mathbf{H}^H)\right)\right\} \text{ (bits/s/Hz)}. \quad (2.28)$$

2.3 Energy-Efficient Wireless Systems

Energy-efficient communications or green radio refers to a research direction for the evolution of wireless techniques and architectures toward high energy efficiency [44]. This is a large research area that covers all layers of the protocol stack of wireless networks. Specifically, the improvement of energy efficiency could be tackled at the component level (e.g., improve power amplifier efficiency), link level (e.g., discontinuous transmission and sleep modes), or network level (e.g., the layout of networks and their management) [45]. This thesis focuses on investigating energy efficiency in point-to-point antenna selection MIMO-OFDM systems from a physical layer perspective. To this end, some basic concepts on energy efficiency communications that are necessary for the analyses and discussions in the subsequent chapters are presented. Comprehensive surveys about research activities in every aspect of energy efficiency in wireless communications could be found in [45-49].

2.3.1 The Needs of Energy-Efficient Wireless Communications

Recently, energy-efficient system design has received increasing attentions from both industry and academic researchers. This research trend is driven by the following main reasons. The first reason is an increasing amount of energy consumption and carbon footprint associated with the operation of mobile networks. It is reported that Information and Communication Technology (ICT) represents around 2% of the global

carbon emissions, of which mobile networks account for about 0.2 percent [47]. Moreover, this portion is expected to increase rapidly in the near future when a mass deployment of 3G and 4G occurs worldwide (i.e., more mobile subscriptions, more mobile data traffic demands, and more network infrastructure). The pressure of social responsibility requires network operators to take an action to reduce energy consumption.

The second reason comes from an economic perspective. In fact, it has been shown that electricity bills account for about 18-32% of the operation expenditure (OpEx) in cellular networks [49]. Also, the radio access part consumes up to 70% of the total energy consumption, of which power amplifiers (PA) account for about 50%–80% [45]. From network operators' perspective, it is clear that improving energy efficiency, especially in the radio access technologies, has significant economic benefits.

In addition to the ecological and economic perspectives, energy-efficient communications is essential from a viewpoint of mobile users' experience [49]. This is because the battery life of mobile devices is limited for emerging energy-hungry applications, such as video games, mobile TV and video sharing. Thus, besides a need of the development of battery technology, energy-efficient system designs may partially tackle this issue.

2.3.2 Power Consumption Model

In order to quantify the energy efficiency of a wireless system, a power consumption model that describes how much power is consumed is required. Thus, a proper power consumption model is of importance for an analysis of energy efficiency. In this thesis, a popular power consumption model, known as the *component power model*, developed by Cui *et al*. [50] is considered. In this model, the total power consumption of a system is the sum of power consumption by its components (i.e., signal processing blocks). Note that this model is for a generic wireless transceiver. Some modifications may be needed for specific systems. For instance, the power consumption model for cellular base stations could be found in [51].

Let us first consider a signal path from a transmitter to a receiver in a generic wireless system as shown in Figure 2.8. At the transmitter, the baseband signal is first converted to an analog signal by the digital-to-analog converter (DAC), then filtered by the low-pass filter and up-converted by the mixer that is driven by the local oscillator

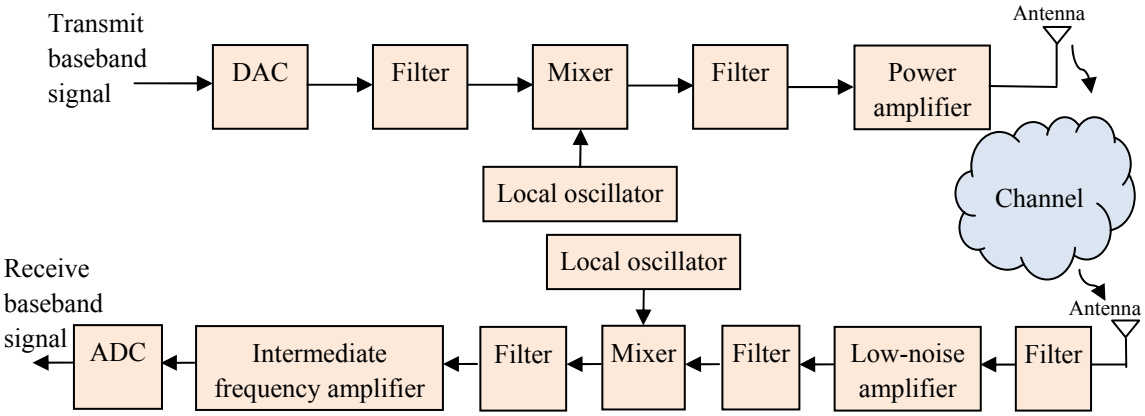

Figure 2.8. Transceiver circuit block in a SISO wireless system.

(LO). The resultant signal is filtered again, and amplified by the high power amplifier (PA) before being transmitted via the antenna. At the receiver, the RF signal is first filtered by the band-pass filter and then amplified by the low-noise power amplifier (LNA). Next, the obtained signal is filtered, down-converted by the mixer, and filtered again before going through the intermediate frequency amplifier (IFA). The resultant signal is finally converted to a digital signal by the analog-to-digital converter (ADC).

To measure the total power consumption, all signal processing blocks mentioned above need to be included in the model. Thus, the total power consumption can be expressed as [50]

$$P_{total} = P_{PA} + P_{bb} + P_c, \tag{2.29}$$

where P_{PA} is the power consumption of the power amplifier, P_{bb} is the power consumption of baseband signal processing blocks at both transmitter and receiver (e.g., channel coding and digital modulation), and P_c is the power consumption of all other circuit blocks, i.e.,

$$P_c = (P_{DAC} + P_{mix} + P_{filt} + P_{syn}) + (P_{LNA} + P_{filr} + P_{mix} + P_{syn} + P_{IFA} + P_{ADC}), \tag{2.30}$$

where P_{DAC}, P_{mix}, P_{filt}, P_{syn}, P_{LNA}, P_{IFA}, P_{filr}, and P_{ADC} are the power consumption values of the DAC, the mixer, the filters at the transmitter side, the frequency synthesizer, the LNA, the IFA, the filters at the receiver side, and the ADC, respectively. Note that the power consumption values in Eq. (2.30) can be estimated using the model introduced in [52]. In addition, the power consumption of power amplifier P_{PA} consisting of the actual transmit power P_t and a wasteful power consumed by the PA can be calculated as [53]

$$P_{PA} = P_t / \eta, \tag{2.31}$$

where η is the power efficiency of a power amplifier.

In MIMO systems, the numbers of signal processing blocks at the transmitter and the receiver increase proportionally with the number of transmit and receive RF chains, excepting the LO that can be shared among RF chains. Thus, a power consumption model in a MIMO system with n_T active transmit RF chains and n_R active receive RF chains is obtained as

$$P_{total} = n_{on}(P_{PA} + P_{ctx}) + n_R P_{crx} + P_{bb}, \tag{2.32}$$

where $P_{ctx} = P_{DAC} + P_{mix} + P_{filt} + P_{syn}/n_T$ is the circuit power consumption per transmit branch excluding both the PA power consumption and the baseband processing power consumption at the transmitter, and $P_{crx} = P_{LNA} + P_{filr} + P_{mix} + P_{syn}/n_R + P_{IFA} + P_{ADC}$ is the circuit power consumption per receive branch excluding the baseband power consumption at the receiver. Here, the frequency synthesizer (LO) is assumed to be shared among the antenna paths.

2.3.3 Energy-Efficiency Metric

In general, there are two definitions for energy-efficiency metric in the literature, namely *energy consumption per bit* and *bit-per-Joule*. These metrics are described in detail below.

❖ ***Bit-per-Joule metric***

One of the most popular energy efficiency metrics is bit-per-Joule. This metric is defined as the ratio between the channel capacity and the corresponding total power consumption, i.e., [54]

$$EE = C / P_{total}, \tag{2.33}$$

where C (bits/s) is the channel capacity and P_{total} is the total power consumption discussed in Section 2.3.2. Recall that the channel capacity C of MIMO and MIMO-OFDM systems have been analysed in previous sections.

❖ ***Energy consumption per bit metric***

In addition to the bit-per-Joule metric, energy-efficiency is often measured in terms of energy consumption per bit. Specifically, this metric calculates the total energy consumption per bit for a given a quality-of-service (QoS) constraint (i.e., a bit-error

rate (BER) requirement). Let R_b denote the bit rate (bps). Then, the total energy consumption per bit can be obtained as [50]

$$E = P_{total} / R_b. \tag{2.34}$$

Note that, given a BER requirement, the actual transmit power P_t (and thus P_{total}) can be computed based on the link budget relationship. In particular, let E_b and P_r denote the required energy per bit and the signal power at the receiver such that the BER requirement is satisfied, respectively. We can express [50]

$$P_t = P_r G_d = E_b R_b G_d, \tag{2.35}$$

where G_d is a factor that represents antenna gain, the path-loss, and noise figure, etc. This factor can be expressed as [52]

$$G_d = G_0 d^{\chi} G_M, \tag{2.36}$$

where G_0 is the factor gain at a unit distance which is defined by antenna gain and carrier frequency, d is a transmission distance, χ is the path-loss exponent, and G_M stands for other parameters such as noise figure and the link margin compensating the variations of hardware process.

Note that it is common in the literature to evaluate a trade-off between energy efficiency (EE) and spectral efficiency (SE) when investigate energy efficiency in wireless systems. This is mainly because EE (bits/Joule or energy consumption per bit) and SE (bits/s/Hz) sometimes conflict with each other. Thus, achieving a balance between these metrics is important from a system-design perspective. Some studies analysed a EE-SE trade-off in MIMO systems in the literature, e.g., [55]. In the subsequent chapters of this thesis, an EE-SE trade-off is considered when evaluating the efficacy of the proposed antenna selection methods for MIMO-OFDM systems.

2.4 Antenna Selection for MIMO-OFDM Wireless Systems

In this section, antenna selection MIMO techniques are introduced. At first, several important aspects in antenna selection MIMO systems, including antenna selection criteria and algorithms, antenna selection training, and the efficacy in terms of capacity and error- performance, are described. Then, the state-of-the-art of antenna selection in single-carrier and multi-carrier systems is reviewed.

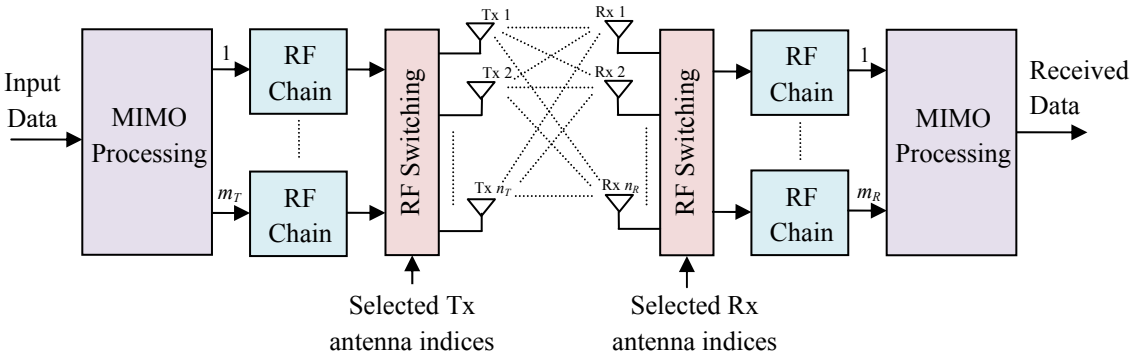

Figure 2.9. Block diagram of an antenna selection MIMO wireless system.

2.4.1 Antenna Selection

As discussed in Section 2.1, MIMO systems can significantly increase system capacity and/or improve link reliability. However, the deployment of multiple antennas incurs a problem of hardware complexity. In fact, while antenna elements are cheap, multiple RF chains associated with antennas introduce high complexity, large power consumption, and increased cost. To overcome these disadvantages, antenna selection is proposed in the literature. In antenna selection, a subset of the best antennas among the available antennas is selected for transmissions, thereby reducing the required number of RF chains.

2.4.1.1 Antenna Selection Criteria and Algorithms

Let us consider an antenna selection MIMO system with n_T transmit antennas and n_R receive antennas as shown in Figure 2.9. The numbers of RF chains at the transmitter and receiver are m_T ($1 \le m_T < n_T$) and m_R ($1 \le m_R < n_R$), respectively. At any channel realization, only m_T out of n_T transmit antennas and m_R out of n_R receive antennas are selected based on a given selection criterion. The received signal can be expressed as (cf. Eq. (2.1))

$$\underline{\mathbf{y}} = \sqrt{\frac{P_t}{m_T}}\underline{\mathbf{H}}\underline{\mathbf{x}} + \underline{\mathbf{n}}, \tag{2.37}$$

where $\underline{\mathbf{x}}$ is a $m_T \times 1$ transmitted signal vector, $\underline{\mathbf{y}}$ is a $m_R \times 1$ received signal vector, $\underline{\mathbf{H}}$ is a $m_R \times m_T$ channel matrix associated with the selected antennas, and $\underline{\mathbf{n}}$ is a $m_R \times 1$ noise vector associated with the selected receive antennas. Note that if the i^{th} ($1 \le i \le n_T$) transmit antenna is chosen, the i^{th} column of $\mathbf{H}$ is selected to form the selected channel matrix $\underline{\mathbf{H}}$. Likewise, the j^{th} receive antenna is corresponding to the j^{th} row of $\mathbf{H}$.

Several criteria can be used for a selection of the best antennas in antenna selection systems, including maximum capacity, maximum post-processing SNR, and minimum mean-squared error.

- *Maximum capacity* [56]: In this criterion, antennas are selected such that the system capacity is maximised. Assume that the channel is unknown to the transmitter, computing the instantaneous capacity $C_{\underline{\mathbf{H}}}$ for every channel matrix $\underline{\mathbf{H}}$, where (cf. Eq. (2.6))

$$C_{\underline{\mathbf{H}}} = \log_2 \det\left(\mathbf{I}_{m_R} + \frac{\rho}{m_T} \underline{\mathbf{H}} \underline{\mathbf{H}}^H \right). \tag{2.38}$$

  The subsets of transmit and receive antennas that attain the largest $C_{\underline{\mathbf{H}}}$ are selected for transmissions.

- *Maximum post-processing SNR* [56]: Let us consider a ZF receiver for simplicity. For every channel matrix $\underline{\mathbf{H}}$, the system computes the minimum post-processing SNR defined as

$$SNR_{\underline{\mathbf{H}}}^{\min} = \min_{i=1,2,\ldots,m_T} \frac{\rho}{m_T [\underline{\mathbf{H}} \underline{\mathbf{H}}^H]_{i,i}^{-1}}, \tag{2.39}$$

  where $[\mathbf{A}]_{i,i}$ denotes the i^{th} diagonal element of the matrix $\mathbf{A}$. The subsets of transmit and receive antennas that achieve the largest $SNR_{\underline{\mathbf{H}}}^{\min}$ are selected.

- *Minimum mean-squared error* (*MSE*) [57]: The optimal antennas are selected by minimising the trace of the error covariance matrix $\mathbf{\Psi}_{\underline{\mathbf{H}}}$. For linear receivers, this matrix is calculated as

$$\mathbf{\Psi}_{\underline{\mathbf{H}}} = \varepsilon\{(\tilde{\mathbf{x}} - \mathbf{x})(\tilde{\mathbf{x}} - \mathbf{x})^H\} = \sigma_n^2 (\underline{\mathbf{H}}^H \underline{\mathbf{H}} + \delta(m_T / \rho)\mathbf{I}_{m_T})^{-1}, \tag{2.40}$$

  where $\delta = 0$ for a ZF receiver and $\delta = 1$ for a MMSE receiver.

The optimal antennas based on the above selection criteria can be obtained by exhaustively searching over all possible antenna subsets. The numbers of subsets in transmit and receive antenna selection systems are $C_{m_T}^{n_T}$ and $C_{m_R}^{n_R}$, respectively. For a joint transmit/receive antenna selection system, the number of subsets is $C_{m_T}^{n_T} \times C_{m_R}^{n_R}$. Note that the complexity of the brute-force search approach can be prohibitive when the numbers of transmit/receive antennas are large. Therefore, several suboptimal algorithms that require much lower complexity were proposed, such as fast incremental

successive selection algorithm [58], decremental algorithms [59], and joint transmit/receive antenna selection algorithm [60]. In addition to greedy algorithms, an optimisation approach was also employed to solve a selection problem in antenna selection systems [61, 62]. This approach could achieve a near-optimal performance with a lower complexity compared to the exhaustive search method.

2.4.1.2 Training in Antenna Selection Systems

In antenna selection systems, to select the best antennas for a given selection criterion, all possible $n_T \times n_R$ links between transmit antennas and receive antennas need to be sounded. As there are only m_T ($m_T < n_T$) transmit RF chains and m_R ($m_R < n_R$) receive RF chains, a sounding process can be accomplished by RF switching [63, 64]. Let us assume that $\Theta_T = n_T / m_T$ and $\Theta_R = n_R / m_R$ are integers for simplicity. The available transmit and receive antennas can be divided into Θ_T and Θ_R disjoint subsets, respectively. During a sounding period, the transmit and receive RF chains are connected to each pair of transmit/receive antenna subsets. The CSI of the associated $m_T \times m_R$ links is obtained by means of a training sequence. Then, the RF chains are switched to another pair of subsets via RF switches. After $\Theta_T \times \Theta_R$ repetitions, all the links have been sounded.

With respect to RF switches, there are generally two switching technologies, namely solid-state RF switches and micro-electro-mechanical systems (MEMS)-based switches [65]. The solid-state RF technologies (i.e., positive-intrinsic-negative (PIN) diodes and field-effect transistors-FET) can achieve a very fast switching speed. However, an insertion loss is quite high (larger than 1 dB). Meanwhile, the MEMS technology has very low insertion loss and a slower switching speed. Therefore, the choice of RF switches depends on particular system requirements. Readers are referred to [65] for more details about RF switching technologies.

2.4.1.3 Efficacy of Antenna Selection Systems

As mentioned earlier, the number of RF chains in antenna selection systems is smaller than the number of available antennas, thereby reducing the hardware complexity. Besides, antenna selection requires a small fraction of the full channel state information. This means that the number of feedback bits in transmit antenna selection systems operating in a frequency-division duplex (FDD) mode is significantly reduced.

Interestingly, antenna selection systems can attain several benefits of full MIMO systems. The efficacy in terms of capacity and error-performance of antenna selection is discussed in detailed below.

❖ *Capacity*: Capacity in spatial multiplexing based antenna selection systems is investigated in several works, e.g., [66, 67]. In a receive antenna selection system with the capacity maximisation criterion, the instantaneous capacity is obtained as (cf. Eq. (2.6))

$$C_{AS} = \max_{S(\underline{\mathbf{H}})} \log_2 \det\left(\mathbf{I}_{m_R} + \frac{\rho}{n_T} \underline{\mathbf{H}} \underline{\mathbf{H}}^H \right). \tag{2.41}$$

where $S(\underline{\mathbf{H}})$ denotes the set of all possible channel matrix $\underline{\mathbf{H}}$. An upper bound for the capacity over i.i.d. fading channels was derived as [66]

$$C_{bound} \le \sum_{j=1}^{m_R} \log_2\left(1 + \frac{\rho}{n_T} \lambda_j \right), \tag{2.42}$$

where λ_j is the squared norm of the ordered j^{th} row of $\mathbf{H}$. This bound is quite tight for $m_R \le n_T$. Also, it is shown that antenna selection preserves most of the capacity promised by MIMO systems provided that the number of selected antennas on one end is not smaller than the antennas on the other end.

❖ *Error-performance*: Many studies have investigated the performance of antenna selection MIMO systems, e.g., [68-71]. These works consider MIMO systems with OSTBC codes and maximum SNR -based antenna selection, in which antenna selection can be implemented at the transmitter and/or the receiver. The error performance of the MIMO systems is analysed by deriving either upper bound of the pairwise error probability (PEP) (e.g., in [68, 69]) or the upper bound of the BER performance (e.g., in [70, 71]). It is shown that antenna selection retains the diversity order compared to the full MIMO system. Also, the reduction in SNR due to antenna selection is upper bounded by $10\log_{10}(m_R/n_R)$ dB. For example, in a MIMO system with OSTBC at the transmitter and antenna selection at the receiver, the BER can be approximated as [71]

$$P_e \approx C_{n_T n_R}^{2n_T n_R - 1} \times \left(4 \frac{m_R}{n_R} \gamma \right)^{-n_T n_R}. \tag{2.43}$$

It is clear from Eq. (2.43) that the achieved diversity order is $n_T n_R$, which is equal to that in a full MIMO system.

The effectiveness of antenna selection systems under imperfect scenarios (e.g., channel estimation error or spatial correlation) is also considered in the literature. In particular, it is shown in [9] that channel estimation errors do not decrease the capacity significantly as long as the SNR of the pilot signals is not smaller than the SNR during the actual data transmission. Also, based on an analysis of the pairwise error probability, it is shown in [72] that the diversity order in space-time coding systems with joint transmit-receive antenna selection is not reduced in the presence of imperfect channel estimation. In addition, in antenna selection systems with closely spaced antennas, it is necessary to maintain the spacing between antenna elements no less than a half of wavelength to guarantee the efficacy of antenna selection schemes [73].

2.4.1.4 Current Research on Antenna Selection for Energy-Efficient Single-Carrier Systems

Antenna selection is traditionally considered for improved capacity and/or error-performance. Recently, some research works have investigated energy efficiency in antenna selection single-carrier (i.e., narrowband) systems [74-78]. The aim of these works is to select antennas such that the energy efficiency (bits/Joule) as defined in Eq. (2.33) is improved. In [74], the authors jointly optimise the transmit power and the number of active antennas to maximise energy efficiency. The optimal solution is obtained by either exhaustive search or (suboptimal) greedy algorithms with low-complexity. This work examines single data stream MIMO systems, while energy-efficiency in multi-stream antenna selection MIMO single-carrier systems is studied in [75, 76]. In general, these works focus on designing low-complexity algorithms for antenna selection to improve energy efficiency. In [77], a trade-off between energy-efficiency (EE) and spectral efficiency (SE) in the context of antenna selection systems is investigated. It is shown that antenna selection can achieve a better EE-SE trade-off performance than spatial multiplexing and MRT MIMO schemes. In addition, antenna selection in systems with a large number of equipped antennas has been recently investigated in [78]. The obtained results show that antenna selection is a good choice for improved energy efficiency in large-scale MIMO systems. As a concluding remark for this subsection, antenna selection has been shown to be promising from an energy-efficiency perspective. However, all of these works only consider narrowband systems.

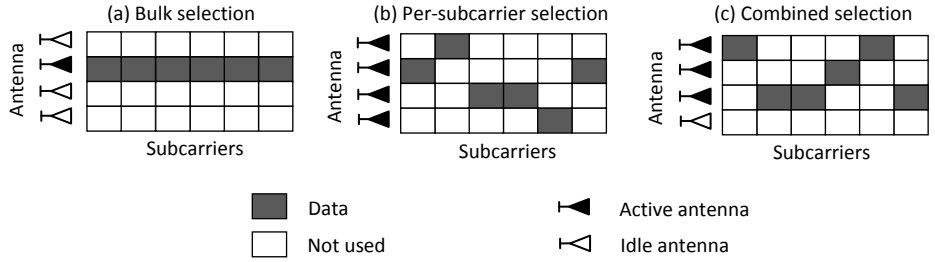

Figure 2.10. Illustrations of the existing antenna selection methods ($n_T = 4$ and $K = 6$).

2.4.2 Antenna Selection for OFDM Systems

In this subsection, a literature review of antenna selection MIMO-OFDM systems is provided. In general, there are three approaches for the deployment of antenna selection in OFDM systems in the literature, namely, bulk selection (i.e., choosing the same antennas for all subcarriers) [79-82], per-subcarrier selection (i.e., selecting antennas independently for each subcarrier) [79, 83-85], and combined selection (i.e., a combination of bulk selection and per-subcarrier selection) [86, 87]. These selection schemes are illustrated in Figure 2.10.

In bulk selection, only one among n_T available antennas is used to transmit data (see Fig. 2.10.a). The antenna that can attain the largest accumulated cost across subcarriers is selected for all subcarriers within one OFDM symbol, i.e.,

$$\hat{i} = \arg \max_{i=1,\ldots,n_T} \sum_{k=0}^{K-1} c_i(k), \tag{2.44}$$

where $c_i(k)$ denote the cost associated with the selection of the i^{th} antenna on the k^{th} subcarrier. The efficacy in terms of capacity and error-performance of this selection scheme was investigated in [80-82]. The diversity and coding gain analysis of this scheme was also performed in [87].

Unlike bulk selection, in per-subcarrier selection, antennas are selected independently for each subcarrier (see Fig. 2.10.b). Assuming that $n_{RF} = n_T$, the selected antenna associated with the k^{th} subcarrier is determined by

$$\hat{i}_k = \arg \max_{i=1,\ldots,n_T} c_i(k). \tag{2.45}$$

Note that all equipped antennas are active in this selection scheme. Thus, the per-subcarrier selection scheme needs a larger number of RF chains than bulk selection. The main benefit of the per-subcarrier selection scheme over bulk selection is that a larger

capacity and/or better error performance can be achieved by exploiting the frequency-selective nature of the fading channels [79, 87]. In addition, an issue of imbalance allocation of data subcarriers among transmit antennas, which may affect power amplifier, was investigated in [83-85]. However, these works only considered single information data stream systems.

Besides the two above fundamental approaches, a combined bulk selection and per-subcarrier selection scheme was considered in [86] for OFDM systems where only $n_{RF} < n_T$ RF chains are equipped (see Fig.2.10.c). Accordingly, the system first selects a subset of n_{RF} antennas and then performs per-subcarrier selection on this subset, i.e.,

$$\widehat{i}_k = \arg\max_{\phi} \sum_{k=0}^{K-1} \max_{i \in S_\phi} c_i(k), \tag{2.46}$$

where $S_\phi \subset \{1,2,...,n_T\}$ is a subset of n_{RF} antennas and $\phi = 1,2,...,C_{n_{RF}}^{n_T}$. It is shown in [86, 87] that the combined selection scheme can achieve the same diversity order as per-subcarrier selection, while suffering a small loss in coding gain. Also, combined selection offers a much larger coding gain than bulk selection. Thus, the system with combined selection scheme can achieve optimal error-performance in the high-SNR regime relative to that with per-subcarrier selection.

2.5 Open Research Problems and Research Approaches

The literature review in Section 2.4 shows that a study on the efficacy of antenna selection in MIMO-OFDM systems from an energy-efficiency viewpoint remains open. In fact, previous studies only investigated the systems from capacity or error performance perspective. Also, it is worth noting that an extension of studies on energy efficiency in narrowband antenna selection systems to wideband OFDM systems is not straightforward. The main reason is that there are several approaches for OFDM systems as mentioned before. Each selection approach possesses both advantages and disadvantages from an energy-efficiency perspective. Specifically, per-subcarrier selection achieves better capacity than bulk selection and combined selection at a cost of higher power consumption due to the requirement of multiple active RF chains. Such behaviours, which are pertinent in the setting of OFDM systems, are never issues in single-carrier systems. Consequently, aiming to achieve energy-efficient antenna selection MIMO-OFDM systems, this thesis focuses on addressing the following important problems.

1. It is currently still unknown whether the existing antenna selection approaches are optimal in terms of energy efficiency for MIMO-OFDM systems. Motivated by this, Chapter 3 of this thesis analyses energy efficiency in MIMO-OFDM systems with several antenna selection schemes. Moreover, this chapter proposes *an adaptive antenna selection method* that outperforms the existing methods from a viewpoint of energy efficiency.
2. It is well known that power amplifier is a major source of RF power consumption. For example, in mobile networks, power amplifiers (PA) consume up to 50%–80% of overall power at a base station [45]. Thus, increasing power efficiency of power amplifiers is of importance to achieve high energy-efficiency in wireless networks. In MIMO-OFDM systems, achieving high power-efficiency of PA is of concern given that PAPR of OFDM signals are large. Motivated by these, the thesis considers antenna selection MIMO-OFDM systems that take into consideration the impacts of PA. Specifically, *power amplifier -aware antenna selection methods* are proposed to improve energy efficiency in the systems in the presence of nonlinear distortions due to power amplifiers (in Chapter 4) and in the systems with linear scaling (in Chapter 5).
3. Recent studies on energy-efficient single-carrier antenna selection systems considered an energy-efficiency metric as a ratio between the ergodic capacity and the total consumed power. Note that this kind of metric does not take into account many important system parameters, such as channel codes, modulation schemes or detection methods. Therefore, it is very important to investigate energy efficiency that involves these system parameters from a practical viewpoint. Such a study is conducted in Chapter 6 of this thesis. Specifically, Chapter 6 proposes and analyses *a joint transmit power allocation and antenna selection method* to improve energy efficiency in antenna selection MIMO and antenna selection MIMO automatic repeat request (ARQ) systems under quality-of-service (QoS) constraints.

2.6 Summary

In this chapter, overviews of MIMO and OFDM techniques have been presented. A MIMO-OFDM system model that is considered throughout this thesis has been described. Also, metrics used to measure energy efficiency in wireless systems have been discussed. These provide the necessary backgrounds for the rest of the thesis.

Based on a thorough literature review of antenna selection in OFDM systems, open research problems considered in this thesis have been identified and stated. Several methods to solve these problems will be proposed and analysed in the subsequent chapters.

Chapter 3

Adaptive Antenna Selection for Energy-Efficient MIMO-OFDM Wireless Systems

In this chapter, antenna selection strategies for MIMO-OFDM wireless systems are investigated from an energy-efficiency perspective. An adaptive antenna selection method, in which both the number of active radio frequency (RF) chains and the antenna indices are jointly selected, is proposed for improved energy-efficiency. This chapter is organized as follows. In Section 3.1, the related works and motivation are presented. In Section 3.2, an antenna selection MIMO-OFDM system model and an energy-efficiency metric are described. In Section 3.3, energy efficiency in the MIMO-OFDM systems that deploy conventional antenna selection approaches is analysed. In Section 3.4, an adaptive antenna selection method to improve energy efficiency is proposed. In Section 3.5, power loading across subcarriers in antenna selection MIMO-OFDM systems is considered. In Section 3.6, simulation results of the achieved energy efficiency are provided. Finally, Section 3.7 concludes the chapter.

3.1 Introduction

As mentioned in Chapter 2, there are three conventional approaches for the deployment of antenna selection in OFDM systems, namely, bulk selection, per-subcarrier selection, and combined selection. Also, all the existing works on antenna selection OFDM systems only considered the systems from either capacity or error-performance perspective, for example, analysing diversity gain and coding gain [79, 86-88], measuring capacity [80], or evaluating error-performance [81, 84]. From an energy-efficiency perspective, it can be noted that each selection approach possesses both advantages and disadvantages. Specifically, per-subcarrier selection achieves better capacity than bulk selection and combined selection at a cost of higher power consumption due to the requirement of multiple active RF chains. Thus, it is not clear if the existing antenna selection approaches are optimal in terms of energy efficiency.

Motivated by the above open problem, this chapter investigates energy efficiency in MIMO-OFDM systems with several antenna selection schemes. The main contributions of this work are summarized as follows.

i) Energy efficiency in conventional antenna selection MIMO-OFDM systems is analysed for the first time. In particular, closed-form expressions for the energy efficiency and the EE-SE trade-off in these systems are derived. The results show that the conventional antenna selection systems are not effective with respect to energy efficiency.

ii) An adaptive antenna selection approach is proposed to improve energy efficiency in MIMO-OFDM systems. In this method, both the number of active RF chains and the antenna indices are selected to maximise energy efficiency. The proposed adaptive selection scheme is shown to achieve better EE-SE trade-off compared to the existing selection schemes.

iii) A greedy algorithm to implement the proposed adaptive selection method is developed. This algorithm can attain near-optimal energy efficiency while requiring much lower complexity compared to that with the optimal exhaustive search method, which is important when a number of antennas is large.

iv) Efficacy of power loading across subcarriers in several antenna selection MIMO-OFDM systems is evaluated from an energy efficiency perspective. The results reveal that power loading can improve energy efficiency in the low signal-to-noise ratio (SNR) region. Also, its effectiveness depends on particular antenna selection schemes.

v) Impacts of a comparison between the transmit power and the circuit power consumption, types of antenna selection criteria, the number of equipped antennas, and spatial correlation, on the energy efficiency in the conventional and proposed systems are numerically evaluated.

3.2 Antenna Selection MIMO-OFDM System Model

3.2.1 System Model

Let us consider a MIMO-OFDM system with K subcarriers, n_T transmit antennas, and n_R receive antennas. The number of equipped transmit RF chains is n_{RF}, $n_{RF} \leq n_T$. A simplified block diagram of the system is shown in Figure 3.1. At the transmitter, the input data stream is mapped onto a unit-energy M-QAM (M-ary Quadrature Amplitude

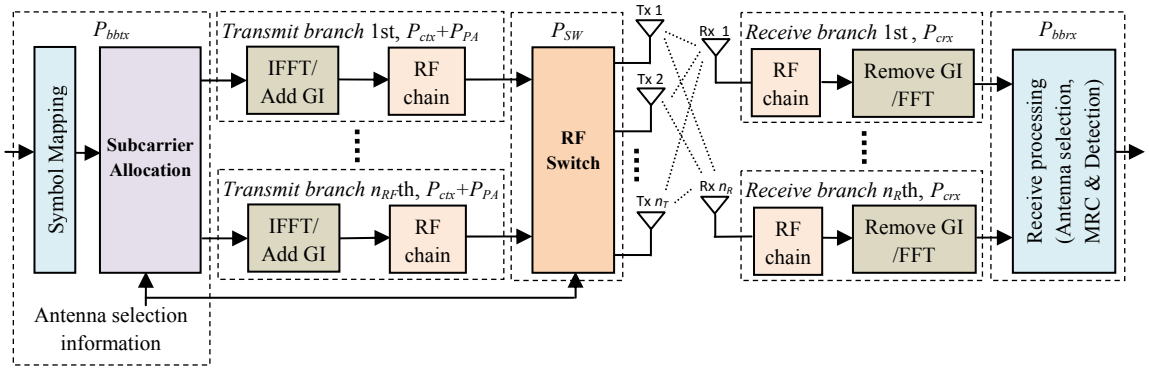

Figure 3.1. A simplified block diagram of an antenna selection MIMO-OFDM wireless system.

Modulation) constellation. The subcarrier allocation block takes in a data frame of $\mathbf{u} = [u(0), u(1),..., u(K-1)],$ and then allocates the data symbol $u(k), 0 \le k \le K-1,$ to the selected antenna, denoted as $\hat{i}_k$, associated with the k^{th} subcarrier. Thus, only one element in a transmit vector $\mathbf{x}(k) = [x_1(k), x_2(k),..., x_{n_T}(k)]^T$ is assigned the data symbol, whereas the others are zero. The output sequences from the subcarrier allocation block are then fed into *K*-point IFFT blocks. Each time-domain OFDM signal is then added with a guard interval (GI) before being transmitted via its corresponding transmit antenna. Note that the transmit branch corresponding to the output of the allocation block that is not allocated any data symbol is turned off to save energy.

At the receiver, the received signal at each antenna is fed into the FFT block after the GI is removed. The received signal in the frequency domain corresponding to the k^{th} subcarrier can be expressed as [2]

$$\mathbf{y}(k) = \sqrt{P_t}\mathbf{H}(k)\mathbf{x}(k) + \mathbf{n}(k) = \sqrt{P_t}\mathbf{h}_{\hat{i}_k}(k)u(k) + \mathbf{n}(k), \tag{3.1}$$

where $\mathbf{H}(k)$ denotes the subchannel matrix associated with the k^{th} subcarrier where its entries are denoted as $h_{j,i}, i = 1,2,..,n_T, j = 1,2,..,n_R,$ $\mathbf{h}_{\hat{i}_k}(k)$ indicates the effective channel vector obtained by selecting the column of $\mathbf{H}(k)$ that is corresponding to the selected transmit antenna $\hat{i}_k$ on the k^{th} subcarrier, and P_t is an equal transmit power allocated to each data symbol. Note that the total transmit power in one OFDM symbol is $P_T = KP_t$. Also, $\mathbf{y}(k) = [y_1(k), y_2(k),..., y_{n_R}(k)]^T$ and $\mathbf{n}(k) = [n_1(k), n_2(k),..., n_{n_R}(k)]^T$, where $y_j(k)$ and $n_j(k)$ denote the received signal and the noise at the j^{th} receive antenna, respectively. Here, the noise is modeled as a Gaussian random variable with

zero-mean and variance σ_n^2. Assume that the receiver uses an MRC (maximum ratio combining) method for signal detection, the detected signal at the k^{th} subcarrier is given as [89]

$$z(k) = \sqrt{P_t}\,\| \mathbf{h}_{\tilde{i}_k}(k) \|^2\, u(k) + \mathbf{h}_{\tilde{i}_k}^H(k)\mathbf{n}(k) = \sqrt{P_t}\, g_{\tilde{i}_k}(k)u(k) + \tilde{n}(k), \tag{3.2}$$

where $g_{\tilde{i}_k}(k) := \| \mathbf{h}_{\tilde{i}_k}(k) \|^2$, and $\tilde{n}(k)$ is the effective noise (after MRC) with variance $g_{\tilde{i}_k}(k)\sigma_n^2$. In this system, the instantaneous post-processing SNR (signal-to-noise ratio) associated with the i^{th} transmit antenna and the k^{th} subcarrier can be calculated as [4]

$$\rho_i(k) = \frac{P_t\left(g_i(k)\right)^2}{g_i(k)\sigma_n^2} = \frac{P_t}{\sigma_n^2} g_i(k) := \bar{\rho} g_i(k). \tag{3.3}$$

With respect to an antenna selection operation, many selection criteria can be used in this system, such as maximising SNR, maximising capacity, or minimising bit-error rate [9]. Details about these criteria associated with different antenna selection approaches are presented in Section 3.3.1. In addition, given that this work focuses on analysing energy efficiency achieved in antenna selection MIMO-OFDM systems, the following assumptions are adopted for simplicity.

A1. Channel state information (CSI) is available at both transmitter and receiver in TDD (time-duplex division) mode. Thus, the transmitter and receiver can determine the selected antenna indices by themselves. Note that channel estimation methods for antenna selection OFDM system were well investigated in the literature, e.g., [90, 91]. In addition, several techniques to obtain CSI of all equipped antennas when only a few antennas are active were also considered in [92].

A2. Effects of power imbalance across transmit antennas is not considered. The issue of power imbalance arises when a large number of subcarriers are allocated to some particular antennas, which may cause problems with power amplifiers (i.e., affects system performance). One approach to deal with this issue is allocating the same number of data symbols to each transmit antenna. This can be accomplished by formulating a linear optimisation for subcarrier allocation [84]. The readers are referred to [84] for further details.

3.2.2 Energy-Efficiency Metric in Antenna Selection MIMO-OFDM Systems

To quantify the fundamental limits of the system, we consider energy efficiency (bits/Joule) defined as a ratio between the achievable rate and the total power consumption (cf. Eq. (2.33)), i.e.,

$$EE = \frac{C}{P_{total}}, \tag{3.4}$$

where C denotes the achievable rate per OFDM symbol (bits/s) and P_{total} is the required total power consumption (watts). Let us denote $I_i(k)$ to be the instantaneous capacity (bits/s/Hz) associated with the i^{th} transmit antenna and the k^{th} subcarrier, i.e.,[4]

$$I_i(k) = \log_2\left(1 + \bar{\rho} g_i(k)\right),\ i = 1,2,...,n_T;\ k = 0,1,...,K-1. \tag{3.5}$$

The achievable rate per OFDM symbol in this system is evaluated by [93]

$$C = W\varepsilon_{\mathbf{H}}\left\{\frac{1}{K}\sum_{k=0}^{K-1} I_{\hat{i}_k}(k)\right\}, \tag{3.6}$$

where $\varepsilon_{\mathbf{H}}\{.\}$ denotes an expectation operation over the fading channel distribution, W (Hz) is the system bandwidth, and $\hat{i}_k$ is the selected antenna on the k^{th} subcarrier.

Also, the total power consumption corresponding to one OFDM symbol is given as (cf. Eq. (2.32))

$$P_{total} = n_{on}(P_{PA} + P_{ctx}) + n_R P_{crx} + P_{bb}, \tag{3.7}$$

where n_{on} is the number of active RF chains (i.e., the number of active transmit branches) at the transmitter, P_{PA} is the power consumption by one power amplifier (PA), P_{ctx} is the power consumption per transmit branch (excluding the associated PA), P_{crx} is the power consumption per receive branch, and $P_{bb} = P_{bbtx} + P_{bbrx}$ where P_{bbtx} and P_{bbrx} are the power consumption of several baseband processing units at the transmitter and receiver, respectively. These values are shown clearly in Figure 3.1. Note that as power and insertion losses caused by a RF switch are negligible [11], we do not include it in Eq. (3.7) for simplicity. When there are n_{on} active RF chains, the number of data symbols allocated per transmit antenna is K/n_{on}. Thus, the total transmit power per antenna is $P_t(K/n_{on})$. Assume that the efficiency η of a power amplifier is invariant to the power output level, we can express the power drawn from a DC source P_{PA} as [53]

$$P_{PA} = \frac{P_t(K/n_{on})}{\eta} = \frac{P_T/n_{on}}{\eta}, \tag{3.8}$$

where $P_T = KP_t$ is the actual total transmit power per OFDM symbol. Note that the above assumption of constant efficiency can be realized by using PA with dynamic power supply [94]. Therefore, Eq. (3.7) can be rewritten as

$$P_{total} = P_T/\eta + n_{on}P_{ctx} + n_R P_{crx} + P_{bb}. \tag{3.9}$$

From Eq. (3.4), Eq. (3.6), and Eq. (3.9), we can rewrite the (average) EE metric as

$$EE = \frac{W\varepsilon_{\mathbf{H}}\left\{\frac{1}{K}\sum_{k=0}^{K-1} I_{\hat{i}_k}(k)\right\}}{P_T/\eta + n_{on}P_{ctx} + n_R P_{crx} + P_{bb}}. \tag{3.10}$$

This metric will be used to evaluate energy efficiency in different antenna selection OFDM systems in the next sections.

3.3 Energy Efficiency Analysis of Conventional Antenna Selection Schemes

3.3.1 Conventional Antenna Selection Schemes

As mentioned in Section 3.2.1, several selection criteria can be used for antenna selection schemes. For notational convenience, let $c_i(k)$ denote the cost associated with the selection of the i^{th} antenna on the k^{th} subcarrier. Then, we can express $c_i(k)$ as

$$c_i(k) = \begin{cases} g_i(k) & \text{for maximum channel power gain criterion (i.e., maximum SNR)} \\ I_i(k) & \text{for a maximum capacity criterion} \\ -BER_i(k) & \text{for a miminum error - rate criterion,} \end{cases} \tag{3.11}$$

where $BER_i(k)$ is a bit-error rate, e.g., for a M-QAM modulation with Gray mapping [95]

$$BER_i(k) = \frac{\sqrt{M}-1}{\sqrt{M}\log_2\sqrt{M}} erfc\left(\sqrt{\frac{3\bar{\rho}g_i(k)}{2(M-1)}}\right), \tag{3.12}$$

where $erfc(.)$ denotes a complementary error function. Note that a negative sign is added to $BER_i(k)$ in Eq. (3.11), as we aim to maximise the cost $c_i(k)$ for all cases.

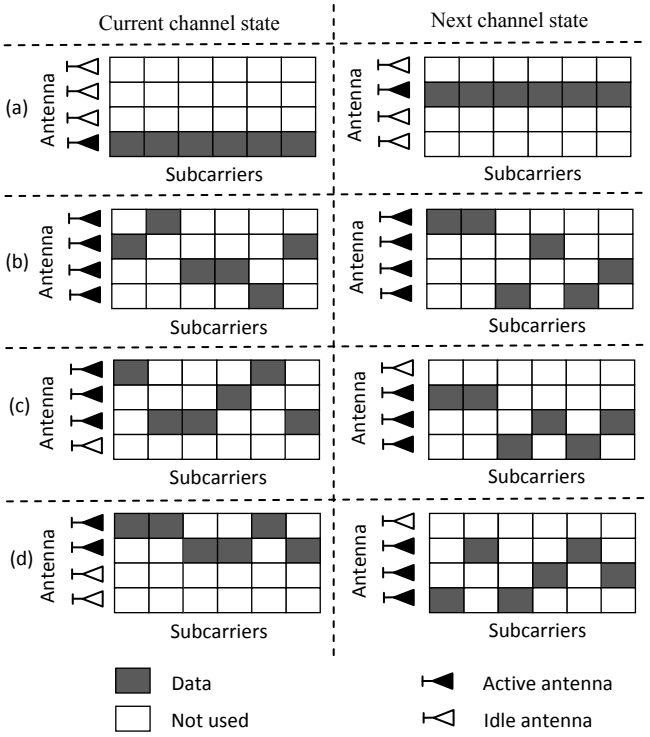

Figure 3.2. Illustrations of antenna selection methods: (a) Bulk selection, (b) Per-subcarrier selection, (c) Combined selection, and (d) Proposed adaptive selection. ($n_T = 4$ and $K = 6$).

As mentioned in Section 2.4.2, there are three conventional antenna selection schemes for OFDM systems, namely per-subcarrier selection, bulk selection, and combined selection (see Figure 3.2). The selected antenna associated with the k^{th} subcarrier in per-subcarrier and bulk selection is determined, respectively, as (cf. Eq. (2.44) and Eq. (2.45))

$$\hat{i}_k = \arg \max_{i=1,\ldots,n_T} c_i(k). \tag{3.13}$$

and

$$\hat{i} = \arg \max_{i=1,\ldots,n_T} \sum_{k=0}^{K-1} c_i(k). \tag{3.14}$$

Note that in per-subcarrier antennas selection with $n_{RF} = n_T$, all equipped antennas are active. Thus, the total power consumption is $P_{total}^{per} = P_T/\eta + n_T P_{ctx} + n_R P_{crx} + P_{bb}$. Meanwhile, in a bulk selection scheme, the total power consumption is $P_{total}^{bulk} = P_T/\eta + P_{ctx} + n_R P_{crx} + P_{bb}$ as only one transmit RF chain is required.

3.3.2 Analysis of Energy Efficiency in the Systems with Conventional Selection Schemes

In this subsection, we derive analytical expressions of energy efficiency in antenna selection OFDM systems with per-subcarrier and bulk selection approaches. For analytical simplicity, we assume that the fading coefficients $h_{j,i}(k)$ are i.i.d. (independent and identically distributed) Rayleigh random variables. This assumption is often adopted to analyse OFDM systems, see e.g., [79, 86-88].

3.3.2.1 Per-Subcarrier Selection Scheme

In an antenna selection OFDM system using a maximum SNR criterion (i.e., maximum channel power gain), assuming that subcarriers are independent, the capacity can be expressed as (cf. Eq. (3.6))

$$C_{per} = W\varepsilon_{\mathbf{H}}\left\{\frac{1}{K}\sum_{k=0}^{K-1} I_{\tilde{i}_k}(k)\right\} = W\varepsilon_{\mathbf{H}}\{\log_2(1+\bar{\rho}g_{\tilde{i}_k}(k))\}, \tag{3.15}$$

which can be evaluated at any subcarrier *k*. Therefore, the energy efficiency is obtained as (cf. Eq. (3.10))

$$EE_{per} = \frac{C_{per}}{P_{total}^{per}} = \frac{W\varepsilon_{\mathbf{H}}\{\log_2(1+\bar{\rho}g_{\tilde{i}_k}(k))\}}{P_T/\eta + n_T P_{ctx} + n_R P_{crx} + P_{bb}}. \tag{3.16}$$

To obtain a closed-form expression of Eq. (3.16), we need to derive an explicit expression for $\varepsilon_{\mathbf{H}}\{\log_2(1+\bar{\rho}g_{\tilde{i}_k}(k))\}$. The final result is stated in the following theorem.

Theorem 3.1 *A closed-form expression of the energy efficiency in per-subcarrier antenna selection OFDM systems is given by*

$$EE_{per} = \frac{W\eta_T}{P_{total}^{per}(n_R-1)!\ln 2}\sum_{u=0}^{n_T-1}\left\{(-1)^u C_u^{n_T-1}\sum_{q=0}^{(n_R-1)u}\left(\alpha_{u,q}\frac{(n_R+q-1)!}{\bar{\rho}^{n_R+q}}e^{(u+1)/\bar{\rho}}\sum_{s=1}^{n_R+q}\left(\frac{u+1}{\bar{\rho}}\right)^{-s}\Gamma\left(-n_R-q+s,\frac{u+1}{\bar{\rho}}\right)\right)\right\}, \tag{3.17}$$

where $C_a^b = b!/a!(b-a)!$ *is the binomial coefficient,* $\alpha_{u,q}$ *denotes the multinomial coefficient, and* $\Gamma(a,x) = \int_x^{+\infty} e^{-t}t^{a-1}dt$ *is the incomplete gamma function.*

Proof: The proof is given in Section 3.A.

3.3.2.2 Bulk Selection Scheme

For a bulk antenna selection, the obtained capacity can be expressed as (cf. Eq. (3.6))

$$C_{bulk} = W\varepsilon_{\mathbf{H}}\left\{\frac{1}{K}\sum_{k=0}^{K-1} I_{\hat{i}}(k)\right\} = W\varepsilon_{\mathbf{H}}\left\{\frac{1}{K}\sum_{k=0}^{K-1}\log_2\left(1+\overline{\rho}g_{\hat{i}}(k)\right)\right\}. \quad (3.18)$$

By using an approximation of $\log_2(1+x) \approx x\log_2 e,$ when x is small, we can express the capacity at a low SNR region as

$$C_{bulk} \approx W(\overline{\rho}\log_2 e)\times\varepsilon_{\mathbf{H}}\left\{\frac{1}{K}\sum_{k=0}^{K-1} g_{\hat{i}}(k)\right\}. \quad (3.19)$$

Consequently, the energy efficiency now becomes (cf. Eq. (3.10))

$$EE_{bulk} = \frac{C_{bulk}}{P_{total}^{bulk}} \approx \frac{W(\overline{\rho}\log_2 e)\times\varepsilon_{\mathbf{H}}\left\{\frac{1}{K}\sum_{k=0}^{K-1} g_{\hat{i}}(k)\right\}}{P_T/\eta + P_{ctx} + n_R P_{crx} + P_{bb}}. \quad (3.20)$$

By calculating the expected value in the numerator of Eq. (3.20), we arrive at the following result.

Theorem 3.2 *The energy efficiency in bulk antenna selection based OFDM systems in the low SNR regime is approximated as*

$$EE_{bulk} \approx \frac{W(\overline{\rho}\log_2 e)n_T}{P_{total}^{bulk}K(n_R K-1)!}\sum_{u=0}^{n_T-1}\left\{(-1)^u C_u^{n_T-1}\sum_{t=0}^{(n_R K-1)u}\beta_{u,t}(n_R K+t)!(u+1)^{-n_R K-t-1}\right\}, \quad (3.21)$$

where $\beta_{u,t}$ *denotes the multinomial coefficient.*

Proof: The proof is given in Section 3.B.

3.3.2.3 Energy Efficiency-Spectral Efficiency Trade-off

In this subsection, we derive closed-from expressions for the EE-SE trade-off in antenna selection MIMO-OFDM systems. Recall that EE (bits/Joule) is defined in Eq. (3.4) as $EE = C/P_{total}$. Also, the spectral efficiency SE (bits/s/Hz) is calculated as $SE = C/W$, where C (bits/s) is the capacity and W (Hz) is the system bandwidth. Thus, the relation between EE and SE can be expressed as

$$EE = \frac{C}{P_{total}} = \frac{W\times SE}{KP_t/\eta + n_{on}P_{ctx} + n_R P_{crx} + P_{bb}} = \frac{W\times SE}{(K/\eta)\times f^{-1}(SE) + n_{on}P_{ctx} + n_R P_{crx} + P_{bb}}, \quad (3.22)$$

where $f^{-1}: SE\in[0,+\infty)\mapsto P_t\in[0,+\infty)$ is the inverse function of SE. In what follows, we consider per-subcarrier and bulk selection schemes at the low SNR region.

In per-subcarrier selection, by using an approximation of $\log_2(1+x) \approx x\log_2 e$, when x is small, we can express the capacity at the low SNR region as (cf. (3.15))

$$C_{per} \approx W(\overline{\rho}\log_2 e)\times \varepsilon_{\mathbf{H}}\{g_{\hat{i}_k}(k)\}. \tag{3.23}$$

By performing similar calculations as in Appendix 3.A, we have

$$\varepsilon_{\mathbf{H}}\{g_{\hat{i}_k}(k)\} = \frac{n_T}{(n_R-1)!}\sum_{u=0}^{n_T-1}\left\{(-1)^u \mathrm{C}_u^{n_T-1}\sum_{q=0}^{(n_R-1)u}\alpha_{u,q}(n_R+q)!(u+1)^{-n_R-q-1}\right\}. \tag{3.24}$$

Thus, Eq. (3.23) can be rewritten as

$$C_{per} \approx W(\overline{\rho}\log_2 e)\times \frac{n_T}{(n_R-1)!}\sum_{u=0}^{n_T-1}\left\{(-1)^u \mathrm{C}_u^{n_T-1}\sum_{q=0}^{(n_R-1)u}\alpha_{u,q}(n_R+q)!(u+1)^{-n_R-q-1}\right\}. \tag{3.25}$$

For notational convenience, let us denote

$$\varphi = \frac{n_T\log_2 e}{(n_R-1)!\sigma_n^2}\sum_{u=0}^{n_T-1}\left\{(-1)^u \mathrm{C}_u^{n_T-1}\sum_{q=0}^{(n_R-1)u}\alpha_{u,q}(n_R+q)!(u+1)^{-n_R-q-1}\right\}. \tag{3.26}$$

Also, recall that $\overline{\rho} = P_t/\sigma_n^2$ .Then, we can express the capacity C_{per} and spectral efficiency SE_{per}, respectively, as

$$C_{per} \approx W \times P_t \times \varphi, \tag{3.27}$$

and

$$SE_{per} \approx P_t \times \varphi. \tag{3.28}$$

From Eq. (3.22), Eq. (3.27), Eq. (3.28), and noting that $P_T = KP_t$, we arrive at the following result.

Proposition 3.1 *The closed-form expression for the EE-SE trade-off in per-subcarrier antenna selection systems in the low SNR regime is approximated as*

$$EE_{per} \approx \frac{W \times SE_{per}}{(K/\eta\varphi)SE_{per} + n_T P_{ctx} + n_R P_{crx} + P_{bb}}. \tag{3.29}$$

For the bulk selection scheme, an expression for the EE-SE trade-off is given below.

Proposition 3.2 *The closed-form expression for the EE-SE trade-off in bulk antenna selection systems in the low SNR regime can be approximated by*

$$EE_{bulk} \approx \frac{W \times SE_{bulk}}{(K/\eta\chi)SE_{bulk} + P_{ctx} + n_R P_{crx} + P_{bb}}, \tag{3.30}$$

where

$$\chi = \frac{n_T \log_2 e}{K(n_R K - 1)!\sigma_n^2} \sum_{u=0}^{n_T-1} \left\{ (-1)^u \mathrm{C}_u^{n_T-1} \sum_{t=0}^{(n_R K-1)u} \beta_{u,t} (n_R K + t)! (u+1)^{-n_R K - t - 1} \right\}. \tag{3.31}$$

Proof: The result is obtained based on Eq. (3.21) and Eq. (3.22).

It is worth noting that the closed-form expressions of the EE-SE trade-off, i.e., Eq. (3.29) and Eq. (3.30), also show the characteristics of the trade-off between the energy efficiency and capacity in antenna selection MIMO-OFDM systems.

3.3.3 Numerical Examples

To validate the analysis above, simulation results for the system with $n_T = 4$, $n_R = 1$, $K = 16$, $W = 1$ MHz, $\eta = 0.35$, and $P_{ctx} = P_{crx} = P_{bb} = 50$ mW are illustrated. Note that although the number of subcarriers K is small, they are assumed independent. Moreover, simulation results under more realistic parameters will be provided in Section 3.6. Figure 3.3 plots the energy efficiency versus the transmit power P_T at the low SNR regime in two scenarios: *Scenario A*: P_T is small compared to the power consumed by hardware, and *Scenario B*: P_T is large. It can be seen that the analytical curves based on *Theorem 3.1* and *Theorem 3.2* match the simulation curves. Also, bulk selection scheme is more effective than per-subcarrier selection when the power P_T is small (Scenario A). Meanwhile, per-subcarrier antenna selection offers better energy-efficiency when P_T is large (Scenario B). In Scenario A, per-subcarrier selection suffers from a loss in energy-efficiency due to the fact that, in this case, the power consumed by hardware is larger than the transmit power P_T. Therefore, the deployment of multiple active RF chains (i.e., $n_{on} = n_T$) in per-subcarrier selection will require large additional RF power consumption, while achieving a small capacity improvement. Unlike Scenario A, in Scenario B, the transmit power P_T dominates the circuit power consumption. Thus, activating multiple RF chains will achieve a larger capacity, while incurring very small additional power consumption due to RF chains. Consequently, in this scenario, multiple antennas, rather than only one antenna, should be activated to achieve improved energy efficiency. This explains why bulk selection attains lower energy efficiency than its counterpart. Motivated by these results, Section 3.4 develops

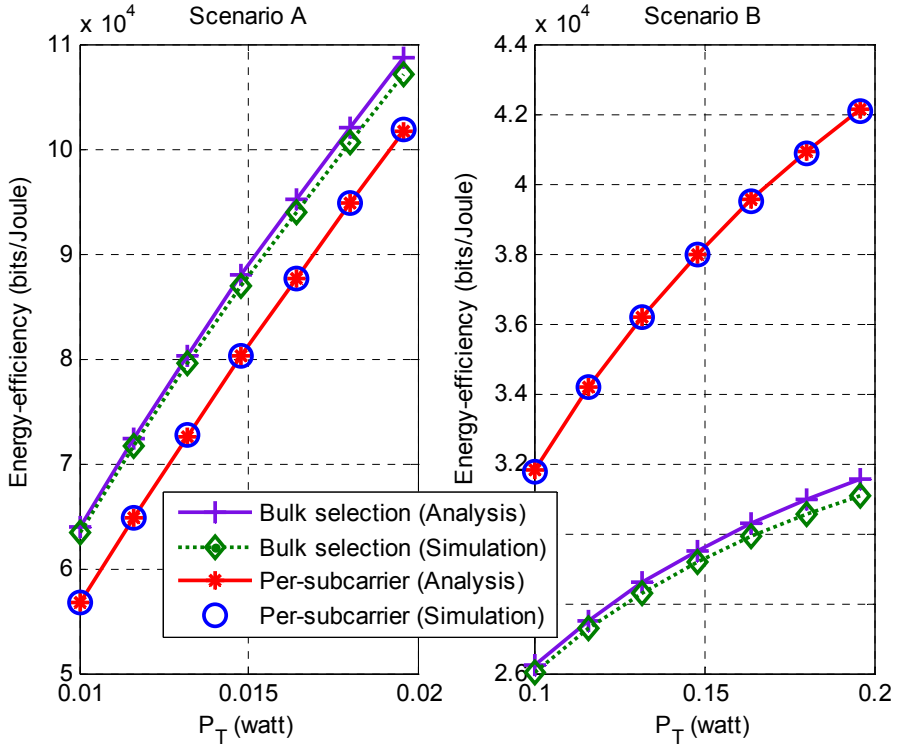

Figure 3.3. Energy-efficiency in bulk selection and per-subcarrier selection: analysis vs. simulation.

an adaptive antenna selection strategy to improve energy efficiency in MIMO-OFDM systems.

3.4 Adaptive Antenna Selection for Improved Energy Efficiency

In Section 3.3, we have shown that the antenna selection MIMO-OFDM systems with a fixed number of RF chains (i.e., $n_{RF} = 1$ in bulk selection, and $n_{RF} = n_T$ in per-subcarrier selection) suffer from a loss in energy efficiency. We note that the average energy efficiency value defined in Eq. (3.10) depends on many factors, including the channel condition, the actual transmit power, as well as the power consumed by the electronics circuits (mainly RF chains). When one antenna (i.e., one RF chain) is activated/deactivated, the system will achieve a higher/lower capacity. Meanwhile, the power consumption due to RF chains is increased/decreased. Consequently, whether the *EE* value is increased or not depends on the changes of the capacity and consumed power. Given fixed values of P_{ctx}, P_{crx}, P_{bb}, and P_T, whether an antenna should be activated or deactivated for improved energy-efficiency depends on the channel condition. Based on these observations, we propose to improve energy efficiency by *adaptively selecting both the number of active RF chains* n_{on} $(1 \le n_{on} \le n_{RF})$ *and the*

transmit antenna indices (see Figure 3.2d for illustration). This proposed selection method can be implemented by either an exhaustive search or a low-complexity algorithm, which are described in detail below.

3.4.1 Exhaustive Search Method

When the number of transmit antennas n_T is small, an exhaustive search method can be used to achieve an optimal antenna allocation. In particular, this method checks all possible subsets of antennas, and selects the subset that attains the highest energy efficiency value. Note that the number of possible subsets is $\sum_{m=1}^{n_{RF}} C_m^{n_T}$, which incurs very high complexity if n_T and/or n_{RF} are large. Thus, a lower complexity method is preferred.

3.4.2 Low-Complexity Algorithm

To realize the proposed adaptive selection method with low complexity, we develop a greedy selection algorithm as described in Table 3.1. This algorithm selects antennas in an incremental fashion and is based on the following principles.

P1. Create n_{RF} subsets of antennas $P_m, m = 1, 2, ..., n_{RF}$, where a subset P_m consists of m antennas. The subset that attains the largest *EE* value is selected as the optimal selected subset.

P2. Given a subset P_{m-1} consisting of (m-1) selected antennas, the best antenna $\hat{i}(m)$ that is added to create the subset P_m is the antenna that makes P_m achieve the largest accumulated cost.

P3. If the cost $c_{\hat{i}(m)}(l)$ is the largest among the available antennas at the l^{th} subcarrier, then the antenna $\hat{i}(m)$ is immediately selected for the l^{th} subcarrier when this antenna is added to the subset P_{m-1}. Note that the value $c_{\hat{i}(m)}(l)$ will be always taken as the cost on the l^{th} subcarrier when measuring the accumulated cost for all n_{RF} subsets $P_m, m = 1, 2, ..., n_{RF}$. Thus, the cost corresponding to the l^{th} subcarrier on the remaining available antennas will not be taken into account when evaluating the accumulated cost of these antennas. Consequently, the optimal antenna $\hat{i}_m$ mentioned in **P2** is the one that has the largest accumulated cost calculated only over a subset of unallocated subcarriers.

Table 3.1. Low-complexity antenna selection algorithm.

1: Initial setting: A subset of unallocated subcarriers $\Omega_0 = \{1, 2, ..., K\}$,
A subset of available transmit antennas $S_0 = \{1, 2, ..., n_T\}$,
A subset of selected antennas $P_0 = \{\varnothing\}$, and an energy-efficiency value $EE_0 = 0$.
2: Calculate the cost $c_i(k), \forall i \in S_0, \forall k \in \Omega_0$, using Eq. (3.11).
3: **for** $m = 1 : n_{RF}$ **do**
4: Calculate the accumulated cost across unallocated subcarriers (used to select antenna)
$\Psi_i^{(m)} = \sum_{k \in \Omega_{m-1}} c_i(k), i \in S_{m-1}$.
5: Select the antenna $\hat{i}(m)$ that satisfies $\hat{i}(m) = \arg\max_{i \in S_{m-1}} \Psi_i^{(m)}$.
6: Add $\hat{i}(m)$ to the subset of selected antennas, i.e., $P_m = \{P_{m-1}, \hat{i}(m)\}$.
7: Assign the selected antenna $\hat{i}(m)$ to the subcarriers l that satisfy
$c_{\hat{i}(m)}(l) = \arg\max_{i \in S_{m-1}} c_i(l)$,
i.e., $\hat{i}_{(m)}(l) = \hat{i}(m), \forall l \in \overline{\Omega}_m$, where $\overline{\Omega}_m$ is the subset of the allocated subcarriers l in the m^{th} loop and $\hat{i}_{(m)}(l)$ is the selected antenna at the subcarrier l in the m^{th} loop.
8: Update the subset of unallocated subcarriers as $\Omega_m = \Omega_{m-1} - \overline{\Omega}_m$.
9: Select antennas in P_m for the remain unallocated subcarriers via
$\hat{i}_{(m)}(\kappa) = \arg\max_{i \in P_m} c_i(\kappa), \forall \kappa \in \Omega_m$.
10: Calculate the accumulated instantaneous capacity (bits/s/Hz) corresponding to the subset P_m (used to calculate the *EE* value) (cf. Eq. (3.5))
$\bar{I}_m = \sum_{k=0}^{K-1} I_{\hat{i}_{(m)}(k)}(k)$.
11: Calculate the *EE* value (cf. Eq. (3.10)):
$EE_m = (W/K) \times \bar{I}_m / (P_T/\eta + mP_{ctx} + n_R P_{crx} + P_{bb})$.
12: **if** $EE_m > EE_0$ **do**
13: $EE_0 = EE_m$,
14: $P_{select} \leftarrow P_m$,
15: $\hat{i}_{select}(k) \leftarrow \hat{i}_{(m)}(k), k = 1, 2, ..., K$.
16: **end if**
17: Update the subset of available antennas as $S_m = S_0 - P_m$.
18: **end for**
19: The subset of selected antennas and the allocation pattern for the maximal *EE* value are P_{select} and $\hat{i}_{select}(k), k = 1, 2, ..., K$, respectively.

3.4.3 Complexity Evaluation

With respect to a complexity comparison between the algorithm in Table 3.1 and the exhaustive search, we consider the number of allocation operations as a measure of complexity. In the exhaustive search, there are $\sum_{m=1}^{n_{RF}} C_m^{n_T}$ possible subsets, and each subset needs K allocations for K subcarriers. Thus, the number of allocations is $\zeta_{opt} = K \sum_{m=1}^{n_{RF}} C_m^{n_T}$. When $n_{RF} = n_T$, the value ζ_{opt} is $\zeta_{opt} = K \sum_{m=1}^{n_T} C_m^{n_T} = K(2^{n_T} - 1)$. Meanwhile, in the proposed algorithm, the m^{th} (m = 1, 2,..., n_{RF}) loop searches for $(n_T - m + 1)$ subsets and performs $|\Omega_{m-1}|$ allocations for each subset. Here, $|\Omega_{m-1}|$

Table 3.2. Complexity Comparison ($n_{RF} = n_T$).

Number of transmit antennas n_T	2	3	4	5	6	7	8
ζ_{opt} (exhaustive search)	$3K$	$7K$	$15K$	$31K$	$63K$	$127K$	$255K$
$\zeta_{sub} = Kn_T(n_T+1)/2$ (worst-case)	$3K$	$6K$	$10K$	$15K$	$21K$	$28K$	$36K$
ζ_{sub} (average)	$2.3K$	$4.1K$	$6.1K$	$8.4K$	$10.9K$	$13.6K$	$16.5K$
ζ_{opt}/ζ_{sub} (average)	1.3	1.7	2.5	3.7	5.8	9.3	15.5

Table 3.3. Number of unallocated subcarriers ($K = 64$).

n_T	$\|\Omega_0\|$	$\|\Omega_1\|$	$\|\Omega_2\|$	$\|\Omega_3\|$	$\|\Omega_4\|$
2	K	$0.34K$			
3	K	$0.46K$	$0.14K$		
4	K	$0.52K$	$0.23K$	$0.07K$	
5	K	$0.56K$	$0.29K$	$0.12K$	$0.03K$

denotes the cardinality of the subset Ω_{m-1}, i.e., $|\Omega_{m-1}| \le K$. Therefore, the proposed algorithm requires only $\zeta_{sub} = \sum_{m=1}^{n_{RF}} (n_T - m + 1)|\Omega_{m-1}|$ allocations. A complexity comparison between the exhaustive search and algorithm methods based on numerical values is shown in Table 3.2. In this table, the results are averaged over 10^5 channel realizations. Details about other simulation parameters are provided in Section 3.6. The obtained results show that the algorithm attains very low complexity compared to the exhaustive search method.

Let us further consider the complexity of the proposed algorithm in the worst case, i.e., $|\Omega_{m-1}| = K, \forall m = 1,2,...,n_{RF}$. In this scenario, the number of allocations is $\zeta_{sub} = K\sum_{m=1}^{n_{RF}} (n_T - m + 1)$. When $n_{RF} = n_T$, we have $\zeta_{sub} = K\sum_{m=1}^{n_T} (n_T - m + 1) = Kn_T(n_T + 1)/2$ (i.e., increase polynomially with respect to n_T) compared to $\zeta_{opt} = K(2^{n_T} - 1)$ (i.e., increase exponentially). Consequently, the proposed algorithm in Table 3.1 still incurs lower complexity, especially when n_T is large. It is also worth mentioning that the value ζ_{sub} (average) is smaller than ζ_{sub} (worst-case) as the number of unallocated subcarriers $|\Omega_{m-1}|$ becomes much smaller after each loop as shown in Table 3.3.

3.5 Power Loading for Antenna Selection MIMO-OFDM Systems

In the previous sections, we have considered the systems with equal power allocation across selected subcarriers, i.e., $P_{t,k} = P_T/K \coloneqq P_t, \forall k$. This equal power allocation may be required in systems where a very strict spectral mask applied on each subcarrier, e.g., multiband-OFDM ultra-wideband (MB-OFDM UWB) [36]. However, if a spectral mask constraint on the kth subcarrier is P_k^{mask}, power loading across selected subcarriers, which means dynamic distribution of the available power among subcarriers, can be employed to further improve energy efficiency. This is because power loading can increase capacity in the system [96], which in turn improves energy efficiency (cf. Eq. (3.10)). Our formulation problem in this section is stated as follows: Suppose that the total transmit power is P_T, find the optimal allocated powers $\{P_{t,k}^*, k = 0,1,..., K-1\}$ that satisfy a spectral mask constraint so that the energy efficiency in antenna selection MIMO-OFDM systems is maximised.

We assume that antennas are selected for all subcarriers based on a given selection scheme (e.g., bulk selection, per-subcarrier selection, combined selection, or adaptive selection scheme) that has been described in the previous sections. In what follows, we will derive the optimal allocation of powers $\{P_{t,k}^*, k = 0,1,..., K-1\}$. Recall that the channel power gain (after MRC) and the allocated power associated with the k^{th} subcarrier are $g_{\tilde{i}_k}(k)$ and $P_{t,k}$, respectively. Hence, the instantaneous energy efficiency can be expressed as (cf. Eq. (3.3), Eq. (3.5), and Eq. (3.10))

$$EE = \frac{(W/K) \times \sum_{k=0}^{K-1} \log_2(1 + P_{t,k} g_{\tilde{i}_k}(k)/\sigma_n^2)}{\sum_{k=0}^{K-1} P_{t,k}/\eta + n_{on} P_{ctx} + n_R P_{crx} + P_{bb}}. \tag{3.32}$$

We aim to allocate powers $\{P_{t,k}\}$ such that the EE value in Eq. (3.32) is maximised subject to the following constraints. The first constraint is that the power allocated on the k^{th} subcarrier $P_{t,k}$ is not larger than the corresponding spectral mask P_k^{mask}, i.e.,

$$0 \le P_{t,k} \le P_k^{mask}, \; k = 0,1,....,K-1. \tag{3.33}$$

The second constraint is related to the total power allocated all over the subcarriers, i.e.,

$$\sum_{k=0}^{K-1} P_{t,k} = P_T. \tag{3.34}$$

Note that this constraint guarantees a fair comparison among antenna selection schemes as our focus in this work is to determine which scheme can attain the highest *EE* value given the same actual transmit power P_T. Due to the second constraint, i.e., Eq. (3.34), the denominator of Eq. (3.32) is a constant with respect to $\{P_{t,k}\}$. Therefore, the power loading problem to maximise energy efficiency can now be expressed as

$$\max_{\{P_{t,k}\}} \sum_{k=0}^{K-1} \log_2(1 + P_{t,k}\, g_{\hat{i}_k}(k) \big/ \sigma_n^2) \tag{3.35}$$

$$\text{s.t.} \quad 0 \le P_{t,k} \le P_k^{mask}, k = 0,1,\ldots, K-1,$$

$$\sum_{k=0}^{K-1} P_{t,k} = P_T.$$

It is clear that Eq. (3.35) is a convex problem. Thus, its solution can be obtained as [97]

$$P_{t,k}^* = \left[\vartheta - \frac{\sigma_n^2}{g_{\hat{i}_k}(k)} \right]_0^{P_k^{mask}}, k = 0,1,\ldots, K-1, \tag{3.36}$$

where $\vartheta > 0$ is the water level that is chosen to satisfy the total power constraint of $\sum_{k=0}^{K-1} P_{t,k}^* = P_T$, and $[x]_a^b$ denotes the Euclidean projection of x on $[a,b]$, i.e., $[x]_a^b = \min(b, \max(x, a))$. Efficacy of power loading on several antenna selection schemes in terms of energy efficiency that is evaluated numerically based on Eq. (3.36) will be discussed in Section 3.6.4.

Remark 3.1 Although power loading has been well studied for single-antenna OFDM systems, an investigation of power loading for antenna selection MIMO-OFDM systems is necessary. The reason is that the effectiveness of power loading over equal allocation depends on a variation of channel power gains. Meanwhile, in antenna selection, statistical distribution properties of channel power gains corresponding to the selected subcarriers are altered due to a selection operation. Note that this characteristic does not occur in single-antenna OFDM systems. Therefore, it is interesting to know, from an energy-efficiency perspective, how effective power allocation is in the context of

Table 3.4. Simulation parameters.

Parameter	Value
Carrier frequency	f_c = 2.4 GHz
Bandwidth	W = 25 MHz
Modulation	4-QAM
FFT size	K = 64
Circuit powers	P_{ctx} = 150 mW, P_{crx} = 120 mW, P_{bb} = 100 mW
Power amplifier efficiency	35%
PSD of noise	-174 dBm/Hz
Path-loss exponent	ϕ = 4
Frequency-selective fading channel	IEEE 802.11n channel models

antenna selection in OFDM systems. This concern has not been addressed in the literature so far.

Remark 3.2 In this work, we perform power loading after antenna selection. The advantage of this approach is that it requires very low additional complexity. In fact, in this approach, the power loading operation, i.e., Eq. (3.36), is performed only once at the transmitter only. Note that one can perform joint power loading and antenna selection. However, for a joint approach, as the allocated powers on subcarriers are involved in the calculation of antenna selection metrics, we need to perform power loading operation several times during an antenna selection process. Moreover, in a TDD mode, this joint method needs to be performed at both transmitter and receiver. This clearly introduces high complexity.

3.6 Simulation Results and Discussions

In this section, we evaluate the energy efficiency in several antenna selection OFDM systems via simulation results. The simulation parameters are listed in Table 3.4. The IEEE 802.11n channel model (channel model B) [98] is adopted in the simulations. This channel model has 9 Rayleigh fading paths and is based on measurements of non-line-of-sight (NLOS) environments.

3.6.1 Energy Efficiency versus Transmit Power

We consider antenna selection MIMO-OFDM systems with n_T = 4, n_R = 1, and the maximum SNR criterion. The number of equipped RF chains in both combined selection and adaptive selection is n_{RF} = 3. Recall that n_{RF} = 1 in the bulk selection, and $n_{RF} = n_T$ in the per-subcarrier selection. Figure 3.4 shows the energy efficiency versus

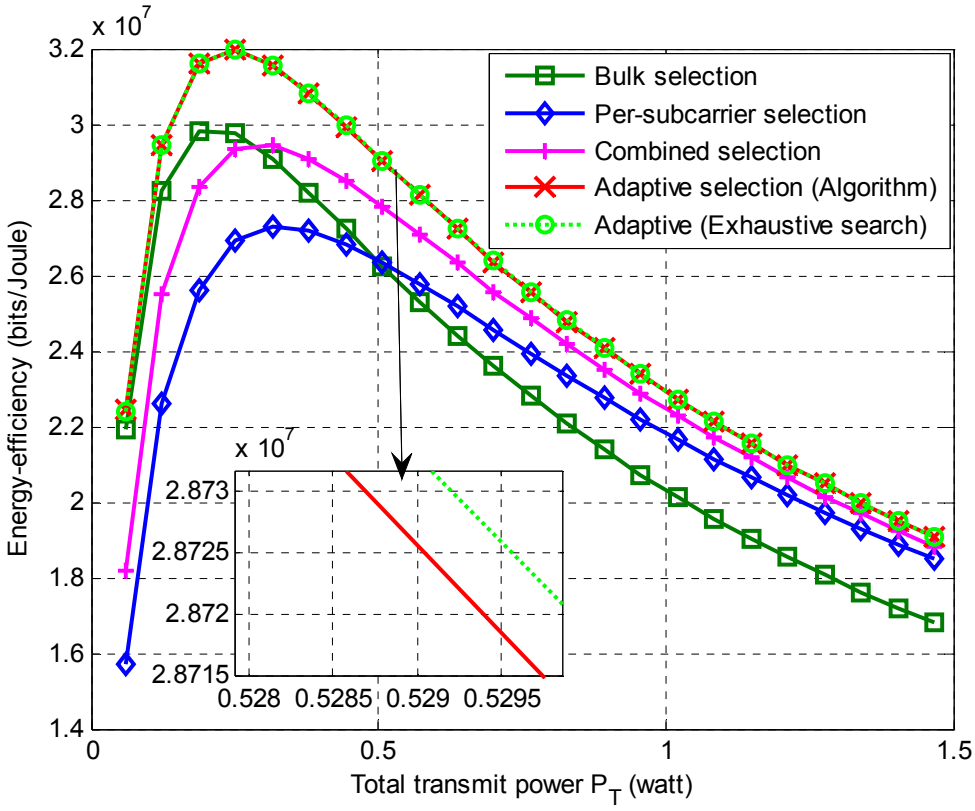

Figure 3.4. Energy efficiency of different antenna selection schemes ($n_T = 4$, $n_R = 1$).

the total transmit power P_T. The obtained results demonstrate the following. First, the proposed adaptive antenna selection method achieves a better energy-efficiency performance than the conventional counterparts. This comes from the fact that the proposed method can adapt the number of active RF chains n_{on} according to the channel condition to achieve the maximal *EE* value. Second, the *EE* value achieved with the proposed low-complexity algorithm is very close to that with the exhaustive search method, which demonstrates the effectiveness of this algorithm from a practical viewpoint. We note that the number of active RF chains in the conventional bulk-selection and the per-subcarrier selection methods are always $n_{on} = 1$ and $n_{on} = n_T$, respectively. Hence, they cannot achieve the maximum energy-efficiency. For the combined selection scheme, as the number of active RF chains is still fixed, i.e., $n_{on} = n_{RF}$, the energy efficiency in this scheme is inferior to that in the adaptive selection scheme.

To have an insight into the adaptive mechanism of the proposed selection approach, we plot in Figure 3.5 the numbers of channel realizations that the numbers of active RF chains equal to one, two, and three, when running a simulation with a total of 10^5

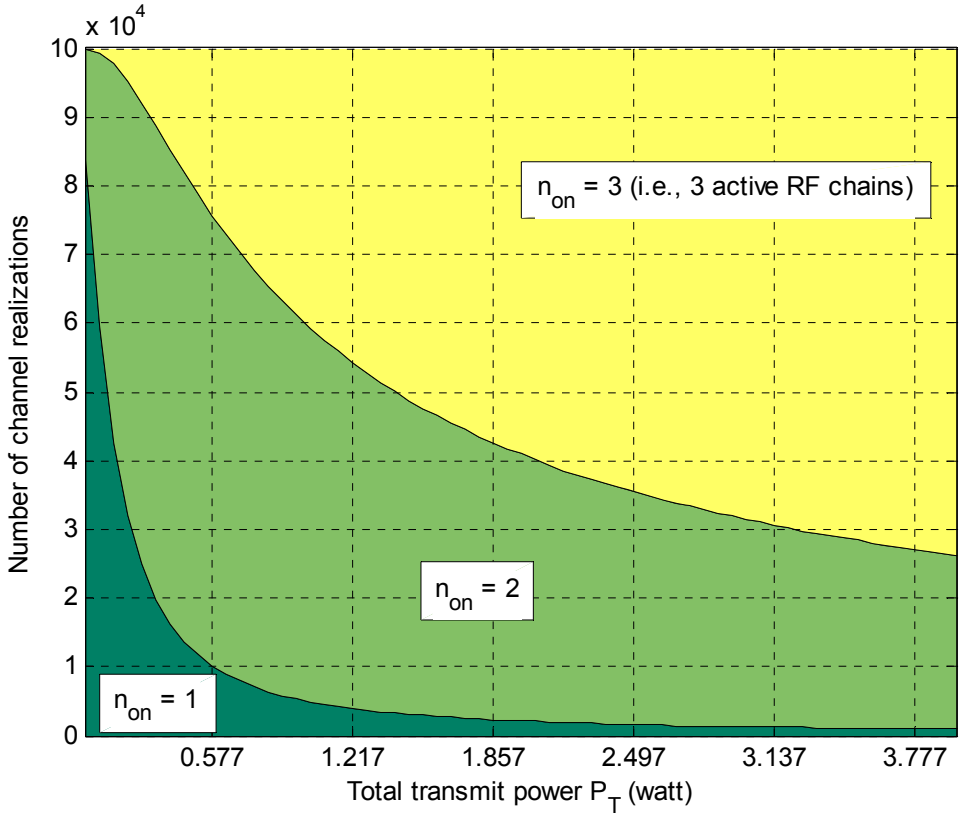

Figure 3.5. Number of active RF chains n_{on} in the adaptive selection scheme ($n_T = 4$, $n_{RF} = 3$, $n_R = 1$).

channel realizations. The result confirms our discussion in Section 3.3.3 that when the transmit power P_T increases, a larger number of active antennas (i.e., number of active RF chains) is likely selected to attain the maximal *EE* value. For example, when P_T = 0.577 W, the percentage of selection of n_{on} = 1, n_{on} = 2, and n_{on} = 3, are about 10%, 66%, and 24%, respectively. Meanwhile, the corresponding numbers at P_T = 2.497 W are about 1% (n_{on} = 1), 34% (n_{on} = 2), and 65% (n_{on} = 3).

In the antenna selection OFDM systems with n_R = 2 receive antennas, as shown in Figure 3.6, we have similar observations as in Figure 3.4. In addition, it can be seen from Figure 3.4 and Figure 3.6 that when the number of receive antenna increases, the energy efficiency is improved. This is because a capacity improvement resulting from the use of multiple receive antennas with an MRC has more impact on the *EE* metric than an additional power required by the second receive RF chain, which leads to an improvement in the energy efficiency (cf. Eq. (3.10)).

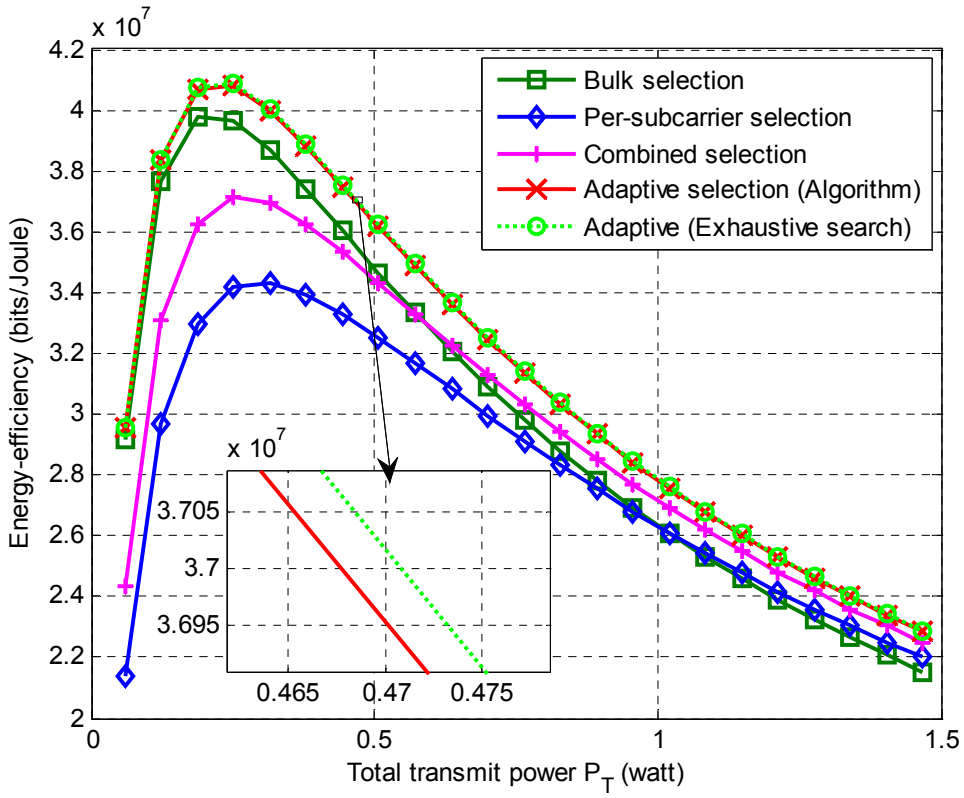

Figure 3.6. Energy efficiency of different antenna selection schemes with two receive antennas ($n_T = 4$).

Remark 3.3 As shown in Figure 3.4 and Figure 3.6, there exists the maximum *EE* value when the transmit power $P_T = P_T^*$. This is because the instantaneous energy-efficiency is a pseudo-concave function with respect to (w.r.t.) P_t (cf. Eq. (3.32)). The unique maximum value occurs when $\partial EE(P_t)/\partial P_t = 0$. Thus, the total transmit power P_T^* can be obtained as $P_T^* = KP_t^*$, where P_t^* is the solution of $\partial EE(P_t)/\partial P_t = 0$ that can be solved numerically.

3.6.2 Energy Efficiency under Different Antenna Selection Criteria

Figure 3.7 shows the energy efficiency in the conventional and proposed selection systems under different antenna selection criteria. Three criteria, namely maximum SNR, maximum capacity, and minimum error-rate, introduced in Eq. (3.11) are considered. The results show that in the per-subcarrier selection scheme, all the selection criteria achieve the same energy efficiency. This is due to the fact that antennas are selected independent for each subcarrier in this case. Moreover, at any subcarrier, the selected antenna for the maximum SNR is the one that attains the maximum capacity and minimum error-rate (cf. Eq. (3.5), Eq. (3.11), Eq. (3.12)). For

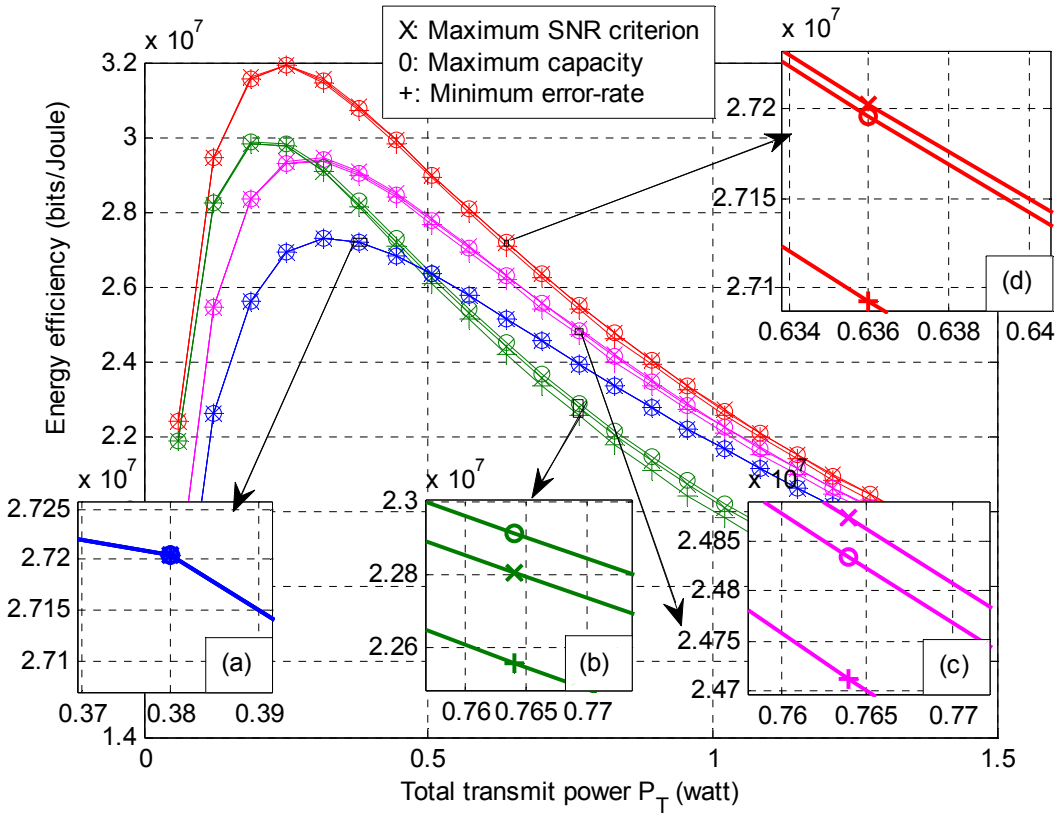

Figure 3.7. Energy efficiency under different antenna selection criteria: (a): Per-subcarrier selection; (b): Bulk selection; (c): Combined selection; (d): Adaptive selection.

the bulk selection scheme, the maximum capacity criterion achieves the largest energy efficiency. This is because this selection criterion directly maximises the accumulated capacity across subcarriers, which in turn maximises energy efficiency (cf. Eq. (3.10)). In the combined and adaptive selection schemes, the maximum SNR criterion can attain higher energy efficiency compared to its counterparts. However, it can be seen that the difference in energy efficiency between the selection criteria is relatively small.

3.6.3 Energy Efficiency versus Number of Transmit Antennas

When antenna selection OFDM systems are investigated from capacity or error performance perspective, it is shown that the more antennas are equipped, the larger the capacity or the better error-rate is achieved, see e.g., [79-81, 88]. In this work, where the system is considered from the energy-efficiency viewpoint, the relation between energy efficiency and the number of equipped transmit antennas is shown in Figure 3.8. It can be seen that, in the bulk selection, combined selection and proposed adaptive selection systems, the *EE* values increase when the number of antennas n_T increases. However, these *EE* values become saturated when n_T becomes very large. This is because the ergodic capacity in antenna selection systems is a logarithmically increasing function

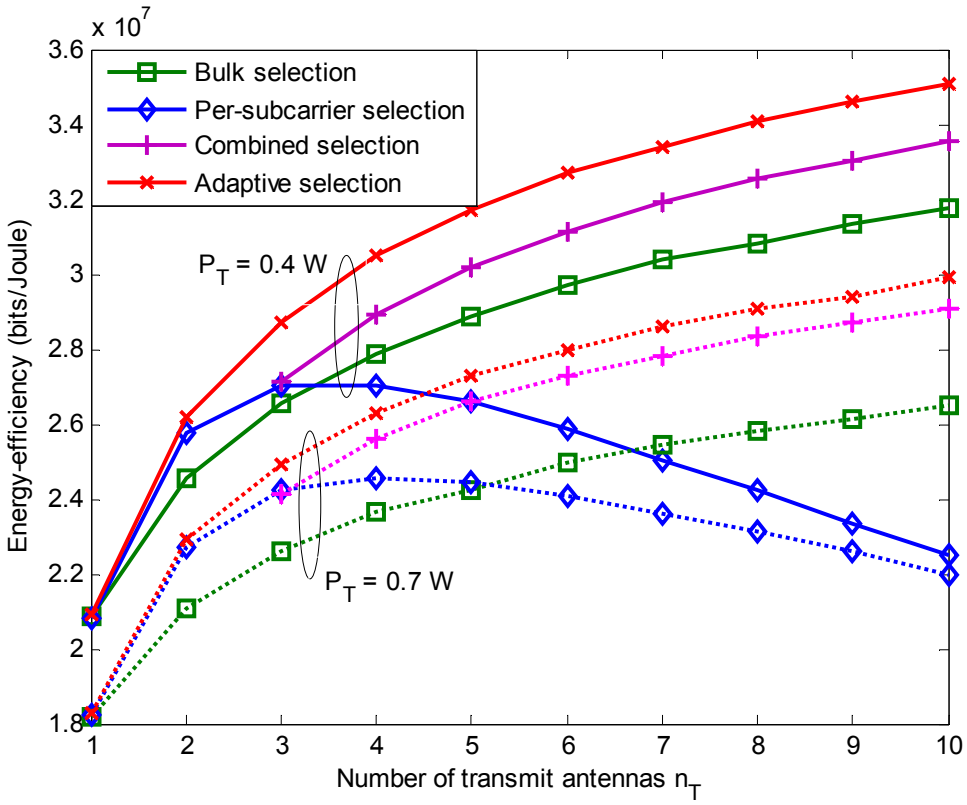

Figure 3.8. Energy efficiency versus the number of transmit antennas ($n_R = 1$, $n_{RF} = 1$ in bulk selection, $n_{RF} = n_T$ in per-subcarrier selection, and $n_{RF} = 3$ in both combined and adaptive selection schemes).

w.r.t. n_T [67]. Meanwhile, in the per-subcarrier selection system, the *EE* value first increases and then decreases. This behaviour can be explained by the fact that, when n_T becomes large, the increased power consumption due to the RF chains has more impact on the energy efficiency than the capacity improvement does, which reduces the *EE* value (cf. Eq. (3.10)). In addition, we note that an *EE* comparison among the selection schemes w.r.t. n_T depends on particular values of the transmit power and power consumed by hardware. For example, bulk selection is better than per-subcarrier selection if $n_T > 3$ when $P_T = 0.4$ W, and if $n_T > 5$ when $P_T = 0.7$ W. It is also important to note that the proposed adaptive selection system outperforms its counterparts for all values of n_T.

Remark 3.4 As shown in Figure 3.8, in the per-subcarrier antenna selection system, there exists an optimal number of equipped antennas such that the energy-efficiency is maximised. This optimal number of antennas can be determined analytically by formulating an optimisation problem for maximising the average energy efficiency with respect to the number of antennas. To solve this optimisation problem, we first derive a closed-form formula expressing the cost function as a function of the number of

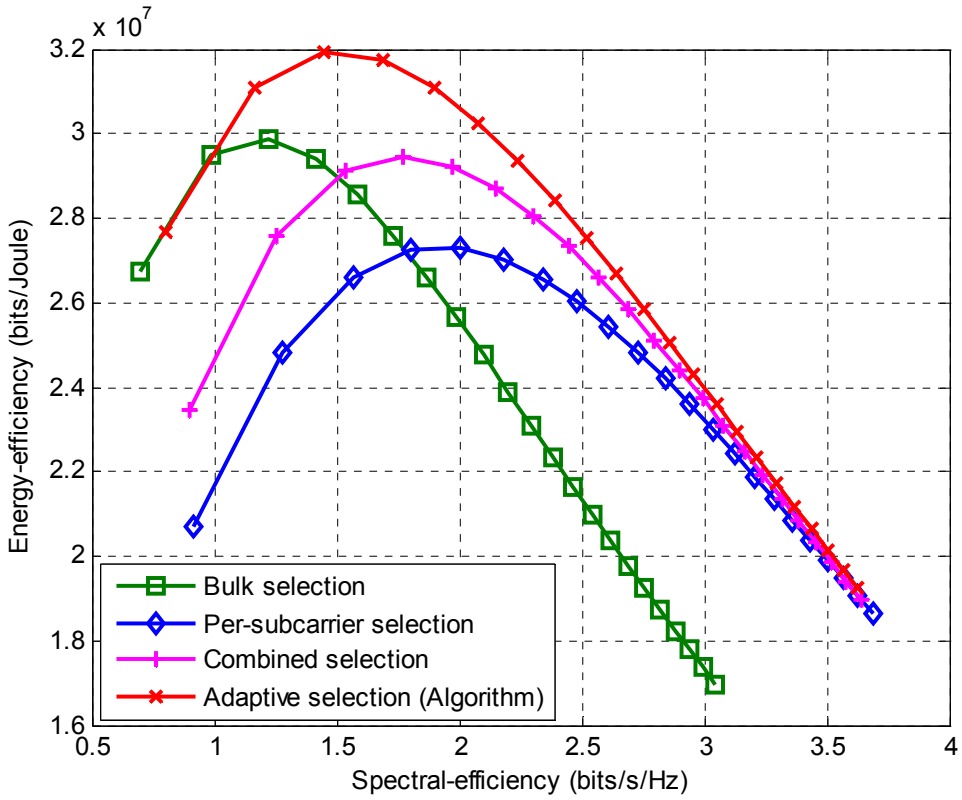

Figure 3.9. Energy efficiency versus spectral efficiency ($n_T = 4$, $n_R = 1$).

antennas. A search algorithm is then designed to obtain the optimal number of antennas (see Section 3.C for more details).

3.6.4 Energy Efficiency versus Spectral Efficiency

We now examine the trade-off between energy efficiency (EE) and spectral efficiency (SE) in OFDM systems with different antenna selection schemes. In Figure 3.9, we plot the achieved energy efficiency (bits/Joule) versus spectral efficiency (bits/s/Hz). From an energy-efficiency perspective, it can be seen that bulk selection is effective in the low-SE regime. Meanwhile, per-subcarrier selection and combined selection are suitable in the high-SE and medium-to-high-SE regimes, respectively. Moreover, the results show that the proposed adaptive selection achieves the best EE-SE tradeoff performance among the considered schemes. Note that the behavior of these EE-SE curves can be explained from the case of *EE*-P_T curves (e.g., Figure 3.4) given that increasing the spectral efficiency is typically associated with the increasing of the transmit power.

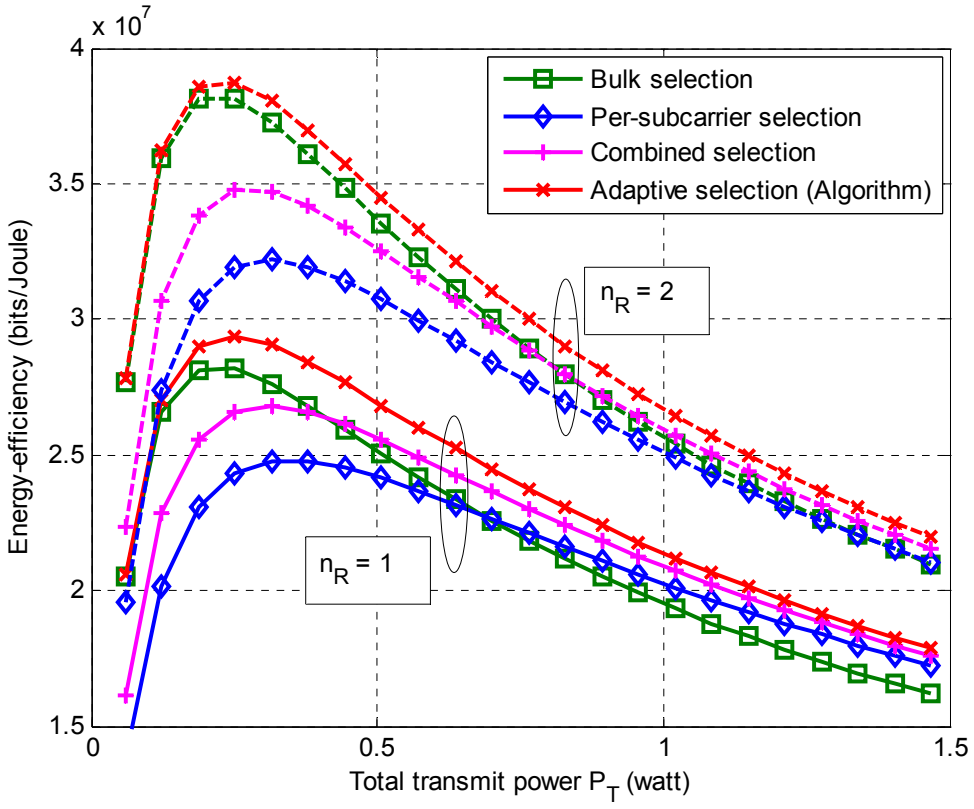

Figure 3.10. Energy efficiency of different antenna selection schemes under spatially correlated channels (correlation coefficient of 0.7, $n_T = 4$, $n_R = 1$).

3.6.5 Impact of Spatial Correlation on Energy Efficiency

We next consider the impact of spatial correlation at the transmitter on energy efficiency in the considered antenna selection OFDM systems. The spatially correlated channel is modelled using the Kronecker model [14], i.e., $\mathbf{H} = \mathbf{R}_R^{1/2}\mathbf{H}_{iid}\mathbf{R}_T^{1/2}$, where $\mathbf{R}_T$ and $\mathbf{R}_R$ are the $n_T \times n_T$ transmit and the $n_R \times n_R$ receive correlation matrices, respectively, and $\mathbf{H}_{iid}$ denotes the $n_R \times n_T$ channel matrix consisting of independent channel realizations. The achieved energy efficiency is shown in Figure 3.10. It can be seen from Figure 3.4, Figure 3.6 and Figure 3.10 that the presence of spatial correlation reduces the achieved energy efficiency. This makes sense as, given a fixed number of antennas, the correlation between transmit antennas reduces the system capacity, which in turns lowers the energy efficiency (cf. Eq. (3.10)). However, it is important to note that the proposed system remains superior with respect to energy efficiency compared to the conventional counterparts.

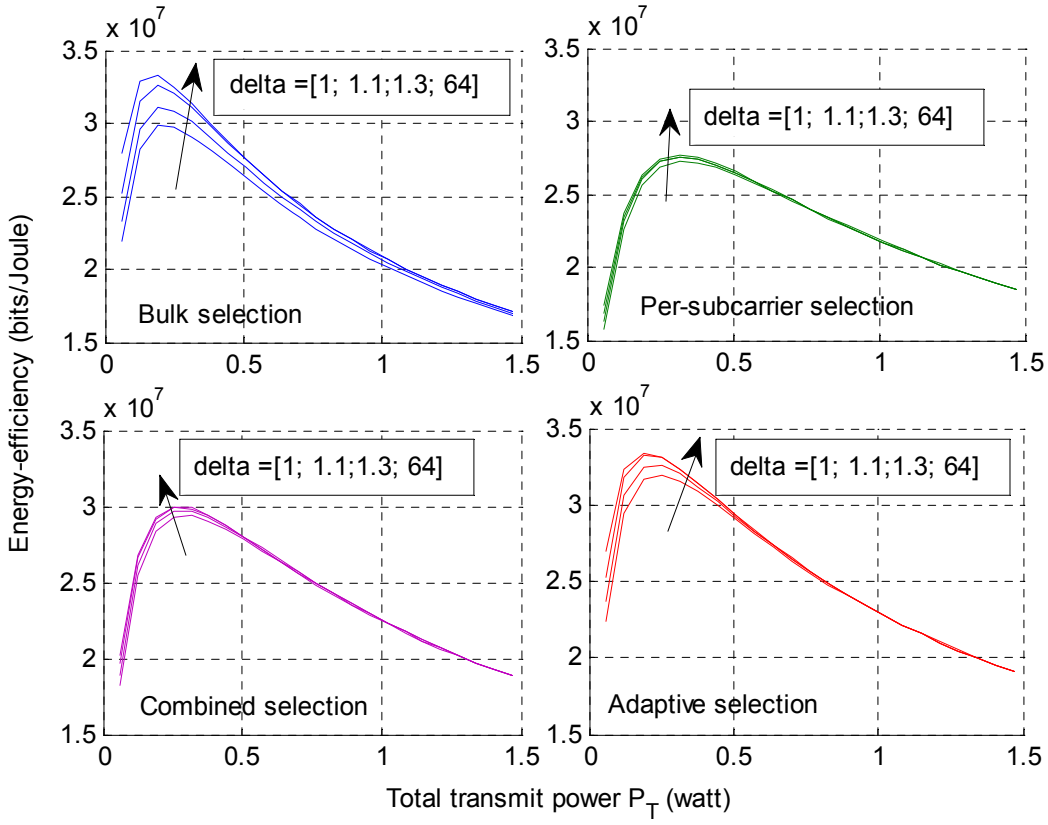

Figure 3.11. Energy efficiency of different antenna selection schemes with power loading ($n_T = 4$, $n_R = 1$).
Notes: 'delta = 1': equal allocation; 'delta = 64': no spectral mask constraint.

3.6.6 Efficacy of Power Loading on Energy Efficiency

We finally examine the effectiveness of power loading across subcarriers on energy efficiency in antenna selection MIMO-OFDM systems. For simplicity, in the simulations, we assume that all subcarriers have a similar spectral mask constraint, i.e., $P_k^{mask} = P^{mask}, \forall k$. Figure 3.11 shows the *EE* values with different levels of spectral mask $\delta \geq 1$, where we define $P^{mask} = \delta \times (P_T / K)$. Note that factors $\delta = 1$ and $\delta = K = 64$ are equivalent to the case of equal power allocation and no spectral mask constraint, respectively. First, it can be seen that performing power loading offers a better energy-efficiency performance than antenna selection with equal power allocation in all the systems. However, the *EE* improvement at the high SNR region is marginal. This can be explained by the fact that *EE* improvement comes from an increase of capacity (cf. Eq. (3.22), Eq. (3.25)). Meanwhile, it was shown in [99] that the capacity improvement based on water-filling power allocation (i.e., Eq. (3.26)) is reduced when SNR increases. Therefore, the *EE* improvement diminishes with an increasing SNR value. The second observation can be made from Figure 3.11 is that the *EE*

improvement becomes larger when δ is larger (i.e., P^{mask} is higher). However, it is important to observe that these *EE* improvements depend on particular antenna selection schemes. In particular, the *EE* value is improved quite significantly in bulk-selection and adaptive antenna selection schemes. Meanwhile, in per-subcarrier antenna selection, the *EE* improvement is not significant. To explain these behaviours, we note that the efficacy of power allocation across subcarriers over equal power allocation comes from a variation of the channel power gains $g_{\hat{i}_k}(k)$ across subcarriers. In per-subcarrier antenna selection, antennas are selected independently for each subcarrier. Thus, it is likely that the difference in the value $c_{\hat{i}_k}(k)$ among the selected subcarriers is insignificant in per-subcarrier selection, compared to bulk selection. As a result, power loading is not effective in terms of energy efficiency in the per-subcarrier antenna selection in comparison to the bulk selection and adaptive antenna selection schemes.

3.7 Summary

This chapter has investigated the energy efficiency in MIMO-OFDM systems with different antenna selection schemes. Several important factors that affect the energy efficiency, including the relation between the actual transmitted power and the power consumed by the transceiver circuits, the number of antennas, and the spatial correlation among antennas, have been examined. The closed-form expressions of energy efficiency in the systems with conventional selection approaches have been derived. It is shown that the conventional antenna selection methods exhibit a loss of energy efficiency. Thus, the adaptive antenna selection scheme has been proposed to deal with this issue. A low-complexity algorithm has also been developed to realize this adaptive selection scheme that can achieve near-optimal performance. In addition, the energy-efficiency improvement when performing power loading in antenna selection MIMO-OFDM systems has been evaluated. The trade-off between energy efficiency and spectral efficiency in all antenna selection schemes has been examined. Simulation results show that the proposed adaptive selection scheme outperforms its counterparts in terms of energy efficiency.

3.A Proof of Theorem 3.1

Let us assume that $|h_{j,i}|$ follows a Rayleigh distribution with $\varepsilon_{\mathbf{H}}\{|h_{j,i}|^2\} = 1$. It is clear that $g_i = \| \mathbf{h}_i \|^2$ is a chi-square distribution with $2n_R$ degrees of freedom. The pdf (probability distribution function) and cdf (cumulative distribution function) of g_i are given as $f(x) = e^{-x}x^{n_R-1}/(n_R-1)!, \forall x > 0,$ and $F(x) = 1 - e^{-x}\sum_{v=0}^{n_R-1} x^v/v!, \forall x > 0$, respectively [4]. By using order statistics [100], we can express the pdf of $g_{\hat{i}_k}(k) = \| \mathbf{h}_{\hat{i}_k}(k) \|^2$ that associated with the selected antennas $\hat{i}_k$ as

$$f_M(x) = n_T f(x) F^{n_T-1}(x) = n_T \frac{e^{-x}x^{n_R-1}}{(n_R-1)!}\left(1 - e^{-x}\sum_{v=0}^{n_R-1}\frac{x^v}{v!}\right)^{n_T-1}$$
$$= \frac{n_T}{(n_R-1)!}e^{-x}x^{n_R-1}\sum_{u=0}^{n_T-1}\left\{(-1)^u \, \mathrm{C}_u^{n_T-1} \, e^{-ux}\left(\sum_{v=0}^{n_R-1}\frac{x^v}{v!}\right)^u\right\}, \tag{3.37}$$

where $\mathrm{C}_a^b = b!/a!(b-a)!$ is the binomial coefficient. By performing a multinomial expansion as $(\sum_{v=0}^{n_R-1} x^v/v!)^u = \sum_{q=0}^{(n_R-1)u}\alpha_{u,q}x^q$, where $\alpha_{u,q}$ is the coefficient resulting from the multinomial expansion corresponding to x^q (i.e., $\alpha_{u,q}$ is the q^{th} element of a vector $\boldsymbol{\alpha}_u$ that is defined as $\boldsymbol{\alpha}_0 = 1$, $\boldsymbol{\alpha}_1 = [1/0!\ \ 1/1!\ \ 1/2!\ \ \ldots 1/(n_R-1)!]$, and $\boldsymbol{\alpha}_u = \boldsymbol{\alpha}_{u-1} \otimes \boldsymbol{\alpha}_1$, where $\otimes$ denotes a discrete convolution [101]), we have

$$f_M(x) = \frac{n_T}{(n_R-1)!}e^{-x}x^{n_R-1}\sum_{u=0}^{n_T-1}\left\{(-1)^u \, \mathrm{C}_u^{n_T-1} \, e^{-ux}\sum_{q=0}^{(n_R-1)u}\alpha_{u,q}x^q\right\}. \tag{3.38}$$

The expected value of $\varepsilon_{\mathbf{H}}\{\log_2(1+\bar{\rho}g_{\hat{i}_k}(k))\}$ can now be calculated as

$$\varepsilon_{\mathbf{H}}\{\log_2(1+\bar{\rho}g_{\hat{i}})\} = \int_0^{+\infty}\log_2(1+\bar{\rho}\,x)f_M(x)dx$$
$$= \int_0^{+\infty}\left(\log_2(1+\bar{\rho}\,x)\frac{n_T}{(n_R-1)!}e^{-x}x^{n_R-1}\sum_{u=0}^{n_T-1}\left\{(-1)^u \, \mathrm{C}_u^{n_T-1} \, e^{-ux}\sum_{q=0}^{(n_R-1)u}\alpha_{u,q}x^q\right\}\right)dx$$
$$= \frac{n_T}{(n_R-1)!}\sum_{u=0}^{n_T-1}\left\{(-1)^u \, \mathrm{C}_u^{n_T-1}\sum_{q=0}^{(n_R-1)u}\alpha_{u,q}\int_0^{+\infty}\log_2(1+\bar{\rho}\,x)x^{n_R+q-1}e^{-(u+1)x}dx\right\}. \tag{3.39}$$

By using the integral result in [102], we can express the integral in Eq. (3.39) as

$$\begin{aligned} Q &= \int_0^{+\infty} \log_2(1+\overline{\rho}\, x) x^{n_R+q-1} e^{-(u+1)x} dx \\ &= \frac{(n_R+q-1)!}{\overline{\rho}^{n_R+q} \ln 2} e^{(u+1)/\overline{\rho}} \sum_{s=1}^{n_R+q} \left(\frac{u+1}{\overline{\rho}}\right)^{-s} \Gamma\left(-n_R-q+s, \frac{u+1}{\overline{\rho}}\right), \end{aligned} \tag{3.40}$$

where $\Gamma(a,x) = \int_x^{+\infty} e^{-t} t^{a-1} dt$ is the incomplete gamma function [103]. From Eq. (3.16), Eq. (3.39), and Eq. (3.40), we finally arrive at Eq. (3.17).

3.B Proof of Theorem 3.2

Let us first denote $w_i = \sum_{k=0}^{K-1} g_i(k)$. Then, we can explicitly express w_i as (cf. Eq. (3.2))

$$w_i = \sum_{k=0}^{K-1} g_i(k) = \sum_{k=0}^{K-1} \| \mathbf{h}_i(k) \|^2 = \sum_{k=0}^{K-1} \sum_{j=1}^{n_R} | h_{j,i}(k) |^2. \tag{3.41}$$

As the channel coefficients $|h_{j,i}(k)|$ are i.i.d. Rayleigh random variables, it follows that w_i in Eq. (3.41) is a chi-square distribution with $2n_RK$ degrees of freedom. Therefore, we can express the pdf and cdf of w_i as $f(y) = e^{-y} y^{n_RK-1} / (n_RK-1)!, \forall y > 0$ and $F(y) = 1 - e^{-y} \sum_{s=0}^{n_RK-1} y^s / s!, \forall y > 0$, respectively [4]. By performing similar calculations as in Section 3.A, we obtain the pdf of $w_{\hat{i}}$ that is corresponding to the selected antenna $\hat{i}$, $\hat{i} = \arg \max_{i=1,\ldots,n_T} w_i$ (cf. Eq. (3.14)), as

$$f_N(y) = \frac{n_T}{(n_RK-1)!} e^{-y} y^{n_RK-1} \sum_{u=0}^{n_T-1} \left\{ (-1)^u \, \mathrm{C}_u^{n_T-1} \, e^{-uy} \sum_{t=0}^{(n_RK-1)u} \beta_{u,t} y^t \right\}, \tag{3.42}$$

where $\beta_{u,t}$ is the coefficient resulting from the multinomial expansion of $\left(\sum_{s=0}^{n_RK-1} y^s / s! \right)^u$, i.e., $\left(\sum_{s=0}^{n_RK-1} y^s / s! \right)^u = \sum_{t=0}^{(n_RK-1)u} \beta_{u,t} y^t$. Consequently, the expected value of $\varepsilon_{\mathbf{H}}\{w_{\hat{i}}\}$ is calculated as

$$\begin{aligned} \varepsilon_{\mathbf{H}}\{w_{\hat{i}}\} &= \int_0^{+\infty} y f_N(y) dy \\ &= \int_0^{+\infty} \left(y \frac{n_T}{(n_RK-1)!} e^{-y} y^{n_RK-1} \sum_{u=0}^{n_T-1} \left\{ (-1)^u \, \mathrm{C}_u^{n_T-1} \, e^{-uy} \sum_{t=0}^{(n_RK-1)u} \beta_{u,t} y^t \right\} \right) dy \\ &= \frac{n_T}{(n_RK-1)!} \sum_{u=0}^{n_T-1} \left\{ (-1)^u \, \mathrm{C}_u^{n_T-1} \sum_{t=0}^{(n_RK-1)u} \beta_{u,t} \int_0^{+\infty} y^{n_RK+t} e^{-(u+1)y} dy \right\} \\ &= \frac{n_T}{(n_RK-1)!} \sum_{u=0}^{n_T-1} \left\{ (-1)^u \, \mathrm{C}_u^{n_T-1} \sum_{t=0}^{(n_RK-1)u} \beta_{u,t} (n_RK+t)! (u+1)^{-n_RK-t-1} \right\}, \end{aligned} \tag{3.43}$$

where, in the last equality, we have used the integral of $\int_0^{+\infty} x^n e^{-\mu x} dx = n!\mu^{-n-1}$ [103]. By substituting Eq. (3.43) into Eq. (3.20), we obtain Eq. (3.21). This completes the proof.

3.C Optimisation Problem Formulation for the Optimal Number of Antennas

In this section, we determine the optimum number of equipped antennas in per-subcarrier antenna selection systems for maximal energy efficiency. The energy-efficiency in a per-subcarrier antenna selection system is derived in Eq. (3.16). Note that this value EE^{per} is the energy-efficiency corresponding to a *Tx*-*Rx* distance of *d*, i.e., $\bar{\rho} = \bar{\rho}(d)$. Let $\bar{\rho}_{\max} = \bar{\rho}(d_{\min})$ and $\bar{\rho}_{\min} = \bar{\rho}(d_{\max})$ denote the largest and smallest average received SNR within the coverage area, respectively. To find out the optimum number of antennas n_T^{opt} that is equipped on the transmitter, the energy-efficiency needs to be evaluated for all possible values of $\bar{\rho}$, i.e., $\forall \bar{\rho} \in [\bar{\rho}_{\min}, \bar{\rho}_{\max}]$. Let $n_T^{\max}$ and $n_T^{\min}$ denote the maximum and minimum numbers of built-in transmit antennas, respectively. Then, the optimisation problem can be expressed as

$$n_T^{opt} = \arg \max_{n_T^{\min} \le n_T \le n_T^{\max}} \frac{\varepsilon_{\bar{\rho}}\{\varepsilon_{\mathbf{H}}\{\log_2(1+\bar{\rho}g_{\hat{i}})\}\}}{P_T/\eta + n_T P_{ctx} + n_R P_{crx} + P_{bb}}. \tag{3.44}$$

In order to solve Eq. (3.44), we first need to explicitly express the term $\varepsilon_{\bar{\rho}}\{\varepsilon_{\mathbf{H}}\{\log_2(1+\bar{\rho}g_{\hat{i}})\}\}$ as a function of n_T (see *Proposition* 3.3 below). The optimal value of n_T^{opt} is then obtained by exhaustive search or bisection search algorithms.

Proposition 3.3 *A closed-form expression of the expected value* $\varepsilon_{\bar{\rho}}\{\varepsilon_{\mathbf{H}}\{\log_2(1+\bar{\rho}g_{\hat{i}})\}\}$ *with* $n_R \ge 2$ *is given as*

$$\varepsilon_{\bar{\rho}}\{\varepsilon_{\mathbf{H}}\{\log_2(1+\bar{\rho}g_{\hat{i}})\}\} = \frac{n_T}{(n_R-1)!(\bar{\rho}_{\max}-\bar{\rho}_{\min})\ln 2} \sum_{u=0}^{n_T-1} \left\{ (-1)^u \mathrm{C}_u^{n_T-1} \times \sum_{q=0}^{(n_R-1)u} \left(\alpha_{u,q} \left[Q(n_R+q-2, \bar{\rho}_{\max}) - Q(n_R+q-2, \bar{\rho}_{\min}) \right.\right.\right.$$
$$\left.\left.\left. + \bar{\rho}_{\max} Q(n_R+q-1, \bar{\rho}_{\max}) - \bar{\rho}_{\min} Q(n_R+q-1, \bar{\rho}_{\min}) - (\bar{\rho}_{\max}-\bar{\rho}_{\min})(n_R+q-1)!(u+1)^{-n_R-q} \right] \right) \right\}, \tag{3.45}$$

where $\alpha_{u,q}$ *denotes the multinomial coefficient, and*

$$Q(n,\overline{\rho}) = \frac{n!}{\overline{\rho}^{n+1}} e^{(u+1)/\rho} \sum_{s=1}^{n+1} \left(\frac{u+1}{\overline{\rho}}\right)^{-s} \Gamma\left(-n-1+s, \frac{u+1}{\overline{\rho}}\right). \tag{3.46}$$

Proof: Let us assume that the average SNR $\overline{\rho}$ is uniformly distributed on $[\overline{\rho}_{\min}, \overline{\rho}_{\max}]$, the pdf of $\overline{\rho}$ is given as

$$f(\overline{\rho}) = 1/(\overline{\rho}_{\max} - \overline{\rho}_{\min}), \ \forall \overline{\rho} \in [\overline{\rho}_{\min}, \overline{\rho}_{\max}]. \tag{3.47}$$

The expected value of $\varepsilon_{\overline{\rho}}\{\varepsilon_{\mathbf{H}}\{\log_2(1+\overline{\rho}g_{\hat{i}})\}\}$ can be calculated as (cf. Eq. (3.38))

$$\begin{aligned}
&\varepsilon_{\overline{\rho}}\{\varepsilon_{\mathbf{H}}\{\log_2(1+\overline{\rho}g_{\hat{i}})\}\} \\
&= \int_{\overline{\rho}_{\min}}^{\overline{\rho}_{\max}} \int_0^{+\infty} \log_2(1+\overline{\rho}x) f_M(x) f(\overline{\rho}) dx d\overline{\rho} = \int_0^{+\infty} \left[\int_{\overline{\rho}_{\min}}^{\overline{\rho}_{\max}} \log_2(1+\overline{\rho}x) f(\overline{\rho}) d\overline{\rho} \right] f_M(x) dx \\
&= \frac{1}{(\overline{\rho}_{\max} - \overline{\rho}_{\min}) \ln 2} \int_0^{+\infty} \left[\left(\frac{1}{x} + \overline{\rho}_{\max}\right) \ln(1+\overline{\rho}_{\max} x) - \left(\frac{1}{x} + \overline{\rho}_{\min}\right) \ln(1+\overline{\rho}_{\min} x) - (\overline{\rho}_{\max} - \overline{\rho}_{\min}) \right] f_M(x) dx \\
&= \frac{n_T}{(n_R-1)!(\overline{\rho}_{\max} - \overline{\rho}_{\min}) \ln 2} \sum_{u=0}^{n_T-1} \left\{ (-1)^u C_u^{n_T-1} \sum_{q=0}^{(n_R-1)u} \left(\alpha_{u,q} \times \left[Q(n_R+q-2, \overline{\rho}_{\max}) + \overline{\rho}_{\max} Q(n_R+q-1, \overline{\rho}_{\max}) \right. \right. \right. \\
&\qquad \left. \left. \left. - Q(n_R+q-2, \overline{\rho}_{\min}) - \overline{\rho}_{\min} Q(n_R+q-1, \overline{\rho}_{\min}) - (\overline{\rho}_{\max} - \overline{\rho}_{\min}) T \right] \right) \right\},
\end{aligned} \tag{3.48}$$

where [103]

$$Q(n,\overline{\rho}) := \int_0^{+\infty} \ln(1+\overline{\rho}x) x^n e^{-(u+1)x} dx = \frac{n!}{\overline{\rho}^{n+1}} e^{(u+1)/\overline{\rho}} \sum_{s=1}^{n+1} \left(\frac{u+1}{\overline{\rho}}\right)^{-s} \Gamma\left(-n-1+s, \frac{u+1}{\overline{\rho}}\right), n \geq 0, \tag{3.49}$$

and

$$T := \int_0^{+\infty} x^{n_R+q-1} e^{-(u+1)x} dx = (n_R+q-1)!(u+1)^{-n_R-q}. \tag{3.50}$$

Chapter 4

Antenna Selection for MIMO-OFDM Systems in the Presence of Nonlinear Distortions

In Chapter 3, antenna selection strategies for MIMO-OFDM systems have been studied from an energy efficiency perspective, in which power amplifiers are assumed ideal. This chapter investigates antenna selection MIMO-OFDM systems that suffer from nonlinear distortions due to power amplifiers (PA). An optimal constrained antenna subset selection scheme is proposed for the MIMO-OFDM systems to improve energy efficiency. This chapter is organized as follows. In Section 4.1, the related works and motivation are presented. In Section 4.2, an antenna selection MIMO-OFDM system model with nonlinear PAs is described. In Section 4.3, per-subcarrier antenna subset selection criterion is investigated in the systems suffering nonlinear distortions. In Section 4.4, an optimisation problem for data subcarrier allocation with power balancing is formulated. Performance analysis is carried out in Section 4.5. Simulation results are provided in Section 4.6. Finally, Section 4.7 concludes the chapter.

4.1 Introduction

Chapter 3 has shown that antenna selection methods that consist of a per-subcarrier selection operation, i.e., conventional per-subcarrier selection, combined selection, and adaptive selection, achieve high energy efficiency in the high spectral-efficiency regime. However, when antennas are selected independently for each subcarrier, a large number of data symbols may be allocated to some particular antennas. The input signal powers of the high power amplifiers (PAs) associated with these antennas might be very large, whereas those at the other antennas might be small. As a result, the PAs on some antennas may operate in their inefficient power regions due to the small average powers of the input signals. Meanwhile, on the other antennas, nonlinear distortions, including in-band and out-of-band distortions, are occurred when the very large signal powers pass thought the PAs. The in-band distortion degrades error-performance and

system capacity, whereas the out-of-band distortion arising from the spectral broadening effect of the PAs interferes the systems operating in the adjacent channels [104, 105].

It is obvious that the unbalance allocation of data subcarriers associated with the conventional per-subcarrier antenna selection scheme reduces the potential benefits of the antenna selection OFDM systems. One possible approach to deal with this problem is selecting transmit antennas under a constraint that the number of data subcarriers allocated to each antenna is equal. As a balance constraint is required, the constrained selection (i.e., power-balance selection) scheme should retain the benefits in terms of error-performance or capacity as large as possible. Some research works have studied the constrained selection approach in the literature, such as [83-85]. In [83, 85], allocation algorithms were developed to realize the constrained selection scheme. Meanwhile, the authors in [84] considered linear optimisation to devise their constrained selection scheme. It was shown that the selection scheme based on optimisation could offer a better performance than the suboptimal solutions in [83, 85]. However, the formulated optimisation problem in [13] is only applicable to OFDM systems where one antenna is active on each subcarrier. More importantly, all the existing works about constrained antenna selection, e.g., [83-85], only consider the effects of nonlinear PAs on the error-performance by means of simulations. This approach obviously has some limitations as it does not fully provide insight into the system characteristics. In particular, the question about whether antenna selection criteria originally derived in linear channels are still effective in nonlinear channels has not been addressed. This issue is of importance as the occurrence of nonlinear distortions may have impacts on the antenna selection criteria. Besides, the benefits in terms of error performance and/or capacity of the power-balance selection over the conventional scheme have not been analysed directly for the systems suffering nonlinear distortions due to PAs. It is clearly worth performing such an analysis given that the efficacy of power-balance selection over its counterpart comes from the PA nonlinearity. In addition, [83-85] only considered antenna selection schemes where data are transmitted from one antenna on each subcarrier. Thus, the achieved spectral efficiency was limited. To fulfil the expectation of delivering very fast data speeds for future wireless applications, antennas subset selection, where multiple data symbols are transmitted simultaneously from multiple antennas on each subcarrier, should be investigated.

In this chapter, a constrained per-subcarrier antenna subset selection is proposed for MIMO-OFDM systems in the presence of nonlinear distortions for improved energy efficiency. The main contributions of this chapter are summarised as follows.

i) A non-causal problem associated with the implementation of conventional per-subcarrier antenna selection in MIMO-OFDM systems suffering nonlinear distortions is identified.

ii) An efficient constrained antenna subset selection scheme is proposed for MIMO-OFDM systems to overcome the drawbacks of the conventional scheme. The proposed scheme is realized based on a linear optimisation problem that is formulated in systems with an arbitrary number of multiplexed data streams.

iii) A reduced-complexity strategy that simultaneously requires a smaller number of feedback bits and lower computational effort to solve the optimisation problem is proposed by exploiting the channel correlation between adjacent OFDM subcarriers.

iv) The efficacy of the proposed antenna selection approach over the conventional approach is analysed directly in the nonlinear fading channels. Specifically, we show that the average mean-squared error (MSE) and energy efficiency in the proposed system with a constrained selection are better than those in its counterpart.

Numerical results are also provided to verify the analyses and demonstrate the improvement in terms of energy efficiency in the proposed system.

4.2 Antenna Selection MIMO-OFDM Systems with Nonlinear Power Amplifiers

4.2.1 Transmitter

Let us consider a MIMO-OFDM system with K subcarriers, n_T transmit antennas, and n_R receive antennas as shown in Figure 4.1. At the transmitter, the input data are demultiplexed into n_D independent streams, where $n_D \le n_T$ and $n_D \le n_R$. Each data bit stream is then mapped onto M-PSK (M-ary Phase Shift Keying) or M-QAM (M-ary Quadrature Amplitude Modulation) constellation. Denote q_u^k and x_i^k, $1 \le u \le n_D, 1 \le i \le n_T, 0 \le k \le K-1,$ to be the symbols that the subcarrier allocation block takes at its u^{th} input and outputs at its i^{th} output, respectively. The allocation block assigns the elements of $\mathbf{q}_k = [q_1^k, q_2^k, ..., q_{n_D}^k]^T$ to n_D selected antennas at the k^{th} subcarrier, based on feedback information. As a result, only n_D elements in a vector

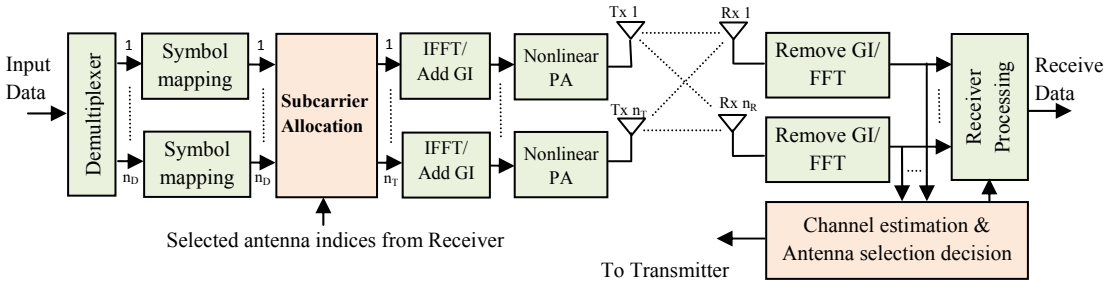

Figure 4.1. A simplified block diagram of antenna selection MIMO-OFDM system.

$\mathbf{x}_k = [x_1^k, x_2^k, ..., x_{n_T}^k]^T$ are assigned values from $\mathbf{q}_k$, whereas the others are zeros. Here, it is assumed that $\varepsilon\{\mathbf{q}_k \mathbf{q}_k^H\} = \sigma^2 \mathbf{I}_{n_D}$. The output sequences from the subcarrier allocation block are then fed into *K*-point IFFT (inverse fast Fourier transform) blocks. In this paper, the Nyquist sampling signal is considered. Thus, the discrete-time baseband OFDM signals can be expressed as

$$s_i(n) = \frac{1}{\sqrt{K}} \sum_{k=0}^{K-1} x_i^k e^{j2\pi nk/K},\ 0 \le n \le K-1,\ 1 \le i \le n_T. \tag{4.1}$$

Many power amplifier models, such as Saleh model, SSPA (or Rapp) model, or SEL (soft envelope limiter) model, can be adopted in this system. However, we only consider the SEL model in this work for simplicity. Moreover, the SEL could model the state-of-the-art amplifier designs [104]. The n^{th} output sample from the SEL is given by [106]

$$\widetilde{s}_i(n) = \begin{cases} s_i(n) & , \text{if } |s_i(n)| \le \sqrt{P_{o,sat}} \\ \sqrt{P_{o,sat}}\, e^{\angle s_i(n)} & , \text{if } |s_i(n)| > \sqrt{P_{o,sat}} \end{cases}, \tag{4.2}$$

where $P_{o,sat}$ is the output saturation power level of PAs, $|s_i(n)|$ and $\angle s_i(n)$ denote the magnitude and phase of $s_i(n)$, respectively. Also, it is assumed that $P_{o,sat} = P_{i,sat}$, where $P_{i,sat}$ is the input saturation power level.

For analytical tractability, let us assume that the signals $s_i(n)$ are asymptotically independent and identically distributed (i.i.d.) Gaussian random variables. Note that this assumption, which is based on the central limit theorem [107], only holds when the number of data subcarriers on the i^{th} antenna, denoted as K_i, is large enough. By using Bussgang's theorem [108], the output of the nonlinear PAs can be expressed as [106]

$$\widetilde{s}_i(n) = \alpha_i s_i(n) + \eta_i(n), \tag{4.3}$$

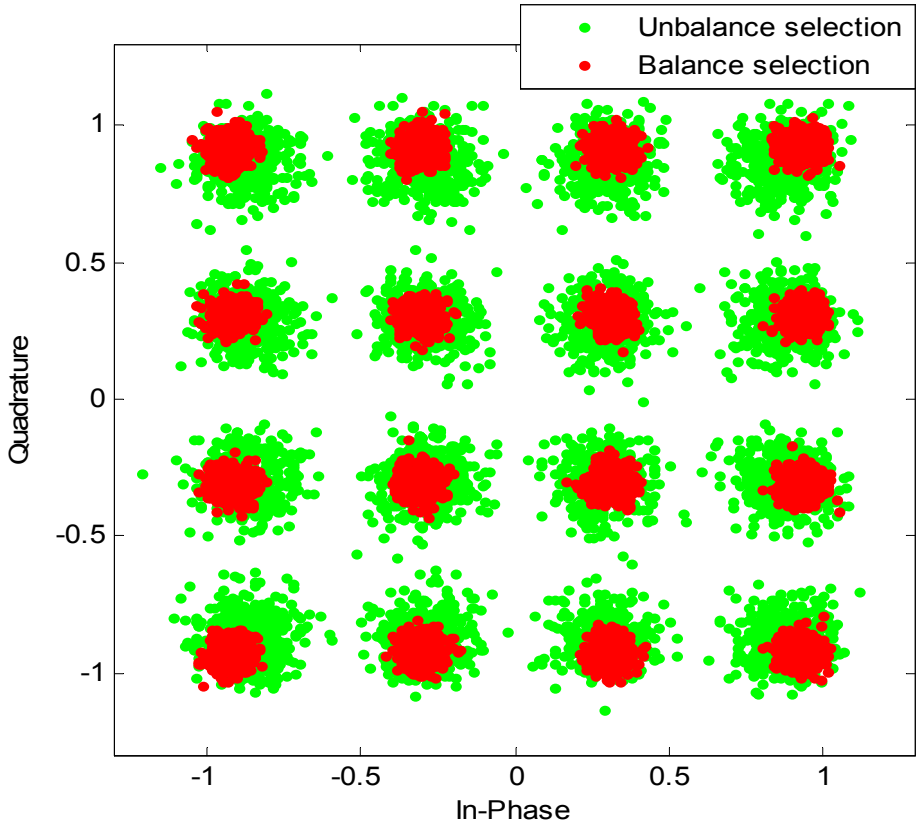

Figure 4.2. Constellation diagrams of estimated 16-QAM data symbols: balance selection versus unbalance selection.

where α_i is a scale factor, and $\eta_i(n)$ represents time-domain distortion noise that is uncorrelated with $s_i(n)$. The factor α_i and the variance $\sigma_{\eta_i}^2$ of $\eta_i(n)$ are, respectively, given by [106]

$$\alpha_i = \frac{\varepsilon\{s_i(n)\tilde{s}_i^*(n)\}}{\varepsilon\{|s_i(n)|^2\}} = 1 - e^{-\vartheta_i^2} + \frac{\sqrt{\pi}}{2}\vartheta_i \operatorname{erfc}(\vartheta_i), \tag{4.4}$$

and

$$\sigma_{\eta_i}^2 = \varepsilon\{|\tilde{s}_i(n)|^2\} - \alpha_i^2\varepsilon\{|s_i(n)|^2\} = \sigma_{K_i}^2[1 - e^{-\vartheta_i^2} - \alpha_i^2], \tag{4.5}$$

where $\sigma_{K_i}^2 := \varepsilon\{|s_i(n)|^2\} = \sigma^2 K_i/K$ is the average power of the input signal of the PA on the i^{th} antenna, $\vartheta_i = \sqrt{P_{i,sat}/\sigma_{K_i}^2}$ is the clipping ratio, and $erfc(x) = \frac{2}{\sqrt{\pi}}\int_x^\infty e^{-t^2}dt$ is a complementary error function. Note that $\sum_{i=1}^{n_T} K_i = n_D K$, thus $\sum_{i=1}^{n_T}\sigma_{K_i}^2 = n_D\sigma^2$. In the system where the same number of data subcarriers is allocated to all antennas, we have $K_i = n_D K/n_T := \overline{K}, \forall i = 1,2,...,n_T$, and $\sigma_{K_i}^2 = n_D\sigma^2/n_T := \sigma_{\overline{K}}^2, \forall i = 1,2,...,n_T$. An input

power back-off (*IBO*) of the PA is defined as $IBO_i = P_{i,sat} \big/ \sigma_{K_i}^2$. Also, all PAs are assumed to have the same nonlinear behaviour. To illustrate the impacts of nonlinear distortions due to nonlinear PAs on transmitted data symbols in the antenna selection OFDM system, we plot in Figure 4.2 the constellation diagrams of 16-QAM symbols in two scenarios: unbalance allocation and balance allocation of data subcarriers. It can be seen that, although the nonlinear distortions is presence in both scenarios, the data symbols in the scenario of imbalance data-subcarrier allocation is more distorted than those in the other scenario. In other words, the level of nonlinear distortion is smallest when data subcarriers are equally allocated across transmit antennas.

4.2.2 Receiver

At the receiver, the received signal at each antenna is fed into the FFT block after the GI (guard interval) is removed. The system model in the frequency domain corresponding to the k^{th} subcarrier can be expressed as [109]

$$\mathbf{y}_k = \mathbf{H}_k \boldsymbol{\alpha} \mathbf{x}_k + \mathbf{H}_k \mathbf{d}_k + \mathbf{n}_k = \underline{\mathbf{H}}_k \underline{\boldsymbol{\alpha}} \underline{\mathbf{q}}_k + \underline{\mathbf{H}}_k \underline{\mathbf{d}}_k + \mathbf{n}_k, \tag{4.6}$$

where

$$\mathbf{x}_k = \begin{bmatrix} x_1^k & x_2^k & \dots & x_{n_T}^k \end{bmatrix}^T, \tag{4.7}$$

$$\mathbf{H}_k = \begin{bmatrix} h_{1,1}^k & h_{1,2}^k & \dots & h_{1,n_T}^k \\ h_{2,1}^k & h_{2,2}^k & \dots & h_{2,n_T}^k \\ \dots & \dots & \dots & \dots \\ h_{n_R,1}^k & h_{n_R,2}^k & \dots & h_{n_R,n_T}^k \end{bmatrix}, \tag{4.8}$$

$$\boldsymbol{\alpha} = \text{diag}([\alpha_1 \quad \alpha_2 \quad .... \quad \alpha_{n_T}]), \tag{4.9}$$

$$\mathbf{d}_k = \begin{bmatrix} d_1^k & d_2^k & \dots & d_{n_T}^k \end{bmatrix}^T, \tag{4.10}$$

$$\mathbf{n}_k = \begin{bmatrix} n_1^k & n_2^k & \dots & n_{n_R}^k \end{bmatrix}^T, \tag{4.11}$$

$$\mathbf{y}_k = \begin{bmatrix} y_1^k & y_2^k & \dots & y_{n_R}^k \end{bmatrix}^T. \tag{4.12}$$

In the above equations, $h_{j,i}^k$ indicates the channel coefficient between the i^{th} transmit antenna and the j^{th} receive antenna. d_i^k denotes the frequency-domain distortion noise at the i^{th} transmit antenna. Also, y_j^k and n_j^k denote the received signal and the thermal

noise at the j^{th} receive antenna, respectively. The effective channel matrix $\underline{\mathbf{H}}_k$, the effective scale factor $\underline{\boldsymbol{\alpha}} = \text{diag}([\underline{\alpha}_1\ \underline{\alpha}_2 \ldots \underline{\alpha}_{n_D}])$, and the effective distortion noise $\underline{\mathbf{d}}_k = [\underline{d}_1^k\ \underline{d}_2^k \ldots \underline{d}_{n_D}^k]^T$ are obtained by eliminating the columns of $\mathbf{H}_k$, the rows of $\boldsymbol{\alpha}$, and the elements of $\mathbf{d}_k$ that are corresponding to the unselected transmit antennas, respectively. The distortion noise d_i^k can be modelled as a zero-mean complex Gaussian random variable with variance $\sigma_{d_i}^2 = \sigma_{\eta_i}^2$ (i.e., $\sigma_{d_i}^2$ is equal to that of the time-domain distortion noise). Note that, as clipping is performed on the Nyquist-rate samples, all the subcarriers on the i^{th} antenna experience the same attenuation α_i and the variance $\sigma_{d_i}^2$ [106]. Therefore, the factors of $\boldsymbol{\alpha}$ and $\underline{\boldsymbol{\alpha}}$, the variance of $\mathbf{d}$, denoted as $\boldsymbol{\sigma}_d^2 = \text{diag}([\sigma_{d_1}^2\ \sigma_{d2}^2 \ldots \sigma_{d_{nT}}^2])$, and the variance of $\underline{\mathbf{d}}$, denoted as $\boldsymbol{\sigma}_{\underline{d}}^2 = \text{diag}([\sigma_{\underline{d}_1}^2\ \sigma_{\underline{d}_2}^2 \ldots \sigma_{\underline{d}_{n_D}}^2])$, are the same for all subcarriers. Here, the index k associated with α_i and $\sigma_{d_i}^2$ are dropped for simplicity. The thermal noise is modelled as a Gaussian random variable with zero mean and $\varepsilon\{\mathbf{n}_k \mathbf{n}_k^H\} = \sigma_n^2 \mathbf{I}_{n_R}$. Also, it is assumed that per-subcarrier power loading is not an option due to the limited feedback rate and the strict regulation of a power spectral mask, such as in ultra-wide band (UWB) systems.

Several MIMO detection techniques can be employed in this system to detect signals. For simplicity, we only consider a ZF (zero-forcing) receiver. Supposed that the perfect channel state information is available at the receiver, the equalized signal at the k^{th} subcarrier is computed as [14]

$$\widetilde{\mathbf{q}}_k = \mathbf{G}_k^{+}\mathbf{y}_k = \mathbf{q}_k + \underline{\boldsymbol{\alpha}}^{-1}\underline{\mathbf{d}}_k + \mathbf{G}_k^{+}\mathbf{n}_k, \tag{4.13}$$

where $\mathbf{G}_k = \underline{\mathbf{H}}_k \underline{\boldsymbol{\alpha}}$ and $\mathbf{G}_k^{+} = (\mathbf{G}_k^H \mathbf{G}_k)^{-1}\mathbf{G}_k^H$ denotes the Moore-Penrose pseudo-inverse of a matrix $\mathbf{G}_k$. It can be seen from Eq. (4.13) that the estimated symbols consist of the desired component $\mathbf{q}_k$, the distortion noise after equalization $\underline{\boldsymbol{\alpha}}^{-1}\underline{\mathbf{d}}_k$, and the thermal noise after equalization $\mathbf{G}_k^{+}\mathbf{n}_k$. Note that to characterize the impacts of nonlinear distortions on the system performance, many other physical layer impairments, such as channel estimation error or I/Q imbalance, have not taken into consideration in this work. For the case of existing errors in channel estimation, the readers are referred to

Table 4.1. Antenna subsets (n_T = 4, n_D = 2, and Γ = 6)

γ	$\mathbf{\Gamma}_\gamma$
1	{1,2}
2	{1,3}
3	{1,4}
4	{2,3}
5	{2,4}
6	{3,4}

[110], where the performance of a MIMO system in the presence of both nonlinear distortions and channel estimation errors is investigated. Although [110] did not consider antenna selection OFDM systems, the obtained results are useful for analysing this system.

4.3 Conventional per-subcarrier antenna selection criterion in the presence of nonlinear distortions

4.3.1 Per-Subcarrier Antenna Subset Selection Criteria

In a MIMO-OFDM system with conventional per-subcarrier subset selection, antenna subsets are selected independently for each subcarrier. On each subcarrier, only n_D antennas out of n_T available transmit antennas are active. Denote $\mathbf{\Gamma}_\gamma, \gamma = 1,2,...,\Gamma,$ to be the γ^{th} subset consisting of n_D selected antennas, where $\Gamma = C_{n_D}^{n_T} = n_T!/n_D!(n_T - n_D)!$ is the number of all possible n_D-element subsets. Each subset consists of n_D transmit antenna indices that are chosen based on the feedback information from the receiver. For example, when n_T = 4 and n_D = 2, then Γ = 6, and all possible subsets $\mathbf{\Gamma}_\gamma, \gamma = 1,2,...,6$ are defined in the Table 4.1. The choice of the best antenna subset depends on a particular antenna selection criterion.

Several antenna selection criteria that originally derived in linear channels, such as MMSE (minimum mean-squared error) [82], maximum capacity [56], or maximum SNR (signal-to-noise ratio) [56] can be extended to this system. For brevity, only the MMSE criterion is analysed in this chapter. The MMSE criterion selects the best antenna subset from the viewpoint of minimum mean-squared error (i.e., minimising the Euclidean distance between the estimated symbols and the transmit symbols). Therefore, it also aims to minimise the error rate. When a ZF receiver is used, the error covariance matrix corresponding to the k^{th} subcarrier and the subset $\mathbf{\Gamma}_\gamma$ is computed as

$$\begin{aligned}\mathbf{MSE}_{\gamma}^{k} &= \varepsilon\left\{(\tilde{\mathbf{q}}_k - \mathbf{q}_k)(\tilde{\mathbf{q}}_k - \mathbf{q}_k)^H\right\} = \varepsilon\left\{(\underline{\boldsymbol{\alpha}}^{-1}\underline{\mathbf{d}}_k + \mathbf{G}_k^{+}\mathbf{n}_k)(\underline{\boldsymbol{\alpha}}^{-1}\underline{\mathbf{d}}_k + \mathbf{G}_k^{+}\mathbf{n}_k)^H\right\} \\ &= \varepsilon\left\{(\underline{\boldsymbol{\alpha}}^{-1}\underline{\mathbf{d}}_k)(\underline{\boldsymbol{\alpha}}^{-1}\underline{\mathbf{d}}_k)^H\right\} + \varepsilon\left\{(\mathbf{G}_k^{+}\mathbf{n}_k)(\mathbf{G}_k^{+}\mathbf{n}_k)^H\right\} = \boldsymbol{\sigma}_{\underline{\tilde{d}}}^2 + \sigma_n^2(\mathbf{G}_k^H\mathbf{G}_k)^{-1}, \end{aligned} \tag{4.14}$$

where $\boldsymbol{\sigma}_{\underline{\tilde{d}}}^2 = \mathrm{diag}\left(\left[\frac{\sigma_{\underline{d}_1}^2}{\underline{\alpha}_1^2} \ \frac{\sigma_{\underline{d}_2}^2}{\underline{\alpha}_2^2} \ldots \frac{\sigma_{\underline{d}_{nD}}^2}{\underline{\alpha}_{nD}^2}\right]\right)$. Note that the third equality comes from the fact that the distortion noise and the thermal noise are independent. Recall that the mean-squared error (MSE) between the estimated symbols and the transmitted symbols is the trace of an error covariance matrix. Hence, the selected subset at the k^{th} subcarrier is determined by minimising the trace of the MSE matrix, i.e.,

$$\boldsymbol{\Gamma}_{\gamma}(k) = \arg\min_{\gamma=1,\ldots,\Gamma} \mathrm{tr}\{\mathbf{MSE}_{\gamma}^{k}\}. \tag{4.15}$$

From Eq. (4.15), we draw two important remarks with respect to the deployment of per-subcarrier antenna selection in the MIMO-OFDM systems in the presence of nonlinear distortions.

1) If the same number of data subcarriers is allocated to all transmit antennas, OFDM symbols in all antennas experience the same distortion characteristics (cf. Eq. (4.3)-Eq. (4.5)). Therefore, Eq. (4.15) can be simplified to as

$$\boldsymbol{\Gamma}_{\gamma}(k) = \arg\min_{\gamma=1,\ldots,\Gamma} \sigma_n^2 \,\mathrm{tr}\{(\mathbf{G}_k^H\mathbf{G}_k)^{-1}\} = \arg\min_{\gamma=1,\ldots,\Gamma} \mathrm{tr}\{(\underline{\mathbf{H}}_k^H\underline{\mathbf{H}}_k)^{-1}\}, \tag{4.16}$$

   which is similar to that in the systems with ideal PAs.

2) On the other hand, if the above condition is not satisfied, per-subcarrier antenna selection criteria, e.g., MMSE criterion in Eq. (4.15), cannot be realized due to a non-causal problem. The non-causality arises because the selection of antenna subset for each subcarrier, i.e., calculating a metric $\mathbf{MSE}_{\gamma}^{k}$, requires the values $\underline{\boldsymbol{\alpha}}$ and $\boldsymbol{\sigma}_{\underline{\tilde{d}}}^2$. Meanwhile, the calculations of these two values require the total number of data subcarriers assigned on each antenna to be known. To realize per-subcarrier antenna selection, the criterion in Eq. (4.16) could be applied. However, as shown in Eq. (4.14) and Eq. (4.15), when the impacts of nonlinear PAs are ignored, the selected antenna subset may not be the one that could obtain minimum MSE. Thus, the optimality of the selection criterion in terms of minimum MSE might not be fully achieved.

4.3.2 Feedback Considerations

With respect to a feedback mechanism used in this system, the selected antenna indices could be directly transmitted through reverse links in a TDD (time-division duplex) mode. In addition, it is typical in indoor wireless applications that the channel might not be changed during the transmission of several consecutive frames. In that scenario, the transmitter will reallocate data subcarriers according to the updated feedback information. Finally, in MIMO-OFDM systems with large values of Γ and/or K, the number of feedback bits might be high. Reduced feedback could be realized by combining subcarriers into a cluster and using only one antenna subset for all subcarriers in the cluster. This is due to the fact that neighbouring subcarriers within each OFDM symbol are correlated. Therefore, it is likely that an optimal antenna subset for a particular subcarrier remains optimal for its neighbour subcarriers. If the cluster size is L, the number of feedback bits is reduced by $1/L$. We propose the following criterion for choosing a proper subset for the m^{th} cluster, $1 \le m \le M, M = K/L$,

$$\mathbf{\Gamma}_{\gamma}(m) = \arg \min_{\gamma=1,\ldots,\Gamma} \left\{ \sum_{k=(m-1)L+1}^{mL} \text{tr}\{\mathbf{MSE}_{\gamma}^{k}\} \right\}. \tag{4.17}$$

Note that the choice of value L is a matter of trade-off between feedback overhead and error performance. Moreover, the value L is chosen based on the correlation characteristic of the channel frequency response. In MIMO-OFDM systems, the cross-correlation coefficients between two arbitrary subcarriers k_1 and k_2 can be expressed as [111]

$$\begin{aligned} \rho_{k_1-k_2} &= \varepsilon\left\{[\mathbf{H}_{k_1}]_{i_1,j_1}[\mathbf{H}_{k_2}]^{*}_{i_2,j_2}\right\} \\ &= \sum_{t=0}^{T-1} \varphi_t^2 e^{-j2\pi(k_1-k_2)t/K} \delta(i_1-i_2)\delta(j_1-j_2), \forall i_1, i_2 \in 1,\ldots,n_R; \forall j_1, j_2 \in 1,\ldots,n_T, \end{aligned} \tag{4.18}$$

where $[\mathbf{H}_k]_{i,j}$ denotes the $(i,j)^{\text{th}}$ entry of the matrix $\mathbf{H}_k$, $\varphi_t, t = 0,1,\ldots,T-1,$ denotes the normalized channel power delay profile, i.e., $\sum_{t=0}^{T-1} \varphi_t^2 = 1$, and $\delta(.)$ is the Kronecker-delta function. It can be seen from Eq. (4.18) that the frequency correlation coefficients depend on the difference between subcarriers (k_1-k_2), rather than on the subcarriers themselves. Thus, given $\rho_{k_1-k_2}$, we can estimate (k_1-k_2). In other words, the number of subcarriers in one cluster (i.e., the value of L) can be estimated given the level of cross-correlation among subcarriers within a cluster. The study of optimal designs regarding

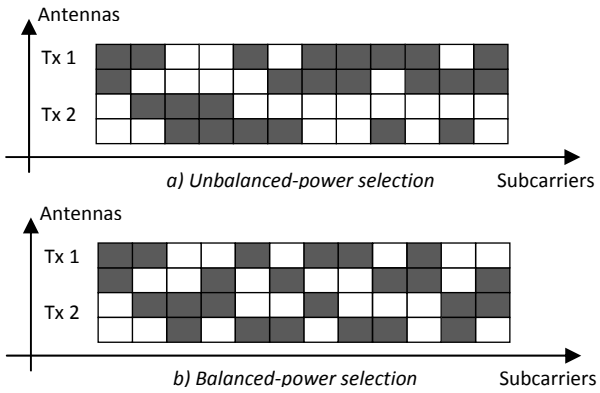

Figure 4.3. Illustration of per-subcarrier antenna subset selection **.** ($n_T = 4$, $n_D = 2$, and $K = 12$).

feedback reduction (e.g., deriving an optimal value of L with respect to error performance-feedback rate trade-off) is beyond the scope of this work. The readers are referred to, e.g., [112, 113], for this topic of research.

4.4 Per-Subcarrier based Antenna Selection with Power Balancing

In Section 4.3, we have developed per-subcarrier transmit antenna subset selection for the MIMO-OFDM system with nonlinear PAs. As the conventional selection scheme selects the best antenna subset for each subcarrier, the number of data subcarriers assigned to each transmit antenna within one OFDM symbol period might be significantly different depending on the channel conditions. Hence, the average input power of PAs might vary significantly between OFDM symbol periods as well as among antennas. When input powers on some antennas are small, the power efficiencies of the corresponding PAs are reduced. On the other hand, large input powers result in severe distortion of signal. In this case, power back-off is required. However, the back-off will degrade the system performance. In addition, the imbalance allocation of data subcarriers on antennas leads to the non-causality as discussed in Section 4.3. It is intuitive that these problems can be avoided if the same number of data subcarriers is allocated to all transmit antennas, as illustrated in Figure 4.3. When a balance selection of data subcarriers is required, the designed selection scheme should retain the benefits in terms of capacity or error performance as large as possible. To this end, we formulate a linear optimisation problem to realize such a scheme.

As mentioned in the Introduction, the linear optimization approach was considered for an OFDM system with $n_D = 1$ in [84]. Before proceeding to formulating a

generalized optimisation problem for systems with $n_D \geq 1$, we make some evaluations with respect to the formulated problem in [84].

1) A selection variable (i.e., optimisation variable) in [84] was defined based on an antenna basis. When $n_D > 1$, a similar definition of a selection variable will result in binary nonlinear optimisation problems. This is clearly not favourable from a practical viewpoint. As shown later in this section, binary linear optimisation could be obtained by defining a selection variable based on a subset basis.
2) Only a system with full feedback was considered in [84]. In OFDM systems with large number of subcarriers, not only a large amount of feedback information is required, but the complexity to solve the optimisation problem also becomes increased. Thus, it is of interest to formulate linear optimisation working in conjunction with feedback reduction.

In the following, linear optimisation problems are formulated for both full feedback and reduced feedback systems with an arbitrary number of data streams $n_D \geq 1$.

4.4.1 Linear optimisation problem formulation

We define a variable z_γ^k, where $z_\gamma^k = 1$ if $\mathbf{\Gamma}_\gamma$ is chosen for the k^{th} subcarrier, and $z_\gamma^k = 0$ otherwise. Also, denote c_γ^k to be the cost associated with the chosen subset $\mathbf{\Gamma}_\gamma$. The type of the cost depends on antenna selection criteria, e.g., $c_\gamma^k = \text{tr}\{\mathbf{MSE}_\gamma^k\}$ if the MMSE selection criterion is used. The total cost function can be expressed as

$$f = \sum_{k=0}^{K-1} \sum_{\gamma=1}^{\Gamma} c_\gamma^k z_\gamma^k. \tag{4.19}$$

As mentioned in Section 4.3, only n_D antennas in this system are allowed to transmit data symbols on each subcarrier. This is equivalent to choosing only one subset of n_D elements among Γ subsets $\mathbf{\Gamma}_\gamma, \gamma = 1,2,...,\Gamma,$ per subcarrier. Thus, the first constraint can be expressed as

$$\sum_{\gamma=1}^{\Gamma} z_\gamma^k = 1, \ \forall k = 0,1,...,K-1. \tag{4.20}$$

The second constraint is that all transmit antennas have the same number of allocated data subcarriers. In the case of Kn_D is not divisible by n_T, some antennas will be allowed to have one more subcarrier than others. This will guarantee that the transmit power will

be evenly distributed over the transmit antennas as much as it could. This constraint can be expressed as

$$\sum_{k=0}^{K-1} z_\gamma^k = \lambda_\gamma,\ \gamma = 1,2,...,\Gamma, \tag{4.21}$$

where the parameter λ_γ is the number of times that the subset $\mathbf{\Gamma}_\gamma$ is selected. The values λ_γ are chosen to satisfy

$$\sum_{\psi \in \mathbf{\Psi}^i} \lambda_\psi \le \left\lceil \frac{n_D K}{n_T} \right\rceil,\ i = 1,2,...,n_T, \tag{4.22}$$

where $\mathbf{\Psi}^i$ denotes a set consisting of $\binom{n_D-1}{n_T-1}$ subsets $\mathbf{\Gamma}_\gamma$ which contains the i^{th} antenna, and $\lceil a \rceil$ indicates the smallest integer that is larger than or equal to a. For example, from Table 4.1, we have $\mathbf{\Psi}^1 = \{\mathbf{\Gamma}_1, \mathbf{\Gamma}_2, \mathbf{\Gamma}_3\}$, $\mathbf{\Psi}^2 = \{\mathbf{\Gamma}_1, \mathbf{\Gamma}_4, \mathbf{\Gamma}_5\}$, $\mathbf{\Psi}^3 = \{\mathbf{\Gamma}_2, \mathbf{\Gamma}_4, \mathbf{\Gamma}_6\}$, and $\mathbf{\Psi}^4 = \{\mathbf{\Gamma}_3, \mathbf{\Gamma}_5, \mathbf{\Gamma}_6\}$. Note that if K is divisible by Γ, Eq. (4.22) can be simplified to as

$$\lambda_\gamma = \frac{K}{\Gamma},\ \forall \gamma = 1,2,...,\Gamma. \tag{4.23}$$

For instance, if n_T = 4, n_D = 2, and K = 12, then $\lambda_\gamma = \frac{12}{6} = 2,\ \forall \gamma = 1,2,...,6$. As all subsets are chosen twice, from Table 4.1, we know that each antenna has six data symbols (cf. Figure 4.3b).

The optimisation problem is now a minimisation of the cost function Eq. (4.19) subject to two constraints Eq. (4.20) and Eq. (4.21). Note that, in the system without power balancing, a problem of subcarrier allocation is equivalent to minimising Eq. (4.19) subject to the constraint Eq. (4.20) only.

In what follows, we will represent the above optimisation problem in a matrix form. Let us define two vectors $\mathbf{z} = (z_1^0 ... z_\Gamma^0 z_1^1 ... z_\Gamma^1 ... z_1^{K-1} ... z_\Gamma^{K-1})^T \in \{0,1\}^{K\Gamma \times 1}$ and $\mathbf{c} = (c_1^0 ... c_\Gamma^0 c_1^1 ... c_\Gamma^1 ... c_1^{K-1} ... c_\Gamma^{K-1})^T \in \Re^{K\Gamma \times 1}$. Then, Eq. (4.19) can be rewritten as $f = \mathbf{c}^T\mathbf{z}$. Also, the first and the second constraints can now be expressed as

$$\mathbf{A}_1 \mathbf{z} = \mathbf{1}_K, \tag{4.24}$$

where $\mathbf{A}_1 = \mathbf{I}_K \otimes \mathbf{1}_\Gamma^T \in \{0,1\}^{K \times K\Gamma}$, and

$$\mathbf{A}_2 \mathbf{z} = \boldsymbol{\lambda}, \tag{4.25}$$

where $\mathbf{A}_2 = \mathbf{1}_K^T \otimes \mathbf{I}_\Gamma \in \{0,1\}^{\Gamma \times K\Gamma}$ and $\boldsymbol{\lambda} = (\lambda_1,...,\lambda_\Gamma)^T \in \Re^{\Gamma \times 1}$. These constraints could be combined in a concise form as

$$\mathbf{Az} = \mathbf{a}, \tag{4.26}$$

where $\mathbf{A} = (\mathbf{A}_1^T, \mathbf{A}_2^T)^T \in \{0,1\}^{(K+\Gamma)\times K\Gamma}$ and $\mathbf{a} = (\mathbf{1}_K^T, \boldsymbol{\lambda}^T)^T \in \Re^{(K+\Gamma)\times 1}$. Therefore, the optimisation problem becomes

$$\min_{\mathbf{z}\in\{0,1\}^{K\Gamma\times 1}} \mathbf{c}^T\mathbf{z},$$

$$\text{subject to } \mathbf{Az} = \mathbf{a}. \tag{4.27}$$

It is obvious that Eq. (4.27) has a canonical form of a binary linear optimisation problem. Moreover, this binary optimisation problem can be relaxed to a linear programming (LP) problem that has a solution $\mathbf{z} \in \{0,1\}^{K\Gamma\times 1}$ (see Section 4.A). As a result, the optimisation problem in Eq. (4.27) can be solved efficiently by well-known linear programming methods, such as simplex methods or interior point methods [114]. When n_D = 1, the formulated problem in Eq. (4.27) is identical to the one in [84]. In addition, it is worth noting that, as the optimisation problem in Eq. (4.27) has been formulated in a way of minimising the cost, a negative sign has to be included in the cost metric if capacity or SNR criterion is used.

4.4.2 Optimisation in the system with reduced feedback

In the system with feedback reduction, an efficient approach to formulate the optimisation problem is based on a cluster basis rather than on a subcarrier basis. Let us define z_γ^m and $c_\gamma^m = \sum_{k=(m-1)L+1}^{mL} \mathrm{tr}\{\mathbf{MSE}_\gamma^k\}$ to be the variable and the cost associated with the m^{th} cluster and the subset $\boldsymbol{\Gamma}_\gamma$ that is applied to all subcarriers within the m^{th} cluster. By doing similar steps as in Section 4.4.1, we arrive at an optimisation formula similar to Eq. (4.27), excepting that:

1) The number of variables is $\Gamma K/L$, i.e., $\mathbf{z} \in \{0,1\}^{(K\Gamma/L)\times 1}$,

2) A cost vector is $\mathbf{c} \in \Re^{(K\Gamma/L)\times 1}$ and its elements are c_γ^m,

3) Matrix **A** and vector **a** in the constraint will need to be modified accordingly.

With respect to the complexity of the proposed selection scheme, we note that the complexity to solve linear optimisation using interior point methods can be reduced to

$O\left([(\Gamma K/L)^3/\ln(\Gamma K/L)]\zeta\right)$, where $O(.)$ denotes an order of complexity, and ζ is the bit size of the optimisation problem [115]. Therefore, solving the optimisation associated with reduced feedback (i.e., $L > 1$) will require much lower computational effort compared to that on a subcarrier basis (i.e., $L = 1$). As a result, the proposed system with this combined strategy could enjoy both small feedback overhead and low complexity for optimisation.

4.5 Performance Analysis

In Section 4.4, a linear optimisation problem has been formulated to realize an optimal (constrained) selection scheme from a viewpoint of minimum MSE (mean-squared error). In this section, we analyse the effectiveness of this selection scheme from MSE and energy-efficiency perspectives. Without loss of generality, it is assumed that all HPAs have the input saturation level of $P_{i,sat}$ and operate with an input back-off of $IBO = P_{i,sat}/\sigma_{\overline{K}}^2$. In the conventional (unconstrained) system, the power back-off is required on the antennas where the numbers of allocated data subcarriers are larger than $\overline{K}$, i.e., $K_i > \overline{K}$, to avoid error floor and other deleterious effects. This is equivalent to scaling the amplitudes of the signals on these antennas by a factor $\beta_i = \sqrt{\sigma_{\overline{K}}^2/\sigma_{K_i}^2} < 1$. Meanwhile, the powers of the signals on the other antennas, i.e., $K_i \le \overline{K}$, are not scaled up due to an EIRP restriction as well as the complexity of power loading.

4.5.1 Analysis of Mean-Squared Error

Let us first rewrite the received signal $\mathbf{y}_k$ in Eq. (4.6) when the back-off operation is included as

$$\mathbf{y}_k = \mathbf{H}_k\boldsymbol{\alpha}\boldsymbol{\beta}\mathbf{x}_k + \mathbf{H}_k\mathbf{d}_k + \mathbf{n}_k = \underline{\mathbf{H}}_k\underline{\boldsymbol{\alpha}}\,\underline{\boldsymbol{\beta}}\mathbf{q}_k + \underline{\mathbf{H}}_k\underline{\mathbf{d}}_k + \mathbf{n}_k, \tag{4.28}$$

where $\boldsymbol{\beta} = \mathrm{diag}([\beta_1\ \beta_2 \ldots \beta_{n_T}])$, and $\underline{\boldsymbol{\beta}} = \mathrm{diag}([\underline{\beta}_1\ \underline{\beta}_2 \ldots \underline{\beta}_{n_D}])$ is obtained by eliminating the rows of $\boldsymbol{\beta}$ that are corresponding to the unselected transmit antennas. Note that $\beta_i = 1$ if no back-off is required on the i^{th} antenna. The error covariance matrix can now be expressed as (cf. Eq. (4.14))

$$\begin{aligned}\mathbf{MSE}^k &= \varepsilon\left\{(\tilde{\mathbf{q}}_k - \mathbf{q}_k)(\tilde{\mathbf{q}}_k - \mathbf{q}_k)^H\right\} \\ &= \varepsilon\left\{\left((\underline{\boldsymbol{\alpha}}\,\underline{\boldsymbol{\beta}})^{-1}\underline{\mathbf{d}}_k\right)\left((\underline{\boldsymbol{\alpha}}\,\underline{\boldsymbol{\beta}})^{-1}\underline{\mathbf{d}}_k\right)^H\right\} + \varepsilon\left\{\left((\underline{\mathbf{H}}_k\underline{\boldsymbol{\alpha}}\,\underline{\boldsymbol{\beta}})^{+}\mathbf{n}_k\right)\left((\underline{\mathbf{H}}_k\underline{\boldsymbol{\alpha}}\,\underline{\boldsymbol{\beta}})^{+}\mathbf{n}_k\right)^H\right\}\end{aligned} \tag{4.29}$$

From Eq. (4.29), we can express the MSE corresponding to the data symbol transmitted at the u^{th} selected antenna on the k^{th} subcarrier as

$$MSE^{k,u} = \frac{\sigma_{\underline{d}_u}^2}{\underline{\alpha}_u^2 \underline{\beta}_u^2} + \frac{\sigma_n^2}{\underline{\alpha}_u^2 \underline{\beta}_u^2}[(\underline{\mathbf{H}}_k^H \underline{\mathbf{H}}_k)^{-1}]_{u,u}, \tag{4.30}$$

where $[\mathbf{A}]_{u,u}$ denotes the *(u,u)*$^{\text{th}}$ entry of the matrix **A**. Thus, the average MSE across subcarriers and transmit antennas can be calculated as

$$\overline{MSE} = \frac{1}{n_D K}\sum_{k=0}^{K-1}\sum_{u=1}^{n_D} MSE^{k,u} = \frac{1}{n_D K}\sum_{k=0}^{K-1}\sum_{u=1}^{n_D} \frac{\sigma_{\underline{d}_u}^2 + \sigma_n^2[(\underline{\mathbf{H}}_k^H \underline{\mathbf{H}}_k)^{-1}]_{u,u}}{\underline{\alpha}_u^2 \underline{\beta}_u^2}. \tag{4.31}$$

For notational simplicity, let us denote

$$F(u, \underline{\mathbf{H}}_k, K_{\Omega_k(u)}) = \frac{\sigma_{\underline{d}_u}^2 + \sigma_n^2[(\underline{\mathbf{H}}_k^H \underline{\mathbf{H}}_k)^{-1}]_{u,u}}{\underline{\alpha}_u^2}, \tag{4.32}$$

where Ω_k is a mapping from the u^{th} selected antenna index to the i^{th} real antenna index at the k^{th} subcarrier, i.e., $i = \Omega_k(u), 1 \le u \le n_D, 1 \le i \le n_T,$ which depends on the selected subset. Note that $\underline{\beta}_u^2$ and $\beta_{\Omega_k(u)}^2$ are the same in this work. We can rewrite Eq. (4.31) as

$$\overline{MSE} = \frac{1}{n_D K}\sum_{k=0}^{K-1}\sum_{u=1}^{n_D} \frac{F(u, \underline{\mathbf{H}}_k, K_{\Omega_k(u)})}{\underline{\beta}_u^2}. \tag{4.33}$$

As mentioned above, in the unconstrained systems, the powers of signals on the antennas that have a large number of data subcarriers will be scaled by a factor $\beta_{\Omega_k(u)}^2 < 1.$ Therefore, the average MSE in this system can now be expressed as

$$\overline{MSE}_{im\_bal} = \frac{1}{n_D K}\sum_{k=0}^{K-1}\left\{ \sum_{u:\Omega_k(u)\in\mathbf{V}} F(u, \underline{\mathbf{H}}_k, K_{\Omega_k(u)}) + \sum_{u:\Omega_k(u)\in\overline{\mathbf{V}}} \frac{F(u, \underline{\mathbf{H}}_k, \overline{K})}{\beta_{\Omega_k(u)}^2} \right\}, \tag{4.34}$$

where **V** denotes a set of antennas that the number of allocated data subcarriers on these antennas are smaller than or equal to $\overline{K}$, and $\overline{\mathbf{V}}$ is a set of the remaining antennas.

In the constrained system, the same number of data subcarriers $\overline{K}$ is allocated to all antennas. Thus, all subcarriers will be scaled by the same factor $\overline{\alpha}$, and distorted by the distortion noises with the same variance $\overline{\sigma}_{\underline{d}}^2$. Recall that, for a given $\overline{K}$, the values of $\overline{\alpha}$ and $\overline{\sigma}_{\underline{d}}^2$ can be calculated using Eq. (4.4) and Eq. (4.5), respectively. In addition, it

is important to note that the effective channel matrix on the k^{th} subcarrier in the constrained system, denoted as $\overline{\underline{\mathbf{H}}}_k$, is generally different from the channel matrix $\underline{\mathbf{H}}_k$ obtained in the unconstrained system because the selected antenna subsets may be different. From Eq. (4.31), we can express the average MSE in this system as

$$\overline{MSE}_{bal} = \frac{1}{n_D K} \sum_{k=0}^{K-1} \sum_{u=1}^{n_D} \frac{\overline{\sigma}_{\underline{d}}^2 + \sigma_n^2 [(\overline{\underline{\mathbf{H}}}_k^H \overline{\underline{\mathbf{H}}}_k)^{-1}]_{u,u}}{\overline{\underline{\alpha}}^2}. \tag{4.35}$$

On the other hand, let us define Δ to be the difference in the total cost between the constrained and unconstrained scheme, i.e., (cf. Eq. (4.16), Eq. (4.19))

$$\Delta = \sum_{k=0}^{K-1} \sum_{u=1}^{n_D} [(\overline{\underline{\mathbf{H}}}_k^H \overline{\underline{\mathbf{H}}}_k)^{-1}]_{u,u} - \sum_{k=0}^{K-1} \sum_{u=1}^{n_D} [(\underline{\mathbf{H}}_k^H \underline{\mathbf{H}}_k)^{-1}]_{u,u}. \tag{4.36}$$

Note that the value Δ is positive due to the fact that the total cost in the constrained optimisation (i.e., minimisation problem) is always larger than that in its unconstrained counterpart. Substitute Eq. (4.36) into Eq. (4.35), we arrive at

$$\begin{aligned} \overline{MSE}_{bal} &= \frac{1}{n_D K} \left\{ \sum_{k=0}^{K-1} \sum_{u=1}^{n_D} \frac{\overline{\sigma}_{\underline{d}}^2 + \sigma_n^2 [(\underline{\mathbf{H}}_k^H \underline{\mathbf{H}}_k)^{-1}]_{u,u}}{\overline{\underline{\alpha}}^2} + \frac{\sigma_n^2}{\overline{\underline{\alpha}}^2} \Delta \right\} \\ &= \frac{1}{n_D K} \left\{ \sum_{k=0}^{K-1} \sum_{u=1}^{n_D} F(u, \underline{\mathbf{H}}_k, \overline{K}) + \frac{\sigma_n^2}{\overline{\underline{\alpha}}^2} \Delta \right\}. \end{aligned} \tag{4.37}$$

The difference in the average MSE between the unconstrained and the constrained systems can now be computed as

$$\begin{aligned} \Theta &= \overline{MSE}_{im\_bal} - \overline{MSE}_{bal} \\ &= \frac{1}{n_D K} \left\{ \sum_{k=0}^{K-1} \sum_{u:\Omega_k(u) \in \mathbf{V}} F(u, \underline{\mathbf{H}}_k, K_{\Omega_k(u)}) + \sum_{k=0}^{K-1} \sum_{u:\Omega_k(u) \in \overline{\mathbf{V}}} \frac{F(u, \underline{\mathbf{H}}_k, \overline{K})}{\beta_{\Omega_k(u)}^2} - \sum_{k=0}^{K-1} \sum_{u=1}^{n_D} F(u, \underline{\mathbf{H}}_k, \overline{K}) - \frac{\sigma_n^2}{\overline{\underline{\alpha}}^2} \Delta \right\} \\ &= \frac{1}{n_D K} \left\{ \sum_{k=0}^{K-1} \sum_{u:\Omega_k(u) \in \mathbf{V}} \left(F(u, \underline{\mathbf{H}}_k, K_{\Omega_k(u)}) - F(u, \underline{\mathbf{H}}_k, \overline{K}) \right) \right. \\ &\qquad \left. + \sum_{k=0}^{K-1} \sum_{u:\Omega_k(u) \in \overline{\mathbf{V}}} \left(\frac{F(u, \underline{\mathbf{H}}_k, \overline{K})}{\beta_{\Omega_k(u)}^2} - F(u, \underline{\mathbf{H}}_k, \overline{K}) \right) - \frac{\sigma_n^2}{\overline{\underline{\alpha}}^2} \Delta \right\} \\ &= \frac{1}{n_D K} \left(I_{\mathbf{V}} + I_{\overline{\mathbf{V}}} + I_{\Delta} \right), \end{aligned} \tag{4.38}$$

where

$$I_{\mathbf{V}} = \sum_{k=0}^{K-1} \sum_{u:\Omega_k(u)\in\mathbf{V}} \left(F(u, \underline{\mathbf{H}}_k, K_{\Omega_k(u)}) - F(u, \underline{\mathbf{H}}_k, \overline{K})\right), \tag{4.39}$$

$$I_{\overline{\mathbf{V}}} = \sum_{k=0}^{K-1} \sum_{u:\Omega_k(u)\in\overline{\mathbf{V}}} F(u, \underline{\mathbf{H}}_k, \overline{K}) \left(\frac{1-\beta_{\Omega_k(u)}^2}{\beta_{\Omega_k(u)}^2}\right), \tag{4.40}$$

$$I_{\Delta} = -\frac{\sigma_n^2}{\underline{\overline{\alpha}}^2}\Delta. \tag{4.41}$$

It can be seen from Eq. (4.38) that the change in the average MSE when implementing balanced allocation compared to the case of unbalanced allocation comes from $I_{\mathbf{V}}$, $I_{\overline{\mathbf{V}}}$, and I_{Δ}, where:

- $I_{\mathbf{V}}$ is a kind of MSE penalty that is associated with data subcarriers on the antennas where $K_i < \overline{K}$. It can be seen from Eq. (4.4) and Eq. (4.5) that when K_i increases, α_i decreases and $\sigma_{\eta_i}^2$ increases. Thus, the value of the function $F(u, \underline{\mathbf{H}}_k, K_i)$, defined in Eq. (4.32), increases when K_i increases. Consequently, the value of $I_{\mathbf{V}}$ in Eq. (4.39) is always negative (i.e., $I_{\mathbf{V}} < 0$).

- $I_{\overline{\mathbf{V}}}$ is a MSE benefit that is associated with data subcarriers on the antennas where $K_i > \overline{K}$, $i = \Omega_k(u)$. As the scale factor $\beta_i^2 < 1$, it is clear that $I_{\overline{\mathbf{V}}} > 0$. The more data subcarriers are allocated to some particular antennas, the smaller the value $\beta_i^2 = \sigma_{\overline{K}}^2 / \sigma_{K_i}^2 = \overline{K}/K_i$ is required, and, thus, $I_{\overline{\mathbf{V}}}$ becomes larger.

- I_{Δ} is a kind of MSE penalty that is incurred because the chosen effective channel matrices in the constrained system are different from the ones in the unconstrained system. Note that $I_{\Delta} < 0$ because $\Delta > 0$ as mentioned before.

It is important to note that, for a given system with defined PAs in terms of nonlinear characteristics, only I_{Δ} among the three components depends on the effective channel matrices $\underline{\overline{\mathbf{H}}}_k, k = 0,1,...,K-1$. Therefore, while different balanced selection schemes introduce different changes in the average MSE, the difference in the average MSE indeed comes from the difference in I_{Δ}. From this observation, it is clear that, to make the value Θ, the difference in the average MSE between the unconstrained and constrained systems, become as positive as possible, the constrained selection method should result in the cost penalty Δ as small as possible. We note that the formulated

optimisation in Eq. (4.27) could achieve the minimum possible value of the total cost. Hence, with the definition of Δ as shown in Eq. (4.36), it is expected that the proposed constrained selection scheme based on linear optimisation will guarantee the minimum achievable value of Δ. In addition, an upper bound of the expected value of the cost penalty is derived in Section 4.B. Based on the obtained bound, it is observed that, for fixed values of n_T and n_D, the cost penalty becomes smaller when the number of receive antennas n_R increases. In addition, as it is too challenging to mathematically evaluate Θ from a statistical viewpoint due to the fact that all components $I_{\mathbf{V}}$, $I_{\overline{\mathbf{V}}}$, and I_{Δ} are complicated and dependent random variables, we perform a numerical evaluation of Eq. (4.38) instead. The results will be provided Section 4.6.1.

4.5.2 Analysis of Energy Efficiency

We consider energy efficiency (bits/Joule) defined as a ratio between the capacity and the total power consumption (cf. Eq. (2.33)), i.e.,

$$EE = C / P_{total}, \tag{4.42}$$

where C denotes the capacity (bits/s) and P_{total} is the required power consumption (watts). In an spatial multiplexing MIMO system with a ZF receiver, we can express the post-processing signal-to-noise-plus-distortion ratio (SNDR) corresponding to the data symbol transmitted at the u^{th} selected antenna on the k^{th} subcarrier as [14]

$$SNDR^{k,u} = P_r / MSE^{k,u}, \tag{4.43}$$

where P_r is the average power per symbol that is calculated via the transmit power per data symbol P_t using Eq. (2.35), and $MSE^{k,u}$ is now the mean-squared error that takes transmitted power P_t the and the path-loss into consideration, i.e., (cf. Eq. (4.30)).

$$MSE^{k,u} = \frac{P_r \sigma_{\underline{d}_u}^2}{\underline{\alpha}_u^2 \underline{\beta}_u^2} + \frac{\sigma_n^2}{\underline{\alpha}_u^2 \underline{\beta}_u^2} [(\underline{\mathbf{H}}_k^H \underline{\mathbf{H}}_k)^{-1}]_{u,u}, \tag{4.44}$$

By substituting Eq. (4.44) into Eq. (4.43), we have

$$SNDR^{k,u} = \frac{P_r \underline{\alpha}_u^2 \underline{\beta}_u^2}{P_r \sigma_{\underline{d}_u}^2 + \sigma_n^2 [(\underline{\mathbf{H}}_k^H \underline{\mathbf{H}}_k)^{-1}]_{u,u}}. \tag{4.45}$$

The capacity of the system can be calculated via SNDR as [25]

$$\begin{aligned} C &= W\varepsilon_{\mathbf{H}}\left\{\frac{1}{K}\sum_{k=0}^{K-1}\sum_{u=1}^{n_D}\log_2(1+SNDR^{k,u})\right\} \\ &= W\varepsilon_{\mathbf{H}}\left\{\frac{1}{K}\sum_{k=0}^{K-1}\sum_{u=1}^{n_D}\log_2\left(1+\frac{P_r\underline{\alpha}_u^2\underline{\beta}_u^2}{P_r\sigma_{\underline{d}_u}^2+\sigma_n^2[(\underline{\mathbf{H}}_k^H\underline{\mathbf{H}}_k)^{-1}]_{u,u}}\right)\right\}, \end{aligned} \tag{4.46}$$

where W is the system bandwidth (Hz).

The total power consumption is given as (cf. Eq. (2.32))

$$\begin{aligned} P_{total} &= \sum_{i=1}^{n_T} P_{PA,i}K_i + n_T P_{ctx} + n_R P_{crx} + P_{bb} \\ &= \sum_{i=1}^{n_T} (IBO_i/\eta)K_i P_t + n_T P_{ctx} + n_R P_{crx} + P_{bb}, \end{aligned} \tag{4.47}$$

where $P_{PA,i} = (IBO_i/\eta)P_t$ is the power consumption by the power amplifier (PA) on the i^{th} transmit antenna corresponding to one data subcarrier, K_i is the number of data symbol on the i^{th} antenna, IBO_i is the input power back-off, P_{ctx} is the circuit power consumption per transmit branch (excluding the associated PA), P_{crx} is the circuit power consumption per receive branch, and P_{bb} is the power consumption of basedband blocks in both transmitter and receiver. Note that the average input signal powers of power amplifiers $\sigma_{K_i}^2 := \varepsilon\{|s_i(n)|^2\} = \sigma^2 K_i/K$ on different transmit antennas are unequal in general. Thus, the efficiency of power amplifiers is not equal even though all power amplifiers have the same characteristics. Consequently, a definition of efficiency of power amplifiers that takes into consideration the peak-to-average power ratio (PAPR) of the signal or the *IBO* values proposed in [52] is considered in Eq. (4.47).

By substituting Eq. (4.46) and Eq. (4.47) into Eq. (4.42), we can express the EE metric in the balance (constrained) and unbalance (unconstrained) systems, respectively, as

$$EE_{bal} = \frac{C_{bal}}{P_{total,bal}} = \frac{W}{P_{total,bal}}\varepsilon_{\mathbf{H}}\left\{\frac{1}{K}\sum_{k=0}^{K-1}\sum_{u=1}^{n_D}\log_2\left(1+\frac{P_r\overline{\underline{\alpha}}^2}{P_r\overline{\sigma}_{\underline{d}}^2+\sigma_n^2[(\overline{\underline{\mathbf{H}}}_k^H\overline{\underline{\mathbf{H}}}_k)^{-1}]_{u,u}}\right)\right\}, \tag{4.48}$$

and

$$EE_{im\_bal} = \frac{C_{im\_bal}}{P_{total,im\_bal}} = \frac{W}{P_{total,im\_bal}}\varepsilon_{\mathbf{H}}\left\{\frac{1}{K}\sum_{k=0}^{K-1}\sum_{u=1}^{n_D}\log_2\left(1+\frac{P_r\underline{\alpha}_u^2\underline{\beta}_u^2}{P_r\sigma_{\underline{d}_u}^2+\sigma_n^2[(\underline{\mathbf{H}}_k^H\underline{\mathbf{H}}_k)^{-1}]_{u,u}}\right)\right\}, \tag{4.49}$$

Table 4.2 Simulation parameters.

Parameter	Value
Bandwidth	528 MHz
FFT size	128
Modulation scheme	16-QAM
Circuit power consumptions	P_{ctx} = 150 mW; P_{crx} = 120 mW P_{bb} = 100 mW
Power efficiency	35%
Gain factor	G_d = 100 dB
PSD of noise	-174 dBm/Hz
IEEE 802.15.3a channel model	CM1

where $P_{total,bal}$ and P_{total,im_bal} are the total power consumptions in the constrained and unconstrained systems, respectively, which are calculated based on the general expression in Eq. (4.47). Simulation results of the energy-efficiency will be provided in Section 4.6.2.

4.6 Simulation Results and Discussions

In this section, simulation results are provided to illustrate the efficacy of the proposed system. The legacy WiMedia Multiband-OFDM UWB (MB-OFDM UWB) [36] is adopted. Note that in this standard, there is a very strict transmit power limit on each subcarrier imposed by the regulatory agencies. The simulation parameters are listed in Table 4.2. The IEEE 802.15.3a channel model (CM1) [116] is based on a measurement of a line-of-sight scenario where the distance between the transmitter and the receiver is up to 4 meters. Additionally, the multipath gains are modeled as independent log-normally distributed random variables. Perfect channel state information is assumed to be available at the receiver. The feedback link is assumed zero-delay and is error-free.

4.6.1 Evaluation of Mean-Squared Error

To evaluate the value of Θ in Eq. (4.38), we plot in Figure 4.4 the empirical CDF (cumulative distribution function) of $I_{\mathbf{V}}$, CDF of I_{Δ}, CCDF (complementary CDF) of $I_{\overline{\mathbf{V}}}$, and CCDF of Θ. These statistical distributions are obtained in the system with n_T = 4, n_D = 2, n_R = 2, K =128, and IBO = 8 dB. The numerical results confirm that $I_{\mathbf{V}} < 0$, $I_{\overline{\mathbf{V}}} > 0$, and $I_{\Delta} < 0$. Moreover, as shown in Figure 4.4d, the probability of Θ being positive is very significant. Therefore, the proposed system could achieve a smaller average MSE (i.e., a better MSE performance) than that in the unconstrained system. In

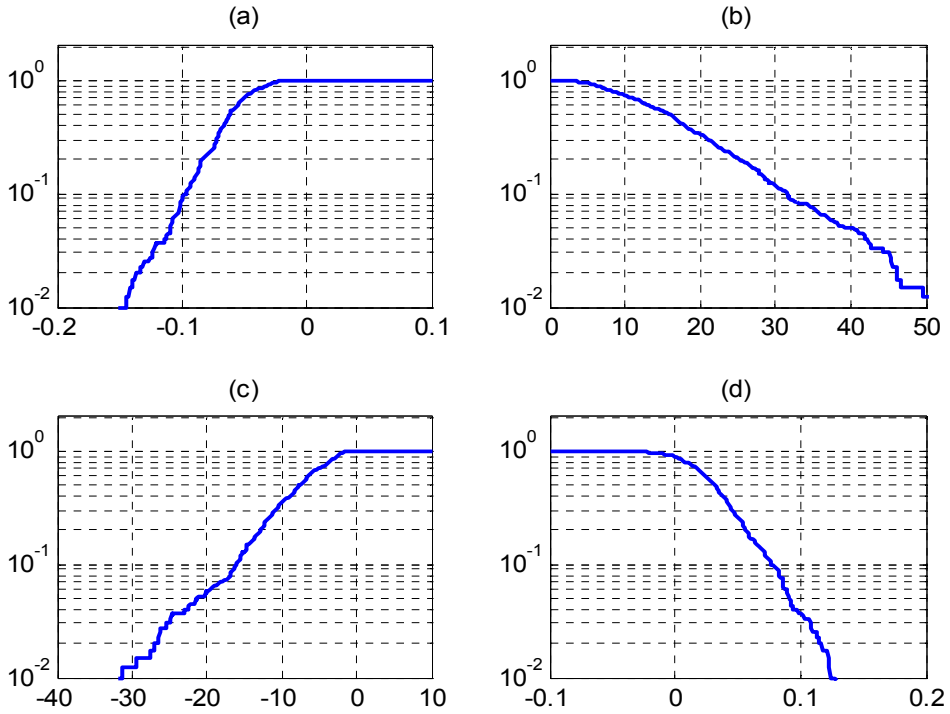

Figure 4.4. Statistical distributions: (a) CDF of I_v ; (b) CCDF of $I_{\bar{v}}$; (c) CDF of I_Δ ; (d) CCDF of Θ .

case that the receiver first estimates the value of Θ and then applies the constrained method only when $\Theta > 0$, the value of Θ is always positive. Note that the small average MSE results in an improved post-processing SNDR value (cf. Eq. (4.43)). Hence, the average SNDR in the proposed system is better than that in the unconstrained system, which results in improved energy efficiency (cf. Eq. (4.46)).

4.6.2 Evaluation of Energy Efficiency

Figure 4.5 plots the energy efficiency versus spectral efficiency (EE-SE) under different numbers of receive antennas. It can be seen that there is a significant improvement in terms of EE performance in the constrained system compared to its counterpart. This agrees with the results in Section 4.6.1 that the constrained system can improve the average MSE and average SNDR values. In addition, when the number of receive antennas increases, the energy efficiency is improved. This EE improvement comes from the fact that the increased capacity when additional antennas are used has more impact on the EE value than the extra power consumption due to additional receive RF chains.

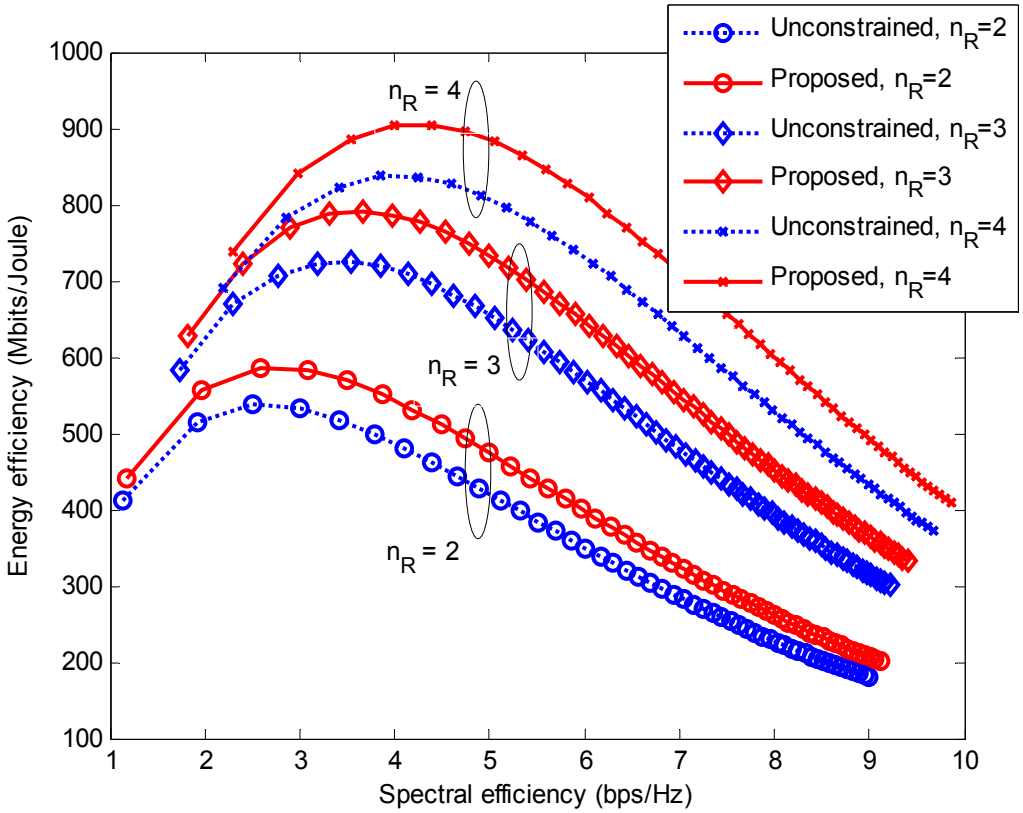

Figure 4.5. Energy efficiency versus spectral efficiency with different numbers of receive antennas ($n_T = 4$, $n_D = 2$, and $IBO = 8$ dB).

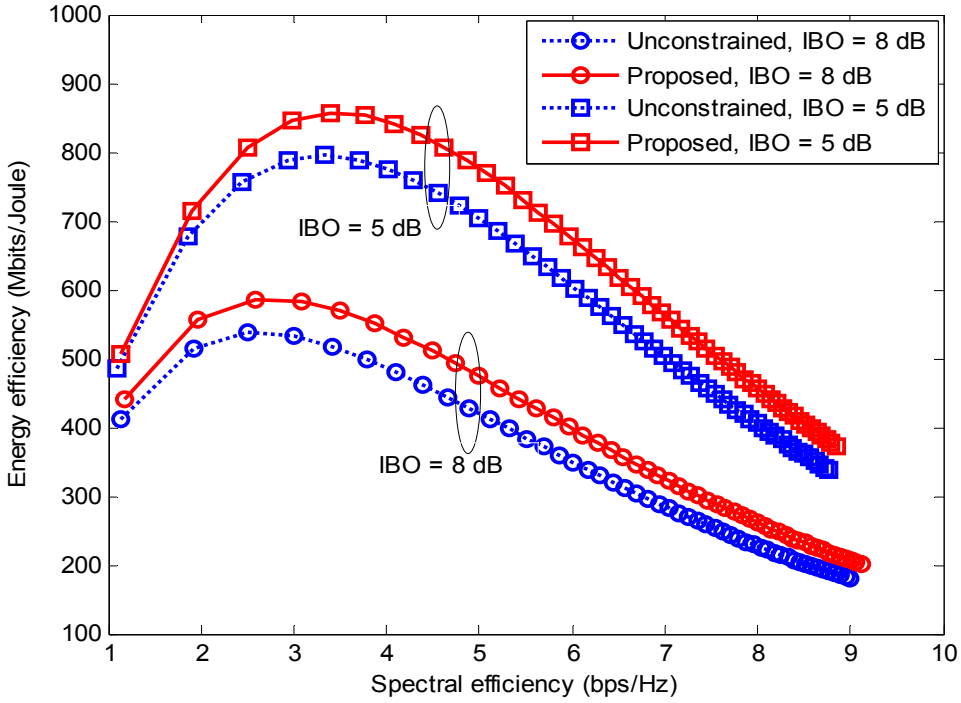

Figure 4.6. Energy efficiency versus spectral efficiency with different *IBO* values ($n_T = 4$, $n_D = 2$, and $n_R = 2$).

In Figure 4.6, we plot EE-SE curves in the two systems under different *IBO* values. The results show that the EE values are improved when *IBO* decreases. This is because, given a saturation level of power amplifiers, a larger power back-off results in lower power efficiency of power amplifiers, which in turn reduces the energy efficiency of the systems. Also, it can be seen that the proposed system offers a better EE-SE performance than its counterpart for all *IBO* values. For example, when *IBO* = 8 dB, the achieved EE values in the proposed system and the conventional system at the SE value of 3 (bits/s/Hz) are 580 (Mbits/J) and 530 (Mbits/J), respectively.

The EE improvement in the proposed system over the conventional system can also be observed in other simulation scenarios, including antenna selection criteria and spatial correlation as shown in Figure 4.7 and Figure 4.8, respectively. In particular, Figure 4.7 shows the EE-SE performance when the MMSE and maximum capacity selection criteria are employed. Meanwhile, Figure 4.8 compares the EE-SE performance in the systems with no spatial correlation and the ones in the presence of transmit spatial correlation.

Figure 4.9 shows the EE-SE performance under reduced feedback. Here, the feedback reduction of $L = 8$ is used. As predicted, there is some loss in EE performance when applying feedback reduction compared to full feedback. However, we note that the system with feedback reduction requires only 12.5 % of the number of feedback bits and has lower computational effort for solving the optimisation problem. Moreover, the proposed system still outperforms its counterpart under reduced feedback. These results illustrate the efficacy of the proposed system with power balancing for energy-efficient MIMO-OFDM wireless systems.

4.7 Summary

In this chapter, an antenna subset selection MIMO-OFDM system in the presence of nonlinear PAs has been investigated. The obtained results have shown that the implementation of the conventional per-subcarrier selection in such a system suffers from the problem of performance degradation due to the large power back-off (resulting from an unequal allocation of data subcarriers across antennas) as well as the non-causality associated with the selection criteria. To overcome these drawbacks, an optimal constrained selection scheme that can equally allocate data subcarriers among

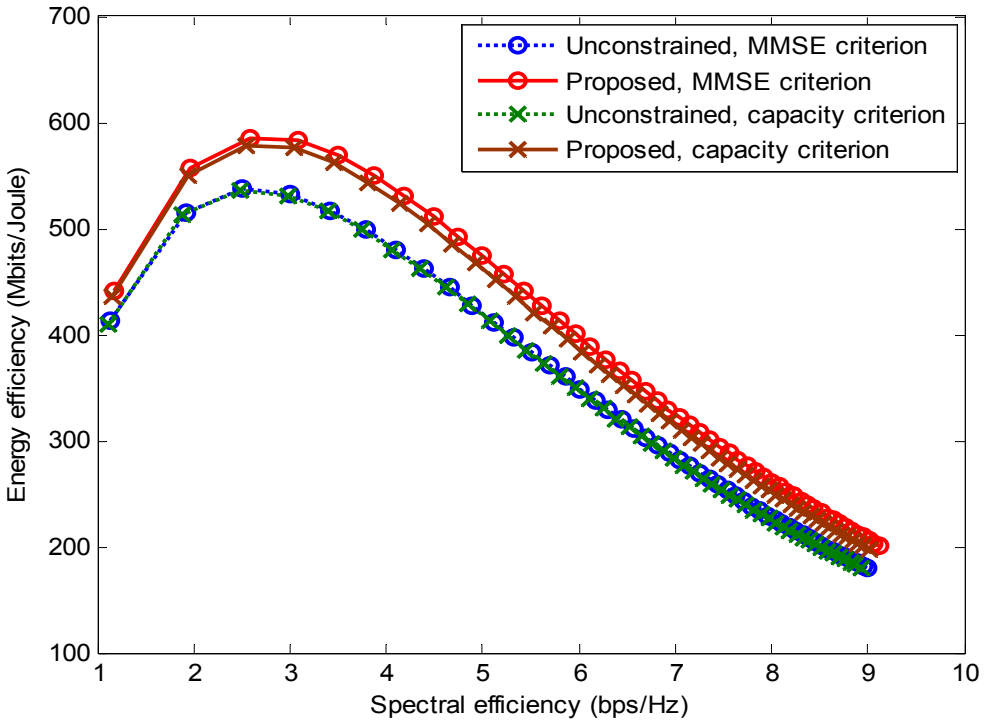

Figure 4.7. Energy efficiency versus spectral efficiency with different selection criteria ($n_T = 4$, $n_D = 2$, $n_R = 2$, and $IBO = 8$ dB).

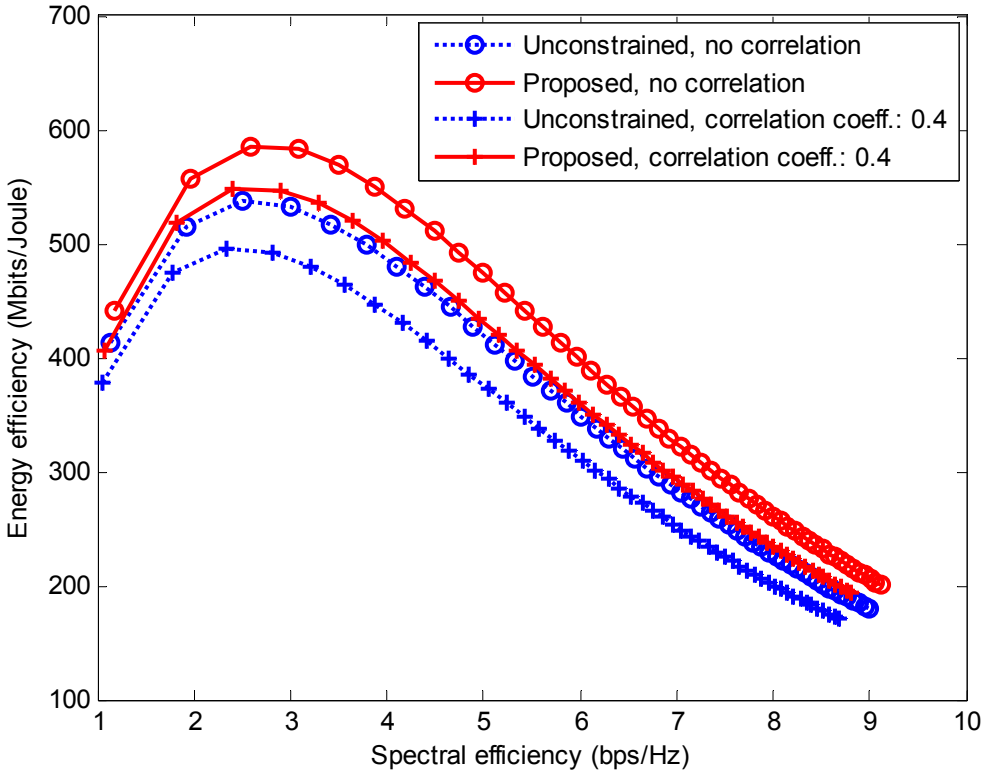

Figure 4.8. Energy efficiency versus spectral efficiency under a spatial correlation scenario ($n_T = 4$, $n_D = 2$, $n_R = 2$, and $IBO = 8$ dB).

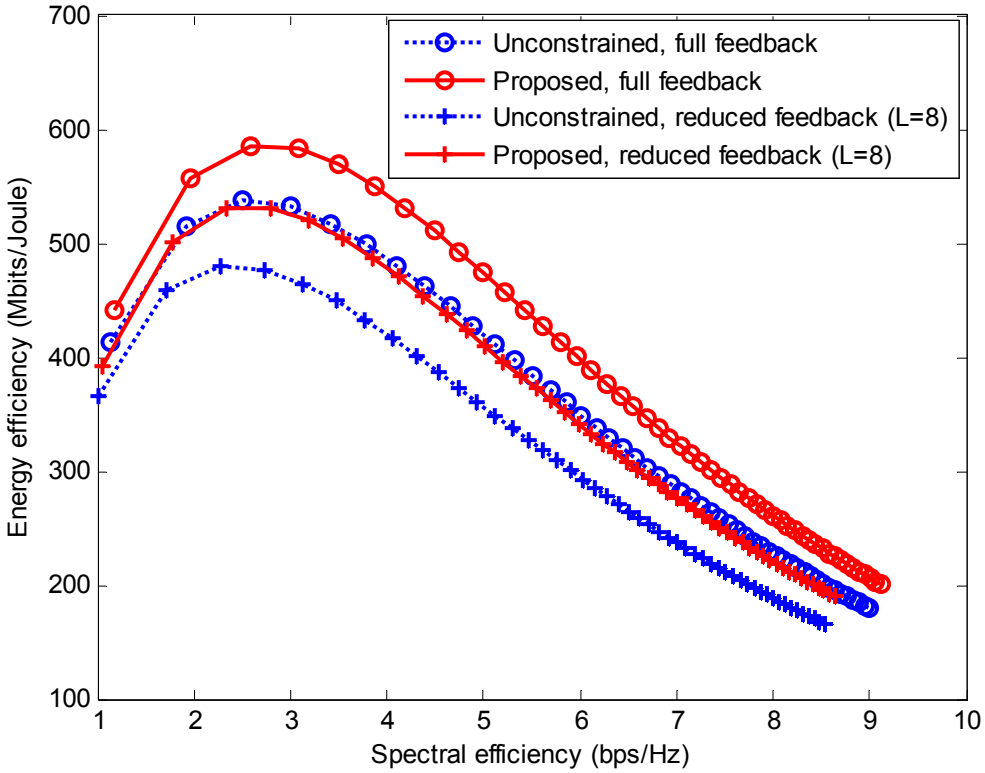

Figure 4.9. Energy efficiency versus spectral efficiency with feedback reduction ($n_T = 4$, $n_D = 2$, $n_R = 2$, and $IBO = 8$ dB).

transmit antennas by means of linear optimisation has been proposed. The optimisation problem to realize the proposed scheme is formulated in the system with an arbitrary number of multiplexed data streams. Moreover, it can be solved efficiently by existing methods. In addition, the reduced-complexity strategy that requires less feedback information and lower computational effort for solving the optimisation problem has been developed. The efficacy of the constrained antenna selection approach over the conventional approach has been analysed directly in the nonlinear fading channels. The analysis could provide an insight into the system characteristics, i.e., the impacts of nonlinear PAs on the error-performance and energy efficiency of the antenna selection OFDM system. Simulation results show that a significant improvement in terms of energy efficiency could be achieved in the system with a constrained antenna selection compared to its counterpart.

4.A Linear Relaxation of the Binary Optimisation in Eq. (4.27)

The optimisation problem in Eq. (4.27) can be relaxed to linear programming (LP) relaxation using a similar approach as in [84], even though the constraint matrices in the two formulated problems are defined differently. Specifically, the feasible set of the LP relaxation of Eq. (4.27) can be expressed as

$$\mathbf{S} = \{\mathbf{z} \in \Re^{KT\times 1} \mid \mathbf{Az} = \mathbf{a},\ \mathbf{0}_{KT} \le \mathbf{z} \le \mathbf{1}_{KT}\}, \tag{4.50}$$

or

$$\mathbf{S} = \{\mathbf{z} \in \Re^{KT\times 1} \mid \mathbf{Bz} \le \mathbf{b}\}, \tag{4.51}$$

where

$$\mathbf{B} \coloneqq \begin{pmatrix} \mathbf{A}^T & -\mathbf{A}^T & \mathbf{I}_{KT} & -\mathbf{I}_{KT} \end{pmatrix}^T, \tag{4.52}$$

$$\mathbf{b} \coloneqq \begin{pmatrix} \mathbf{a}^T & -\mathbf{a}^T & \mathbf{1}_{KT}^T & \mathbf{0}_{KT}^T \end{pmatrix}^T. \tag{4.53}$$

As the matrix **A**, defined in Eq. (4.26), is totally unimodular (i.e., every square submatrix of **A** has determinant +1, -1, or 0), it follows from [117] (also in [84], *Proposition 1*] that **B** is also a totally unimodular matrix. On the other hand, the vector **b** in Eq. (4.53) is an integer vector. Therefore, the solution obtained by solving the LP relaxation using known programming methods is integral [117]. Consequently, the optimal solution of the LP relaxation is optimal for the original problem in Eq. (4.27).

4.B Derivation of an Upper Bound of the Cost Penalty in Eq. (4.36)

Let us first rewrite Eq. (4.36) as

$$\Delta = \sum_{k=0}^{K-1} \mathrm{tr}\{(\overline{\underline{\mathbf{H}}}_k^H \overline{\underline{\mathbf{H}}}_k)^{-1}\} - \sum_{k=0}^{K-1} \mathrm{tr}\{(\underline{\mathbf{H}}_k^H \underline{\mathbf{H}}_k)^{-1}\} = \sum_{k=0}^{K-1} \Delta_k, \tag{4.54}$$

where

$$\Delta_k = \mathrm{tr}\{(\overline{\underline{\mathbf{H}}}_k^H \overline{\underline{\mathbf{H}}}_k)^{-1}\} - \mathrm{tr}\{(\underline{\mathbf{H}}_k^H \underline{\mathbf{H}}_k)^{-1}. \tag{4.55}$$

We now derive an upper bound of the expected value of Δ_k. From Eq. (4.15), it can be seen that among all possible matrices $\underline{\mathbf{H}}_k$, the matrix $\underline{\mathbf{H}}_k$ with the lowest value of

$\mathrm{tr}\{(\underline{\mathbf{H}}_k^H \underline{\mathbf{H}}_k)^{-1}\}$ will be selected as the effective channel matrix for the k^{th} subcarrier in the unconstrained system. Meanwhile, the effective channel matrix associated with the k^{th} subcarrier in the constrained system is not necessarily the one with the lowest $\mathrm{tr}\{(\underline{\mathbf{H}}_k^H \underline{\mathbf{H}}_k)^{-1}\}$, i.e., $\mathrm{tr}\{(\overline{\underline{\mathbf{H}}}_k^H \overline{\underline{\mathbf{H}}}_k)^{-1}\} \geq \mathrm{tr}\{(\underline{\mathbf{H}}_k^H \underline{\mathbf{H}}_k)^{-1}$, due to the balance constraint. Hence, the expected value of Δ_k can be computed by using order statistics. In particular, an upper bound on the expected difference of two order statistics, the 1st and the γ^{th}, $1 < \gamma \leq \Gamma$, is given by [118]

$$\varepsilon\{\Delta_k\} = \varepsilon\{\mathrm{tr}\{(\overline{\underline{\mathbf{H}}}_k^H \overline{\underline{\mathbf{H}}}_k)^{-1}\}\} - \varepsilon\{\mathrm{tr}\{(\underline{\mathbf{H}}_k^H \underline{\mathbf{H}}_k)^{-1}\}\} \leq \sigma_w \sqrt{\frac{\Gamma(\Gamma-\gamma+2)}{\Gamma-\gamma+1}}, \tag{4.56}$$

where σ_w^2 is the variance of $\mathrm{tr}\{(\underline{\mathbf{H}}_k^H \underline{\mathbf{H}}_k)^{-1}\}$ that is assumed to be the same for all $\underline{\mathbf{H}}_k$.

On the other hand, suppose that the entries of the $n_R \times n_T$ matrix $\mathbf{H}_k$ are i.i.d. complex Gaussian random variables with zero-mean and unit-variance, then for any effective channel matrix $\underline{\mathbf{H}}_k$, $(\underline{\mathbf{H}}_k^H \underline{\mathbf{H}}_k)^{-1}$ follows complex inverse Wishart distribution with n_R degrees of freedom [119]. When $n_R > n_D + 1$, it is shown in [119] that

$$\varepsilon\{\mathrm{tr}\{(\underline{\mathbf{H}}_k^H \underline{\mathbf{H}}_k)^{-1}\}\} = \frac{n_D}{n_R - n_D}, \tag{4.57}$$

and

$$\varepsilon\left\{\left(\mathrm{tr}\{(\underline{\mathbf{H}}_k^H \underline{\mathbf{H}}_k)^{-1}\}\right)^2\right\} = \frac{n_D}{n_R - n_D}\left(\frac{n_R}{(n_R-n_D)^2-1} - \frac{n_D-1}{n_R-n_D+1}\right). \tag{4.58}$$

Thus, the variance of $\mathrm{tr}\{(\underline{\mathbf{H}}_k^H \underline{\mathbf{H}}_k)^{-1}\}$ can be computed as [107]

$$\begin{aligned}\sigma_w^2 &= \varepsilon\left\{\left(\mathrm{tr}\{(\underline{\mathbf{H}}_k^H \underline{\mathbf{H}}_k)^{-1}\}\right)^2\right\} - \left(\varepsilon\left\{\mathrm{tr}\{(\underline{\mathbf{H}}_k^H \underline{\mathbf{H}}_k)^{-1}\}\right\}\right)^2 \\ &= \frac{n_D n_R}{(n_R-n_D)^2[(n_R-n_D)^2-1]}.\end{aligned} \tag{4.59}$$

Substitute Eq. (4.59) into Eq. (4.56), we finally arrive at

$$\varepsilon\{\Delta_k\} \leq \sqrt{\frac{n_D n_R}{(n_R-n_D)^2[(n_R-n_D)^2-1]} \cdot \frac{\Gamma(\Gamma-\gamma+2)}{\Gamma-\gamma+1}}. \tag{4.60}$$

Chapter 5

Peak-Power Reduction based Antenna Selection for Energy-Efficient MIMO-OFDM Systems

In Chapter 4, antenna selection MIMO-OFDM systems in the presence of nonlinear distortions due to high-power amplifiers had been investigated. This chapter continues to consider energy efficiency in antenna selection MIMO-OFDM systems from a power amplifier perspective. Unlike Chapter 4, this chapter focuses on an antenna selection MIMO-OFDM system with linear scaling for non-distortion transmissions. In particular, peak-power reduction antenna selection method is proposed to improve the power efficiency of power amplifiers and the energy efficiency of the system. This chapter is organized as follows. In Section 5.1, the related works and the motivation of this chapter are introduced. In Section 5.2, a system model for per-subcarrier antenna selection MIMO-OFDM system with linear scaling is described. In Section 5.3, a data allocation strategy that could allocate evenly data subcarriers across antennas with a low peak-power is proposed. Analysis of power efficiency is carried out in Section 5.4. The achievable capacity and energy efficiency are considered in Section 5.5. Numerical results are provided in Section 5.6. Finally, Section 5.7 concludes the chapter.

5.1 Introduction

As mentioned in Chapter 2, high-power amplifier (PAs) is a major source of RF (radio frequency) power consumption. For example, in mobile networks, PAs consume up to 50% - 80% of overall power at a base station [45, 120]. Thus, increasing power-efficiency of PAs is of importance to achieve high energy-efficient wireless networks. In antenna selection MIMO-OFDM systems, the peak power and average power of the signals on some antennas may be very large, whereas those on the other antennas might be small. This phenomenon is due to both the high peak-to-average power ratio (PAPR) of time-domain OFDM signals and an unbalance allocation of data subcarriers across transmit antennas. The fluctuation of the powers clearly affects the power efficiency of

PAs, which in turn reduces the energy efficiency of the antenna selection OFDM systems.

One possible approach to deal with the problem of unbalance allocation of data subcarriers is selecting antennas under a constraint that the number of data subcarriers allocated to each antenna is equal as shown in Chapter 4. However, even though the same number of data subcarriers is allocated to each transmit antenna (i.e., all antennas have an equal average power), an occurrence of high PAPR still affects the system. This problem becomes crucial in the OFDM systems where linear scaling (i.e., scale the peak power of the time-domain OFDM signals to the saturation level of the PAs [121, 122]) is implemented to realize OFDM transmissions with no nonlinear distortions. Motivated by this, this chapter proposes a method to improve power efficiency of PAs and the energy efficiency in antenna selection MIMO-OFDM system with linear scaling. The main contributions are summarized as follows.

i) A two-step data allocation strategy is proposed to deliver a maximum overall power efficiency of PAs. This strategy consists of an equal allocation of data subcarriers among transmit antennas based on linear optimisation and a peak-power reduction algorithm via cross-antenna permutations.

ii) Analytical expressions characterizing the achieved power efficiency of PAs, including the complementary cumulative distribution function (*CCDF*) and the average power efficiency, are derived. The results show that, from the power-efficiency perspective, the proposed allocation scheme outperforms the conventional scheme.

iii) The improvements in capacity and energy efficiency resulting from the improved power efficiency of PAs are analysed.

In addition, numerical results are provided to verify the analysis as well as demonstrate the benefits in terms of the power efficiency of PAs, system capacity as well as the achieved energy efficiency.

5.2 System Model

Let us consider a MIMO-OFDM system with K subcarriers, n_T transmit antennas, and n_R receive antennas as shown in Figure 5.1. At the transmitter, the input data are demultiplexed into n_D independent data streams. Each data stream is then mapped onto M-QAM (M-ary quadrature amplitude modulation) constellations. For the k^{th} subcarrier,

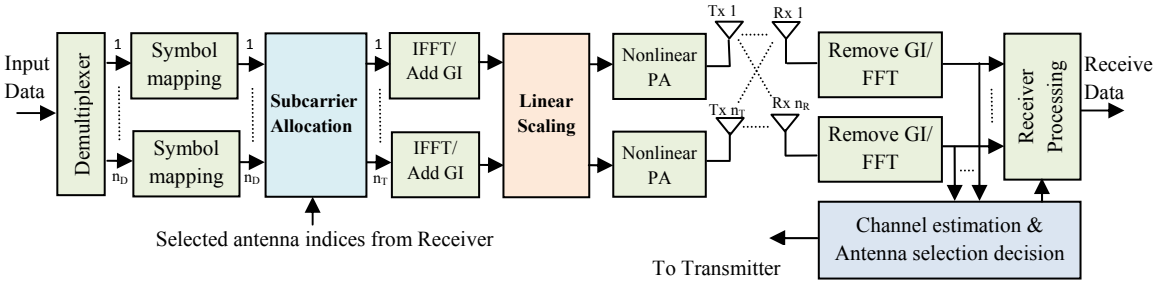

Figure 5.1. A simplified block diagram of an antenna selection MIMO-OFDM system with linear scaling.

let u_l^k and x_i^k, $1 \le l \le n_D, 1 \le i \le n_T, 0 \le k \le K-1$, denote the symbols that the subcarrier block takes at its l^{th} input and outputs at its i^{th} output, respectively. The allocation block assigns the elements of $\mathbf{u}_k = [u_1^k, u_2^k, ..., u_{n_D}^k]^T$ to n_D selected antennas at the k^{th} subcarrier based on feedback information. As a result, only n_D elements in a vector $\mathbf{x}_k = [x_1^k, x_2^k, ..., x_{n_T}^k]^T$ are assigned values from $\mathbf{u}_k$, whereas the others are zeros. It is assumed that $\varepsilon\{\mathbf{u}_k \mathbf{u}_k^H\} = \sigma^2 \mathbf{I}_{n_D}$. The output sequences from the subcarrier allocation block are then fed into K-point IFFT blocks. In this work, the Nyquist sampling signal is considered. Thus, the discrete-time baseband OFDM signals can be expressed as

$$s_i(n) = \frac{1}{\sqrt{K}} \sum_{k=0}^{K-1} x_i^k e^{j2\pi nk/K}, \; 0 \le n \le K-1, \; 1 \le i \le n_T. \tag{5.1}$$

For simplicity, we consider ideal predistortion PAs (i.e., soft envelope limiters) with a unity gain and class-A operation. To deliver the maximum power efficiency with no nonlinear distortions in the system with nonlinear PAs, the peak power across transmit antennas are linearly scaled to the saturation level P_{sat} of the PAs. In addition, as feedback information (i.e., the selected antenna indices which are calculated based on the channel state information) is deployed by the transmitter, all transmit branches are scaled with the same scaling factor [122]. Thus, the signal after linear scaling can be expressed as

$$\tilde{s}_i(n) = \sqrt{\alpha} s_i(n), \tag{5.2}$$

where the scaling factor $\alpha = P_{sat}/P$, and the peak power across antennas $P = \max\{s_i(n) \mid n = 0,...,K-1; i = 1,...,n_T\}$. Each time-domain OFDM signal is then amplified by the PA before being transmitted via its corresponding transmit antenna.

At the receiver, the received signal at each antenna is fed into the FFT block after the GI (guard interval) is removed. The system model in the frequency domain corresponding to the k^{th} subcarrier can be expressed as

$$\mathbf{y}_k = \sqrt{\alpha}\mathbf{H}_k\mathbf{x}_k + \mathbf{n}_k = \sqrt{\alpha}\underline{\mathbf{H}}_k\mathbf{u}_k + \mathbf{n}_k, \tag{5.3}$$

where

$$\mathbf{x}_k = \begin{bmatrix} x_1^k & x_2^k & \dots & x_{n_T}^k \end{bmatrix}^T, \tag{5.4}$$

$$\mathbf{H}_k = \begin{bmatrix} h_{1,1}^k & h_{1,2}^k & \dots & h_{1,n_T}^k \\ h_{2,1}^k & h_{2,2}^k & \dots & h_{2,n_T}^k \\ \dots & \dots & \dots & \dots \\ h_{n_R,1}^k & h_{n_R,2}^k & \dots & h_{n_R,n_T}^k \end{bmatrix}, \tag{5.5}$$

$$\mathbf{y}_k = \begin{bmatrix} y_1^k & y_2^k & \dots & y_{n_R}^k \end{bmatrix}^T, \tag{5.6}$$

$$\mathbf{n}_k = \begin{bmatrix} n_1^k & n_2^k & \dots & n_{n_R}^k \end{bmatrix}^T. \tag{5.7}$$

In the above equations, $h_{j,i}^k$ indicates the channel coefficient between the i^{th} transmit antenna and the j^{th} receive antenna. The effective channel matrix $\underline{\mathbf{H}}_k$ is obtained by eliminating the columns of $\mathbf{H}_k$ corresponding to the unselected transmit antennas. Also, y_j^k and n_j^k denote the received signal and the noise at the j^{th} receive antenna, respectively. Here, the noise is modeled as a Gaussian random variable with zero mean and $\varepsilon\{\mathbf{n}_k\mathbf{n}_k^H\} = \sigma_n^2\mathbf{I}_{n_R}$. Also, we assume that the receiver can perfectly estimate the channel coefficients, e.g., using a block-type pilot arrangement for channel estimation [123].

Several antenna selection criteria, such as maximum capacity or maximum SNR can be employed in this system. In this work, we consider the capacity criterion for simplicity. Accordingly, the optimal subset at the k^{th} subcarrier is determined by maximising the instantaneous capacity of the k^{th} subchannel, i.e.,

$$\mathbf{\Gamma}_{\gamma^*}(k) = \arg \max_{\mathbf{\Gamma}_\gamma, \gamma=1,\dots,\Gamma} I_\gamma^k, \tag{5.8}$$

where $\mathbf{\Gamma}_\gamma, \gamma = 1,2,...,\Gamma,$ denotes the γ^{th} subset that consists of n_D selected transmit antennas, $\Gamma = C_{n_D}^{n_T}$ is the number of all possible n_D-element subsets, and

$$I_{\gamma}^{k} = \log_2\left(\det\left(\mathbf{I}_{n_R} + \frac{\rho}{n_D}\underline{\mathbf{H}}_k\underline{\mathbf{H}}_k^H\right)\right) \tag{5.9}$$

is the instantaneous capacity associated with the k^{th} subchannel [93]. Here, $\rho = P_t/\sigma_n^2 = \alpha n_D\sigma^2/\sigma_n^2$, and $P_t = \alpha n_D\sigma^2$ is the total transmit power per subchannel. Also, we have assumed in Eq. (5.9) that the transmit power is allocated uniformly across antennas. This is because the feedback information in this system is only the selected antenna indices (i.e., not sufficient enough to perform power allocation algorithms across subcarriers as well as antennas). The average capacity across subcarriers can now be expressed as

$$I(\rho, \underline{\mathbf{H}}) = \frac{1}{K}\sum_{k=0}^{K-1} I_{\gamma^*}^{k}. \tag{5.10}$$

5.3 Antenna Selection Strategy for Peak-Power Reduction

In Section 5.2, we have described the non-distortion MIMO-OFDM system with the conventional antenna selection scheme. It can be noted that the number of data subcarriers assigned to each transmit antenna might be significantly different depending on the channel condition. In the system with identical linear scaling, to achieve the maximal overall power efficiency of PAs, the peak power across antennas should be as small as possible. We note that the peak power of the signal on each branch depends on both the transmitted constellation symbols and the number of data subcarriers allocated in each OFDM symbol (cf. Eq. (5.1)). Thus, it is not sufficient to reduce the peak power by solely implementing PAPR reduction techniques. In other words, PAPR reduction techniques themselves cannot solve the problem of imbalance allocation of data subcarriers across antennas. To reduce the peak power across antennas, we propose a two-step strategy below.

Step1: *Allocate the same number of data subcarriers to all transmit antennas (i.e., selecting antennas under a constraint that all antennas have the same number of data subcarriers. Once this is achieved, the time-domain signals on all transmit branches have the same average power. Moreover, as we will mathematically prove in Section 5.4.1, the peak power across antennas is reduced.*

Step2: *Reallocate data symbols across antennas. This process will alter the statistical distribution of signals, and thus further reduce the peak power.*

We note that this work does not focus on developing original techniques for either equal allocation of data subcarriers or peak-power reduction. Instead, we are interested in analysing power-efficiency of PAs and energy-efficiency in per-subcarrier antenna selection OFDM systems, which has not been considered so far. The two steps in the proposed strategy, which are described in Section 5.3.1 and Section 5.3.2, are accomplished by extending the suitable approaches available in the literature to the context of the considered system.

5.3.1 Optimal Equal Allocation of Data Subcarriers

The optimal constrained antenna selection scheme based on linear optimisation has been considered Chapter 4 to improve error performance of OFDM systems suffering nonlinear distortions due to PAs. We now consider this method for the first step of the proposed strategy to achieve a better power delivery in a linearly scaled MIMO-OFDM system. Specifically, we define a variable z_γ^k, where $z_\gamma^k = 1$ if $\mathbf{\Gamma}_\gamma$ is chosen for the k^{th} subcarrier, and $z_\gamma^k = 0$ otherwise. Also, denote c_γ^k to be the cost associated with the chosen subset $\mathbf{\Gamma}_\gamma$. Here, $c_\gamma^k = I_\gamma^k$ since the maximum capacity criterion is considered. By denoting two vectors $\mathbf{z} = (z_1^0,...,z_\Gamma^0, z_1^1,...,z_\Gamma^1,...,z_1^{K-1},...,z_\Gamma^{K-1})^T \in \{0,1\}^{K\Gamma\times 1}$, and $\mathbf{c} = (c_1^0,...,c_\Gamma^0, c_1^1,...,c_\Gamma^1,...,c_1^{K-1},...,c_\Gamma^{K-1})^T \in \Re^{K\Gamma\times 1}$, an optimal solution for an equal allocation of data subcarriers is obtained by solving the following linear optimisation problem (cf. Eq. (4.27))

$$\begin{aligned} &\max_{\mathbf{z}\in\{0,1\}^{K\Gamma\times 1}} \mathbf{c}^T\mathbf{z}, \\ &\text{subject to} \quad \mathbf{A}\mathbf{z} = \mathbf{a}, \end{aligned} \tag{5.11}$$

where $\mathbf{A}_1 = \mathbf{I}_K \otimes \mathbf{1}_\Gamma^T \in \{0,1\}^{K\times K\Gamma}$, $\mathbf{A}_2 = \mathbf{1}_K^T \otimes \mathbf{I}_\Gamma \in \{0,1\}^{\Gamma\times K\Gamma}$, $\mathbf{A} = (\mathbf{A}_1^T, \mathbf{A}_2^T)^T \in \{0,1\}^{(K+\Gamma)\times K\Gamma}$, $\mathbf{a} = (\mathbf{1}_K^T, \boldsymbol{\lambda}^T)^T$, and $\boldsymbol{\lambda} = (\lambda_1, \lambda_2, ..., \lambda_\Gamma)^T$, where λ_γ is the number of times that the subset $\mathbf{\Gamma}_\gamma$ is selected.

5.3.2 Data Allocation with Peak-Power Reduction

To further reduce the peak power of the whole system, various available PAPR reduction techniques (e.g., see [35] and the references therein) can be now adopted. In this work, we are interested in a selected mapping (SLM) technique [124] as SLM is an undistorted PAPR technique that could achieve a good PAPR reduction. One of the most important steps in SLM is creating a set of candidates that represents the same data

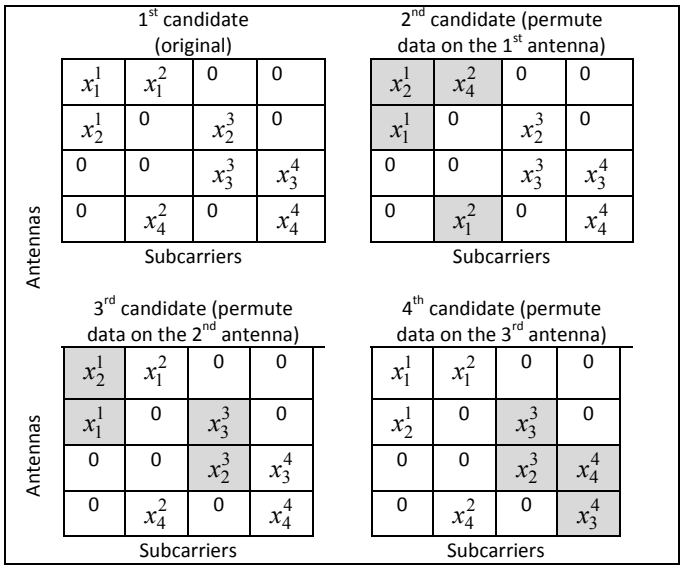

Figure 5.2. Illustration of cross-antenna permutations ($n_T = 4$, $n_D = 2$, and $K = 4$).

information. To exploit the available degrees of freedom in multiple-antenna systems for peak-power reduction, we propose to create a set of candidates using cross-antenna permutations. In the literature, a SLM-based scheme that could exploit the available the available degrees of freedom was first developed in [125]. The scheme in [125] creates candidates by performing cross-antenna rotation and inversion (CARI) based on a defined random matrix. However, that scheme is proposed for an Alamouti code based MIMO-OFDM system only. In a per-subcarrier antenna selection OFDM system, CARI cannot be implemented directly as only n_D out of n_T antennas are active on each subcarrier. To create candidates in our scheme, we perform cross-antenna permutations instead of CARI. In addition, we utilize an antenna allocation pattern that is already known by the transmitter and receiver, instead of storing a pre-defined random matrix at both transmitter and receiver as in [125]. The proposed algorithm is described as follows.

1) Create W candidates by performing cross-antennas permutations. An illustration of this process in the system with $n_D = 2$, $n_T = 4$, and $K = 4$ is shown in Figure 5.2. Accordingly, the first candidate is the original data allocation. The second candidate is obtained by permuting all symbols on the first antennas with their associated symbols on the other antennas. The third and fourth candidates are created in a similar manner. To obtain a larger number of candidates, all symbols on the antenna that are going be

permutated need first have their phase rotated (i.e., being multiplied with an element of a phase set, e.g., a 4-phase set is $\{0, \pi/2, \pi, 3\pi/2\}$).

2) Calculate the peak powers of all available candidates.

3) Select the candidate with the minimum peak power for transmission.

To recover the transmitted data, the transmitter needs to inform the receiver which candidate has been selected. Thus, the number of side information bits in this scheme is $\log_2 W$, which is similar to that in [125].

5.3.3 Complexity Considerations

In this subsection, the complexity of the proposed allocation scheme is compared to that of the conventional (unbalance) allocation scheme. In the first step of the proposed scheme, to realize an equal allocation of data subcarriers, the optimisation problem in Eq. (5.11) needs to be solved at the receiver. As shown in Chapter 4, this linear optimisation problem can be solved in polynomial time. In addition, it is noted that this step is transparent to the transmitter (i.e., no additional complexity is required at the transmitter). In the second step, a major additional complexity lies in the required IFFT operations due to additional W candidates. As an K point-IFFT requires $K\log_2 K$ complex additions and $(K/2)\log_2 K$ complex multiplications, the numbers of complex additions and complex multiplications in the conventional scheme are $n_T K\log_2 K$ and $n_T(K/2)\log_2 K$, respectively. Meanwhile, in the proposed scheme with W candidates, $Wn_T K\log_2 K$ complex additions and $Wn_T(K/2)\log_2 K$ complex multiplications are required. However, as we will show analytically in Section 5.4 and numerically in Section 5.6, an improvement in the peak-power reduction reduces when W becomes large. Thus, it is better to select a small value of W, which does not incur much additional complexity. Finally, the amount of feedback information in the proposed scheme is similar to that in the conventional scheme.

5.4 Analysis of Power Efficiency of Power Amplifiers

5.4.1 Statistical Distribution of Peak-Powers of Time-Domain OFDM Signals

Before proceeding to analyse the power efficiency of PAs, we need to investigate the distribution of the peak power of the time-domain MIMO-OFDM signals (i.e., the peak power across transmit antennas). Let us consider the complementary cumulative

distribution function (*CCDF*) of the peak power, defined as the probability that the peak power P exceeds a given threshold P_0, i.e.,

$$CCDF^{P}(P_0) = \Pr(P > P_0). \tag{5.12}$$

Note that although a procedure for calculating *CCDF* of PAPR in OFDM systems is known, all the *CCDF* expressions with respect to MIMO-OFDM signals available in the literature assume that all data subcarriers are active. This can be considered as a special case in the considered system when all the transmit antennas have the same number of allocated data symbols. In the following, we calculate the *CCDF* of the peak power.

Let us begin with the discrete-time OFDM signal $s_i(n), n = 0,1,...,K-1,$ corresponding to the i^{th} transmit antenna. The peak power of this signal is defined as

$$P_i = \max_{0 \le n \le K-1} |s_i(n)|^2 . \tag{5.13}$$

For analytical tractability, we assume that both the real part and imaginary part of the signal $s_i(n)$ are asymptotically independent and identically distributed Gaussian random variables. Note that this assumption, which is based on the central limit theorem [107], only holds when the number of assigned data subcarriers on the i^{th} antenna, denoted as K_i, is large enough. As a result, $|s_i(n)|$ follows the Rayleigh distribution, and $|s_i(n)|^2$ has a chi-square distribution with two degrees of freedom. The probability density function of the signal $|s_i(n)|^2$ can be expressed as [107]

$$p_{|s|^2}(|s_i|^2) = \frac{1}{\sigma_{K_i}^2} e^{-|s_i|^2/\sigma_{K_i}^2}, \tag{5.14}$$

where $\sigma_{K_i}^2 = \sigma^2 K_i / K$ is the variance of the signal $|s_i(n)|$. Note that $\sum_{i=1}^{n_T} K_i = n_D K$, thus we have $\sum_{i=1}^{n_T} \sigma_{K_i}^2 = n_D \sigma^2$. The *CDF* (cumulative distribution function) of the signal $|s_i(n)|^2$ is given as

$$\Pr(|s_i|^2 \le \theta) = 1 - e^{-\theta/\sigma_{K_i}^2}, \ \theta \ge 0. \tag{5.15}$$

Suppose that K samples of $|s_i(n)|, n = 0,1,...,K-1,$ are independent, the *CDF* of the peak power P_i can be expressed as

$$\begin{aligned} CDF^{P_i} &= \Pr(P_i \le P_0) = \Pr(|s_i(0)|^2 \le P_0) \Pr(|s_i(1)|^2 \le P_0) ... \Pr(|s_i(K-1)|^2 \le P_0) \\ &= (1 - e^{-P_0/\sigma_{K_i}^2})^K. \end{aligned} \tag{5.16}$$

In MIMO-OFDM systems with linear scaling, the peak power across transmit antennas P can be defined as

$$P = \max_{1 \le i \le n_T} P_i. \tag{5.17}$$

Given the statistical independence of data among transmit antennas, which is the case in the considered spatial multiplexed OFDM system, the *CDF* of the peak power P is calculated as

$$\begin{aligned} CDF^P &= \Pr(P \le P_0) = \Pr(P_1 \le P_0)\Pr(P_2 \le P_0)...\Pr(P_{n_T} \le P_0) \\ &= \prod_{i=1}^{n_T} (1 - e^{-P_0/\sigma_{K_i}^2})^K. \end{aligned} \tag{5.18}$$

Therefore, the *CCDF* of the peak power of the antenna selection MIMO-OFDM signals can be expressed as

$$CCDF_{imbalance}^P(P_0) = 1 - CDF^P = 1 - \prod_{i=1}^{n_T} (1 - e^{-P_0/\sigma_{K_i}^2})^K. \tag{5.19}$$

In the MIMO-OFDM system with a power balancing constraint, the number of allocated data subcarriers per transmit antenna is equal to one another (i.e., $K_i = n_D K / n_T := \overline{K}, \forall i = 1,2,...,n_T$). Thus, the variances of the signals are $\sigma_{K_i}^2 = n_D \sigma^2 / n_T := \sigma_{\overline{K}}^2, \forall i = 1,2,...,n_T$. As a result, the *CCDF* expression can be simplified to as

$$CCDF_{balance}^P(P_0) = 1 - (1 - e^{-P_0/\sigma_{\overline{K}}^2})^{n_T K}. \tag{5.20}$$

A comparison of the *CCDF* of the peak powers in the two systems is presented in the following theorem:

Theorem 5.1 *In MIMO-OFDM transmission schemes that consist of inactive data subcarriers (e.g., per-subcarrier antenna selection), the probability of occurrences of high peak power is smallest when the same number of data symbols is allocated to all transmit antennas, i.e.,*

$$CCDF_{balance}^P(P_0) \le CCDF_{imbalance}^P(P_0). \tag{5.21}$$

Proof: The proof is provided in Section 5.A.

When the peak-power reduction algorithm proposed in Section 5.3.2 is implemented in the MIMO-OFDM system with a power-balancing constraint, the *CCDF* of the peak power can be expressed as

$$CCDF^{P}_{balance+reduced}(P_0) = \left(CCDF^{P}_{balance}(P_0)\right)^W = \left(1-(1-e^{-P_0/\sigma^2_K})^{n_T K}\right)^W, \tag{5.22}$$

where W is the number of candidates that are assumed to be independent. Recall that, by definition, the *CCDF* value is always smaller than one (cf. Eq. (5.12)). Therefore, the *CCDF* value in Eq. (5.22) is smaller than that in Eq. (5.20), i.e.,

$$CCDF^{P}_{balance+reduced}(P_0) \le CCDF^{P}_{balance}(P_0). \tag{5.23}$$

5.4.2 Power Efficiency of Power Amplifiers

We now analyse the power efficiency (PE) of high-power amplifiers (PAs). The *drain efficiency* of PAs, which is defined as a ratio between the power drawn from the DC source P_{dc} and the average output power P_{out} is considered in this work. Denote P^i_{in} and P^i_{out} to be the average input and output powers of the PA for the i^{th} antenna, respectively. Recall that all PAs are assumed to have an unity gain, i.e., $P^i_{out} = P^i_{in}, \forall i = 1,2,...,n_T$. Hence, the instantaneous overall power efficiency of PAs in the MIMO-OFDM system can be expressed as [122]

$$\eta^{PE} = \frac{1}{n_T P_{dc}} \sum_{i=1}^{n_T} P^i_{out} = \frac{1}{n_T P_{dc}} \sum_{i=1}^{n_T} P^i_{in} = \alpha \frac{n_D \sigma^2}{n_T P_{dc}} = \frac{n_D \sigma^2 P_{sat}}{n_T P_{dc}} \frac{1}{P} = \frac{n_D \sigma^2}{2 n_T} \frac{1}{P}. \tag{5.24}$$

In the above manipulations, we have used the fact that $\sum_{i=1}^{n_T} P^i_{in} = \alpha n_D \sigma^2$ and $P_{dc} = 2P_{sat}$ for class-A PAs, regardless of the average powers of the input time-domain signals. Denoting $CCDF^{PE}(\eta^{PE}_0) = \Pr(\eta^{PE} > \eta^{PE}_0)$ to be the *CCDF* of the power efficiency, we obtain the following result with respect to η^{PE}.

Theorem 5.2 *In per-subcarrier antenna selection MIMO-OFDM systems with linear scaling, the probability of achieving high instantaneous overall power efficiency of PAs is largest when all transmit antennas have the same number of allocated data symbols, i.e.,*

$$CCDF^{PE}_{balance}(\eta^{PE}_0) \ge CCDF^{PE}_{imbalance}(\eta^{PE}_0), \tag{5.25}$$

where

$$CCDF_{balance}^{PE}(\eta_0^{PE}) = (1 - e^{-1/2\eta_0^{PE}})^{n_T K}, \tag{5.26}$$

and

$$CCDF_{imbalance}^{PE}(\eta_0^{PE}) = \prod_{i=1}^{n_T} (1 - e^{-n_D K / 2 n_T K_i \eta_0^{PE}})^K. \tag{5.27}$$

Proof: From Eq. (5.21) and Eq. (5.24), it is readily to obtain Eq. (5.25), Eq. (5.26), and Eq. (5.27).

With respect to the average value of the overall power efficiency, from Eq. (5.24), we can express the average overall power efficiency of PAs as

$$\overline{\eta}^{PE} = \varepsilon\{\eta^{PE}\} = \frac{n_D \sigma^2}{2n_T} \varepsilon\{\frac{1}{P}\} = \frac{n_D \sigma^2}{2n_T} \int \frac{1}{x} p(x) dx, \tag{5.28}$$

where *p(x)* is the *pdf* (probability distribution function) of the peak power. In the system with a balance constraint (i.e., only use *Step 1*), the *pdf* of the peak power can be calculated as

$$p_{balance}(x) = \frac{d}{dx} CDF_{balance}^{P}(x) = \frac{d}{dx} (1 - e^{-x/\sigma_{\overline{K}}^2})^{n_T K} = \frac{n_T K}{\sigma_{\overline{K}}^2} e^{-x/\sigma_{\overline{K}}^2} (1 - e^{-x/\sigma_{\overline{K}}^2})^{n_T K - 1}. \tag{5.29}$$

Hence,

$$\begin{aligned} \overline{\eta}_{balance}^{PE} &= \frac{n_D \sigma^2}{2n_T} \int \frac{1}{x} p_{balance}(x) dx = \frac{n_T K}{2} \int_{\sigma_{\overline{K}}^2}^{\overline{K}\sigma_{\overline{K}}^2} \frac{1}{x} e^{-x/\sigma_{\overline{K}}^2} (1 - e^{-x/\sigma_{\overline{K}}^2})^{n_T K - 1} dx \\ &= \frac{n_T K}{2} \int_{1}^{\overline{K}} \frac{1}{x} e^{-x} (1 - e^{-x})^{n_T K - 1} dx. \end{aligned} \tag{5.30}$$

Similarly, the power efficiency of PAs in the conventional system is

$$\begin{aligned} \overline{\eta}_{imbalance}^{PE} &= \frac{n_D \sigma^2}{2n_T} \int \frac{1}{x} p_{imbalance}(x) dx \\ &= \frac{n_D K \sigma^2}{2n_T} \int_{\sigma_{\max}^2}^{K_{\max}\sigma_{\max}^2} \frac{1}{x} \left\{ \sum_{j=1}^{n_T} \frac{e^{-x/\sigma_{K_j}^2}}{(1 - e^{-x/\sigma_{K_j}^2}) \sigma_{K_j}^2} \right\} \prod_{i=1}^{n_T} (1 - e^{-x/\sigma_{K_i}^2})^K dx, \end{aligned} \tag{5.31}$$

where $\sigma_{\max}^2 = \max\{\sigma_{K_1}^2, ..., \sigma_{K_{n_T}}^2\}$ and $K_{\max} = \max\{K_1, ..., K_{n_T}\}$.

When the peak-power reduction algorithm is also implemented (i.e., the system employs both *Step 1* and *Step 2*), it is readily from Eq. (5.23) and Eq. (5.24) that

$$CCDF^{PE}_{balance+reduced}(\eta_0^{PE}) \geq CCDF^{PE}_{balance}(\eta_0^{PE}), \tag{5.32}$$

where

$$CCDF^{PE}_{balance+reduced}(\eta_0^{PE}) = 1-\left(1-(1-e^{-1/2\eta_0^{PE}})^{n_T K}\right)^{W}. \tag{5.33}$$

Also, the average power efficiency can now be calculated as

$$\begin{aligned}\overline{\eta}^{PE}_{balance+reduced} &= \frac{n_D\sigma^2}{2n_T}\int \frac{1}{x} p_{balance+reduced}(x)dx \\ &= \frac{n_T K W}{2}\int_1^{\overline{K}} \frac{1}{x} e^{-x}(1-e^{-x})^{n_T K-1}\left(1-(1-e^{-x})^{n_T K}\right)^{W-1} dx.)\end{aligned} \tag{5.34}$$

It can be seen from Eq. (5.34) that the smaller the peak power is reduced (i.e., the larger the number of candidates W is used), the higher the power efficiency could be achieved. Note that although the integrals in Eq. (5.30), Eq. (5.31), and Eq. (5.34) have no closed-form solutions, they can be evaluated numerically. Also, the average power efficiencies in Eq. (5.30), Eq. (5.31), and Eq. (5.34) are taken with respect to the input data. In other words, they are considered as instantaneous power efficiencies with respect to the channel distribution. Consequently, the power efficiency in the systems is obtained by averaging these values over the fading channel distribution.

5.5 Analyses of Capacity and Energy Efficiency

It has been shown in Eq. (5.25) and Eq. (5.32) that the proposed system could achieve a better power efficiency of PAs than its counterpart. Thus, when the power P_{dc} is fixed, it is intuitive that an increased average power efficiency results in an increased average transmit power, which in turn leading to an increase in the achievable rate. Moreover, an increase in the data rate under a constant consumption power will translate into an improvement in energy efficiency. The improved capacity and energy efficiency are now investigated in this section.

5.5.1 Ergodic Capacity

Let us begin by rewriting the capacity in Eq. (5.10) with respect to the average SNR value of $\overline{\rho} = \overline{P}_t/\sigma_n^2$, where $\overline{P}_t = \overline{\alpha} n_D \sigma^2 = \overline{\eta}^{PE} n_T P_{dc}$ (cf. Eq. (5.24)). The ergodic capacity

is then calculated by averaging the instantaneous capacity over the fading channel distribution, i.e., $C(\overline{\rho}) = \varepsilon_{\mathbf{H}}\{I(\overline{\rho}, \underline{\mathbf{H}})\}$. From Eq. (5.9) and Eq. (5.10), the capacity in the proposed and conventional systems can be expressed, respectively, as

$$I(\overline{\rho}_{proposed}, \underline{\overline{\mathbf{H}}}) = \frac{1}{K}\sum_{k=0}^{K-1}\log_2\left(\det\left(\mathbf{I}_{n_R} + \frac{\overline{\rho}_{proposed}}{n_D}\underline{\overline{\mathbf{H}}}_k\underline{\overline{\mathbf{H}}}_k^H\right)\right), \tag{5.35}$$

and

$$I(\overline{\rho}_{imbalance}, \underline{\mathbf{H}}) = \frac{1}{K}\sum_{k=0}^{K-1}\log_2\left(\det\left(\mathbf{I}_{n_R} + \frac{\overline{\rho}_{imbalance}}{n_D}\underline{\mathbf{H}}_k\underline{\mathbf{H}}_k^H\right)\right), \tag{5.36}$$

where $\overline{\rho}_{proposed} = \overline{\eta}_{proposed}^{PE} n_T P_{dc}/\sigma_n^2$ and $\overline{\rho}_{imbalance} = \overline{\eta}_{imbalance}^{PE} n_T P_{dc}/\sigma_n^2$. Here, $\overline{\eta}_{proposed}^{PE} = \overline{\eta}_{balance+reduced}^{PE}$ if the peak-power reduction algorithm is implemented; otherwise $\overline{\eta}_{proposed}^{PE} = \overline{\eta}_{balance}^{PE}$. Also, $\underline{\overline{\mathbf{H}}}_k$ in Eq. (5.35) denotes the effective channel matrix on the k^{th} subcarrier in the proposed system, which is obtained when solving the problem in Eq. (5.11). This channel matrix is generally different from the effective channel matrix $\underline{\mathbf{H}}_k$ in the conventional system because the selected antenna subset may be different. The difference in the mutual information between the two systems can be now calculated as

$$\Delta I = I(\overline{\rho}_{proposed}, \underline{\overline{\mathbf{H}}}) - I(\overline{\rho}_{imbalance}, \underline{\mathbf{H}}) = \frac{1}{K}\sum_{k=0}^{K-1}\Delta I_k, \tag{5.37}$$

where

$$\Delta I_k = \log_2\left(\det\left(\mathbf{I}_{n_R} + \frac{\overline{\rho}_{proposed}}{n_D}\underline{\overline{\mathbf{H}}}_k\underline{\overline{\mathbf{H}}}_k^H\right)\right) - \log_2\left(\det\left(\mathbf{I}_{n_R} + \frac{\overline{\rho}_{imbalance}}{n_D}\underline{\mathbf{H}}_k\underline{\mathbf{H}}_k^H\right)\right). \tag{5.38}$$

For analytical simplicity, we focus on the high-SNR regime. At the high SNR, the capacity at the k^{th} subcarrier can be approximated as [126]

$$I_k = \log_2\left(\det\left(\frac{\overline{\rho}}{n_D}\mathbf{\Omega}_k\right)\right), \tag{5.39}$$

where

$$\mathbf{\Omega}_k = \Omega(\underline{\mathbf{H}}_k) = \begin{cases}\underline{\mathbf{H}}_k\underline{\mathbf{H}}_k^H & , n_R \le n_D \\ \underline{\mathbf{H}}_k^H\underline{\mathbf{H}}_k & , n_R > n_D\end{cases}. \tag{5.40}$$

Thus, the difference in the mutual information can be rewritten as

$$\begin{aligned}\Delta I &= \frac{1}{K}\sum_{k=0}^{K-1}\left(\log_2\left(\det\left(\frac{\overline{\rho}_{proposed}}{n_D}\overline{\mathbf{\Omega}}_k\right)\right)-\log_2\left(\det\left(\frac{\overline{\rho}_{imbalance}}{n_D}\mathbf{\Omega}_k\right)\right)\right)\\ &= p\log_2\frac{\overline{\eta}^{PE}_{proposed}}{\overline{\eta}^{PE}_{imbalance}}-\frac{1}{K}\sum_{k=0}^{K-1}\Delta_k := T_1+T_2,\end{aligned} \tag{5.41}$$

where $p=\min(n_D,n_R)$, $\overline{\mathbf{\Omega}}_k=\Omega(\overline{\underline{\mathbf{H}}}_k)$, and

$$\Delta_k=\log_2\left(\det\left(\mathbf{\Omega}_k\right)\right)-\log_2\left(\det\left(\overline{\mathbf{\Omega}}_k\right)\right) \tag{5.42}$$

is the loss in the mutual information associated with the k^{th} subcarrier due to the constrained allocation. Note that if both systems have the same selected antenna subset at the k^{th} subcarrier, then $\Delta_k = 0$; otherwise, $\Delta_k > 0$. Thus, the total loss in the mutual information $\Delta=\frac{1}{K}\sum_{k=0}^{K-1}\Delta_k>0$.

We have some important observations with respect to the value of ΔI in Eq. (5.41):

- The change of ΔI comes from two sources. The first source T_1 is a benefit in capacity due to the improvement in the power efficiency of PAs. The second source T_2 is a penalty that incurs because the chosen effective channel matrices in the proposed system are different from the ones in the conventional system.
- For each channel realization, the matrix $\underline{\mathbf{H}}_k$ is fixed and the first term T_1 in Eq. (5.41) is a constant. Thus, the value of ΔI depends on how the effective channel matrix $\overline{\underline{\mathbf{H}}}_k$ is selected in the constrained selection scheme. From this observation, it is clear that, to make the value ΔI become as positive as possible, the constrained selection method should result in the cost penalty Δ as small as possible. We note that the formulated optimisation in Eq. (5.11) could achieve the minimum possible value of the total cost. Hence, it is expected that the constrained selection scheme based on linear optimisation will guarantee the maximum achievable value of ΔI. In addition, to have an insight into the cost penalty, we derive the upper bound of the expected value of the cost penalty in Section 5.B. Based on the obtained bound, it is observed that, for fixed values of n_T and n_D, the cost penalty becomes smaller with an increasing value of $q=\max(n_D,n_R)$.
- As $\Delta > 0$, the upper bound of the capacity improvement can be given as

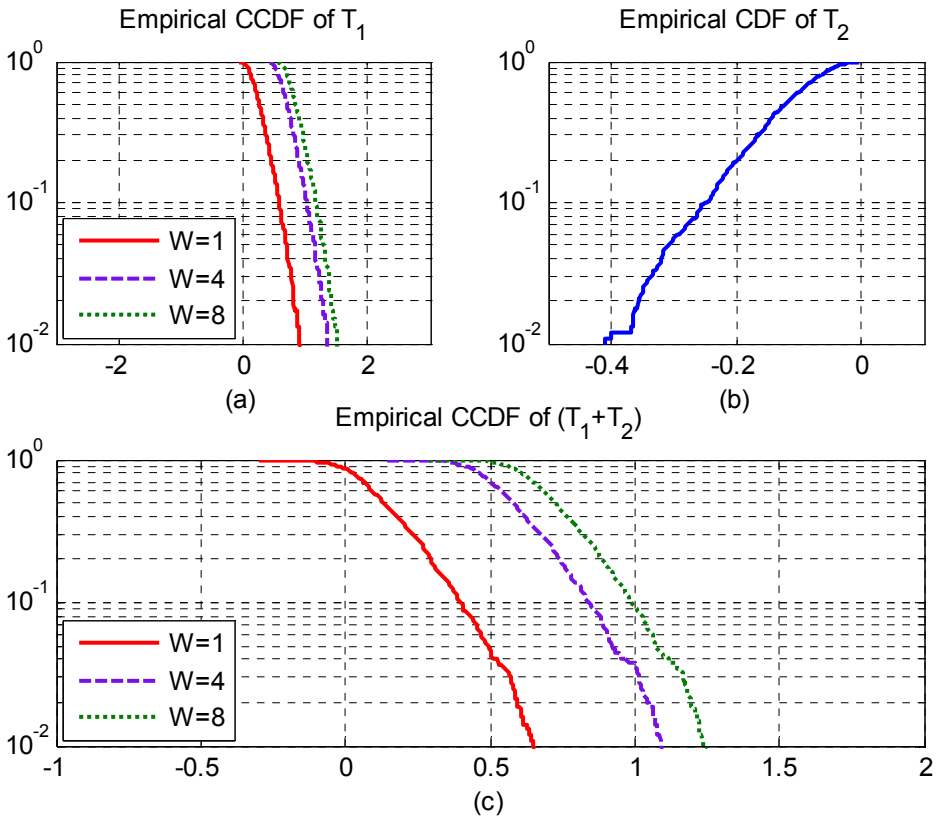

Figure 5.3. Statistical distributions (Note: T_2 is independent of W).

$$\Delta C = \varepsilon_{\mathbf{H}}\{\Delta I\} \le p \log_2 \varepsilon_{\mathbf{H}}\left\{\frac{\overline{\eta}^{PE}_{proposed}}{\overline{\eta}^{PE}_{imbalance}}\right\}. \tag{5.43}$$

In Eq. (5.43), we have used Jensen's inequality of $\varepsilon\{\log(x)\} \le \log(\varepsilon\{x\})$ as $\log(x)$ is a concave function. Based on this bound, we could estimate the maximum improvement in capacity that could be realized in the proposed system compared to its counterpart.

It is now necessary to evaluate the change in capacity, i.e., ΔC. We note that although the distribution of the mutual information at high SNRs can be well approximated by a Gaussian distribution [126], it is still challenging to perform a mathematical evaluation of ΔC from a statistical viewpoint. This is mainly due to the fact that the two terms in Eq. (5.41) are complicated, dependent random variables. Thus, we perform a numerical evaluation of ΔC instead. Figure 5.3 plots the empirical C*CDF* of T_1, *CDF* of T_2, and *CCDF* of ΔI. In the figure, 'W=1' stands for the case in which only Step 1 in Section 5.3.1 is implemented. The results are obtained in the systems with n_T = 4, n_D = 2, n_R = 2, K=128, and are averaged over 10^3 channel realizations. Details about other simulation parameters are described in Section 5.6. The numerical

results confirm that $T_1 > 0$ and $T_2 < 0$. Moreover, as shown in Figure 3c, ΔI is always positive when the peak-power reduction algorithm is implemented (i.e., $W = 4$ and $W = 8$). For the case of $W = 1$, the probability of ΔI being positive is significant. Therefore, the proposed system attains a better ergodic capacity than that in the conventional system. Numerical results of the achieved capacities in the considered systems will be provided in Section 5.6.

5.5.2 Energy Efficiency

In this subsection, we examine the efficacy of the proposed system from an energy-efficiency (EE) perspective. Energy efficiency (bits/Joule) in MIMO-OFDM systems can be defined as (cf. Eq. (2.33))

$$EE = \frac{BW \times C(\overline{\rho})}{P_{total}}, \tag{5.44}$$

where $C(\overline{\rho})$ is the achievable rate in bits/s/Hz, i.e., $C(\overline{\rho}) = \varepsilon_{\mathbf{H}}\{I(\overline{\rho}, \underline{\mathbf{H}})\}$, BW is the bandwidth, and $P_{total} = n_T P_{dc} + n_T P_{ctx} + n_R P_{crx} + P_{bb}$ is the total power consumption. It can be seen from Eq. (5.44) that given a fixed value of P_{total}, a comparison of energy efficiency achieved in the two systems is based on the capacity comparison that has been analysed in Section 5.5.1. We are now interested in evaluating a useful metric of energy efficiency-spectral efficiency performance. Recall that the average SNR $\overline{\rho}$ is given as $\overline{\rho} = \overline{P}_t / \sigma_n^2 = \overline{\eta}^{PE} n_T P_{dc} / \sigma_n^2$. Thus, we can rewrite the energy efficiency in Eq. (5.44) as a function of P_{dc} as

$$EE(P_{dc}) = \frac{BW \times C(\overline{\eta}^{PE} n_T P_{dc} / \sigma_n^2)}{n_T P_{dc} + n_T P_{ctx} + n_R P_{crx} + P_{bb}}. \tag{5.45}$$

The energy efficiency of the proposed and conventional systems can now be, respectively, expressed as

$$\begin{aligned} EE_{proposed}(P_{dc}) &= \frac{BW \times C_{proposed}(\overline{\eta}_{proposed}^{PE} n_T P_{dc} / \sigma_n^2)}{n_T P_{dc} + n_T P_{ctx} + n_R P_{crx} + P_{bb}} \\ &= \frac{BW \times \varepsilon_{\mathbf{H}}\{I(\overline{\eta}_{proposed}^{PE} n_T P_{dc} / \sigma_n^2, \overline{\underline{\mathbf{H}}})\}}{n_T P_{dc} + n_T P_{ctx} + n_R P_{crx} + P_{bb}}, \end{aligned} \tag{5.46}$$

and

$$EE_{imbalance}(P_{dc}) = \frac{BW \times C_{imbalance}(\overline{\eta}_{imbalance}^{PE} n_T P_{dc} / \sigma_n^2)}{n_T P_{dc} + n_T P_{ctx} + n_R P_{crx} + P_{bb}} = \frac{BW \times \varepsilon_{\mathbf{H}}\{I(\overline{\eta}_{imbalance}^{PE} n_T P_{dc} / \sigma_n^2, \underline{\mathbf{H}})\}}{n_T P_{dc} + n_T P_{ctx} + n_R P_{crx} + P_{bb}}. \quad (5.47)$$

Similarly to the case of capacity, we compare the energy efficiency achieved in the two systems by means of numerical results in the next section. Note that the calculation of energy efficiency in the proposed system (i.e., Eq. (5.46)) has assumed that a reduction in spectral efficiency due to the side information as well as additional processing power required for the peak-power reduction algorithm are negligible. In fact, a reduction in spectral efficiency is very small. For example, in a system with 16-QAM, FFT size of 128, $n_D = 2$, and $W = 4$ (i.e., 2 bits are needed for side information), a spectral efficiency loss is0.19% (i.e., 2*bits*/(128×4×2+2)*bits*). Also, it was shown in [127] that the additional power cost when implementing SLM schemes is minuscule. Thus, the proposed peak-power reduction algorithm in Section 5.3.2, which is a SLM-based scheme, requires a small additional power cost.

5.6 Simulation Results and Discussions

In this section, we provide numerical results to validate the analyses performed in the previous sections, as well as demonstrate the effectiveness of the proposed allocation scheme. A MIMO-OFDM system with $n_T = 4$, $n_D = 2$, and $n_R = 2$ is considered in the simulations. The system parameters are listed in Table 5.1. These parameters are chosen based on the legacy WiMedia MB-OFDM UWB standard [36]. We assume that perfect channel state information is available at the receiver. Also, the feedback link has no delay and is error-free.

5.6.1 Evaluation of Peak-Power Distribution

In Figure 5.4, we plot the *CCDFs* of the peak power of time-domain signals. The analytical curves are based on Eq. (5.19), Eq. (5.20), and Eq. (5.22). Meanwhile, the simulation curves are empirical *CCDF* values. The simulation result confirms that a system with the proposed allocation scheme offers a better *CCDF* performance than its counterpart. As expected, the occurrence of high peak power is significantly reduced when the peak-power reduction algorithm is implemented. Also, it can be seen that the improvement associated with this algorithm is reduced with increasing *W*. In other words, a very large value of *W*, while requiring higher complexity in terms on the

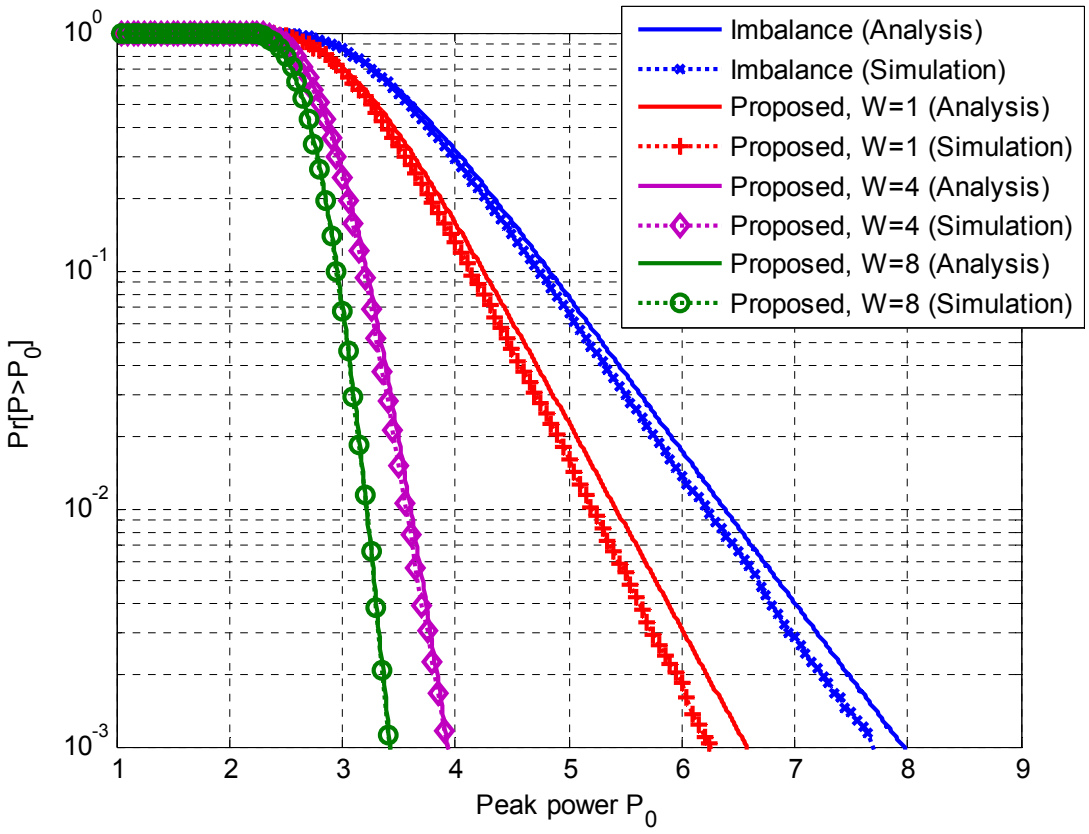

Figure 5.4. Comparison of *CCDF*s of the peak-powers.

Table 5.1. Simulation parameters.

Parameter	Value
Bandwidth	528 MHz
FFT size	128
Number of samples in zero-padded suffix	37
Modulation scheme	4-QAM
IEEE 802.15.3a channel model [116]	CM1

number of IFFT operations, results in a marginal improvement. Thus, it is reasonable to choose a relatively small value for W (e.g., W = 4). It is also worth noting that the analytical curves are relatively close to the simulation curves. The small gaps exist due to the fact that the assumption of independent samples $|s_i(n)|$ to obtain Eq. (5.16) does not strictly hold as we have $\sum_{n=0}^{K-1}|s_i(n)|^2 = \sigma^2 K_i$ by Parseval's relation [107].

5.6.2 Evaluation of Power Efficiency of Power Amplifiers

Figure 5.5 compares the *CCDF*s of the power efficiency achieved in the proposed and conventional systems. It can be seen that the probability of power efficiency being

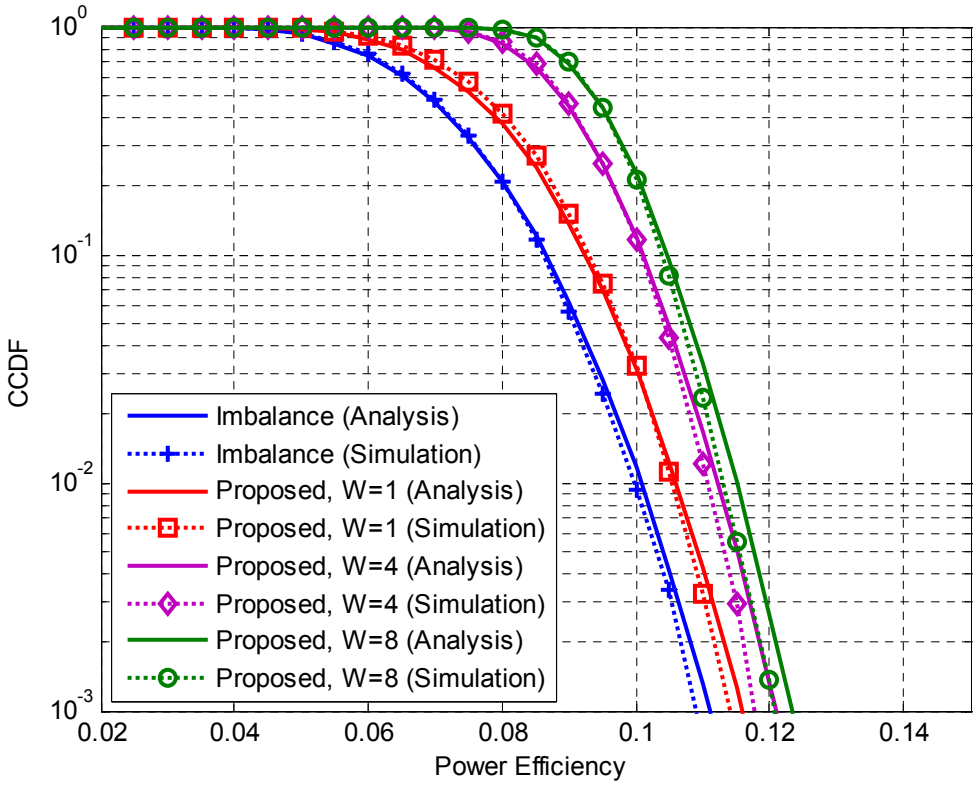

Figure 5.5. Comparison of *CCDF*s of the power efficiencies.

Table 5.2. A comparison of average power efficiencies.

	Imbalance	Proposed (W=1)	Proposed (W=4)	Proposed (W=8)
$\overline{\eta}^{PE}$ (Simulation)	0.0697	0.0768	0.0894	0.0942
$\overline{\eta}^{PE}$ (Analysis)	0.0691	0.0757	0.0892	0.0943
Improvement $\frac{\overline{\eta}^{PE}_{proposed}-\overline{\eta}^{PE}_{imbalance}}{\overline{\eta}^{PE}_{imbalance}}$	–	10.19%	28.26%	35.15%

large highly likely occurs in the proposed system, compared to its counterpart. Also, the simulation results agree well with the analytical results derived in Eq. (5.26), Eq. (5.27), and Eq. (5.33). In Table 5.2, we compare the average power efficiencies. Here, the analytical values are obtained according to Eq. (5.30), Eq. (5.31), and Eq. (5.34). Meanwhile, the simulation values are empirical values based on the original definition of the drain efficiency in Eq. (5.24). Also, these values are averaged over the fading channel realizations. It can be seen that the derived expressions approximate well the achieved power efficiencies. Table 5.2 also provides relative improvements of the

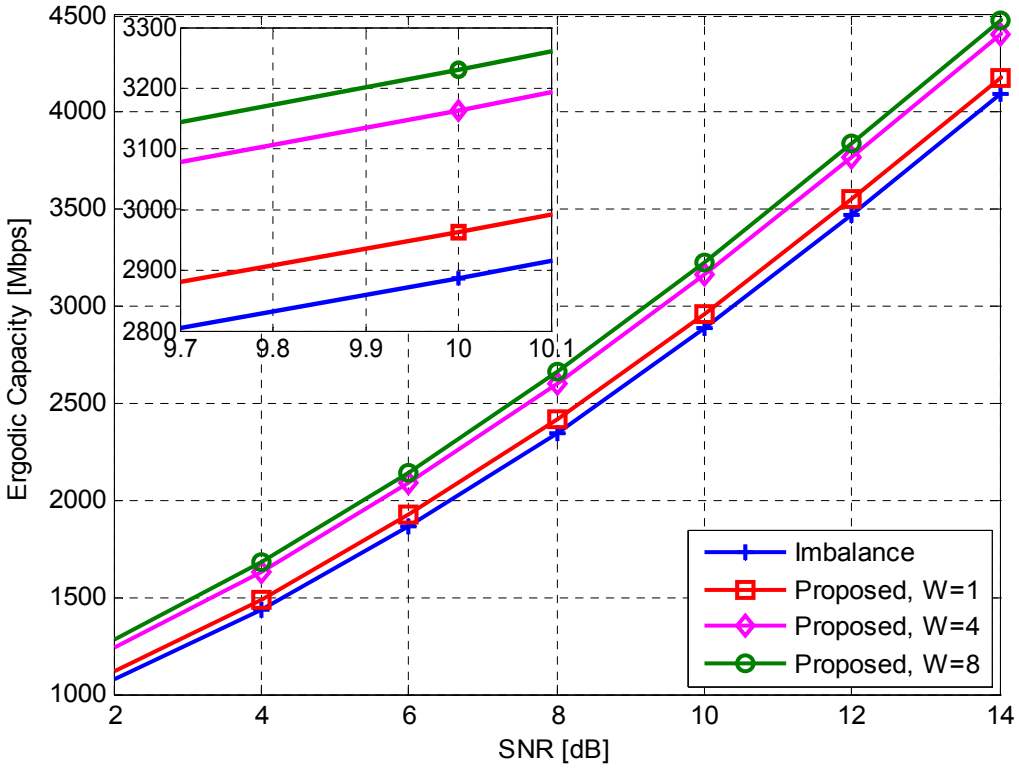

Figure 5.6. Comparison of the ergodic capacities.

power efficiencies achieved in the proposed system over the conventional system. These improvements are calculated based on the $\overline{\eta}^{PE}$ (Simulation) values. It is clear that the proposed system could achieve a significant improvement in terms of average power efficiency.

5.6.3 Evaluations of Capacity and Energy Efficiency

Figure 5.6 shows the system capacity in Mbps (i.e., the normalized value in Eq. (5.9) is scaled up with the system bandwidth *BW*) versus the SNR value of σ^2/σ_n^2. It is clear that a system with the proposed allocation scheme achieves a higher capacity than its counterpart. This agrees with the analysis in Section 5.5.1 that the change in capacity ΔC is positive. In Figure 5.7, we plot the energy efficiency (Mbits/Joule) versus spectral efficiency (bps/Hz). This figure is obtained based on Eq. (5.46) and Eq. (5.47) when varying P_{dc}. Other parameters are P_{ctx} = 60 mW, P_{crx} =60 mW, P_{bb} = 50 mW, and $\sigma^2/\sigma_n^2 = 15dB$. As expected, the improvement in the power efficiency of PAs results in improved energy-efficiency. In addition, it can be observed that there exists an energy efficiency-spectral efficiency (EE-SE) trade-off in the systems. The proposed system can achieve a better EE-SE trade-off performance than its counterparts.

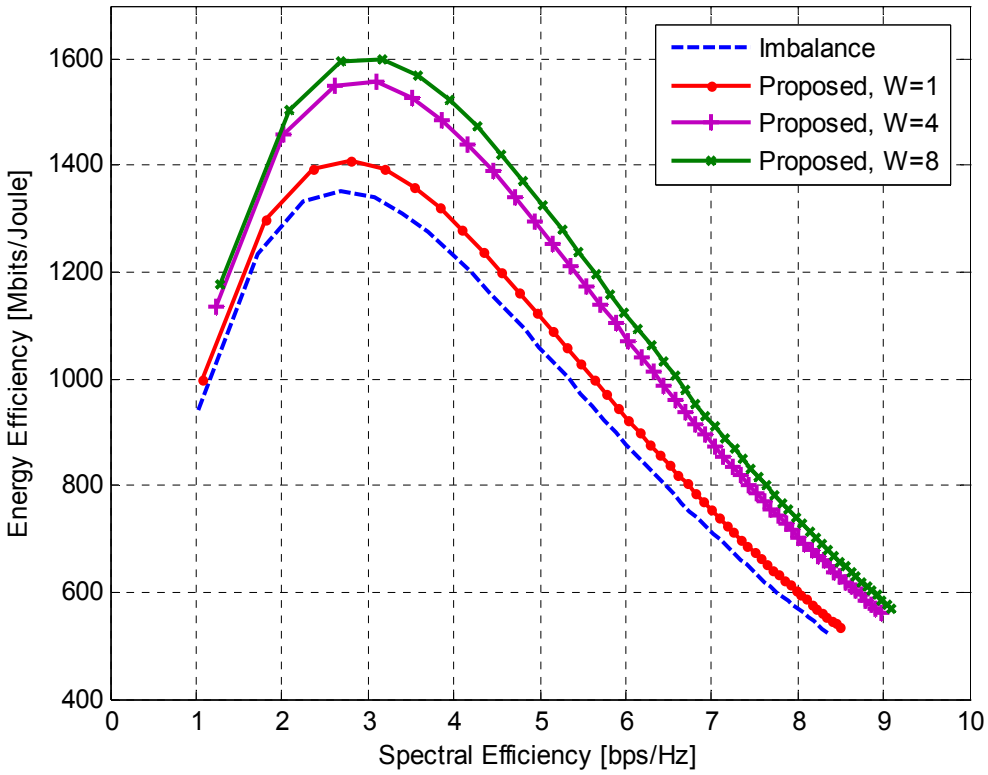

Figure 5.7. Energy efficiency versus spectral efficiency.

5.7 Summary

In this chapter, an antenna selection MIMO-OFDM system with linear scaling has been investigated from an energy-efficiency perspective. It has been shown that an unbalance allocation of data subcarriers associated with the conventional per-subcarrier antenna selection scheme affects the power efficiency of PAs, as well as the energy efficiency of the whole system. To deliver the maximum overall power efficiency, a two-step strategy has been proposed, which consists of equal allocation data subcarriers across antennas and peak-power reduction. It has been proved from the power-efficiency viewpoint that the proposed allocation scheme outperforms the conventional scheme. The expressions of the average power efficiency have been derived. Moreover, the improvements in terms of capacity and energy efficiency resulting from the improved power efficiency have been analysed. The analytical results are validated by simulation results. The simulation results also show that the system with the proposed allocation scheme could achieve a better EE-SE trade-off, compared to its counterpart.

5.A Proof of Theorem 5.1

Let us begin by considering a function $f(\upsilon) = 1 - e^{-P_0/\upsilon}, 0 < \upsilon \le \sigma^2_{\max}$, where $\sigma^2_{\max} = \max\{\sigma^2_{K_1}, \sigma^2_{K_2}, ..., \sigma^2_{K_{n_T}}\}$. The second derivative of this function is

$$f''(\upsilon) = \frac{2P_0\upsilon - P_0^2}{\upsilon^4} e^{-P_0/\upsilon}. \tag{5.48}$$

From a power amplifier perspective, it is of interest to consider the situation when the peak power across antennas P_0 is large. Thus, we consider the scenarios of $P_0 > 2\sigma^2_{\max}$, where $\sigma^2_{\max}$ is the maximum average power across antennas. Under these situations, it is clear that $f''(\upsilon) < 0, \forall \upsilon \in (0, \sigma^2_{\max}]$. Hence, the function $f(\upsilon)$ is concave. By applying Jensen's inequality, we obtain a following inequality

$$\frac{1}{n_T}\sum_{i=1}^{n_T} f(\sigma^2_{K_i}) \le f\left(\frac{1}{n_T}\sum_{i=1}^{n_T}\sigma^2_{K_i}\right) = f\left(\frac{1}{n_T}\sum_{i=1}^{n_T}\sigma^2_{\overline{K}}\right) = f(\sigma^2_{\overline{K}}), \tag{5.49}$$

where the equality comes from the fact that $\sum_{i=1}^{n_T}\sigma^2_{K_i} = \sum_{i=1}^{n_T}\sigma^2_{\overline{K}} = n_D\sigma^2$. Eq. (5.49) can also be rewritten as

$$\sum_{i=1}^{n_T}(1 - e^{-P_0/\sigma^2_{K_i}}) \le n_T(1 - e^{-P_0/\sigma^2_{\overline{K}}}), \tag{5.50}$$

with equality if and only if $\sigma^2_{K_i} = \sigma^2_{\overline{K}}, \forall i = 1, ..., n_T$.

On the other hand, by applying the arithmetic-geometric mean inequality, and note that $(1 - e^{-x}) > 0, \forall x > 0$, we have

$$\prod_{i=1}^{n_T}(1 - e^{-P_0/\sigma^2_{K_i}}) \le \left(\frac{1}{n_T}\sum_{i=1}^{n_T}(1 - e^{-P_0/\sigma^2_{K_i}})\right)^{n_T}. \tag{5.51}$$

Note that the equality in Eq. (5.51) holds if and only if $\sigma^2_{K_i} = \sigma^2_{\overline{K}}, \forall i = 1, ..., n_T$. Combining Eq. (5.50) and Eq. (5.51) results in

$$\prod_{i=1}^{n_T}(1 - e^{-P_0/\sigma^2_{K_i}}) \le \left(1 - e^{-P_0/\sigma^2_{\overline{K}}}\right)^{n_T}, \tag{5.52}$$

with equality if and only if $\sigma_{K_i}^2 = \sigma_{\overline{K}}^2, \forall i = 1,...,n_T$. Thus, we get the following desired inequality

$$1 - \prod_{i=1}^{n_T} (1 - e^{-P_0/\sigma_{K_i}^2})^K \geq 1 - \left(1 - e^{-P_0/\sigma_{\overline{K}}^2}\right)^{n_T K}, \tag{5.53}$$

or

$$CCDF_{imbalance}^{P}(P_0) \geq CCDF_{balance}^{P}(P_0). \tag{5.54}$$

This completes the proof.

5.B Derivation of an Upper Bound of the Cost Penalty in Eq. (5.42)

In this section, we derive an upper bound of the expected value of Δ_k. It can be seen from Eq. (5.8) that, among all possible matrices $\underline{\mathbf{H}}_k$, the matrix $\underline{\mathbf{H}}_k$ with the highest value of $\log_2(\det(\mathbf{\Omega}_k)), \mathbf{\Omega}_k = \Omega(\underline{\mathbf{H}}_k),$ will be selected as the effective channel matrix for the k^{th} subcarrier in the conventional scheme. Meanwhile, in the proposed scheme, due to the balance constraint, the effective channel matrix associated with the k^{th} subcarrier is not necessarily the one with the highest $\log_2(\det(\mathbf{\Omega}_k))$, i.e., $\log_2(\det(\overline{\mathbf{\Omega}}_k)) \leq \log_2(\det(\mathbf{\Omega}_k))$. Thus, the expected value of Δ_k can be computed by using order statistics. In particular, an upper bound on the expected difference of two order statistics, the Γ^{th} and γ^{th}, $1 \leq \gamma < \Gamma$, is given by [118]

$$\varepsilon\{\Delta_k\} = \varepsilon\{\log_2(\det(\mathbf{\Omega}_k))\} - \varepsilon\{\log_2(\det(\overline{\mathbf{\Omega}}_k))\} \leq \sigma_C \sqrt{\frac{\Gamma(\gamma+1)}{\gamma}}, \tag{5.55}$$

where σ_C^2 is the variance of $\log_2(\det(\mathbf{\Omega}_k))$ that is assumed to be the same for all possible matrices $\underline{\mathbf{H}}_k$.

On the other hand, suppose that the entries of the $n_R \times n_T$ matrix $\mathbf{H}_k$ are *i.i.d.* complex Gaussian random variables with zero-mean and unit-variance, then for any effective channel matrix $\underline{\mathbf{H}}_k$, $\mathbf{\Omega}_k$ is a complex Wishart matrix. It follows from [126] that the variance of $\log_2(\det(\mathbf{\Omega}_k))$ can be expressed as

$$\sigma_C^2 = [\log_2(e)]^2 \sum_{m=1}^{p} \psi'(q-m+1), \tag{5.56}$$

where $p = \min(n_D, n_R)$, $q = \max(n_D, n_R)$, and $\psi'(x) = \sum_{\varphi=1}^{\infty} \frac{1}{(\varphi+x-1)^2}$ is the first derivative of the digamma function. By approximating $\psi'(x) \approx 1/x$ [126], the simpler expression for σ_C^2 in Eq. (5.56) is given as

$$\sigma_C^2 = \left[\log_2(e)\right]^2 \sum_{m=1}^{p} \frac{1}{q-m+1}. \tag{5.57}$$

By substituting Eq. (5.57) into Eq. (5.55), we finally arrive at

$$\varepsilon\{\Delta_k\} \le \log_2(e) \sqrt{\left(\sum_{m=1}^{p} \frac{1}{q-m+1} \right) \times \frac{\Gamma(\gamma+1)}{\gamma}}. \tag{5.58}$$

Chapter 6

Energy-Efficient Antenna Selection MIMO Systems under QoS Constraints

In the previous chapters, improved energy efficiency in antenna selection systems has been achieved by using adaptive RF chains and power amplifier aware selection methods. In this chapter, energy efficiency in antenna selection MIMO systems with/without an automatic repeat request (ARQ) mechanism is investigated from a viewpoint of transmitted energy allocation. In particular, the optimal energy per transmitted data symbol that maximises the energy efficiency subject to a quality-of-service (QoS) constraint is analysed. This chapter is organized as follows. In Section 6.1, the related works and motivation of this chapter are presented. In Section 6.2, a system model for an antenna selection MIMO system over Nakagami-*m* fading channels is described. In Section 6.3, an approximation expression for frame-error rate (FER) is derived. Energy efficiency in antenna selection MIMO systems and MIMO-ARQ systems is analysed in Section 6.4 and Section 6.5, respectively. Simulation results are provided in Section 6.6. Finally, Section 6.7 concludes the chapter.

6.1 Introduction

As discussed in Chapter 2, some research works have studied energy efficiency in antenna selection single-carrier systems, e.g., [74-78]. However, in all of these works, the metric of energy efficiency is defined as a ratio between the ergodic capacity and the total consumed power. Thus, it does not take into account many important system parameters, such as channel codes, modulation schemes or detection methods.

In this chapter, energy efficiency in antenna selection systems is analysed that takes into consideration the aforementioned system parameters. Two system configurations are considered, including an antenna selection MIMO system and an antenna selection MIMO ARQ (automatic repeat request) system. The aim is to maximise the energy

efficiency subject to a quality-of-service constraint (i.e., an error-performance requirement). The main contributions of this chapter are summarised as follows.

i) An analytical expression that can accurately approximate a frame-error rate (FER) in antenna selection MIMO systems over quasi-static Nakagami-*m* fading is derived.

ii) An energy-efficiency metric that is defined as the number of successfully received bits per unit energy consumption is shown to be a quasi-concave function with respect to (w.r.t.) the average signal-to-noise ratio (SNR). Similarly, the total energy required to successfully deliver one information bit in the ARQ system, is a quasi-convex function.

iii) The optimal value of the average energy per transmitted symbol to maximise the energy efficiency in antenna selection MIMO system with/without ARQ is determined.

iv) Antenna selection MIMO systems are shown to outperform a single-input single output (SISO) system from an energy-efficiency perspective. Moreover, the energy efficiency in antenna selection MIMO systems will be improved when the number of equipped antennas is increased.

6.2 System Model

Let us consider an antenna selection MIMO system with n_T transmit antennas and n_R receive antennas over a Nakagami-*m* fading channel. A block diagram of the system with/without an ARQ mechanism is shown in Figure 6.1. In this system, there is only one RF chain available at the transmitter and receiver. Each frame of L_f bits, consisting of L_d information bits and $L_h = (L_f - L_d)$ overhead bits, is first encoded by a rate-r_c channel encoder, and then mapped into a *M*-ary quadrature amplitude modulation (*M*-QAM) constellation. At any time instant, only one out of n_T transmit antennas and only one out of n_R receive antennas are selected for data transmission. Assuming that the flat fading channel is quasi-static (i.e., fading coefficients remain constant during one frame, and vary from one frame to another), the received signal can be expressed as

$$y = \sqrt{E_r} h_{i,j} x + n_j, \tag{6.1}$$

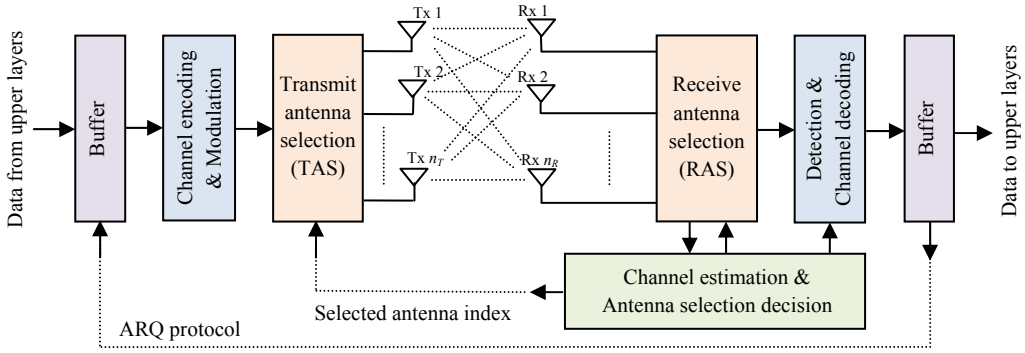

Figure 6.1. Block diagram of an antenna selection MIMO system (with/without ARQ).

where x is a modulation symbol drawn from a unit-energy constellation, E_r is the average received energy per symbol, $h_{i,j}$ is the flat Nakagami-m fading channel coefficient between the i^{th} transmit antenna and the j^{th} receive antenna with $\varepsilon\{|h_{i,j}|^2\} = 1$, where $\varepsilon\{.\}$ denotes an expectation operator, and n_j is the additive white Gaussian noise at the j^{th} receive antenna with power spectral density (PSD) of N_0.

Denote E_s to be the average transmitted energy per symbol. Note that this energy E_s is the actual average transmitted energy (i.e., after a power amplifier-PA). Then, we have a relation

$$E_{\text{s}} = E_{\text{r}} G_d, \tag{6.2}$$

where G_d is a factor that represents antenna gain, the path-loss, noise figure, etc. This factor can be expressed as $G_d = G_0 d^{\chi} G_M$, where G_0 is the factor gain at the unit distance which is defined by antenna gain and carrier frequency, d is the transmission distance, χ is the path-loss exponent, and G_M stands for other parameters such as noise figure and the link margin compensating the variations of hardware process [52].

Let us define the average signal-to-noise ratio (SNR) in terms of E_b/N_0 as

$$\bar{\gamma} = \frac{E_b}{N_0} = \frac{E_r}{N_0 r_c \log_2 M} = \frac{E_s}{G_d N_0 r_c \log_2 M}, \tag{6.3}$$

where $E_b = E_r / (r_c \log_2 M)$. Also, the instantaneous SNR between the i^{th} transmit and the j^{th} receive antennas can be expressed as

$$\gamma_{i,j} = \frac{E_s \,|\, h_{i,j} \,|^2}{G_d N_0 r_c \log_2 M}. \tag{6.4}$$

In this work, we consider a maximum SNR criterion for simplicity. Accordingly, the transmit and receive antennas are selected to maximise the instantaneous SNR value $\gamma_{i,j}$, i.e.

$$(\hat{i},\hat{j}) = \arg \max_{\substack{i=1,2..,n_T \\ j=1,2..,n_R}} \gamma_{i,j}. \tag{6.5}$$

Assuming that the channel state information (CSI) is available at the receiver, the receiver can select the optimal transmit and receive antennas based on Eq. (6.5). The transmitter is then informed of the selected transmit antenna index via a low-rate feedback link. Note that the CSI can be obtained by using pilot symbols. In addition, in the system with a time-division duplex (TDD) mode, the transmitter can estimate the CSI due to the channel reciprocity. In such case, there is no need to feedback the selected transmit antenna index.

With respect to the employed ARQ protocol, we consider type-I ARQ in this system. This type of protocol is simple, which is important for low cost and low energy systems. For each transmission round, the receiver decodes data only based on the received signal in that round. If the receiver recovers the data frame successfully, it sends a positive acknowledgement (ACK) to the transmitter. In case the data frame cannot be recovered, it will be discarded, and a negative acknowledgement (NACK) will be sent to the transmitter. The data frame will be retransmitted if the transmitter receives a NACK. In this work, we assume that there is no limit on the number of retransmissions, i.e., delay tolerant systems. Thus, the average number of transmissions is given as [128]

$$\upsilon = \frac{1}{1 - FER}, \tag{6.6}$$

where *FER* is the average frame-error rate. Note that, as the fading channel is assumed quasi-static, the selected antennas during the first transmission round and retransmission rounds (if required) of the same information data frame are not necessarily the same.

6.3 Frame-Error Rate Approximation over Nakagami-*m* Fading Channels

In this section, we derive an expression for FER approximation in antenna selection systems. It is well known that a Nakagami-*m* distribution can model a wide range of fading channel conditions depending on the parameter *m*. Thus, in this work, an

expression for FER approximation is derived directly in Nakagami-*m* fading channels. The obtained result will be used to analyse the energy efficiency in Section 6.4 and Section 6.5. As the exact expression for the average FER over quasi-static fading channels is hard to derive, a threshold-based FER approximation approach was considered in the literature, i.e., in turbo codes based single-antenna systems [129], or non-iterative decoded single-antenna systems [130]. In antenna selection systems, we can express the average FER as

$$FER(\bar{\gamma}) = \int_0^{\infty} FER_G(\gamma) p_{AS}(\bar{\gamma},\gamma) d\gamma \approx \int_0^{\gamma_{th}} p_{AS}(\bar{\gamma},\gamma) d\gamma = F_{AS}(\bar{\gamma},\gamma_{th}), \tag{6.7}$$

where $FER_G(\gamma)$ is the FER over the Gaussian channel, $p_{AS}(\bar{\gamma},\gamma)$ is the probability density function (PDF) of the received SNR in antenna selection systems, γ_{th} is a threshold SNR with an assumption that $FER_G(\gamma \mid \gamma \le \gamma_{th}) \approx 1$ and $FER_G(\gamma \mid \gamma > \gamma_{th}) \approx 0,$ and $F_{AS}(.)$ is the cumulative distribution function (CDF) of the received SNR, i.e., $F_{AS}(\bar{\gamma},\gamma_0) = \Pr(\gamma \le \gamma_0) = \int_0^{\gamma_0} p_{AS}(\bar{\gamma},\gamma) d\gamma$.

In Nakagami-*m* fading channels, the PDF and CDF of the received SNR can be expressed, respectively, as $p_{\bar{\gamma}}(\gamma) = (m/\bar{\gamma})^m \gamma^{m-1} e^{-m\gamma/\bar{\gamma}} / \Gamma(m),\ \gamma \ge 0,$ and $F_{\bar{\gamma}}(\gamma) = \psi(m, m\gamma/\bar{\gamma})/\Gamma(m),\ \gamma \ge 0,$ where $\Gamma(x) = \int_0^{+\infty} e^{-t} t^{x-1} dt$ and $\psi(a,x) = \int_0^x e^{-t} t^{a-1} dt,\ \mathrm{Re}\{a\} > 0,$ denote the Gamma function and the incomplete Gamma function, respectively [103, 131]. Moreover, when the parameter *m* is an integer value, we can rewrite the CDF of the received SNR as $F_{\bar{\gamma}}(\gamma) = 1 - e^{-m\gamma/\bar{\gamma}} \sum_{k=0}^{m-1} (m\gamma/\bar{\gamma})^k / k!,\ \gamma \ge 0$ [103]. Thus, $p_{AS}(\bar{\gamma},\gamma)$ in antenna selection systems can be calculated by means of order statistics [100] as

$$\begin{aligned} p_{AS}(\bar{\gamma},\gamma) &= n_T n_R \times p_{\bar{\gamma}}(\gamma) \times [F_{\bar{\gamma}}(\gamma)]^{n_T n_R - 1} \\ &= n_T n_R \left(\frac{m}{\bar{\gamma}}\right)^m \frac{\gamma^{m-1} e^{-m\gamma/\bar{\gamma}}}{\Gamma(m)} \left(1 - e^{-m\gamma/\bar{\gamma}} \sum_{k=0}^{m-1} \frac{(m\gamma/\bar{\gamma})^k}{k!}\right)^{n_T n_R - 1}, \ \gamma \ge 0. \end{aligned} \tag{6.8}$$

Also, the CDF of the received SNR in antenna selection systems is calculated as

$$F_{AS}(\bar{\gamma},\gamma) = \left(F_{\bar{\gamma}}(\gamma)\right)^{n_T n_R} = \left(1 - e^{-m\gamma/\bar{\gamma}} \sum_{k=0}^{m-1} \frac{(m\gamma/\bar{\gamma})^k}{k!}\right)^{n_T n_R}, \ \gamma \ge 0. \tag{6.9}$$

By substituting Eq. (6.9) into Eq. (6.7), we obtain the FER approximation as

$$FER(\bar{\gamma}) \approx F_{AS}(\bar{\gamma}, \gamma_{th}) = \left(1 - e^{-m\gamma_{th}/\bar{\gamma}} \sum_{k=0}^{m-1} \frac{(m\gamma_{th}/\bar{\gamma})^k}{k!}\right)^{n_T n_R}. \quad (6.10)$$

Note that Eq. (6.10) can also be obtained by substituting Eq. (6.8) into the integral in Eq. (6.7). When the parameter m = 1 (i.e., Rayleigh fading channel), Eq. (6.10) can be simplified to as

$$FER(\bar{\gamma}) \approx \left(1 - e^{-\gamma_{th}/\bar{\gamma}}\right)^{n_T n_R}. \quad (6.11)$$

We now consider a calculation of the SNR threshold γ_{th} in Eq. (6.10). For diversity systems, a threshold γ_{th} can be obtained by using a criterion proposed in [132]. However, this method only offers a good FER approximation at the high SNR region. It was shown in [133] that SISO ARQ systems achieve the optimal energy efficiency at the low SNR region. Thus, it is important to obtain γ_{th} that could offer an accuracy approximation of FER at the low SNR region. For diversity systems operating over Nakagami-*m* fading channels, a derivation of a mathematical expression of γ_{th} that is optimised for a low SNR region is hard. Hence, in this work, we investigate the following two approaches to obtain γ_{th}.

- *Least-square* (*LS*) *matching* (*i.e., curve fitting*): In this method, the threshold γ_{th} is obtained by matching (i.e., fitting) the FER curve based on the approximation expression in Eq. (6.10) with the simulation FER curve using a least-square criterion.
- *Minimum sum-error* (*MSE*) *criterion*: This criterion was considered to obtain the threshold γ_{th} over Rayleigh fading channels in SISO systems [130], and orthogonal space-time block codes based (OSTBC) MIMO systems [134]. Although this criterion is not necessarily optimised for the low SNR region, it was shown in [130, 132] that it can offer a good FER approximation in this region. Moreover, this method requires less complexity compared to the least-square matching approach. In our antenna selection MIMO system operating in the Nakagami-*m* fading channel, the optimal SNR threshold γ_{th} is derived as (see Section 6.A for a derivation)

$$\gamma_{th} = \frac{A}{B}\left(\int_0^{\infty} \frac{1 - FER_G(\gamma)}{\gamma^2} d\gamma\right)^{-1}, \quad (6.12)$$

where $A=\sum_{q=1}^{n_T n_R}(-1)^q C_q^{n_T n_R}\sum_{u=0}^{(m-1)q}\omega_{u,q}u!/q^{u+1}$, $B=(\sum_{q=1}^{n_T n_R}(-1)^q C_q^{n_T n_R}\sum_{u=0}^{(m-1)(q-1)}\omega_{u,q-1}(u+m)!/q^{u+m})/\Gamma(m)$, C_a^b and $\omega_{u,q}$ denote the binomial coefficient and multinomial coefficient, respectively. We note that it is easy to calculate coefficients A and B. When m = 1 (i.e., Rayleigh fading channels), it is readily observed that $A = B$. Therefore, Eq. (6.12) can be simplified to as

$$\gamma_{th}=\left(\int_0^{\infty}\frac{1-FER_G(\gamma)}{\gamma^2}d\gamma\right)^{-1}. \tag{6.13}$$

Note that, $FER_G(\gamma)$, the FER over the Gaussian channel, can be expressed in a closed-form in uncoded systems [130]. For coded system, it can be numerically calculated using Monte-Carlo methods. An approximation accuracy of the two considered approaches, LS matching and MSE, will be provided in Section 6.6.

6.4 Energy Efficiency in Antenna Selection MIMO Systems

We consider the number of successfully received data bits per the total energy consumption as a metric to measure the energy efficiency, i.e.

$$EE=N_b/E_{total},\quad (bits/Joule) \tag{6.13}$$

where N_b is the average number of successfully received data bits in one data frame and E_0 is the total energy consumption at both transmitter and receiver corresponding to one frame.

Assuming that a data frame is accepted and sent for upper-layer processing only if there is no bit-error within that frame, we can express the number of bits N_b as

$$N_b=L_d\times(1-FER),\quad (bits) \tag{6.14}$$

where *FER* is the average frame-error rate that can be approximated using Eq. (6.10).

The total energy consumption per frame E_{total} can be expressed as

$$E_{total}=L_d\times E_0, \tag{6.15}$$

where E_0 is the energy per information bit, which can be calculated via the energy per symbol E_t as

$$E_0=\frac{L_f}{L_d}\times\frac{E_t}{r_c\log_2 M}, \tag{6.16}$$

where $E_t = E_s + E_c$ is the energy per symbol, which consists of the actual transmitted energy per symbol E_s and the energy consumed by electronics circuits E_c. Note that a factor (L_f / L_d) is included in Eq. (6.16) to take into consideration the energy waste due to a transmission of $L_h = (L_f - L_d)$ overhead bits (i.e., non-information data bits). Also, the circuit energy consumption E_c is given as $E_c = (\xi/\eta - 1)E_s + P_c / R_s$ [52, 133], where $\xi \approx 3(\sqrt{M} - 1/\sqrt{M} + 1), M \geq 4,$ is the peak-to-average power ratio of M-QAM signals, η is the drain efficiency of power-amplifier (PA), P_c is a power consumption of baseband processing units and RF chains at both transmitter and receiver (excluding the PA), and R_s is the symbol rate that is related to the information bit rate R_b as $R_b = R_s r_c (L_d / L_f) \log_2 M.$ Thus, we can rewrite E_0 in Eq. (6.16) as

$$\begin{aligned} E_0 &= \frac{L_f}{L_d} \times \frac{1}{r_c \log_2 M} \times \left(E_s + \left(\frac{\xi}{\eta} - 1 \right) E_s + \frac{P_c}{R_s} \right) = \frac{L_f}{L_d} \times \frac{1}{r_c \log_2 M} \times \left(\frac{\xi}{\eta} E_s + \frac{P_c}{R_s} \right) \\ &= \frac{L_f}{L_d} \times \frac{\xi}{\eta} \times \frac{E_s}{r_c \log_2 M} + \frac{P_c}{R_b} := \alpha \bar{\gamma} + \beta, \end{aligned} \tag{6.17}$$

where $\bar{\gamma} = E_s / (G_d N_0 r_c \log_2 M)$ is the average SNR value (cf. Eq. (6.3)), $\alpha = (L_f / L_d) \times (\xi / \eta) \times G_d N_0$, and $\beta = P_c / R_b$.

Substituting Eq. (6.10), Eq. (6.14), Eq. (6.15), and Eq. (6.17) into Eq. (6.13) results in

$$EE(\bar{\gamma}) = \frac{1 - \left(1 - e^{-m\gamma_{th}/\bar{\gamma}} \sum_{k=0}^{m-1} (m\gamma_{th}/\bar{\gamma})^k / k! \right)^{n_T n_R}}{\alpha \bar{\gamma} + \beta}. \tag{6.18}$$

The energy-efficiency maximisation problem can be now formulated as

$$\begin{aligned} &\textit{maximise } EE(\bar{\gamma}) \\ &\textit{subject to } FER(\bar{\gamma}) \leq FER_0, \end{aligned} \tag{6.19}$$

where FER_0 is the required frame-error rate. Assuming that bit-errors are uncorrelated, we have $FER_0 = 1 - (1 - BER_0)^{L_d}$, where BER_0 is the required bit-error rate. To solve the optimisation problem in Eq. (6.19), we first analyse characteristics of the cost function and the constraint.

Theorem 6.1 *The energy-efficiency metric* $EE(\bar{\gamma})$ *defined in Eq.* (6.18) *is a quasi-concave function with respect to* $\bar{\gamma}$. *Also, the optimal value* $\bar{\gamma}_m$ *that maximises* $EE(\bar{\gamma})$ *is the root of the equation* $\partial EE(\bar{\gamma})/\partial\bar{\gamma} = 0.$

Proof: The proof of the first part is provided in Section 6.B. For the second part, as $EE(\bar{\gamma})$ is quasi-concave, it clear that $EE(\bar{\gamma})$ has a unique maximum value at $\bar{\gamma}_m$.

Note that due to the complexity of the function $EE(\bar{\gamma})$, it is hard to derive the closed-form expression for $\bar{\gamma}_m$. However, it is easy to numerically evaluate $\bar{\gamma}_m$, e.g. using bisection search or Newton's method [135]. The explicit expression of $\partial EE(\bar{\gamma})/\partial\bar{\gamma} = 0$ is obtained as

$$\alpha\left(1-\left(1-e^{-m\gamma_{th}/\bar{\gamma}}\sum_{k=0}^{m-1}\frac{(m\gamma_{th}/\bar{\gamma})^k}{k!}\right)^{n_T n_R}\right)- (\alpha\bar{\gamma}+\beta)n_T n_R\frac{(m\gamma_{th})^m}{(m-1)!}\left(\frac{1}{\bar{\gamma}^{m+1}}\right)e^{-m\gamma_{th}/\bar{\gamma}}\left(1-e^{-m\gamma_{th}/\bar{\gamma}}\sum_{k=0}^{m-1}\frac{(m\gamma_{th}/\bar{\gamma})^k}{k!}\right)^{n_T n_R-1}=0. \tag{6.20}$$

Proposition 6.1 *There exists a positive value* $\bar{\gamma}_0$ *such that* $FER(\bar{\gamma}) \le FER_0$ *when* $\bar{\gamma} \ge \bar{\gamma}_0$. *The value* $\bar{\gamma}_0$ *is the root of the equation* $g(\bar{\gamma}) = 1-(FER_0)^{1/n_T n_R}$, *where* $g(\bar{\gamma}) = e^{-m\gamma_{th}/\bar{\gamma}}\sum_{k=0}^{m-1}(m\gamma_{th}/\bar{\gamma})^k/k!$.

Proof: We can rewrite Eq. (6.10) as $FER(\bar{\gamma}) = (1-g(\bar{\gamma}))^{n_T n_R}$. Thus, a constraint of $FER(\bar{\gamma}) \le FER_0$ is equivalent to $g(\bar{\gamma}) \ge 1-(FER_0)^{1/n_T n_R}$. Let us denote $\Xi = 1-(FER_0)^{1/n_T n_R}$ for convenience. As $0 < \Xi < 1,$ what we need to do is showing that $g(\bar{\gamma})$ is an increasing function within an interval (0,1). This is indeed the case as $\partial g(\bar{\gamma})/\partial\bar{\gamma} = (m\gamma_{th})^m e^{-m\gamma_{th}/\bar{\gamma}}/\bar{\gamma}^{m+1}(m-1)! > 0, \quad \forall\bar{\gamma} > 0,$ $\lim_{\bar{\gamma}\to 0} g(\bar{\gamma}) = 0,$ and $\lim_{\bar{\gamma}\to+\infty} g(\bar{\gamma}) = 1.$ This completes the proof.

Note that when m = 1 (i.e. a Rayleigh fading channel), the explicit expression of $\bar{\gamma}_0$ is given as $\bar{\gamma}_0 = \gamma_{th}/\log_e(1/\Xi)$. Also, when m = 2, we have $\bar{\gamma}_0 = -2\gamma_{th}/(W_{-1}(-\Xi/e)+1)$, where $W_k(.)$ is the k^{th} branch of the Lambert W function, and e is the Euler's number, i.e. $e \approx 2.71828$. For other values of m, the value $\bar{\gamma}_0$ can be evaluated numerically.

The solution $\bar{\gamma}^{opt}$ of the problem in Eq. (6.19) can be obtained as follow.

Theorem 6.2 *If the optimal value* $\bar{\gamma}_m$ *satisfies* $FER(\bar{\gamma}_m) \le FER_0$, *it will be the solution to the problem in Eq.* (6.19)*, i.e.* $\bar{\gamma}^{opt} = \bar{\gamma}_m$. *Otherwise,* $\bar{\gamma}^{opt} = \bar{\gamma}_0$.

Proof: The result is obtained directly based on Theorem 6.1 and Proposition 6.1.

Once the optimal value $\bar{\gamma}^{opt}$ is calculated, we can get the optimal average energy per transmitted symbol by using Eq. (6.3), i.e.,

$$E_s^{opt} = \bar{\gamma}^{opt} r_c G_d N_0 \log_2 M. \tag{6.21}$$

Simulation results that corroborate the analysis are provided in Section 6.6.

6.5 Energy Efficiency in Antenna Selection MIMO ARQ Systems

In this section, we focus on optimizing energy efficiency in antenna selection MIMO ARQ systems. The total energy E required to successfully deliver one information bit is considered as a metric to measure energy efficiency of the system, i.e.,

$$E = \upsilon E_0, \tag{6.22}$$

where υ is the average number of transmissions per successful bit (cf. Eq. (6.6)) and E_0 is the energy required to transmit one information bit for each transmission attempt (cf. Eq. (6.17)).

Substituting Eq. (6.6), Eq. (6.10) and Eq. (6.17) into Eq. (6.22) results in

$$E(\bar{\gamma}) = \frac{1}{1-\left(1-e^{-m\gamma_{th}/\bar{\gamma}}\sum_{k=0}^{m-1}\frac{(m\gamma_{th}/\bar{\gamma})^k}{k!}\right)^{n_T n_R}} \times (\alpha\bar{\gamma}+\beta). \tag{6.23}$$

To achieve energy-efficient transmission, the total energy $E(\bar{\gamma})$ in Eq. (6.23) should be as small as possible. For fixed values of n_T, n_R, α and β, we could find the optimal value of $\bar{\gamma}$, denoted as $\bar{\gamma}^{opt}$, so that the total energy $E(\bar{\gamma})$ is minimised. This is based on the following theorem.

Theorem 6.3 *The energy-efficiency metric* $E(\bar{\gamma})$ *defined in Eq. (6.23) is a quasi-convex function with respect to the average SNR* $\bar{\gamma}$. *Also, the optimal value* $\bar{\gamma}^{opt}$ *that minimises* $E(\bar{\gamma})$ *is the root of the equation* $\partial E(\bar{\gamma})/\partial\bar{\gamma} = 0$.

Table 6.1. Simulation parameters.

Parameter	Value
Frame length	L_f = 1000 bits or L_f = 2000 bits
Data rate	R_b = 20 kbps or R_b = 300 kbps
Modulation scheme	4-QAM
Convolutional coding	Generator polynomial $[5,7]_8$ and a code rate $r_c = 1/2$
Decoding method	Soft Viterbi
Circuit power consumption	P_c = 310 mW
Power amplifier efficiency	η = 0.35
Path-loss exponent	χ = 3.5
PSD of noise	$N_0/2$ = - 174 dBm/Hz
Nakagami-*m* fading channels	m =1 or m = 2
Other factors	G_0 = 30 dB
	G_M = 40 dB

Proof: A proof is obtained directly based on the proof of Theorem 6.1. In particular, as the energy efficiency $E(\bar{\gamma}) > 0$, to prove that $E(\bar{\gamma})$ is a quasi-convex function w.r.t. $\bar{\gamma}$, we will show that its reciprocal, i.e., $EE(\bar{\gamma}) = 1/E(\bar{\gamma})$, is a quasi-concave function w.r.t. $\bar{\gamma}$. This is the result of Theorem 6.1. In addition, it is worth noting that the root of the equation $\partial E(\bar{\gamma})/\partial\bar{\gamma} = 0$ is identical to that of $\partial EE(\bar{\gamma})/\partial\bar{\gamma} = 0$ (cf. Eq. (6.20)).

Once the optimal value $\bar{\gamma}^{opt}$ is obtained, we can get the optimal average transmitted energy per symbol E_s^{opt} using Eq. (6.3) (cf. Eq. (6.21)).

So far, we have derived the threshold-based FER approximation expression in Eq. (6.10), where the SNR threshold γ_{th} can be obtained by using either Eq. (6.12) or the curve-fitting approach. Based on Eq. (6.10), we have formulated the analytical expressions of the energy efficiency $EE(\bar{\gamma})$ in Eq. (6.18) for MIMO systems and the total energy consumption $E(\bar{\gamma})$ in Eq. (6.23) for MIMO-ARQ systems. The optimal value $\bar{\gamma}^{opt}$ to maximise $EE(\bar{\gamma})$ is obtained based on *Theorem* 6.2. Also, the optimal value $\bar{\gamma}^{opt}$ to minimise $E(\bar{\gamma})$ is determined based on *Theorem* 6.3. To realize the optimal value $\bar{\gamma}^{opt}$, the optimal average transmitted energy per symbol follows Eq. (6.21). In the next section, we will provide some numerical and simulation results to validate the analyses.

6.6 Simulation Results and Discussions

We use the simulation parameters shown in Table 6.1, most of which follow those in [52, 133]. We assume that perfect channel state information is available at the receiver.

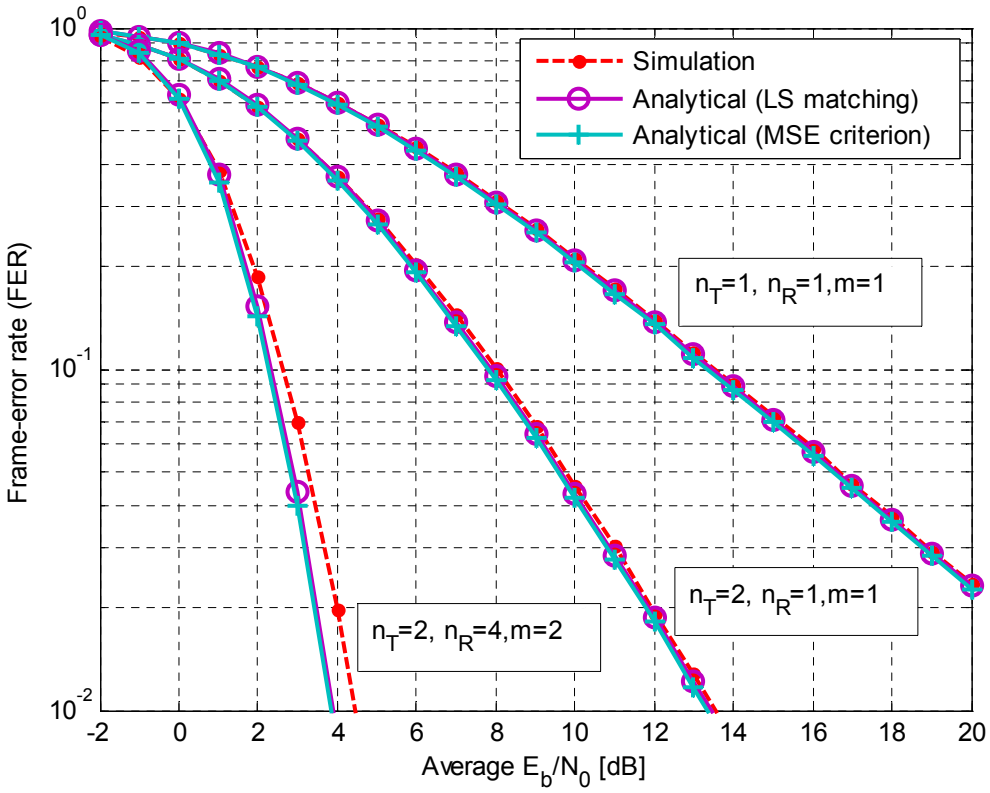

Figure 6.2. Comparison of the simulated FER and approximated FER ($L_f = L_d = 1000$ bits).

Also, the feedback link is zero-delay and error-free.

6.6.1 Evaluation of the FER Approximation

Figure 6.2 plots the frame-error rates (FER) of the antenna selection systems versus SNR over Nakagami-*m* channels. It can be seen that the analytical curves based on the FER approximation expression in Eq. (6.10) agree well with the simulation curves. Also, the analytical curve based on the MSE criterion is very close to that with the least-square matching approach. Therefore, using the simple FER approximation expression in Eq. (6.10) facilitates the analysis of energy efficiency in both antenna selection MIMO systems and antenna selection MIMO-ARQ systems.

6.6.2 Energy Efficiency in Antenna Selection MIMO Systems

In Figure 6.3, we plot the energy efficiency $EE(\bar{\gamma})$ versus the average SNR $\bar{\gamma}$. In this simulation, we adopt the follow parameters: $L_f = L_d = 2000$ bits, $BER_0 = 10^{-4}$ and $R_b = 20$ kbps. The obtained results demonstrate the following. First, it can be seen that the analytical curves based on the FER approximation in Eq. (6.10) agree well with the

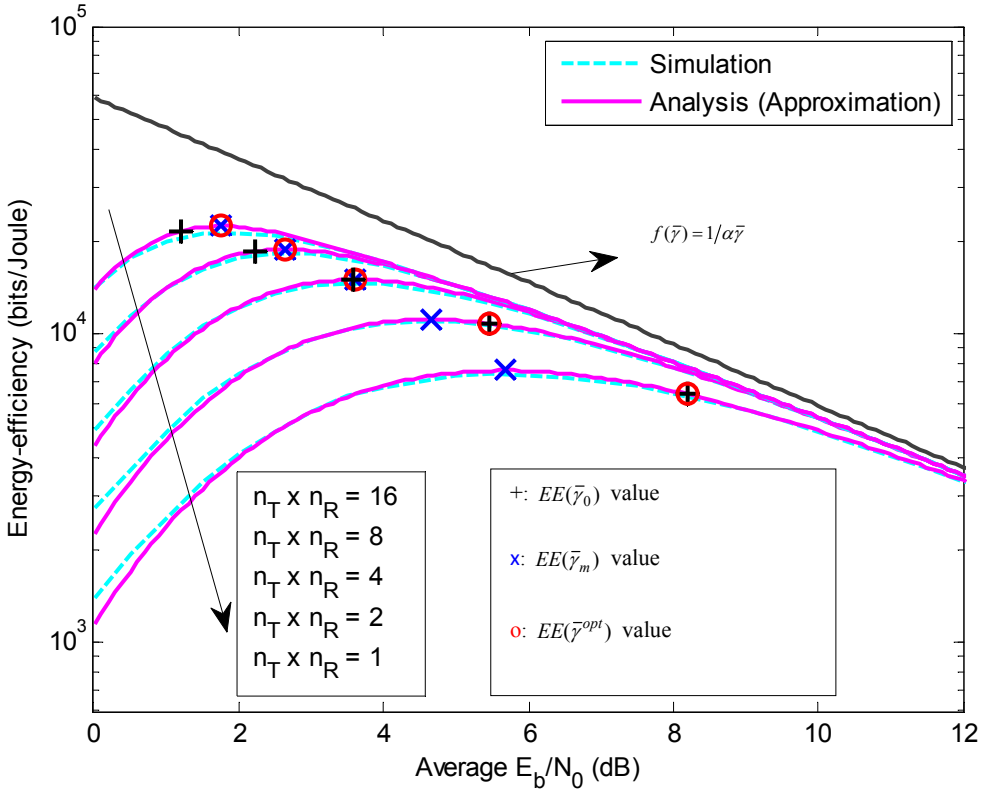

Figure 6.3. Energy efficiency $EE(\bar{\gamma})$ versus the average SNR $\bar{\gamma}$ (d = 100m).

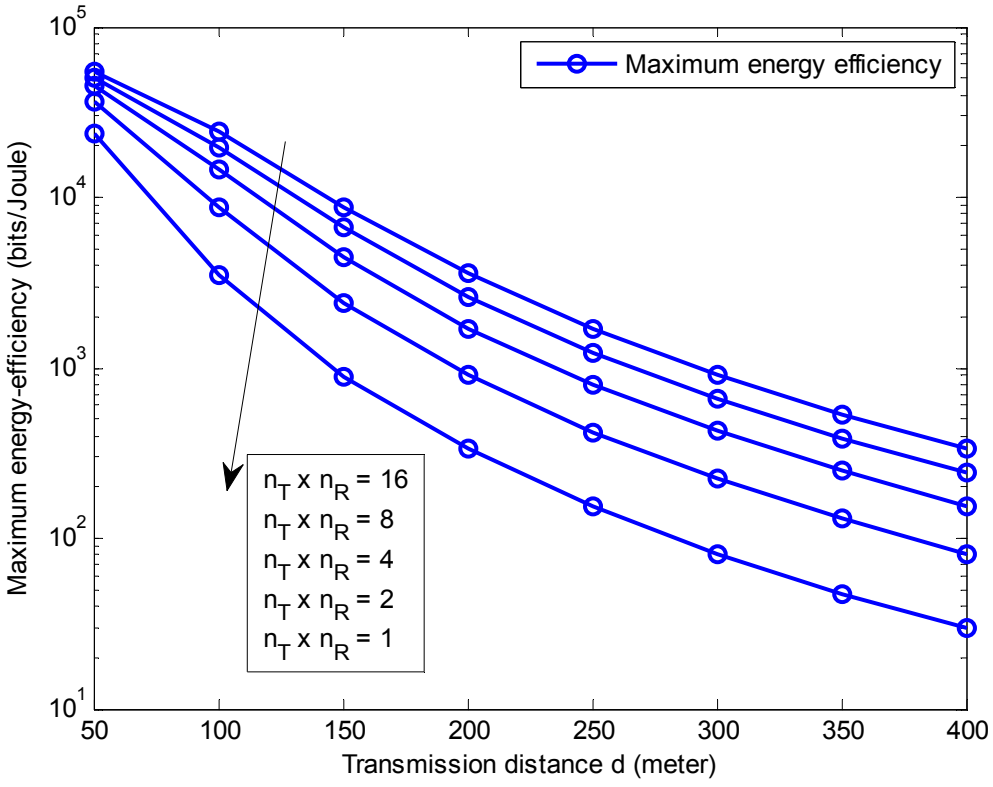

Figure 6.4. Maximum energy efficiency versus the transmission distance (m = 1).

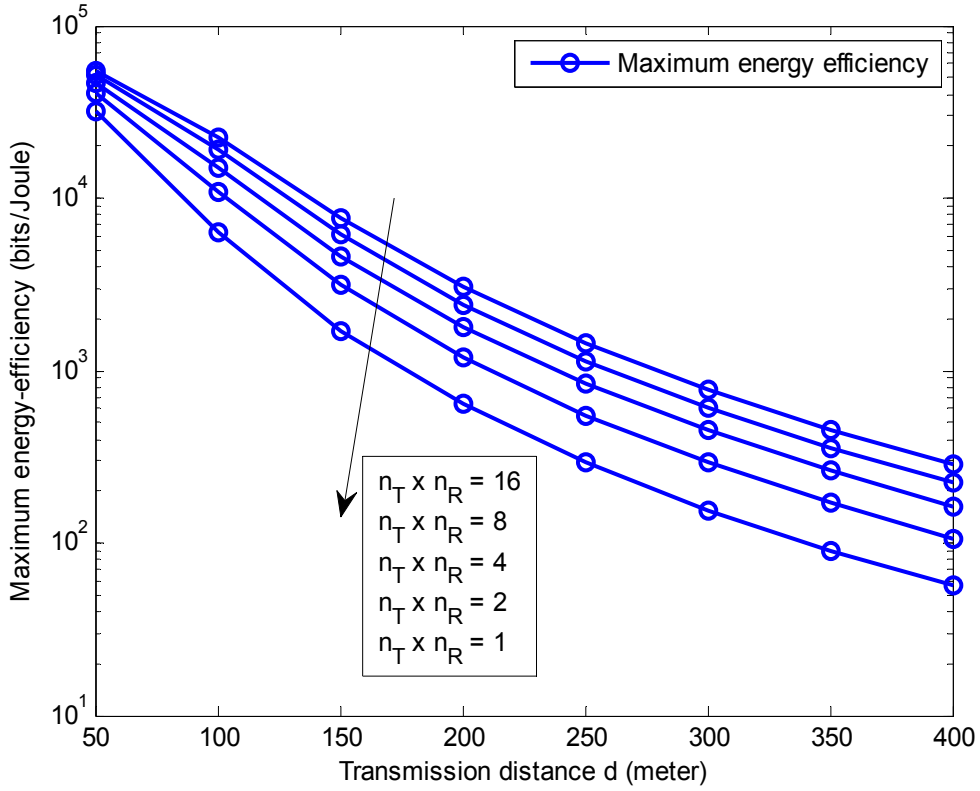

Figure 6.5. Maximum energy efficiency versus the transmission distance (m = 2).

simulation curves. Second, the AS system outperforms the single-input single-output (SISO) system from an energy-efficiency perspective. Moreover, the energy efficiency is improved when the number of antennas is increased. This is because a larger diversity gain leads to a lower FER, which in turns improves energy efficiency. Note that in the high SNR regime, the FER values become very small. Also, the transmitted energy E_s dominates the circuit energy consumption E_c. Hence, the EE value is asymptotic to $f(\bar{\gamma}) = 1/\alpha\bar{\gamma}$ (cf. Eq. (6.18)). Third, the average SNR values $\bar{\gamma}_0, \bar{\gamma}_m$, and thus $\bar{\gamma}^{opt}$ reduces when the number of antennas increases. Consequently, by employing more antennas, the optimal transmitted energy E_s^{opt} is reduced. This is an advantage of antenna selection systems especially when the transmitted power is limited, e.g., due to strict regulations.

In Figure 6.4, we show the maximum energy efficiency $EE(\bar{\gamma}^{opt})$ versus the transmission distance d when the parameter m = 1. It can be seen that $EE(\bar{\gamma}^{opt})$ decreases when the distance d increases. This makes sense as a larger transmitted energy is required to compensate for the increasing path-loss so that the FER constraint

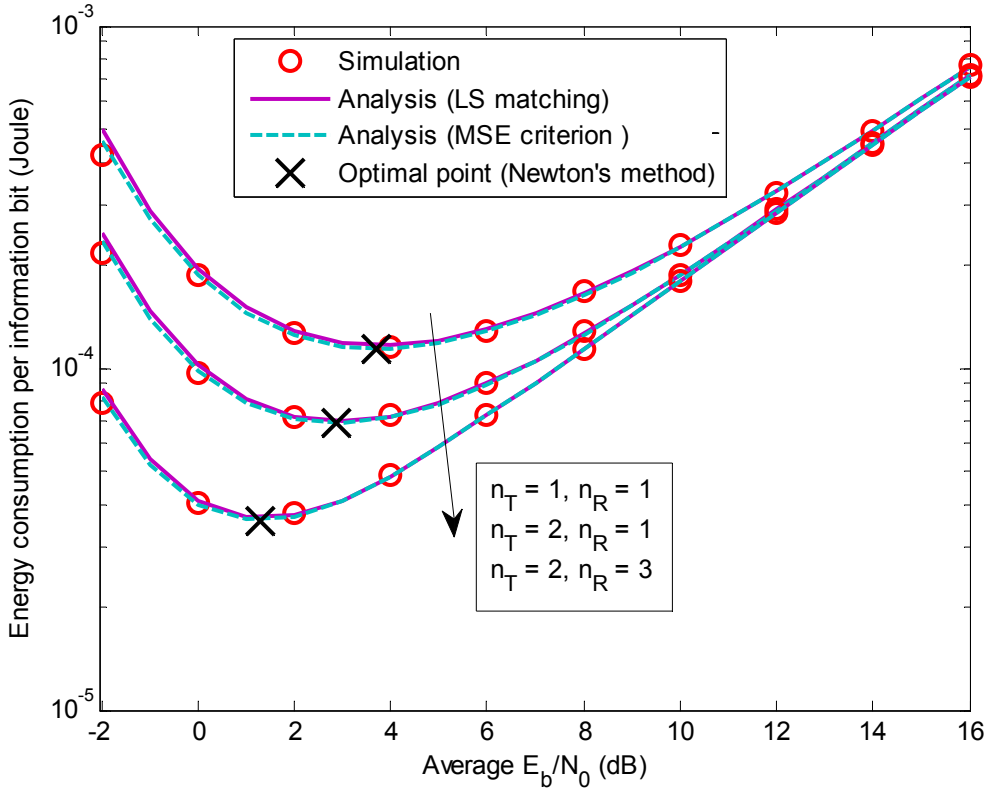

Figure 6.6. Energy consumption per information bit $E(\bar{\gamma})$ versus the average SNR $\bar{\gamma}$. ($m = 1$, $L_f = 1000$ bits, $L_h = 48$ bits, and $R_b = 300$ kbps).

is satisfied. However, we note that the AS system can achieve higher energy-efficiency than the SISO system in all scenarios. Similar observations can be made when $m = 2$ as shown in Figure 6.5.

6.6.3 Energy Efficiency in Antenna Selection MIMO-ARQ Systems

The energy consumption per information bit $E(\bar{\gamma})$ versus the average SNR is shown in Figure 6.6. First, it can be seen that the antenna selection MIMO ARQ system outperforms the SISO ARQ system (i.e., $n_T \times n_R = 1$) from an energy-efficiency perspective. The energy saving of the antenna selection system over the SISO system comes from diversity gain offered by the use of multiple antennas. In fact, a larger diversity gain leads to a lower FER, which in turn reduces the number of transmissions υ (cf. Eq. (6.6)). On the other hand, as only one RF chain is equipped at the transmitter and receiver in all systems, the energy E_0 in Eq. (6.17) is constant regardless of how many antennas are equipped. Consequently, the total energy $E = \upsilon E_0$ defined Eq. (6.22)

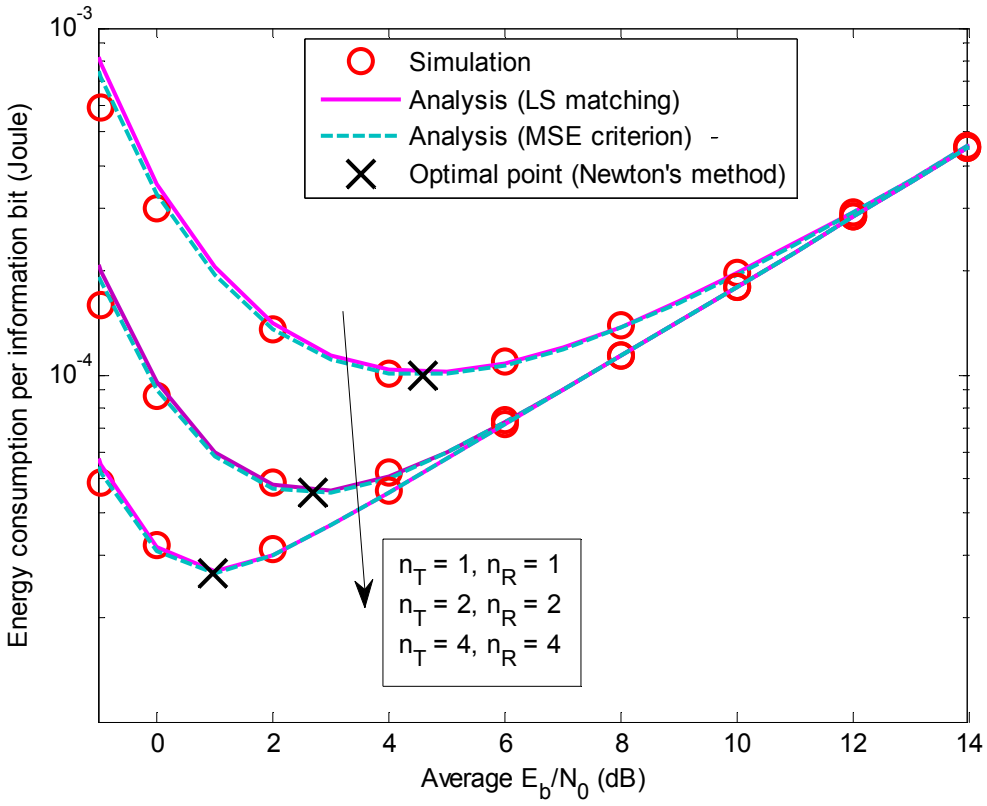

Figure 6.7. Energy consumption per information bit $E(\bar{\gamma})$ versus the average SNR $\bar{\gamma}$. ($m = 2$)

is reduced. Second, the optimal average SNR values $\bar{\gamma}^{opt}$ (marked as '×' in the figure) calculated using Newton's method match exactly with the analytical curves. Third, the optimal SNR value $\bar{\gamma}^{opt}$ and minimum energy $E^{opt}(\bar{\gamma})$ are reduced when the number of equipped antennas is increased. This behaviour can be explained by an additional diversity gain that is achieved when increasing the number of antennas as mentioned above. We also have the similar observations when $m = 2$ as shown in Fig. 6.7.

It is also worth noting that the optimal SNR value $\bar{\gamma}^{opt}$ results from the energy-delay trade-off (EDT) in the systems [136]. Specifically, when $\bar{\gamma} < \bar{\gamma}^{opt}$, the frame-error rate (FER) is high. Therefore, a large number of retransmissions is required to guarantee reliable transmission. As a result, the energy consumption is high (i.e., $E(\bar{\gamma})$ is dominated by retransmissions in this case). When $\bar{\gamma} > \bar{\gamma}^{opt}$, FER is small enough, and thus the impact of retransmissions is negligible. Also, the energy consumption $E(\bar{\gamma})$ increases when the average SNR value $\bar{\gamma}$ increases. Consequently, it is important to select the optimal operating point (i.e., obtain $\bar{\gamma}^{opt}$) for energy saving.

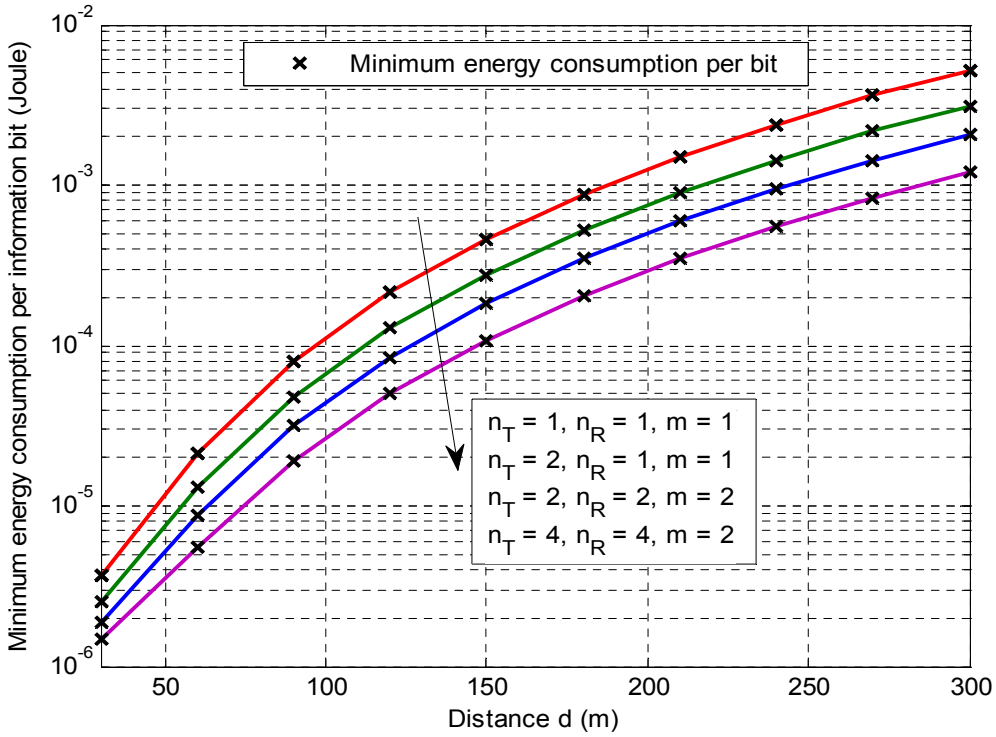

Figure 6.8. Minimum energy consumption per information bit versus the transmission distance.

Figure 6.8 shows the minimum energy consumption required to successfully deliver one information bit, i.e., $E^{opt}(\bar{\gamma})$, versus the transmission distance $d(m)$ in different systems. It can be seen that when the distance d increases (i.e., the path-loss is increasing), the energy consumption $E^{opt}(\bar{\gamma})$ increases. However, it is worth noting that the antenna selection MIMO ARQ system requires lower energy consumption compared to the SISO ARQ system for all values of the distance d. For example, at d = 150 m, the values of $E^{opt}(\bar{\gamma})$ in the antenna selection MIMO ARQ system with $n_T = 2$, $n_R = 1$ and the SISO ARQ system are 2.77×10^{-4} Joule and 4.63×10^{-4} Joule, respectively. Thus, an energy saving of about 40% can be achieved by the antenna selection system. Finally, the impact of some system parameters, such as frame length L_f and data rate R_b, on the energy efficiency is illustrated in Fig. 6.9.

6.7 Summary

In this chapter, antenna selection MIMO systems with/without an ARQ mechanism have been investigated from an energy-efficiency perspective. In particular, an EE metric that takes into account several important system parameters such as channel coding and modulation, has been considered, which is important from a practical

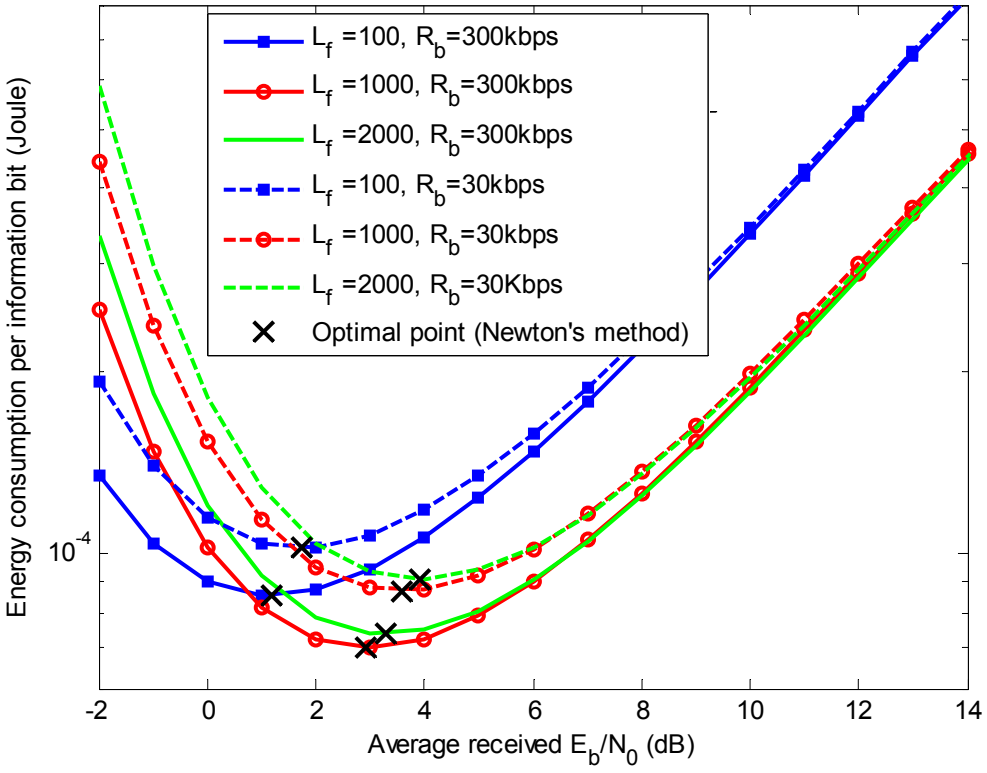

Figure 6.9. Energy consumption $E(\bar{\gamma})$ versus the average SNR $\bar{\gamma}$ under different values of L_f and R_b. ($n_T = 2$, $n_R = 1$, $m = 1$).

viewpoint. An analytical expression that can accurately approximate the FER over quasi-static Nakagami-*m* fading channels has been derived. Also, the energy efficiency $EE(\bar{\gamma})$ has been proved to be a quasi-convex function with respect to the average SNR value. Thus, the optimal value of the average energy of the transmitted symbols E_s^{opt} is obtained such that the energy efficiency in antenna selection MIMO system is maximised. Similarly, the optimal value E_s^{opt} in antenna selection MIMO-ARQ systems is determined. In addition, it has been shown analytically and numerically that the antenna selection MIMO systems offer a significant improvement in terms of energy efficiency, compared to the SISO system.

6.A Derivation of the SNR threshold γ_{th}

In this section, we derive the optimal SNR threshold γ_{th} for antenna selection systems over Nakagami-*m* fading channels. According to the minimum sum-error criterion [130], the optimal SNR value γ_{th} is the one that satisfies the following condition (cf. Eq. (6.7))

$$\lim_{\Lambda\to\infty}\left(\int_0^{\Lambda} F_{AS}(\lambda,\gamma_{th})d\lambda - \int_0^{\Lambda} FER(\lambda)d\lambda\right) = 0, \tag{6.24}$$

where $\lambda = 1/\bar{\gamma}$. The first integral in Eq. (6.24) can be expressed as

$$\begin{aligned}\int_0^{\Lambda} F_{AS}(\lambda,\gamma_{th})d\lambda &= \int_0^{\Lambda}\left(1-e^{-\lambda m\gamma_{th}}\sum_{k=0}^{m-1}\frac{(\lambda m\gamma_{th})^k}{k!}\right)^{n_T n_R} d\lambda \\ &= \int_0^{\Lambda}\left(\sum_{q=0}^{n_T n_R} C_q^{n_T n_R}(-1)^q e^{-q\lambda m\gamma_{th}}\left(\sum_{k=0}^{m-1}\frac{(\lambda m\gamma_{th})^k}{k!}\right)^q\right)d\lambda,\end{aligned} \tag{6.25}$$

where $C_a^b = b!/a!(b-a)!$ is the binomial coefficient. By performing a multinomial expansion as $(\sum_{k=0}^{m-1} x^k/k!)^q = \sum_{u=0}^{(m-1)q}\omega_{u,q}x^u$, where a coefficient $\omega_{u,q}$ is the u^{th} element of a vector $\boldsymbol{\omega}_q$ that is defined as $\boldsymbol{\omega}_0 = 1$, $\boldsymbol{\omega}_1 = [1\ \ 1/1!\ \ 1/2!\ \ldots.\ \ 1/(m-1)!]$, and $\boldsymbol{\omega}_q = \boldsymbol{\omega}_{q-1}\otimes\boldsymbol{\omega}_1$, where $\otimes$ denotes a discrete convolution [101], we can rewrite Eq. (6.25) as

$$\begin{aligned}\int_0^{\Lambda} F_{AS}(\lambda,\gamma_{th})d\lambda &= \sum_{q=0}^{n_T n_R}\left((-1)^q C_q^{n_T n_R}\sum_{u=0}^{(m-1)q}\left(\omega_{u,q}\int_0^{\Lambda}(\lambda m\gamma_{th})^u e^{-q\lambda m\gamma_{th}}d\lambda\right)\right) \\ &= \Lambda + \sum_{q=1}^{n_T n_R}\left((-1)^q C_q^{n_T n_R}\sum_{u=0}^{(m-1)q}\left(\omega_{u,q}\int_0^{\Lambda}(\lambda m\gamma_{th})^u e^{-q\lambda m\gamma_{th}}d\lambda\right)\right) \\ &= \Lambda + \sum_{q=1}^{n_T n_R}\left((-1)^q C_q^{n_T n_R}\sum_{u=0}^{(m-1)q}\left(\omega_{u,q}\frac{1}{m\gamma_{th}}\left(\frac{u!}{q^{u+1}} - e^{-q\Lambda/(m\gamma_{th})}\sum_{s=0}^{u}\frac{u!}{s!}\times\frac{(\Lambda/(m\gamma_{th}))^s}{q^{u-s+1}}\right)\right)\right),\end{aligned} \tag{6.26}$$

where the integral of $\int_0^a x^n e^{-bx}dx = n!/b^{n+1} - e^{-ab}\sum_{s=0}^{n}\left(n!a^s/s!b^{n-s+1}\right)$ [103] has been used in the last equality.

The second integral in Eq. (6.24) can be expressed as

$$\begin{aligned}\int_0^{\Lambda} FER(\lambda)d\lambda &= \int_0^{\Lambda}\int_0^{\infty} FER_G(\gamma)\,p_{AS}(\lambda,\gamma)\,d\gamma d\lambda \\ &= \int_0^{\Lambda}\int_0^{\infty} p_{AS}(\lambda,\gamma)d\gamma d\lambda - \int_0^{\Lambda}\int_0^{\infty}\left(1-FER_G(\gamma)\right)p_{AS}(\lambda,\gamma)\,d\gamma d\lambda \\ &= \int_0^{\Lambda}\int_0^{\infty} p_{AS}(\lambda,\gamma)d\gamma d\lambda - \int_0^{\infty}\left(\left(1-FER_G(\gamma)\right)\int_0^{\Lambda} p_{AS}(\lambda,\gamma)\,d\lambda\right)d\gamma \\ &= \Lambda - \int_0^{\infty}\left(\left(1-FER_G(\gamma)\right)\int_0^{\Lambda} p_{AS}(\lambda,\gamma)\,d\lambda\right)d\gamma,\end{aligned} \tag{6.27}$$

where the first term in the third equality is evaluated based on the fact that $\int_0^{\infty} p_{AS}(\lambda,\gamma)d\gamma = 1$. By performing a similar calculation as done to obtain Eq. (6.26), we can calculate the inner integral in the second term in Eq. (6.27) as follows (cf. Eq. (6.8))

$$\begin{aligned}\int_0^{\Lambda} p_{AS}(\lambda,\gamma)d\lambda &= \int_0^{\Lambda} n_T n_R (m\lambda)^m \frac{\gamma^{m-1}e^{-m\lambda\gamma}}{\Gamma(m)}\left(1-e^{-m\lambda\gamma}\sum_{k=0}^{m-1}\frac{(m\lambda\gamma)^k}{k!}\right)^{n_T n_R-1} d\lambda \\ &= \int_0^{\Lambda}\left(n_T n_R (m\lambda)^m \frac{\gamma^{m-1}e^{-m\lambda\gamma}}{\Gamma(m)}\sum_{q=0}^{n_T n_R-1}\left(C_q^{n_T n_R-1}(-1)^q e^{-qm\lambda\gamma}\left(\sum_{k=0}^{m-1}\frac{(m\lambda\gamma)^k}{k!}\right)^q\right)\right)d\lambda \\ &= \int_0^{\Lambda}\left(n_T n_R (m\lambda)^m \frac{\gamma^{m-1}e^{-m\lambda\gamma}}{\Gamma(m)}\sum_{q=0}^{n_T n_R-1}\left((-1)^q C_q^{n_T n_R-1} e^{-qm\lambda\gamma}\sum_{u=0}^{(m-1)q}\omega_{u,q}(m\lambda\gamma)^u\right)\right)d\lambda \\ &= \frac{n_T n_R}{\Gamma(m)}\sum_{q=0}^{n_T n_R-1}\left((-1)^q C_q^{n_T n_R-1}\sum_{u=0}^{(m-1)q}\omega_{u,q}m^{u+m}\gamma^{u+m-1}\int_0^{\Lambda}\lambda^{u+m}e^{-(q+1)m\lambda\gamma}d\lambda\right) \\ &= \frac{n_T n_R}{\Gamma(m)}\sum_{q=0}^{n_T n_R-1}\left((-1)^q C_q^{n_T n_R-1}\sum_{u=0}^{(m-1)q}\omega_{u,q}m^{u+m}\gamma^{u+m-1}\left(\frac{(u+m)!}{\left((q+1)m\gamma\right)^{u+m+1}}-\right.\right. \\ &\qquad \left.\left. e^{-\Lambda(q+1)m\gamma}\sum_{s=0}^{u+m}\frac{(u+m)!}{s!}\times\frac{\Lambda^s}{\left((q+1)m\gamma\right)^{u+m-s+1}}\right)\right) \\ &= \frac{n_T n_R}{\Gamma(m)}\sum_{q=0}^{n_T n_R-1}\left((-1)^q C_q^{n_T n_R-1}\sum_{u=0}^{(m-1)q}\omega_{u,q}\left(\frac{(u+m)!}{m(q+1)^{u+m+1}\gamma^2}-\right.\right. \\ &\qquad \left.\left. m^{u+m}\gamma^{u+m-1}e^{-\Lambda(q+1)m\gamma}\sum_{s=0}^{u+m}\frac{(u+m)!}{s!}\times\frac{\Lambda^s}{\left((q+1)m\gamma\right)^{u+m-s+1}}\right)\right).\end{aligned} \tag{6.28}$$

By substituting Eq. (6.26), Eq. (6.27) and Eq. (6.28) into Eq. (6.24), and noting that all terms containing $e^{-\Lambda}$ are eliminated as $e^{-\Lambda} \to 0$ when $\Lambda \to \infty$, we arrive at

$$\sum_{q=1}^{n_T n_R}\left((-1)^q C_q^{n_T n_R}\sum_{u=0}^{(m-1)q}\left(\omega_{u,q}\frac{1}{m\gamma_{th}}\times\frac{u!}{q^{u+1}}\right)\right)+$$
$$\int_0^{\infty}\left(\left(1-FER_G(\gamma)\right)\frac{n_T n_R}{\Gamma(m)}\sum_{q=0}^{n_T n_R-1}\left((-1)^q C_q^{n_T n_R-1}\sum_{u=0}^{(m-1)q}\omega_{u,q}\left(\frac{(u+m)!}{m(q+1)^{u+m+1}\gamma^2}\right)d\gamma=0,\right.\right. \tag{6.29}$$

or, equivalently,

$$\frac{1}{\gamma_{th}}\sum_{q=1}^{n_T n_R}\left((-1)^q C_q^{n_T n_R}\sum_{u=0}^{(m-1)q}\omega_{u,q}\frac{u!}{q^{u+1}}\right)=$$
$$-\frac{n_T n_R}{\Gamma(m)}\sum_{q=0}^{n_T n_R-1}\left((-1)^q C_q^{n_T n_R-1}\sum_{u=0}^{(m-1)q}\omega_{u,q}\frac{(u+m)!}{(q+1)^{u+m+1}}\right)\int_0^{\infty}\frac{1-FER_G(\gamma)}{\gamma^2}d\gamma. \tag{6.30}$$

For notational convenience, let us denote

$$A=\sum_{q=1}^{n_T n_R}\left((-1)^q C_q^{n_T n_R}\sum_{u=0}^{(m-1)q}\omega_{u,q}\frac{u!}{q^{u+1}}\right), \tag{6.31}$$

and

$$\begin{aligned}B&=-\frac{n_T n_R}{\Gamma(m)}\sum_{q=0}^{n_T n_R-1}\left((-1)^q C_q^{n_T n_R-1}\sum_{u=0}^{(m-1)q}\omega_{u,q}\frac{(u+m)!}{(q+1)^{u+m+1}}\right)\\&=\frac{1}{\Gamma(m)}\sum_{q=1}^{n_T n_R}\left((-1)^q C_q^{n_T n_R}\sum_{u=0}^{(m-1)(q-1)}\omega_{u,q-1}\frac{(u+m)!}{q^{u+m}}\right),\end{aligned} \tag{6.32}$$

where the equality in Eq. (6.32) is obtained by changing a variable (q+1) by q, and using a binomial identity of $C_q^{n_T n_R}=(n_T n_R/q)C_{q-1}^{n_T n_R-1}$. Then, from Eq. (6.30), we can express the optimal SNR threshold as

$$\gamma_{th}=\frac{A}{B}\left(\int_0^{\infty}\frac{1-FER_G(\gamma)}{\gamma^2}d\gamma\right)^{-1}. \tag{6.33}$$

This completes the derivation.

6.B Proof of Theorem 6.1

It is well-established that if $f(x)$ is a sigmoid function (or S-shaped, i.e., it is initially convex and then concave), then $f(x)/x$ is a quasi-concave function [137]. Therefore, to prove Theorem 6.1, we will show that

$$f(\bar{\gamma}) = 1 - \left(1 - e^{-m\gamma_{th}/\bar{\gamma}} \sum_{k=0}^{m-1} \frac{(m\gamma_{th}/\bar{\gamma})^k}{k!}\right)^{n_T n_R} \tag{6.34}$$

is a sigmoid function for all $\bar{\gamma} > 0$. It then follows that $EE(\bar{\gamma})$ is a quasi-concave function.

Let us denote $g(\bar{\gamma}) = e^{-m\gamma_{th}/\bar{\gamma}} \sum_{k=0}^{m-1} (m\gamma_{th}/\bar{\gamma})^k / k!$, then Eq. (6.34) can be rewritten as

$$f(\bar{\gamma}) = 1 - \left(1 - g(\bar{\gamma})\right)^{n_T n_R}. \tag{6.35}$$

The first-order and second-order derivatives of $g(\bar{\gamma})$ with respect to $\bar{\gamma}$ are calculated, respectively, as

$$g'(\bar{\gamma}) = \frac{(m\gamma_{th})^m}{(m-1)!}\left(\frac{1}{\bar{\gamma}^{m+1}}\right)e^{-m\gamma_{th}/\bar{\gamma}}, \tag{6.36}$$

and

$$g''(\bar{\gamma}) = \frac{(m\gamma_{th})^m}{(m-1)!}\left(\frac{m\gamma_{th} - (m+1)\bar{\gamma}}{\bar{\gamma}^{m+3}}\right)e^{-m\gamma_{th}/\bar{\gamma}}. \tag{6.37}$$

As $g'(\bar{\gamma}) > 0, \forall \bar{\gamma} > 0$, the function $g(\bar{\gamma})$ is increasing over its domain. Also, we have $g''(\bar{\gamma}) > 0$ when $\bar{\gamma} < m\gamma_{th}/(m+1)$, and $g''(\bar{\gamma}) < 0$ when $\bar{\gamma} > m\gamma_{th}/(m+1)$. Thus, $g(\bar{\gamma})$ is initially convex and then concave with the inflection point of $\bar{\gamma}_0 = m\gamma_{th}/(m+1)$, i.e., $g(\bar{\gamma})$ is a sigmoid function.

We now prove that $f(\bar{\gamma}) = 1 - \left(1 - g(\bar{\gamma})\right)^{n_T n_R}$ is also a sigmoid function w.r.t. $\bar{\gamma}$. We note that it is very hard, if not impossible, to obtain an explicit solution of $f''(\bar{\gamma}) = 0$. Therefore, we will show that $f(\bar{\gamma})$ satisfies all the properties of a sigmoid function described in [137] as follows:

1) It is clear that its domain is the interval [0, ∞).

2) We have $f'(\bar{\gamma}) = n_T n_R g'(\bar{\gamma})\left(1 - g(\bar{\gamma})\right)^{n_T n_R - 1} > 0$ because $g'(\bar{\gamma}) > 0, \forall \bar{\gamma} \in [0, \infty)$ (cf. Eq. (6.36)). Thus, $f(\bar{\gamma})$ is increasing.

3) We have $\lim_{\bar{\gamma}\to 0} g(\bar{\gamma}) = 0$, $\lim_{\bar{\gamma}\to +\infty} g(\bar{\gamma}) = 1$, and $g(\bar{\gamma})$ is increasing. Thus, the range of $g(\bar{\gamma})$ is the interval [0,1). As $f(\bar{\gamma})$ is increasing, it is readily from Eq. (6.35) that the range of $f(\bar{\gamma})$ is also [0,1).

4) The second-order derivative of $f(\bar{\gamma})$ is calculated as

$$f''(\bar{\gamma}) = n_T n_R [g''(\bar{\gamma})(1-g(\bar{\gamma})) - (n_T n_R - 1)(g'(\bar{\gamma}))^2](1-g(\bar{\gamma}))^{n_T n_R - 2}. \tag{6.38}$$

Recall that $g''(\bar{\gamma}) < 0$ when $\bar{\gamma} > \bar{\gamma}_0$, and the range of $g(\bar{\gamma})$ is the interval [0,1). Thus, it is clear from Eq. (6.38) that $f''(\bar{\gamma}) < 0$ when $\bar{\gamma} > \bar{\gamma}_0$. In other words, in the interval $(\bar{\gamma}_0, \infty)$, $f(\bar{\gamma})$ is concave (i.e., eventually concave).

5) We first note that

$$\begin{aligned}\lim_{\bar{\gamma}\to 0} f'(\bar{\gamma}) &= \lim_{\bar{\gamma}\to 0}\left\{ n_T n_R g'(\bar{\gamma})(1-g(\bar{\gamma}))^{n_T n_R - 1} \right\} \\ &= \lim_{\bar{\gamma}\to 0}\left\{ n_T n_R \frac{(m\gamma_{th})^m}{(m-1)!}\left(\frac{1}{\bar{\gamma}^{m+1}}\right) e^{-m\gamma_{th}/\bar{\gamma}}\left(1 - e^{-m\gamma_{th}/\bar{\gamma}} \sum_{k=0}^{m-1} \frac{(m\gamma_{th}/\bar{\gamma})^k}{k!}\right)^{n_T n_R - 1}\right\} = 0.\end{aligned} \tag{6.39}$$

As mentioned earlier, $f'(\bar{\gamma}) > 0$. Thus, $f'(\bar{\gamma}_0) = \theta, \theta > 0$. By applying the mean value theorem, we have $f''(\bar{\gamma}_c) = (f'(\bar{\gamma}_0) - f'(0))/(\varepsilon - 0) = \theta/\varepsilon > 0$ at some point $\bar{\gamma}_c \in (0, \bar{\gamma}_0)$. Recall that $f''(\bar{\gamma}) < 0, \forall \bar{\gamma} \in (\bar{\gamma}_0, +\infty)$. This implies that when $\bar{\gamma}$ decreases from $\bar{\gamma}_0$ toward zero, $f''(\bar{\gamma})$ increases from a negative value to a positive value. Moreover, it can be shown that $f''(\bar{\gamma}) = 0$ has a unique solution, denoted as $\bar{\gamma}_z$, in the interval $(0, \bar{\gamma}_0)$ (see Section 6.C). Therefore, $f''(\bar{\gamma}) > 0, \forall \bar{\gamma} < \bar{\gamma}_z$, and $f''(\bar{\gamma}) < 0, \forall \bar{\gamma} > \bar{\gamma}_z$. In other words, the function $f(\bar{\gamma})$ is convex in $(0, \bar{\gamma}_z)$ and concave in $(\bar{\gamma}_z, \infty)$, with the unique inflection point of $\bar{\gamma}_z$.

6) It is readily that $f(\bar{\gamma})$ has a continuous derivative.

This completes the proof.

6.C Proof that $f''(\bar{\gamma}) = 0$ has a Unique Solution

It is noted from Eq. (6.38) that $f''(\bar{\gamma}) = 0$ is equivalent to

$$g''(\bar{\gamma})(1-g(\bar{\gamma}))-(n_T n_R-1)(g'(\bar{\gamma}))^2 = 0. \tag{6.40}$$

By using Eq. (6.36) and Eq. (6.37), we can express the left hand side in Eq. (6.40) as

$$g''(\bar{\gamma})(1-g(\bar{\gamma}))-(n_T n_R-1)(g'(\bar{\gamma}))^2 = \frac{(m\gamma_{th})^m}{(m-1)!}\left(\frac{m\gamma_{th}-(m+1)\bar{\gamma}}{\bar{\gamma}^{m+3}}\right)e^{-m\gamma_{th}/\bar{\gamma}}\left(1-e^{-m\gamma_{th}/\bar{\gamma}}\sum_{k=0}^{m-1}\frac{(m\gamma_{th}/\bar{\gamma})^k}{k!}\right)-(n_T n_R-1)\left(\frac{(m\gamma_{th})^m}{(m-1)!\bar{\gamma}^{m+1}}e^{-m\gamma_{th}/\bar{\gamma}}\right)^2. \tag{6.41}$$

Thus, the equation $f''(\bar{\gamma}) = 0$ is now equivalent to

$$\left(m\gamma_{th}-(m+1)\bar{\gamma}\right)\left(1-e^{-m\gamma_{th}/\bar{\gamma}}\sum_{k=0}^{m-1}\frac{(m\gamma_{th}/\bar{\gamma})^k}{k!}\right)-(n_T n_R-1)\frac{(m\gamma_{th})^m}{(m-1)!\bar{\gamma}^{m-1}}e^{-m\gamma_{th}/\bar{\gamma}} = 0, \tag{6.42}$$

or

$$h(\bar{\gamma}) := m\gamma_{th}-(m+1)\bar{\gamma}+\left[\left(-m\gamma_{th}+(m+1)\bar{\gamma}\right)\sum_{k=0}^{m-1}\frac{(m\gamma_{th}/\bar{\gamma})^k}{k!}-(n_T n_R-1)\frac{(m\gamma_{th})^m}{(m-1)!\bar{\gamma}^{m-1}}\right]e^{-m\gamma_{th}/\bar{\gamma}} = 0. \tag{6.43}$$

It is straightforward to show that

$$\lim_{\bar{\gamma}\to 0} h(\bar{\gamma}) = m\gamma_{th} > 0, \tag{6.44}$$

and

$$h(\bar{\gamma}_0) = -(n_T n_R-1)\frac{m\gamma_{th}}{(m-1)!}(m+1)^{m-1}e^{-m-1} < 0, \tag{6.45}$$

where $\bar{\gamma}_0 = m\gamma_{th}/(m+1)$ is the inflection point of $g(\bar{\gamma})$ as mentioned in Appendix 6.B. Therefore, to prove that $f''(\bar{\gamma}) = 0$ has a unique solution in the interval $(0,\bar{\gamma}_0)$, we only need to show that $h'(\bar{\gamma}) < 0, \forall \bar{\gamma} \in (0,\bar{\gamma}_0)$ (i.e., $h(\bar{\gamma})$ is strictly decreasing).

The first-order derivative of $h(\bar{\gamma})$ is calculated as

$$h'(\bar{\gamma}) = -(m+1) + \left[\left(-m\gamma_{th} + (m+1)\bar{\gamma}\right) \sum_{k=0}^{m-1} \frac{(m\gamma_{th}/\bar{\gamma})^k}{k!} - (n_T n_R - 1) \frac{(m\gamma_{th})^m}{(m-1)!\bar{\gamma}^{m-1}} \right] \frac{m\gamma_{th}}{\bar{\gamma}^2} e^{-m\gamma_{th}/\bar{\gamma}} +$$

$$\left[(m+1) \sum_{k=0}^{m-1} \frac{(m\gamma_{th}/\bar{\gamma})^k}{k!} + \left(-m\gamma_{th} + (m+1)\bar{\gamma}\right) \frac{-m\gamma_{th}}{\bar{\gamma}^2} \sum_{k=0}^{m-2} \frac{(m\gamma_{th}/\bar{\gamma})^k}{k!} + (n_T n_R - 1)(m-1) \frac{(m\gamma_{th})^m}{(m-1)!\bar{\gamma}^m} \right] e^{-m\gamma_{th}/\bar{\gamma}}$$

$$= -(m+1) + \left[\left(-m\gamma_{th} + (m+1)\bar{\gamma}\right) \frac{m\gamma_{th}}{\bar{\gamma}^2} \frac{(m\gamma_{th}/\bar{\gamma})^{m-1}}{(m-1)!} - (n_T n_R - 1) \frac{(m\gamma_{th})^{m+1}}{(m-1)!\bar{\gamma}^{m+1}} + \right.$$

$$\left. (m+1) \sum_{k=0}^{m-1} \frac{(m\gamma_{th}/\bar{\gamma})^k}{k!} + (n_T n_R - 1)(m-1) \frac{(m\gamma_{th})^m}{(m-1)!\bar{\gamma}^m} \right] e^{-m\gamma_{th}/\bar{\gamma}}$$

$$= -(m+1) + \left[(m+1) \sum_{k=0}^{m-1} \frac{(m\gamma_{th}/\bar{\gamma})^k}{k!} - n_T n_R \frac{(m\gamma_{th}/\bar{\gamma})^{m+1}}{(m-1)!} + \left((n_T n_R - 1)(m-1) + m + 1\right) \frac{(m\gamma_{th}/\bar{\gamma})^m}{(m-1)!} \right] e^{-m\gamma_{th}/\bar{\gamma}}$$

$$= -e^{-m\gamma_{th}/\bar{\gamma}} \left[(m+1) e^{m\gamma_{th}/\bar{\gamma}} - (m+1) \sum_{k=0}^{m-1} \frac{(m\gamma_{th}/\bar{\gamma})^k}{k!} + \right.$$

$$\left. n_T n_R \frac{(m\gamma_{th}/\bar{\gamma})^{m+1}}{(m-1)!} - \left((n_T n_R - 1)(m-1) + m + 1\right) \frac{(m\gamma_{th}/\bar{\gamma})^m}{(m-1)!} \right].$$

(6.46)

We note that the Maclaurin series of the function $e^{m\gamma_{th}/\bar{\gamma}}$ is expressed as $e^{m\gamma_{th}/\bar{\gamma}} = \sum_{k=0}^{+\infty} (m\gamma_{th}/\bar{\gamma})^k / k!$ [103]. Thus, it is clear that

$$(m+1) e^{m\gamma_{th}/\bar{\gamma}} - (m+1) \sum_{k=0}^{m-1} \frac{(m\gamma_{th}/\bar{\gamma})^k}{k!} = (m+1) \sum_{k=m}^{+\infty} \frac{(m\gamma_{th}/\bar{\gamma})^k}{k!} > 0, \forall \bar{\gamma} > 0. \tag{6.47}$$

On the other hand, as $\bar{\gamma} \in (0, \bar{\gamma}_0)$, we have $\bar{\gamma} < \bar{\gamma}_0 = m\gamma_{th}/(m+1)$, or $m\gamma_{th}/\bar{\gamma} > m+1$. Thus, it is readily that

$$n_T n_R \frac{(m\gamma_{th}/\bar{\gamma})^{m+1}}{(m-1)!} - \left((n_T n_R - 1)(m-1) + m + 1\right) \frac{(m\gamma_{th}/\bar{\gamma})^m}{(m-1)!} > 2(n_T n_R - 1) \frac{(m\gamma_{th}/\bar{\gamma})^m}{(m-1)!} > 0. \tag{6.48}$$

By combining Eq. (6.46), Eq. (6.47) and Eq. (6.48), we obtain the desired result of $h'(\bar{\gamma}) < 0, \forall \bar{\gamma} \in (0, \bar{\gamma}_0)$. Thus, $f''(\bar{\gamma}) = 0$ has a unique solution in the interval $(0, \bar{\gamma}_0)$. Also, recall that $f''(\bar{\gamma}) < 0, \forall \bar{\gamma} \in (\bar{\gamma}_0, +\infty)$. Therefore, $f''(\bar{\gamma}) = 0$ has a unique solution for all $\bar{\gamma} \in (0, +\infty)$.

Chapter 7

Conclusions and Future Work

This chapter summarises the research results and highlights the major contributions of the thesis. Several potential research directions based on this research work are also provided.

7.1 Summary of the Thesis

This thesis has studied antenna selection MIMO-OFDM wireless systems from an energy-efficiency perspective. Three antenna selection methods have been proposed to improve energy efficiency of the systems, including: *i*) adaptive antenna selection (i.e., jointly selecting antenna indices and the number of active RF chains); *ii*) power amplifier aware antenna selection; and *iii*) jointly optimising transmit power allocation and antenna selection under QoS constraints. These methods have been presented in Chapter 3 to Chapter 6. The key results in each chapter are summarised below.

Chapter 3 has investigated energy efficiency in MIMO-OFDM systems with different antenna selection strategies. Several important factors that affect energy efficiency, including the relation between the actual transmitted power and the power consumed by the transceiver circuits, the number of equipped antennas, and the spatial correlation among antennas, have been considered. The results are as follows.

- Conventional antenna selection schemes, in which the number of active RF chains is fixed, exhibit a loss of energy efficiency.
- There exists the optimal number of equipped transmit antennas so that the energy-efficiency in per-subcarrier antenna selection MIMO-OFDM systems is maximised. Specifically, a large number of antennas should be equipped when the transmitted power significantly dominates the circuit power consumption, and vice versa.

- A proposed adaptive antenna selection that jointly selects the antenna indices and the number of active RF chains achieves better energy efficiency than its counterparts.
- Power loading can improve energy efficiency quite significantly in the systems that deploy bulk-selection and adaptive selection. However, in per-subcarrier antenna selection, the energy efficiency improvement is marginal.
- Bulk selection is only effective in the low spectral efficiency (SE) regime (i.e., the low-power regime). Meanwhile, conventional per-subcarrier selection and combined selection are suitable in the high-SE and medium-to-high-SE regimes, respectively. Moreover, the proposed adaptive selection achieves the best EE-SE trade-off performance.

Chapter 4 has considered antenna selection MIMO-OFDM systems in the presence of nonlinear distortions due to high-power amplifiers. An optimal constrained selection scheme that equally allocates data subcarriers among transmit antennas by means of linear optimisation has been proposed to improve energy efficiency. This chapter has gained the following insights.

- Conventional per-subcarrier selection suffers from performance degradation due to the large required power back-off.
- A proposed constrained antenna selection offers better performance than the conventional scheme in terms of error rate, energy efficiency, and the EE-SE trade-off.

Chapter 5 has focused on an antenna selection MIMO-OFDM system with linear scaling for undistorted transmission. A two-step strategy for data-subcarrier allocation, which consists of an equal allocation of data subcarriers based on linear optimisation and peak-power reduction via cross-antenna permutations, has been proposed to improve energy efficiency. The following results have been obtained based on the analytical results.

- Unbalance allocation of data subcarriers associated with the conventional per-subcarrier selection affects the power efficiency of power amplifiers.
- A proposed strategy significantly improves the power efficiency of power amplifiers and the energy efficiency of the whole system.

Chapter 6 has been devoted to investigate energy efficiency in antenna selection MIMO systems under QoS constraints over Nakagami-*m* fading channels. Two MIMO schemes have been considered, namely antenna selection MIMO and antenna selection MIMO ARQ. The analytical results have revealed the following insights.

- An energy-efficiency metric, defined as the number of successfully received data bits per the total energy consumption, is a quasi-concave function with respect to (w.r.t.) the average SNR. Similarly, the total energy required to successfully deliver one information bit in ARQ systems, is a quasi-convex function w.r.t. the average SNR.
- There exists the optimal value of the average energy per transmitted data symbols so that the energy efficiency in the antenna selection MIMO and antenna selection MIMO ARQ systems is maximised. These optimal values have been determined.
- Energy efficiency in these systems is improved when the number of equipped antennas is increased.

7.2 Suggestions for Future Work

This thesis has proposed several techniques to improve the energy efficiency in antenna selection MIMO-OFDM wireless systems. Besides, the obtained results reveal some open research problems that require further investigation. Below are some of potential directions for future research.

❖ ***Antenna selection for MIMO-OFDM systems under practical impairments***

In this thesis, channel estimation process and feedback link are assumed perfect. However, it is very hard in reality to obtain perfect CSI. Also, feedback delay and errors inevitably occur. The presence of such impairment factors will affect the efficacy of the systems. Consequently, it would be important and interesting to further investigate the systems under these practical conditions. The motivation of this research direction is twofold. In the one hand, it could provide more insightful into the effectiveness of the proposed systems under practical conditions. On the other hand, based on the obtained results, one can come up with solutions for robustness against these impairments.

❖ ***Antenna selection for multi-data streams MIMO-OFDM systems***

In Chapter 3 and Chapter 6, single-data stream MIMO systems have been investigated. It is important to note that these systems can be extended to multi-data

streams (i.e., spatial multiplexing) cases to exploit multiplexing gain. Toward this end, one of the main tasks would be how to jointly select antennas and allocate power among the selected antennas to maximise energy efficiency. While antenna selection can be obtained in a similar manner, the challenges lie in performing mathematical analysis for optimal power allocation. In addition, interference among data streams does affect the energy efficiency. Substantial research efforts might be needed to deal with these issues.

❖ ***Antenna selection for single-user large-scale MIMO-OFDM systems***

Massive MIMO, in which a large number of antennas (possibly hundreds or even thousands) are equipped at base stations or on devices, is an emerging area of research. This MIMO technique promises to offer a significant improvement in spectral efficiency as well as energy efficiency [138, 139]. Currently, some research works, for instance [78], have studied energy-efficient antenna selection for massive MIMO single-carrier systems. Thus, it would be interesting to investigate antenna selection in massive MIMO-OFDM systems from an energy-efficiency perspective. To this end, major focuses would be designing efficient antenna selection algorithms and analysing the system characteristics when the number of equipped antennas are very large. It is worth noting that the proposed adaptive antenna selection scheme in Chapter 3 is suitable for a system with a very large number of antennas (i.e., massive MIMO). However, further theoretical analysis is needed to understand the system behaviour in the large-scale regime.

❖ ***Antenna selection for multiuser MIMO-OFDM systems***

This thesis focuses on point-to-point wireless systems. As a natural extension of this research work, antenna selection can be considered for downlink multiuser MIMO-OFDM systems. In multiuser MIMO-OFDM scenarios, one of the main challenges is the presence of multi-user interference (i.e., interference between different active users) [3]. Consequently, proposed strategies for improved energy efficiency will involve not only antenna selection and power allocation among users, but also designs of precoding matrix for interference mitigation. It would also be very interesting to further consider energy-efficient antenna selection for multiuser massive MIMO-OFDM wireless systems.

Bibliography

[1] A. Fehske, G. Fettweis, J. Malmodin, and G. Biczok, "The global footprint of mobile communications: The ecological and economic perspective," *IEEE Communications Magazine,* vol. 49, no. 8, pp. 55- 62, Aug. 2011.

[2] G. L. Stuber, J. R. Barry, S. W. Mclaughlin, M. A. I. Y. Li, and T. G. Pratt, " Broadband MIMO-OFDM wireless communications," *Proceedings of the IEEE,* vol. 92, no. 2, pp. 271-294, Feb. 2004.

[3] M. Jiang and L. Hanzo, "Multiuser MIMO-OFDM for next-generation wireless systems," *Proceeding of the IEEE,* vol. 95, no. 7, pp. 1430-1469, July 2007.

[4] D. Tse and P. Viswanath, *Fundamentals of Wireless Communication*: Cambridge University Press, 2005.

[5] "The draft IEEE 802.16m system description document," IEEE 802.16m-08/003r7, Feb. 2009.

[6] "Draft amendment to wireless LAN media access control (MAC) and physical layer (PHY) specifications: enhancements for higher throughput," Tech. Rep. P802.11n/D0.04, March 2006.

[7] "Evolved universal terrestrial radio access (E-UTRA); LTE physical layer-general description (Release 8)," 3GPP, TS 36.201.

[8] "Requirements for further advancements for E-UTRA (LTE-Advanced) (Release 8)," 3GPP, TR 36.913.

[9] A. F. Molisch and M. Z. Win, "MIMO systems with antenna selection," *IEEE Microwave Magazine,* vol. 5, no. 1, pp. 45-56, March 2004.

[10] C. M. Vithanage, J. P. Coon, and S. C. J. Parker, "On capacity-optimal precoding for multiple antenna systems subject to EIRP restrictions," *IEEE Trans. Wireless Commun.,* vol. 7, no. 12, pp. 5182-5187, Dec. 2008.

[11] N. B. Mehta, A. F. Molisch, and S. Kashyap, "Antenna selection in LTE: from motivation to specification," *IEEE Communications Magazine,* vol. 50, no. 10, pp. 144-150, Oct. 2012.

[12] E. Eraslan, C. Y. Wang, and B. Daneshrad, "Practical energy-aware link adaptation for MIMO-OFDM systems," *IEEE Trans. on Wireless Commun.,* vol. 13, pp. 246-258, Jan. 2014.

[13] X. Ge *et al.*, "Energy-efficiency optimization for MIMO-OFDM mobile multimedia communication systems with QoS constraints," *IEEE Trans. Veh. Technol.,* vol. 63, pp. 2127-2138, June 2014.

[14] A. Paulraj, R. Nabar, and D. Gore, *Introduction to Space-Time Wireless Communications*, 1st ed.: Cambridge University Press, 2003.

[15] C. Shannon, "A mathematical theory of communication," *Bell Labs Tech. Journal,* vol. 27, pp. 379-423, 623-656, 1948.

[16] E. Telatar, "Capacity of multi-antenna Gaussian channels," *European Trans. Telecommun.,* vol. 10, no. 6, pp. 585–595, Nov./Dec. 1999.

[17] G. J. Foschini and M. J. Gans, "On limits of wireless communications in a fading environment when using multiple antennas," *Wireless Personal Commun.,* vol. 6, pp. 311-335, Feb. 1998.

[18] J. Mietzner, R. Schober, L. Lampe, W. H. Gerstacker, and P. A. Hoher, "Multiple–antenna techniques for wireless communications - A comprehensive literature survey," *IEEE Communications Surveys and Tutorials,* vol. 11, no. 2, pp. 87-105, June 2009.

[19] S. M. Alamouti, "A simple transmit diversity technique for wireless communications," *IEEE J. Select. Areas Commun.,* vol. 16, no. 8, pp. 1451-1458, Oct. 1998.

[20] V. Tarokh *et al.*, "Space-time block coding from orthogonal designs," IEEE Transactions on Information Theory," vol. 45, no. 5, pp. 1456-1467, July 1999.

[21] H. Jafarkhani, "A quasi-orthogonal space-time block code," *IEEE Trans. Commun.,* vol. 49, no. 1, pp. 1-4, Jan. 2001.

[22] B. Hassibi and B. M. Hochwald, "High-rate codes that are linear in space and time," *IEEE Trans. Inf. Theory,* vol. 48, no. 7, pp. 1804-1824, July 2002.

[23] V. Tarokh *et al.*, " Space-time codes for high data rate wireless communication: performance criterion and code construction," *IEEE Transactions on Information Theory,* vol. 44, pp. 744-765, March 1998.

[24] Q. Yan and R. S. Blum, "Improved space time convolutional codes for quasi-static slow fading channels," *IEEE Trans. Wireless Commun.,* vol. 1, no. 4, pp. 563-571, Oct. 2002.

[25] G. J. Foschini *et al.*, "Analysis and performance of some basic space–time architectures," *IEEE J. Sel. Areas Commun.,* vol. 21, no. 3, pp. 303-320, April 2003.

[26] G. D. Golden, C. J. Foschini, R. A. Valenzuela, and P. W. Wolniansky, "Detection algorithm and initial laboratory results using V-BLAST space-time communication architecture," *IEE Electronics Letters,* vol. 35, no. 1, pp. 14-16, Jan. 1999.

[27] E. Viterbo and J. Boutros, "A universal lattice code decoder for fading channels," *IEEE Trans. Inf. Theory,* vol. 45, no. 5, pp. 1639-1642, July 1999.

[28] H. Yao and G. Wornell, "Lattice reduction aided detectors for MIMO communication systems," in *Proc. IEEE Global Communications Conference, GLOBECOM 2002*, Nov. 2002, pp. 17-21.

[29] L. C. Godara, "Application of antenna arrays to mobile communications, Part II: Beam-forming and direction-of-arrival considerations," *Proceeding of the IEEE,* vol. 85, no. 8, pp. 1195-1245, Aug. 1997.

[30] M. E. Hajjar and L. Hanzo, "Multifunctional MIMO schemes: a combined diversity and multiplexing design perspective," *IEEE Wireless Communication Magazine,* vol. 17, no. 2, pp. 73-79, April 2010.

[31] G. Jongren, M. Skoglund, and B. Ottersten, "Combining beamforming and space-time block coding," *IEEE Trans. Inf. Theory,* vol. 48, no. 3, pp. 611-627, March 2002.

[32] E. N. Onggosanusi, A. G. Dabak, and T. M. Schmidl, "High rate spacetime block coded scheme: performance and improvement in correlated fading channels," in *Proc. IEEE WCNC 2002*, March 2002, pp. 194-199.

[33] L. Zheng and D. N. C. Tse, "Diversity and multiplexing: A fundamental tradeoff in multiple-antenna channels," *IEEE Trans. Inform. Theory,* vol. 49, no. 5, pp. 1073-1096, May 2003.

[34] T. D. Chiueh and P. Y. Tsai, *OFDM Baseband Receiver Design for Wireless Communications*: John Willey, 2007.

[35] T. Jiang and J. Wu, "An overview: Peak-to-average power ratio reduction techniques for OFDM signals," *IEEE Trans. on Broadcasting,* vol. 54, no. 2, pp. 257-268, 2008.

[36] A. Batra *et al*., " Multiband OFDM physical layer specification," *WiMedia Alliance,* Release 1.5, August 2009.

[37] W. Su, Z. Safar, and K. J. L. Liu, "Towards maximum achievable diversity in space, time, and frequency: Performance analysis and code design," *IEEE Trans. Wireless Commun.,* vol. 4, no. 4, pp. 1847-1857, July 2005.

[38] L. C. Tran and A. Mertins, "Space-time-frequency code implementation in MB-OFDM UWB communications: Design criteria and performance," *IEEE Trans. Wireless Commun.,* vol. 8, no. 2, pp. 701-713, Feb. 2009.

[39] H. Bolcskei and A. Paulraj, "Space-frequency coded broadband OFDM systems," in *Proc. IEEE Wireless Communications and Networking Conference*, 2000, pp. 1-6.

[40] D. Wang, G. Zhu, and Z. Hu, "Optimal pilots in frequency domain for channel estimation in MIMO-OFDM systems in mobile wireless channels," in *Proc. IEEE Vehicular Technology Conference*, May 2004, pp. 608-612.

[41] Z. Wu, J. He, and G. Gu, "Design of optimal pilot-tones for channel estimation in MIMO-OFDM sysems," in *Proc. IEEE Wireless Communications and Networking Conference*, March 2005, pp. 12-17.

[42] Y. G. Li, N. Seshadri, and S. Ariyavisitakul, "Channel estimation for OFDM systems with transmitter diversity in mobile wireless channels," *IEEE J. Sel. Areas Commun.,* vol. 17, pp. 461-471, March 1999.

[43] G. Raleigh and J. Cioffi, "Spatio-tempotal coding for wireless communication," *IEEE Trans. Commun.,* vol. 46, no. 3, pp. 357-366, March 1998.

[44] Y. Chen, S. Zhang, and S. Xu, "Fundamental Trade-offs on Green Wireless Networks," *IEEE Communications Magazine,* vol. 49, no. 6, pp. 30-37, June 2011.

[45] L. M. Correia *et al.*, "Challenges and enabling technologies for energy aware mobile radio networks," *IEEE Communications Magazine,* vol. 48, no.11, pp. 66-72, 2010.

[46] G. Y. Li *et al*., "Energy-efficient wireless communications: Tutorial, survey, and open issues," *IEEE Wireless commun.,* vol. 18, no. 6, pp. 28-35, Dec. 2011.

[47] Z. Hasan, H. Boostanimehr, and V. K. Bhargava, "Green cellular networks: A survey, some research issues and challenges," *IEEE Commun. Surveys & Tutorials,* vol. 13, no. 4, pp. 524-540, 2011.

[48] G. Miao, N. Himayat, Y. Li, and A. Swami, "Cross-layer optimization for energy-efficient wireless communications: a survey," *Wireless Communications and Mobile Computing,* vol. 48, pp. 529–542, April 2009.

[49] D. Feng *et al.*, "A survey of energy-efficient wireless communications," *IEEE Comm. Surveys and Tutorials,* vol. 15, no. 1, pp. 167-177, 2013.

[50] S. Cui, A. Goldsmith, and A. Bahai, "Energy-efficiency of MIMO and cooperative MIMO techniques in sensor networks," *IEEE J. Sel. Areas Commun.,* vol. 22, pp. 1089-1098, Aug. 2004.

[51] O. Arnold, F. Richter, G. Fettweis, and O. Blume, "Power consumption modeling of different base station types in heterogeneous cellular networks," in *Future Network and Mobile Summit*, June 2010, pp. 1-8.

[52] S. Cui, A. Goldsmith, and A. Bahai, "Energy-constrained modulation optimization," *IEEE Trans. on Wireless Communications,* vol. 4, no. 5, pp. 2349-2360, 2005.

[53] S. C. Cripps, *RF Power Amplifiers for Wireless Communications*: Artech House, 2006.

[54] H. M. Kwon and T. G. Birdsall, "Channel capacity in bits per Joule " *IEEE Journal of Oceanic Engineering,* vol. OE-11, no. 1, pp. 97-99, Jan. 1986.

[55] F. Heliot, M. Imran, and R. Tafazolli, "On the energy efficiency-spectral efficiency trade-off over the MIMO Rayleigh fading channel," *IEEE Trans. Commun.,* vol. 60, no. 5, pp. 1345-1356, May 2012.

[56] R.W. Heath, A. Paulraj, and S. Sandhu, "Antenna selection for spatial multiplexing systems with linear receivers," *IEEE Communications Letters,* vol. 5, pp. 142-144, April 2001.

[57] L. Zhou, "Low complexity optimum transmit antenna selection algorithms in spatial multiplexing systems," *Proc. IEEE PIMRC,* pp. 825-830, 2010.

[58] M. Gharavi-Alkhansari and A. Gershman, "Fast antenna subset selection in MIMO systems," *IEEE Trans. Signal Process.,* vol. 52, no. 2, pp. 339- 347, Jan. 2004.

[59] A. Gorokhov, D. A. Gore, and A. J. Paulraj, "Receive antenna selection for MIMO flat-fading channels: theory and algorithms," *IEEE Trans. Inf. Theory,* vol. 49, no. 10, pp. 2687-2696, Oct. 2003.

[60] R. S. Blum, Z. Xu, and S. Sfar, "A near-optimal joint transmit and receive antenna selection algorithm for MIMO systems," in *Proc. Radio and Wireless Sympsium*, Jan. 2009, pp. 554-557.

[61] H. Yongqiang, L. Wentao, and L. Xiaohui, "Particle swarm optimization for antenna selection in MIMO systems," *Wireless Personal Commun.,* pp. 1-10, Dec. 2011.

[62] A. Dua, K. Medepalli, and A. J. Paulraj, "Receive antenna selection in MIMO systems using convex optimization," *IEEE Trans. Wireless Commun.,* vol. 5, no. 9, pp. 2353-2357, Sep. 2006.

[63] A. F. Molisch *et a*l., "Implementation aspects of antenna selection for MIMO systems," in *Proc. Int. Conf. Commun. Network. China (China Com)*, 2006, pp. 1 -7.

[64] V. Kristem, N. B. Mehta, and A. F. Molisch, "A novel, balanced, and energy-efficient training method for receive antenna selection," *IEEE Trans. Wireless Commun.,* vol. 9, pp. 2742-2753, Sep. 2010.

[65] R. Poisel, *Antenna Systems and Electronic Warfare Applications*: Artech House, Jan. 2012.

[66] A. F. Molisch, M. Z. Win, Y.-S. Choi, and J. H. Winters, "Capacity of MIMO systems with antenna selection," *IEEE Trans. Wireless Commun.,* vol. 4, no. 4, pp. 1759-1772, Jul. 2005.

[67] S. Sanayei and A. Nosratinia, "Capacity of MIMO channels with antenna selection," *IEEE Transactions on Information Theory,* vol. 53, no. 11, pp. 4356-4362, 2007.

[68] I. Bahceci, T. M. Duman, and Y. Altunbasak, "Antenna selection for multiple-antenna transmission systems: performance analysis and code construction," *IEEE Trans. Inf. Theory,* vol. 49, no. 10, pp. 2669-2681, 2003.

[69] T. Gucluoglu and T. M. Duman, "Performance analysis of transmit and receive antenna selection over flat fading channels," *IEEE Transactions on Wireless Comm.,* vol. 7, no. 8, pp. 3056-3065, August 2008.

[70] Z. Chen, J. Yuan, B. Vucetic, and Z. Zhou, "Performance of Alamouti scheme with transmit antenna selection," *IEE Electronics Letters,* vol. 39, pp. 1666-1668, Nov. 2003.

[71] X. Zeng and A. Ghrayeb, "Performance bounds for space-time block codes with receive antenna selection," *IEEE Trans. Inf. Theory,* vol. 50, no. 9, pp. 2130-2137, Sept. 2004.

[72] T. Gucluoglu and E. Panayirci, "Performance of transmit and receive antenna selection in the presence of channel estimation errors," *IEEE Comm. Letters,* vol. 12, no. 5, pp. 371-373, May 2008.

[73] Y. Yang, R. S. Blum, and S. Sfar, "Antenna selection for MIMO systems with closely spaced antennas," *EURASIP J. Wireless Commun. Netw.,* vol. 2009, 2009.

[74] C. Jiang and L. J. Cimini, "Antenna selection for energy-efficient MIMO transmission," *IEEE Wireless Communications Letters,* vol. 1, no. 6, pp. 577-580, Dec. 2012.

[75] X. Zhou, B. Bai, and W. Chen, "Iterative antenna selection for multi-stream MIMO under a holistic power model," *IEEE Wireless Communications Letters,* vol. 3, no. 1, pp. 82-85, Feb. 2014.

[76] X. Zhou, B. Bai, and W. Chen, "An iterative algorithm fot joint antenna selection and power adaptation in energy-efficient MIMO," in *Proc. IEEE International Conference on Communications (ICC)*, June 2014, pp. 3812-3816.

[77] O. K. Rayel *et al.*, "Energy efficiency-spectral efficiency trade-off of transmit antenna selection," *IEEE Trans. Commun.,* vol. early access, 2014.

[78] H. Li, L. Song, and M. Debbah, "Energy-efficiency of large-scale multiple antenna systems with transmit antenna selection," *IEEE Trans. Communications,* vol. 62, no. 2, pp. 638-647, Feb. 2014.

[79] H. Zhang and R. U. Nabar, "Transmit antenna selection in MIMO-OFDM systems: bulk versus per-tone selection," in *Proc. IEEE Intern. Conf. Commun., ICC 2008*, May 2008, pp. 4371-4375.

[80] Z. Tang, H. Suzuki, and I. B. Collings, "Performance of antenna selection for MIMO-OFDM systems based on measured indoor correlated frequency selective channels," in *Proc. Australian Telecom. Networks and Applications Conference*, Dec. 2006, pp. 435-439.

[81] H. Zhang, A. F. Molisch, and J. Zhang, " Applying antenna selection in WLAN for achieving broadband multimedia communications," *IEEE Transactions on Broadcasting,* vol. 52, no. 4, pp. 475-482, Dec. 2006.

[82] Y. Liu, Y. Zhang, C. Ji, W. Q. Malik, and D. J. Edwards, " A low complexity receive antenna selection algorithm for MIMO-OFDM wireless systems," *IEEE Transactions on Vehicular Technology,* vol. 58, no. 6, pp. 2793-2802, July 2009.

[83] H. Shi, M. Katayama, T. Yamazato, H. Okada, and A. Ogawa, " An adaptive antenna selection scheme for transmit diversity in OFDM systems," in *Proc. IEEE Vehicular Technology Conference, VTC 2001-Fall*, Oct. 2001, pp. 2168 - 2172.

[84] M. Sandell and J. Coon, "Per-subcarrier antenna selection with power constraints in OFDM systems," *IEEE Transactions on Wireless Communications,* vol. 8, no. 2, pp. 673-677, Feb. 2009.

[85] K. H. Park, Y. C. Ko, and M. S. Alouini, " Low complexity transmit antenna selection with power balancing in OFDM systems," *IEEE Trans. on Wireless Commu.,* vol. 9, no. 10, pp. 3018-3023, Oct. 2010.

[86] J. P. Coon and M. Sandell, "Combined bulk and per-tone transmit antenna selection in OFDM systems," *IEEE Comm. Letters,* vol. 14, no. 5, pp. 426-428, May 2010.

[87] M. Sandell and J. Coon, "Performance of combined bulk and per-tone antenna selection precoding in coded OFDM systems," *IEEE Trans. Commun.,* vol. 60, no. 3, pp. 655-660, March 2012.

[88] J. P. Coon and M. Sandell, "Performance of transmit antenna selection in space-time-coded OFDM systems," *IEEE Transactions on Vehicular Technology,* vol. 60, no. 6, pp. 2824-2828, July 2011.

[89] Z. Chen, J. Yuan, and B. Vucetic, "Analysis of transmit antenna selection/maximal-ratio combining in Rayleigh fading channels," *IEEE Trans. Veh. Technol.,* vol. 54, no. 4, pp. 1312-1321, July 2005.

[90] N. B. Mehta , A. F. Molisch , J. Zhang, and E. Bala, "Antenna selection training in MIMO-OFDM/OFDMA cellular systems," in *Proc. IEEE International Workshop on Computational Advances in Multi-Sensor Adaptive Processing*, Dec. 2007, pp. 113-116.

[91] Y. (G.) Li, N. Seshadri, and S. Ariyavisitakul, "Channel estimation for OFDM systems with transmitter diversity in mobile wireless channels," *IEEE J. Select. Areas Commun.,* vol. 17, pp. 461-471, March 1999.

[92] M. Sandell and J. Coon, "Joint data detection and channel sounding for TDD systems with antenna selection," in *Proc. IEEE Vehicular Tech. Conf., VTC-Spring 2011*, May 2011, pp. 1-5.

[93] H. Bolcskei, D. Gesbert, and A. J. Paulraj, "On the capacity of OFDM based spatial multiplexing systems," *IEEE Transactions on Communications,* vol. 50, no. 2, pp. 225-234, 2002.

[94] F. Wang *et al*., "Design of wide-bandwidth envelope-tracking power amplifiers for OFDM applications," *IEEE Trans. Microwave Theory and Techniques,* vol. 53, no. 4, pp. 1312-1321, April 2005.

[95] K. Cho and D. Yoon, "On the general BER expression of one-and two-dimensional amplitude modulations," *IEEE Trans. Commun.,* vol. 50, no. 7, pp. 1074 -1080, Nov. 2002.

[96] A. Leke and J. Cioffi, "A maximum rate loading algorithm for discrete multitone modulation systems," in *Proc. IEEE Global Telecommunications Conf., Globecom 1997*, Nov. 1997, pp. 1514-1518.

[97] S. Boyd and L. Vandenbergh, *Convex Optimization*: Cambridge University Press, 2004.

[98] V. Erceg *et al.* , "TGn channel models," IEEE 802.11-03/940r4, May 2004.

[99] H. Moon, "Water-filling power allocation at high SNR regimes," *IEEE Trans. Commun.,* vol. 59, no. 3, pp. 708-715, March 2011.

[100] H. A. David, *Order Statistics*: John Wiley & Sons, 1981.

[101] M. Lari, A. Mohammadi, A. Abdolali, and I. Lee, "Characterization of effective capacity in antenna selection MIMO systems," *KICS/IEEE Journal of Communications and Networks,* vol. 15, no. 5, pp. 476-485, Oct. 2013.

[102] M. S. Alouini and A. J. Goldsmith, "Capacity of Rayleigh fading channels under different adaptive transmission and diversity-combining techniques," *IEEE Transactions on Vehicular Technology,* vol. 48, no. 4, pp. 1165-1181, July 1999.

[103] I. S. Gradshteyn and I. M. Ryzhik, *Table of Integrals, Series and Products*: Academic Press, 2007.

[104] I. Ahmad, A. I. Sulyman, A. Alsanie, A. Alasmari, and A. Saleh, " Spectral broadening effects of high power amplifiers in MIMO-OFDM relaying channels," *EURASIP J. Wireless Commun. Netw.,* vol. 2013, 2013.

[105] K. G. Grad, L. E. Larson, and M. B. Steer, "The impact of RF front-end characteristics on the spectral regrowth of communications signals," *IEEE Trans. Microw. Theory,* vol. 53, no. 6, pp. 2179-2186, 2005.

[106] H. Ochiai and H. Imai, "Performance of the deliberate clipping with adaptive symbol selection for strictly band-limitted OFDM systems," *IEEE Journal on Selected Areas in Communications,* vol. 18, no. 11, pp. 2270-2277, Nov. 2000.

[107] J. G. Proakis, *Digital Communications*, 4th ed.: McGraw Hill Inc., 2001.

[108] J. J. Bussgang, "Crosscorrelation functions of amplitude-distorted Gaussian signals," Technical Report 216, Research Laboratory Electronics, M. I. T., Cambridge, MA, . March 1952.

[109] P. Banelli, "Theoretical analysis and performance of OFDM signals in nonlinear fading channels," *IEEE Transactions on Wireless Communications,* vol. 2, no. 2, pp. 284-293, March 2003.

[110] E. K. S. Au and W. H. Mow, "Effect of non-linearity on the performance of a MIMO zero-forcing receiver with channel estimation errors," in *Proc. IEEE International Conference on Communications*, June 2007, pp. 4150-4155.

[111] M. R. McKay, P. J. Smith, H. A. Suraweera, and I. B. Collings, "On the mutual information distribution of OFDM-based spatial multiplexing: exact variance and outage approximation," *IEEE Trans. Inf. Theory,* vol. 54, no. 7, pp. 3260-3278, 2008.

[112] J. Choi, B. Mondal, and R. W. Heath Jr, " Interpolation based unitary precoding for special multiplexing MIMO-OFDM with limited feedback," *IEEE Trans. Signal Processing,* vol. 54, no. 12, pp. 4730-4740, 2006.

[113] H. Zhang, Y. Li, V. Stolpman, and N. V. Waes, "A reduced CSI feedback approach for precoded MIMO-OFDM systems," *IEEE Trans. Wireless Commun.,* vol. 6, no. 1, pp. 55-58, 2007.

[114] R. Fletcher, *Practical Methods of Optimization*, 2nd ed.: John Willey & Sons, 1987.

[115] K. M. Anstreicher, " Linear programming in O((n^3/ln$n$)L) operations," *SIAM Journal on Optimization,* vol. 9, no. 4, pp. 803-812, Sept. 1999.

[116] J. Foerster *et al.*, " Channel modeling sub-committee report final," IEEE P802.15-02/490r1-SG3a, Feb. 2003.

[117] D. Bertsimas and R. Weismantel, *Optimization Over Integers*, 2nd ed.: Dynamic Ideas, 2005.

[118] B. C. Arnold and R. A. Groeneveld, "Bounds on expectations of linear systematic statistics based on dependent samples," *The Annals of Statistics,* vol. 7, no. 1, pp. 220-223, Oct. 1979.

[119] A. Lozano, A. M. Tulino, and S. Verdu, "Multiple-antenna capacity in the low power-regime," *IEEE Transactions on Information Theory,* vol. 49, no. 10, pp. 2527-2544, Oct. 2003.

[120] J. Joung, C. K. Ho, and S. Sun, "Spectral efficiency and energy efficiency of OFDM systems: Impact of power amplifiers and countermeasures," *IEEE J. Select. Area Commun.,* vol. 32, no. 2, pp. 208-220, Feb. 2014.

[121] H. Ochiai, "Performance analysis of peak power and band-limited OFDM systems with linear scaling," *IEEE Trans. on Wireless Communications,* vol. 2, no. 5, pp. 1055-1065, 2003.

[122] C. Zhao, R. J. Baxley, and G. T. Zhou, "Peak-to-average power ratio and power efficiency considerations in MIMO-OFDM systems," *IEEE Communications Letters,* vol. 12, no. 4, pp. 268-270, 2008.

[123] S. Coleri, A. P. M. Ergen, and A. Bahai, "Channel estimation techniques based on pilot arrangement in OFDM systems," *IEEE Trans. on Broadcasting,* vol. 48, no. 3, pp. 223-229, 2002.

[124] R. W. Bauml, R. F. H. Fischer, and J. B. Huber, "Reducing the peak-toaverage power ratio of multicarrier modulation by selected mapping," *IEE Electronics Letters,* vol. 32, no. 22, pp. 2056-2057, 1996.

[125] M. Tan, Z. Latinovic, and Y. Bar-Ness, "STBC MIMO-OFDM peak-toaverage power ratio reduction by cross-antenna rotation and inversion," *IEEE Communications Letters,* vol. 9, no. 7, pp. 592-594, 2005.

[126] O. Oyman, R. U. Nabar, H. Bolcskei, and A. J. Paulraj, "Characterizing the statistical properties of mutual information in MIMO channels," *IEEE Trans. on Signal Proc.,* vol. 51, no. 11, pp. 2784-2795, 2003.

[127] R. J. Baxley and G. T. Zhou, "Power savings analysis of peak-toaverage power ratio reduction in OFDM," *IEEE Trans. on Consumer Electronics,* vol. 50, no. 3, pp. 792-797, 2004.

[128] R. A. Comroe and D. J. Costello, "ARQ schemes for data transmission in mobile radio systems," *IEEE Trans. Vehicular Technology,* vol. 33, no. 3, pp. 88-97, 1984.

[129] H. E. Gamal and J. A. R. Hammons, "Analyzing the Turbo decoder using the Gaussian approximation," *IEEE Trans. Information Theory,* vol. 47, no. 2, pp. 671-686, Feb. 2001.

[130] I. Chatzigeorgiou, I. J. Wassell, and R. Carrasco, "On the frame error rate of transmission schemes on quasi-static fading channel," in *Proc. 42nd Annual Conf. Infor. Sciences Systems.*, 2008, pp. 577-581.

[131] A. F. Coskun and O. Kucur, "Performance analysis of joint transmit and receive antenna selection in Nakagami-m fading channels," *IEEE Communications Letters,* vol. 15, no. 2, pp. 211-213, Feb. 2011.

[132] T. Liu, L. Song, Y. Li, Q. Huo, and B. Jiao, "Performance analysis of hybrid relay selection in cooperative wireless systems," *IEEE Trans. on Communications,* vol. 60, no. 3, pp. 779-787, March 2012.

[133] G. Wang, J. Wu, and Y. R. Zheng, "Cross-layer design of energy efficient coded ARQ systems," in *Proc. IEEE GLOBECOM*, Dec. 2012, pp. 2351-2355.

[134] I. Chatzigeorgiou, I. J. Wassell, and R. Carrasco, "Threshold-based frame error rate analysis of MIMO systems over quasistatic fading channels," *Electronics Letters,* vol. 45, no. 4, pp. 216-217, Feb. 2009.

[135] K. E. Atkinson, *An Introduction to Numerical Analysis*: John Wiley & Sons, 1989.

[136] I. Stanojev, O. Simeone, Y. Bar-Ness, and D. H. Kim, "Energy efficiency of non-collaborative and collaborative hybrid-ARQ protocols," *IEEE Trans. Wireless Commun.,* vol. 8, pp. 326–335, 2009.

[137] V. Rodriguez, "An analytical foundation for resource management in wireless communication," in *Proc. IEEE GLOBECOM*, Dec. 2003, pp. 898-902.

[138] F. Rusek *et al.*, "Scaling up MIMO: Opportunities and challenges with very large arrays," *IEEE Trans. Signal Process.,* vol. 30, no. 1, pp. 40-60, Jan. 2013.

[139] H. Ngo, E. G. Larsson, and T. L. Marzetta, "Energy and Spectral Efficiency of Very Large Multiuser MIMO Systems," *IEEE Trans. Commun.,* vol. 61, no. 4, pp. 1436-1449, April 2013.